SUPPORTING INFORMATION

Amino-Terphenyl Covalent Triazine Polymers as Visible-Light Heterogeneous Photocatalysts for Aerobic Sulfoxidation and Cross-Dehydrogenative Coupling Reactions

Andrea Odoardo,[a] Martina Milani,[b] Alessandra Molinari,[a] Lorenzo Poletti,[b] Carmela De Risi,[a] Stefano Caramori,[a] Carmine D'Agostino,[c,d] Min Hu,[c] Paolo Dambruoso,[e] Daniele Cortecchia,[f] Graziano Di Carmine,[b] Daniele Ragno,[*,a] and Alessandro Massi[*,a]

[a]Department of Chemical, Pharmaceutical and Agricultural Sciences, University of Ferrara, Via L. Borsari, 46 – 44121 Ferrara (Italy)

[b]Department of Environmental and Prevention Sciences, University of Ferrara, Via L. Borsari, 46 – 44121 Ferrara (Italy)

[c]Department of Chemical Engineering, University of Manchester, Oxford Road, Manchester M13 9PL (U.K.)

[d]Department of Civil, Chemical, Environmental, and Materials Engineering, Alma Mater Studiorum - University of Bologna, Via Terracini 28 – 40131 Bologna (Italy)

[e]Institute for the Organic Synthesis and Photoreactivity of the Italian National Research Council, Area della Ricerca di Bologna, Via P. Gobetti, 101 – 40129 – Bologna (Italy)

[f]Department of Industrial Chemistry Toso Montanari, University of Bologna, Via Piero Gobetti 85 – 40129 Bologna (Italy)

Table of contents

1. General informations S2

2. Experimental procedures and DAPT-CTP$_s$ characterization S6

3. Characterization data S42

4. Comparison of different triazine-based photocatalysts in the aerobic oxidation of sulfides S57

5. References S58

6. NMR Spectra S61

1. General informations

Commercially available reagents were purchased from commercial sources and used without any subsequent purification. Anhydrous solvents were freshly distilled and dried over a standard drying agent prior to use. Flash column chromatography was performed on silica gel 60 (230−400 mesh). Kessil lamp PR160L (390 nm, 52W), Hg-Xe LC8 lamp (-06A type, 200W) and a light-emitting diodes (LEDs) array (6 LEDs, 10 W each, λ = 418 nm) were used as the irradiation source for the photochemical reactions. Hg-Xe LC8 lamp was purchased from Hamamatsu Photonics K.K. The long-pass filters at 400 or 420 nm were purchased from Thorlabs, Inc. Flow reactions were performed using an HPLC pump (Agilent Technologies, series 1100) and mass flow controller (Brooks Instrument, series SLA5800, with secondary electronics model 0251). The flow reaction takes place inside an Omnifit® column (EZ Solventplus Column 6.6 mm/150).

Attenuated Total Reflectance-Fourier Trasform Infrared (ATR-FTIR)

Attenuated total reflectance (ATR) analyses of samples were obtained with a universal ATR accessory coupled to an FT-IR spectrometer (PerkinElmer Spectrum 100 FTIR).

Nuclear Magnetic Resonance (NMR)

^{1}H, ^{13}C and ^{19}F NMR spectra were recorded by a Varian Mercury Plus 300 and a Varian Mercury plus 400 equipped with an Oxford NMR AS400 MHz autosampler, at room temperature in $CDCl_3$, CD_3OD, D_2O, DMSO-d_6 and acetone-d_6. The chemical shifts in ^{1}H and ^{13}C NMR spectra were referenced to tetramethylsilane (TMS).

Solid State Nuclear Magnetic Resonance (ssNMR)

Solid state nuclear magnetic resonance (ssNMR) measurements were performed on a Bruker Avance NEO WB with a wide-bore magnet (89 mm) operating at a ^{1}H frequency of 400 MHz using a 1.9 mm cross polarization magic angle spinning (CP-MAS) probe employing 1.9 mm zirconia rotors with VESPEL turbines. The ^{13}C spectrum was measured via cross-polarization $^{13}C\{^{1}H\}$ with a number of scans of 1800. The spin-rotation frequency was set to 15 kHz. The 90° pulse length was 1.66 ms for ^{1}H and 2.94 ms for ^{13}C. A spin–lattice relaxation time T_1 of 2 s for ^{1}H was determined with the inversion recovery pulse sequence and used as reference value to set a recycle delay of $3xT_1$ = 6 s for the CP experiment. Heteronuclear decoupling was applied through the SPINAL64 sequence. The contact time was 3ms. The chemical shift was referenced to the ^{13}C signal of adamantane at 37.77 ppm.

Powder X-Ray Diffraction (XRD)

The powder XRD data of all the samples were collected on a Bruker D8 Discover GIXRD Autochanger diffractometer operating with CuKα radiation (λ=1.542 Å) at 30 kV. The powder XRD data were collected in the 2θ range 3–90° with a step size of 0.02°.

Thermogravimetric analysis (TGA)

Thermogravimetric analysis (TGA) was performed on a Discovery TGA 550 analyzer. Samples were subjected to a linear temperature ramp from 30 °C to 800 °C at a rate of 10 °C min^{-1} under an air flow of 40 mL min^{-1}.

Nitrogen adsorption-desorption

Nitrogen adsorption-desorption isotherms were obtained using a Micromeritics ASAP 2060 physisorption analyzer. Prior to analysis, approximately 100 mg of sample was degassed at 200 °C under vacuum (0.3

mmHg) for 12 h. The physisorption measurements were conducted at -196 °C (77 K). The Brunauer-Emmett-Teller (BET) method was employed to determine the specific surface area, while the pore size distribution was obtained according to the Barrett−Joyner−Halenda (BJH) method.

Scanning electron microscope (SEM) and Energy Dispersive X-ray Spectroscopy (EDX)

Microscopic analyses were performed with a Gemini 460 (Zeiss, Germany), scanning electron microscope (SEM) working under high vacuum with a FEG source, voltage 5 kV and 200 pA probe. Samples were deposited on stubs with carbon adhesive tabs and covered with gold using Sputter Q150R S (Quorum Technologies).

The elemental distribution was determined by collecting energy dispersive X-ray spectroscopy (EDX) map with a Zeiss EVO40 scanning electron microscope (SEM) equipped with an Oxford Instruments INCAx-act detector, working at 50 Pa with a working distance of 9 mm, a probe current of 3 nA and an electron high tension (EHT) of 5 kV.

Elemental analyses

Elemental analyses were performed using a FLASH 2000 series CHNS/O analyzer (ThermoFisher Scientific).

Steady State Optical Absorption and Emission.

UV−Vis absorption spectrum of the reference p-terphenyl (**PT**) in CH_3CN was recorded using an Agilent Cary-300 UV-Vis spectrophotometer in absorbance mode in the range 200-800 nm. The absorption spectrum of solid **DAPT-CTPs** was recorded using a Jasco V-570 spectrophotometer equipped with an integrating sphere (2 nm bandwidth) in diffuse reflectance mode in the range 200-800 nm. The Tauc plot of **DAPT-CTPs** was obtained according to $(F(R)\ x\ h\nu)^{\alpha} = A\ x\ (h\nu - E_g)$, where α = 1/2 for a direct band gap, $(F(R) = (1 - R)^2/2R)$ is Kubelka-Munk function, A is a proportionality coefficient and E_g is the material band gap.
Emission spectra were obtained at room temperature with an Edinburgh Instruments FLS 920 spectrofluorometer (Edinburgh Instrument Ltd) using a dedicated thin cell holder when needed. All spectra were corrected for the lamp and photomultiplier response and averaged over 10 subsequent scans with a 0.5 nm step.
Emission spectra of **PT** in CH_3CN were recorded with λ_{exc} = 278 nm and excitation spectra of the same was collected at λ_{em} = 350 nm. Emission spectra of **DAPT-CTPs** dispersed in CH_3CN were carried out with λ_{exc} = 300 nm while their excitation spectra were recorded by collecting the emission at λ_{em} = 430 nm.

Electrochemical measurements

Electrochemical measurements were carried out using a PGSTAT302N potentiostat (Autolab-Eco Chemie) in a three-electrode cell configuration. A leakless Ag/AgCl or Standard Calomel Electrode (SCE) was used as the reference electrode, a Pt wire as counter electrode and either a glassy carbon electrode, a **DAPT-CTP** modified FTO (Fluorine-Tin-Oxide) or a **DAPT-CTP** graphite sheet (CP) as the working electrodes.
Cyclic Voltammetry (CV) was performed by suspending **DAPT-CTPs** in acetonitrile containing 0.1 M $LiClO_4$ as supporting electrolyte, in a nitrogen-purged sealed electrochemical cell, by sweeping the voltage in the +2.0 to -2.8 V range at a scan rate of 10 mV/s.
Cyclic Voltammetry (CV) of **FTO/DAPT-CTPs** and **CP/DAPT-CTPs** was carried out in either nitrogen or oxygen purged electrochemical cell, using $LiClO_4$ in acetonitrile as supporting electrolyte. The potential was swept from 0.0 to -1.5 V at a scan rate of 10 mV/s. The working electrodes were prepared by dispersing approximately 20 mg of **DAPT-CTPs** in 2 mL of ethanol, followed by drop-casting the resulting suspension

onto pre-cleaned FTO glass or carbon paper substrates. The electrodes were then allowed to dry under ambient conditions prior to electrochemical measurements.

Single photon counting

Emission lifetimes of **PT** and **DAPT-CTPs** samples were acquired with a Picoquant Picoharp 300 time correlated single photon counting at a 4 ps resolution by using a 290/280 nm pulsed LED source. The fitting and deconvolution of the decay histogram were performed using mono- or bi-exponential functions with the Fluofit program. Overall, the fits met the statistical acceptability criteria, achieving χ^2 values close to 1. The residuals, defined as R(i)=(W(i)Decay(i)-Fit(i)), remained within 4 standard deviations of zero across all fitting intervals. Here, W(i) = 1/((Decay(i))$^{(1/2)}$ represents the intensity weight for each channel (i) based on the Poisson distribution, while Decay(i) and Fit(i) denote the experimentally measured and calculated decay values, respectively.

Nanosecond Transient Absorption Spectra

Nanosecond-transient absorption spectra (TAS) were obtained by excitation of either a **PT** solution or **DAPT-CTP** powder finely suspended in CH_3CN contained in a quartz cell. A frequency tripled (355 nm) or quadrupled (266 nm) Continuum Surelite II Nd/YAG laser (1064 nm, fwhm = 6−8 ns) was used as an excitation source. The probe source was provided by an Applied Photophysics Xe lamp (150 W), equipped with an Action SpectraPro 2300i monocromator (150 grooves/mm grating) and a Hamamatsu R3896 photomultiplier tube detector biased at 490 V. By acting on the Q switch, flash lamp voltage supply and by optically defocusing the laser beam, the excitation fluence was set to ca. 15 mJ/cm^2/pulse. This relatively high value is needed to obtain an acceptable S/N ratio in the oscillographic traces of the samples. When needed, the solution/suspension was sealed and bubbled with N_2 to remove oxygen. The resulting transient traces were averaged over 200 laser shots and corrected for the baseline (i.e. the background noise generated by the probe beam in the absence of the laser excitation pulse). Fitting of the traces to extract the lifetime was achieved with either a monoexponential (**PT**) or bi-exponential function (**DAPT-CTP)**. In the case of the bi-exponential decay, an amplitude weighted lifetime was calculated.

Quantum chemical calculations

DFT and TD-DFT calculations on **PT** and representative **DAPT-CTP** fragments were carried out with Gaussian 09 [1] with the B3LYP functional. Geometry optimization was carried out in vacuo with the 6-31g(d) basis set, an ultrafine integration grid and a maximum step=3. Force constants were calculated after each optimization step to ensure localization of an appropriate stationary point. TD-DFT calculations were accomplished on the respective optimized ground state geometry of the selected closed shell molecular fragments at the B3LYP-6311g(d,p) level by including the solvent treated as a dielectric continuum (IEFPCM). The lowest 30 singlet transitions were considered. In the same fashion, the energy of the lowest triplet states was obtained. Computed optical spectra (3000 cm^{-1} FWHM) and orbital isosurfaces were plotted with Gaussview 5. EDDMs (Electron Density Difference Maps) associated with the strongest transitions were generated with Multiwfn [2].

Electron Spin Resonance (ESR) Spin Trapping

ESR spin trapping experiments were carried out with a Bruker ER200 MRD spectrometer equipped with a TE201 resonator (microwave frequency of 9.4 GHz). The samples were EtOH or EtOH/H_2O 1/1 suspensions of **DAPT-CTP$_{sc}$** and 5,5' -dimethyl 1-pyrroline N-oxide (**DMPO**) or 2,2,6,6-tetra-methyl-1-piperidine (**TEMP**) as spin trap. The suspensions were transferred into a flat quartz cell and directly irradiated (Hg medium pressure lamp with a cut off filter, $\lambda \geq 400$ nm) in the ESR cavity.

2. Experimental procedures and DAPT-CTP$_s$ characterization

2.1 Elemental composition and Morphological Properties of DAPT-CTPs

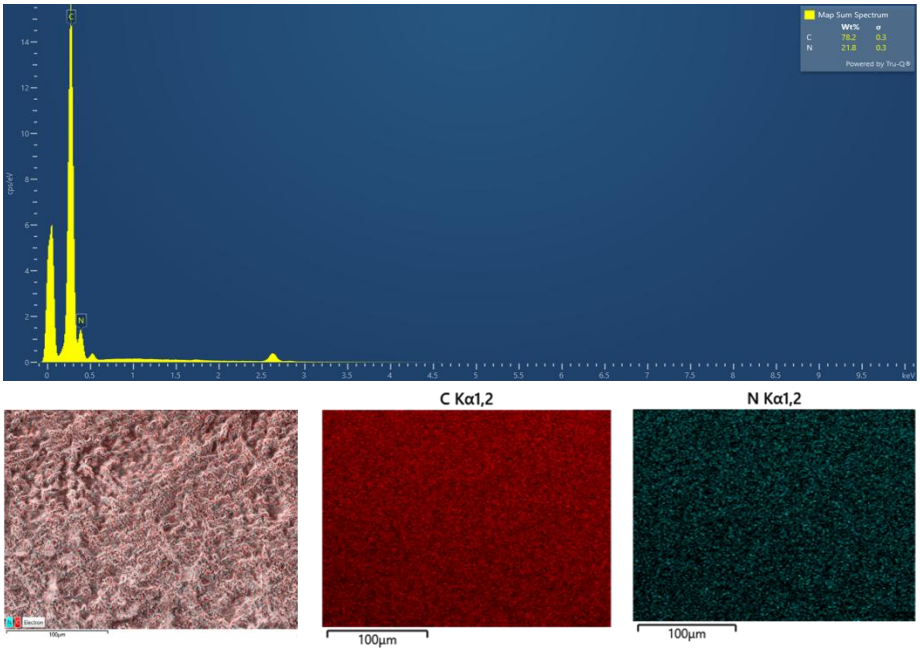

Figure S1. DAPT-CTP$_{sc}$ EDX elemental mapping.

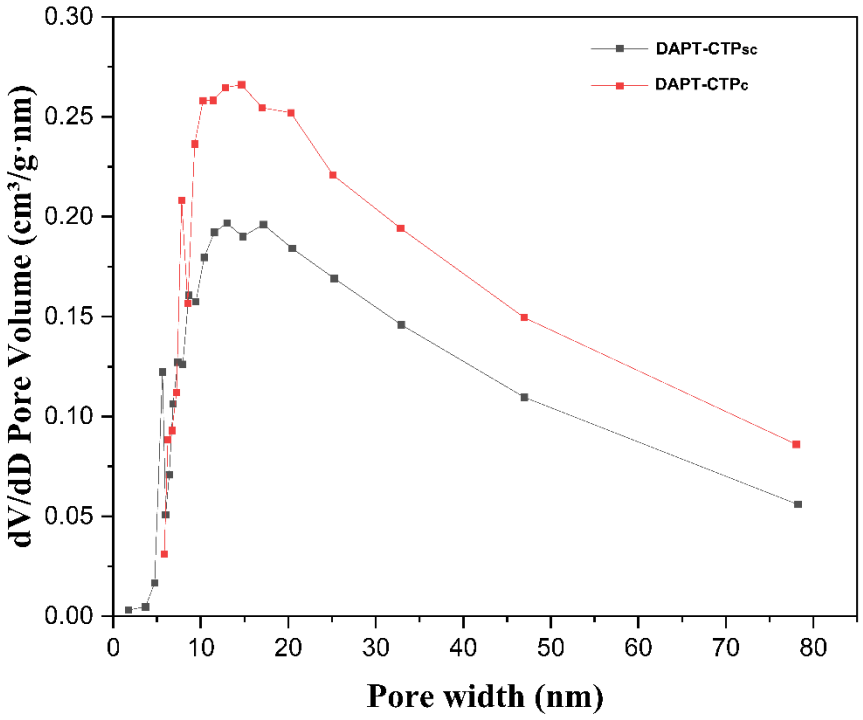

Figure S2. DAPT-CTP$_{sc}$ and **DAPT-CTP$_c$** Barrett-Joyner-Halenda (BJH) pore size plots.

2.2 Synthesis of Covalent Triazine Polymers photocatalysts

2.2.1 Procedure for the synthesis of DAPT-CTP$_{sc}$

In a two-neck round-bottom flask, 4,4”-diamino-*p*-terphenyl (1 g, 1.9 mmol) was dissolved in anhydrous dimethylacetamide (DMA) (38 mL), and *N*,*N*-diisopropylethylamine (DIPEA) (5.7 mL, 16.3 mmol) was added to the mixture under nitrogen atmosphere. After cooling to 0°C, a solution of cyanuric chloride (0.71 g, 1.9 mmol) in anhydrous DMA (57 mL) was added dropwise into the mixture within 30 minutes under stirring. Then the reaction solution was heated at 50°C for 16 hours and then at 95°C for 24 hours. The suspension was filtered and extracted with THF in a Soxhlet apparatus over at least 16 hours.
After vacuum-drying for 16 hours, the final product was obtained as a beige powder. Elemental analysis (%) found: C = 72.2, N = 20.6.

2.2.2 Procedure for the synthesis of DAPT-CTP$_{c}$ [3]

In a two-neck round-bottom flask, cyanuric chloride (0.10 g, 0.54 mmol) was dissolved in anhydrous 1,4-dioxane (250 mL) under nitrogen atmosphere. Then, 50 mL of 4,4′′-diamino-*p*-terphenyl (0.21 g, 0.81 mmol) and *N*,*N*-diisopropylethylamine (DIPEA) (0.33 ml, 1.94 mmol) solution in anhydrous 1,4-dioxane were added dropwise into the stirring solution of cyanuric chloride within 30 minutes under nitrogen atmosphere at room temperature. Four hours later, the temperature was raised to 90 °C and heated for 24 hours. The suspension was filtered, and the filter cake was washed with 1,4-dioxane, THF and distilled water. After vacuum-drying for 16 hours, the final product was obtained as a white powder. Elemental analysis (%) found: C = 71.1, N = 23.6.

2.3 Optical properties of DAPT-CTPs

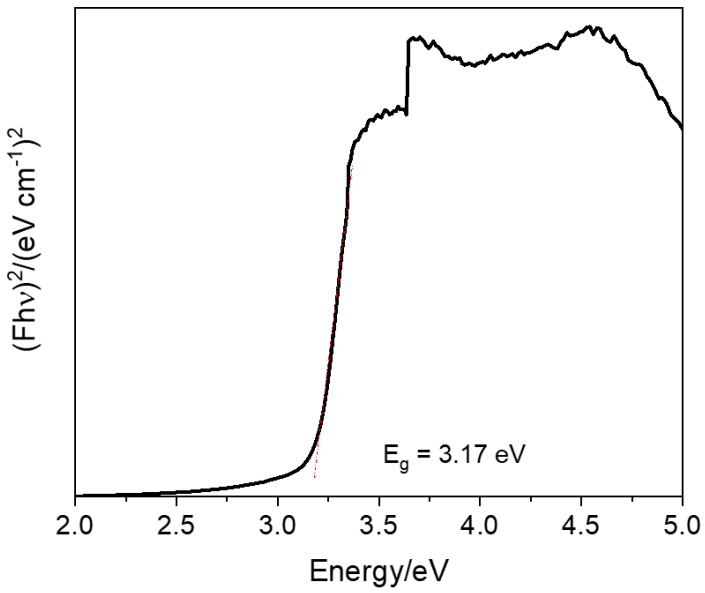

(a)

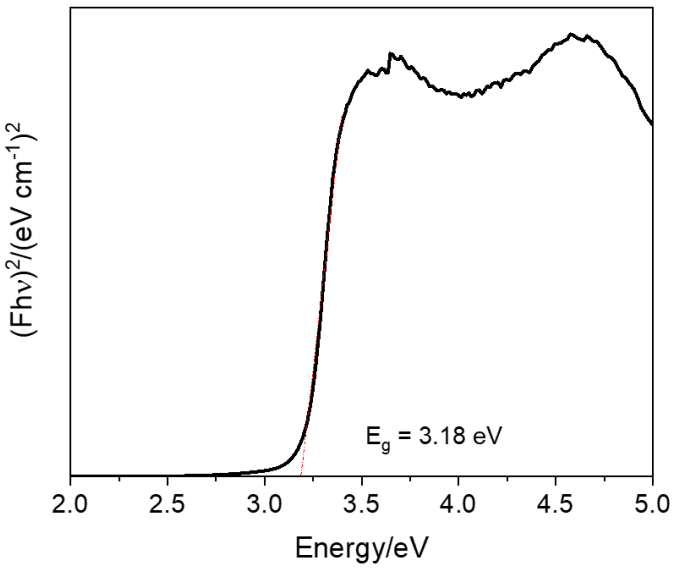

(b)

Figure S3. Tauc plots of **DAPT-CTP$_{sc}$** (a) and **DAPT-CTP$_{c}$** (b) recorded in diffuse reflectance mode.

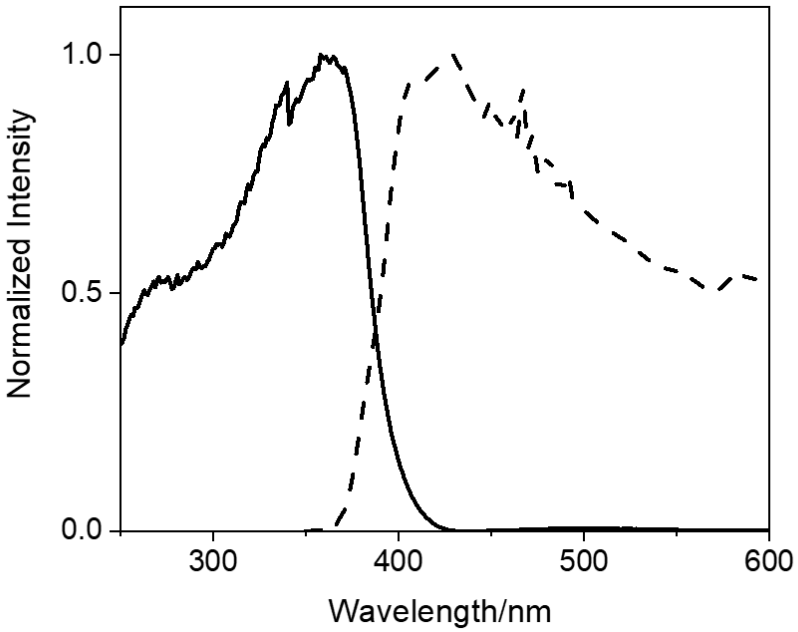

(a)

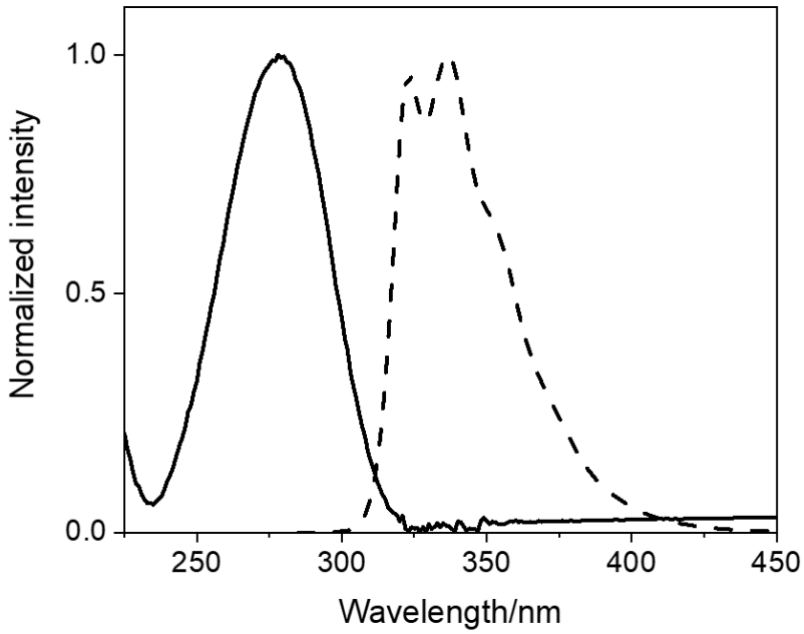

(b)

Figure S4. Normalized absorption and emission spectra of **DAPT-CTP$_{sc}$** (a) and of **PT** as a reference (b).

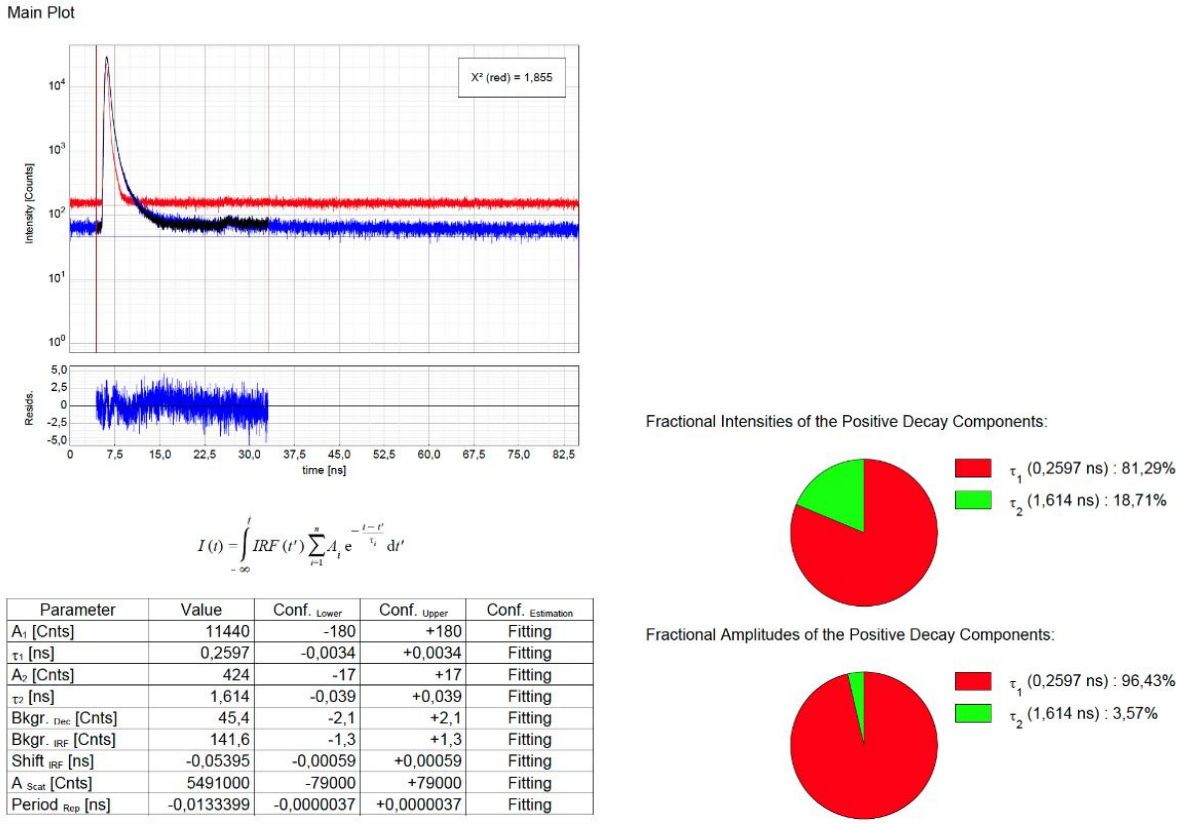

Parameter	Value	Conf. Lower	Conf. Upper	Conf. Estimation
A_1 [Cnts]	11440	-180	+180	Fitting
τ_1 [ns]	0,2597	-0,0034	+0,0034	Fitting
A_2 [Cnts]	424	-17	+17	Fitting
τ_2 [ns]	1,614	-0,039	+0,039	Fitting
Bkgr. $_{Dec}$ [Cnts]	45,4	-2,1	+2,1	Fitting
Bkgr. $_{IRF}$ [Cnts]	141,6	-1,3	+1,3	Fitting
Shift $_{IRF}$ [ns]	-0,05395	-0,00059	+0,00059	Fitting
A $_{Scat}$ [Cnts]	5491000	-79000	+79000	Fitting
Period $_{Rep}$ [ns]	-0,0133399	-0,0000037	+0,0000037	Fitting

(a)

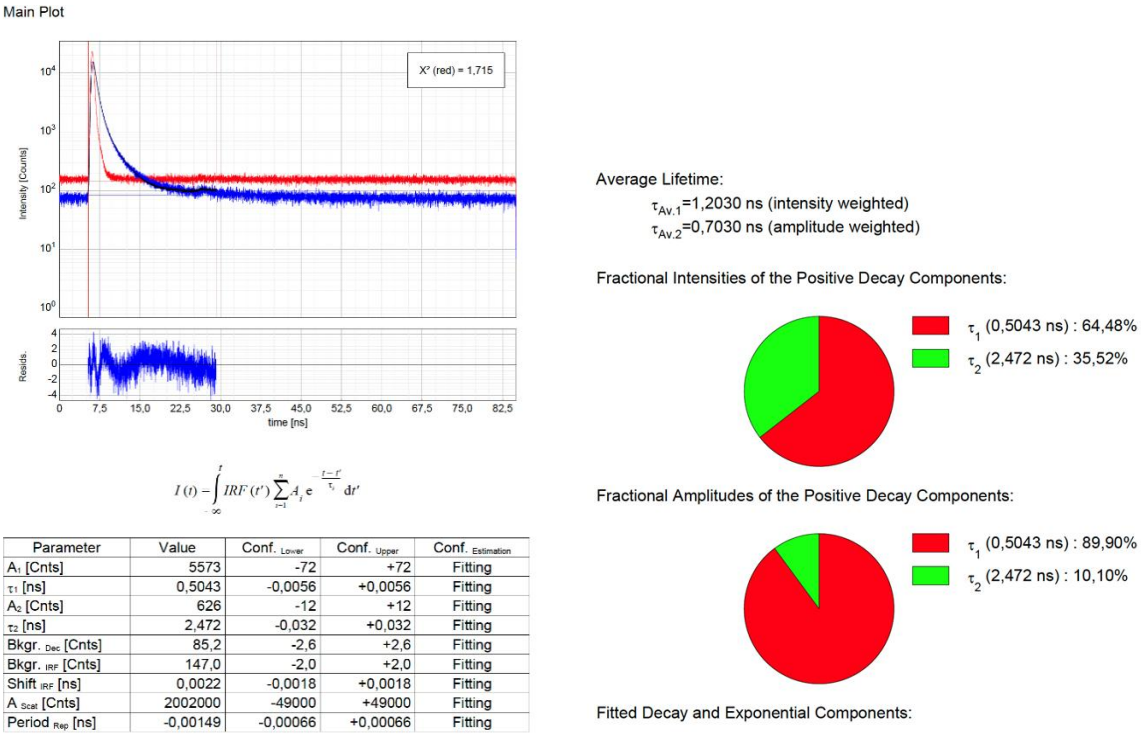

$$I(t) = \int_{-\infty}^{t} IRF(t') \sum_{i=1}^{n} A_i \, e^{-\frac{t-t'}{\tau_i}} \, dt'$$

Parameter	Value	Conf. Lower	Conf. Upper	Conf. Estimation
A_1 [Cnts]	5573	-72	+72	Fitting
τ_1 [ns]	0,5043	-0,0056	+0,0056	Fitting
A_2 [Cnts]	626	-12	+12	Fitting
τ_2 [ns]	2,472	-0,032	+0,032	Fitting
Bkgr. Dec [Cnts]	85,2	-2,6	+2,6	Fitting
Bkgr. IRF [Cnts]	147,0	-2,0	+2,0	Fitting
Shift IRF [ns]	0,0022	-0,0018	+0,0018	Fitting
A Scat [Cnts]	2002000	-49000	+49000	Fitting
Period Rep [ns]	-0,00149	-0,00066	+0,00066	Fitting

(b)

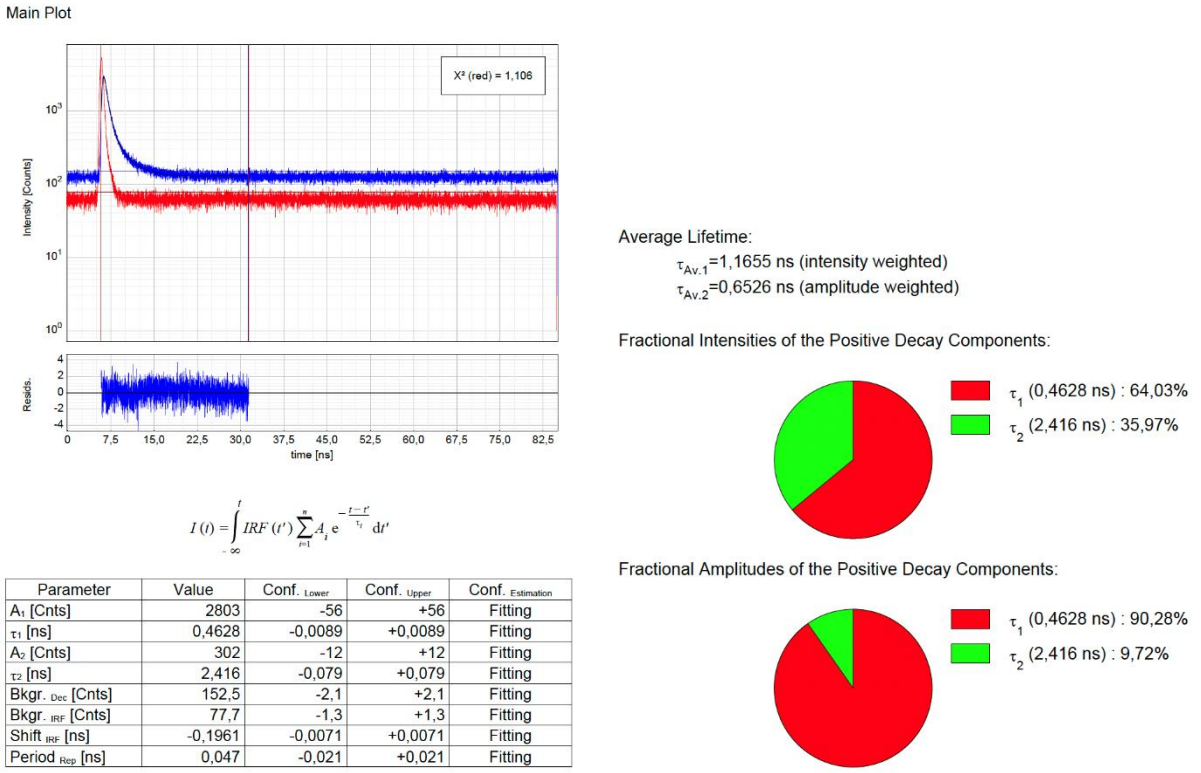

$$I(t) = \int_{-\infty}^{t} IRF(t') \sum_{i=1}^{n} A_i \, e^{-\frac{t-t'}{\tau_i}} \, dt'$$

Parameter	Value	Conf. Lower	Conf. Upper	Conf. Estimation
A_1 [Cnts]	2803	-56	+56	Fitting
τ_1 [ns]	0,4628	-0,0089	+0,0089	Fitting
A_2 [Cnts]	302	-12	+12	Fitting
τ_2 [ns]	2,416	-0,079	+0,079	Fitting
Bkgr. Dec [Cnts]	152,5	-2,1	+2,1	Fitting
Bkgr. IRF [Cnts]	77,7	-1,3	+1,3	Fitting
Shift IRF [ns]	-0,1961	-0,0071	+0,0071	Fitting
Period Rep [ns]	0,047	-0,021	+0,021	Fitting

(c)

Figure S5. Emission decays of **DAPT-CTP$_{sc}$** powder in contact with acetonitrile fitted with biexponential decay sampled at 425 nm (a), 525 nm (b), and 620 nm (c).

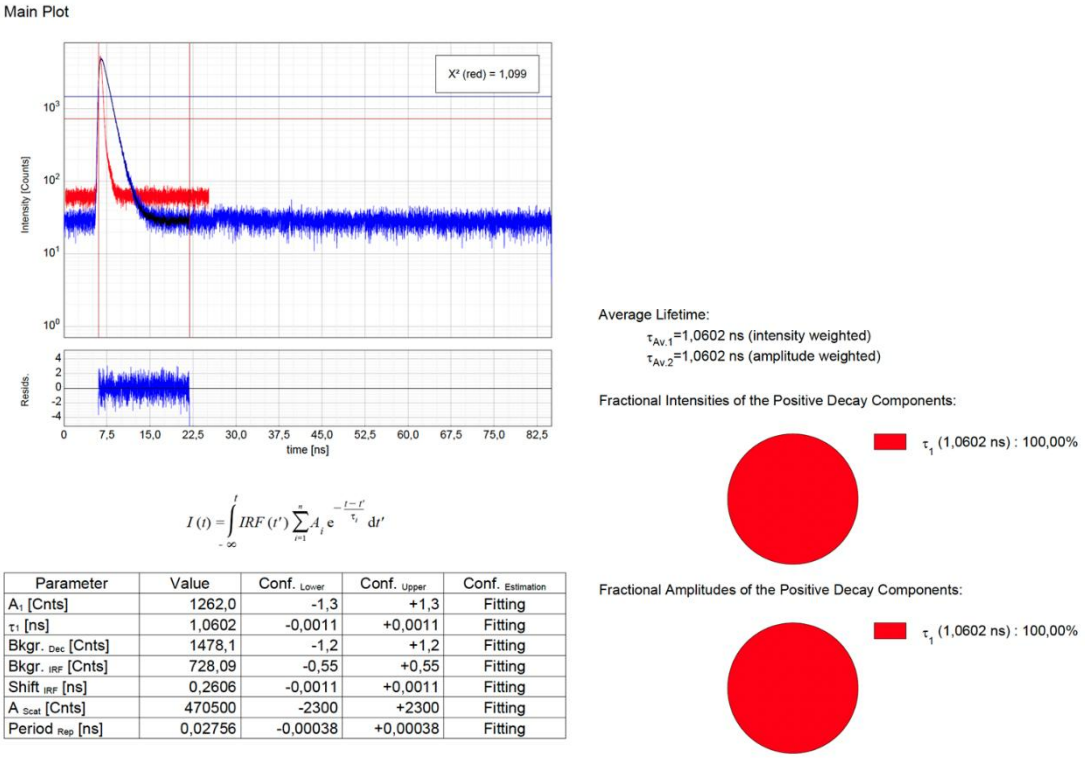

$$I(t) = \int_{-\infty}^{t} IRF(t') \sum_{i=1}^{n} A_i \, e^{-\frac{t-t'}{\tau_i}} \, dt'$$

Parameter	Value	Conf. Lower	Conf. Upper	Conf. Estimation
A_1 [Cnts]	1262,0	-1,3	+1,3	Fitting
τ_1 [ns]	1,0602	-0,0011	+0,0011	Fitting
Bkgr. Dec [Cnts]	1478,1	-1,2	+1,2	Fitting
Bkgr. IRF [Cnts]	728,09	-0,55	+0,55	Fitting
Shift IRF [ns]	0,2606	-0,0011	+0,0011	Fitting
A Scat [Cnts]	470500	-2300	+2300	Fitting
Period Rep [ns]	0,02756	-0,00038	+0,00038	Fitting

Figure S6. Emission decay of **PT** in acetonitrile.

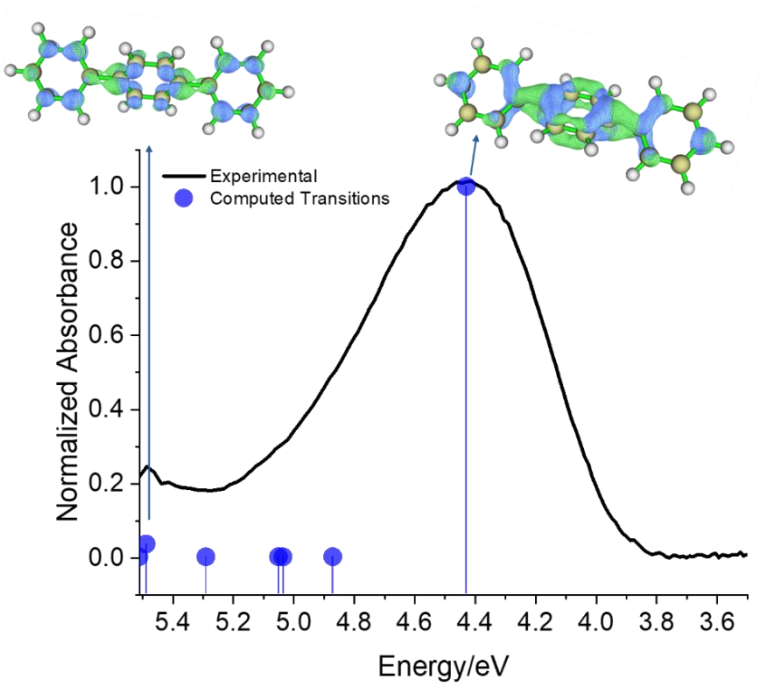

Figure S7. Experimental spectrum of **PT** and vertical transitions computed at the B3LYP 6-311g(d,p) level and electron density difference map (EDDM) associated with the transitions with the largest oscillator strength. Green isosurfaces represent electron accumulation, blue ones indicate hole accumulation.

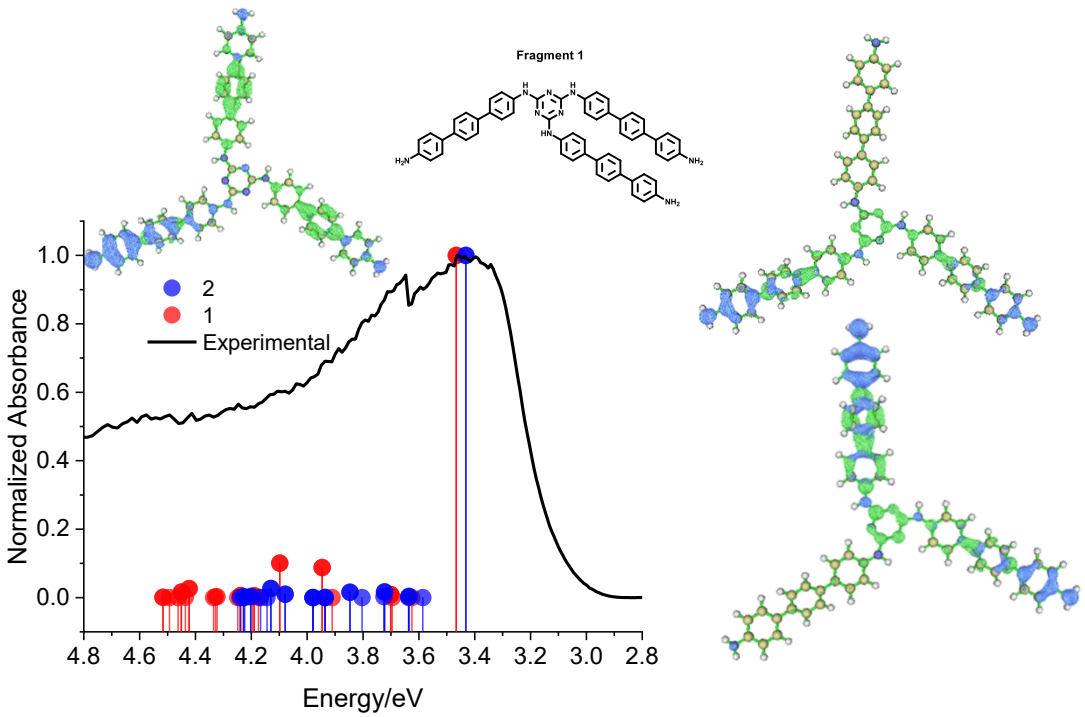

Figure S8. Experimental spectrum and computed vertical excitations in fragments 1 and 2 at the TDDFT B3LYP 6-311g(d,p) + IEFCPM. EDDM associated to the most intense transition of fragment 1 are shown. Green isosurfaces represent electron accumulation, blue ones are associated to hole accumulation.

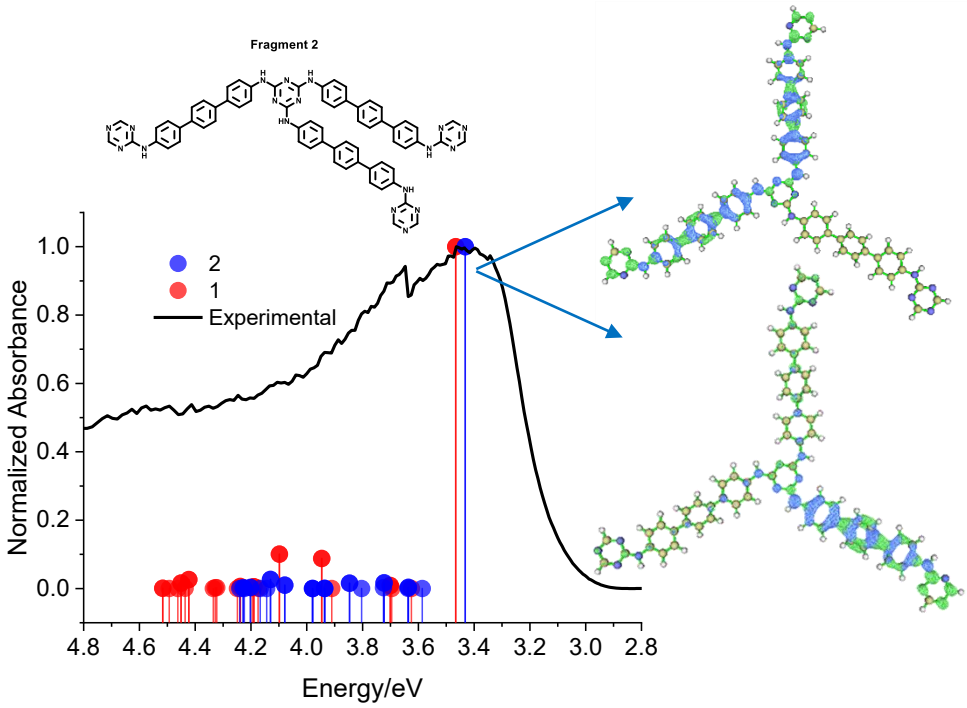

Figure S9. Experimental spectrum of **DAPT-CTP$_{sc}$** and computed vertical excitations in the fragments 1 and 2 at the TDDFT B3LYP 6-311g(d,p) + IEFCPM level. EDDMs associated to the most intense transitions in fragment 2 are shown. Green isosurfaces represent electron accumulation, blue ones are associated to hole accumulation.

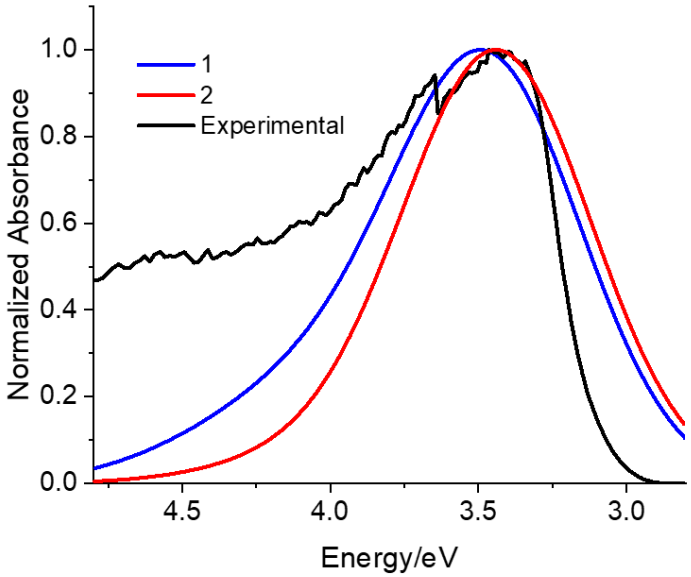

Figure S10. Comparison of the experimental spectrum (black) of **DAPT-CTP$_{sc}$** and theoretical spectra computed for fragments 1 and 2 and plotted with an FWHM of 3000 cm^{-1}.

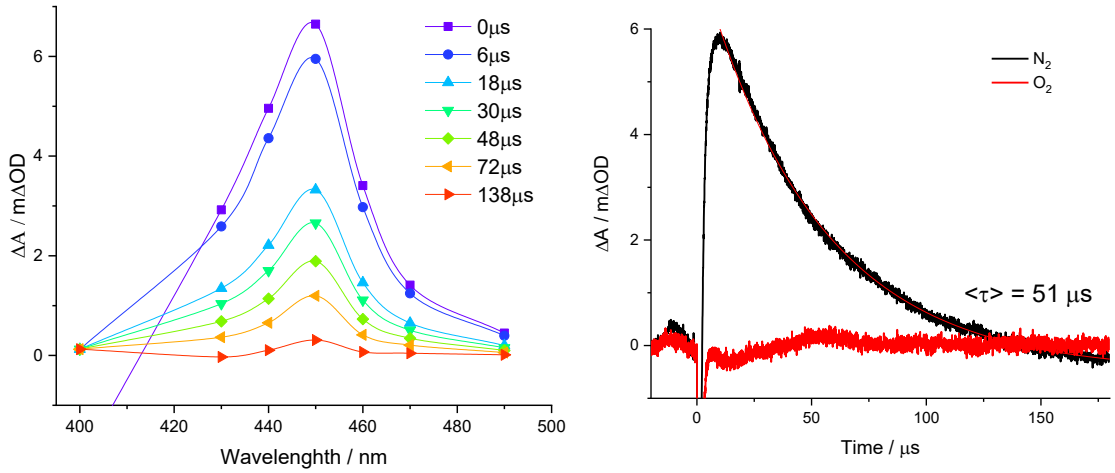

Figure S11. Left: Transient absorption spectrum of **PT** following 266 nm laser excitation; right: mono-exponential excited state decay kinetics in the absence (black) and in the presence of air.

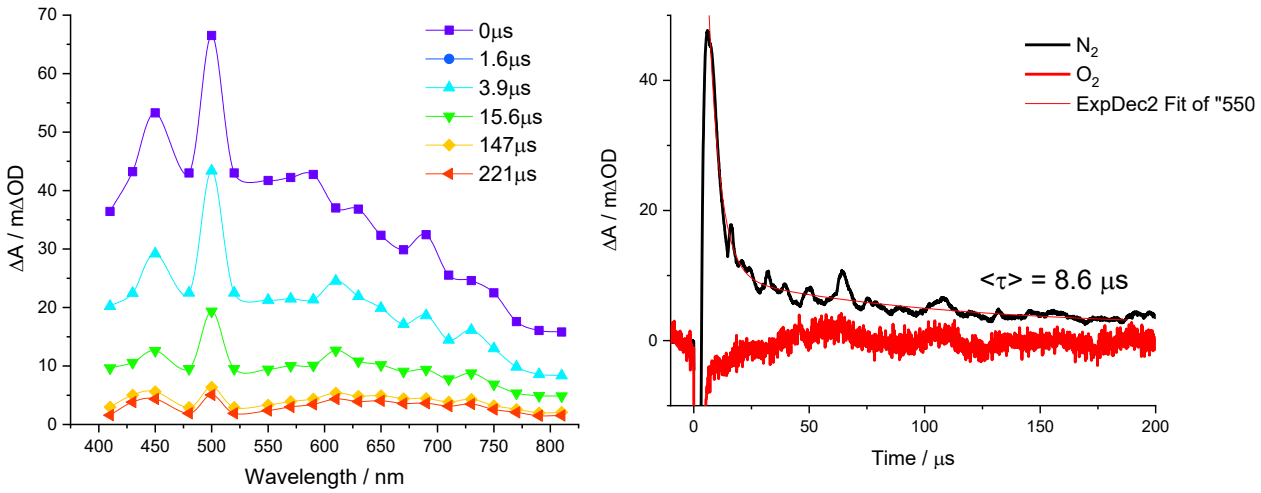

Figure S12. Left: Transient absorption spectrum of **DAPT-CTP$_{sc}$** following 355 nm laser excitation; right: multiexponential excited state decay kinetics in the absence (black) and in the presence of air.

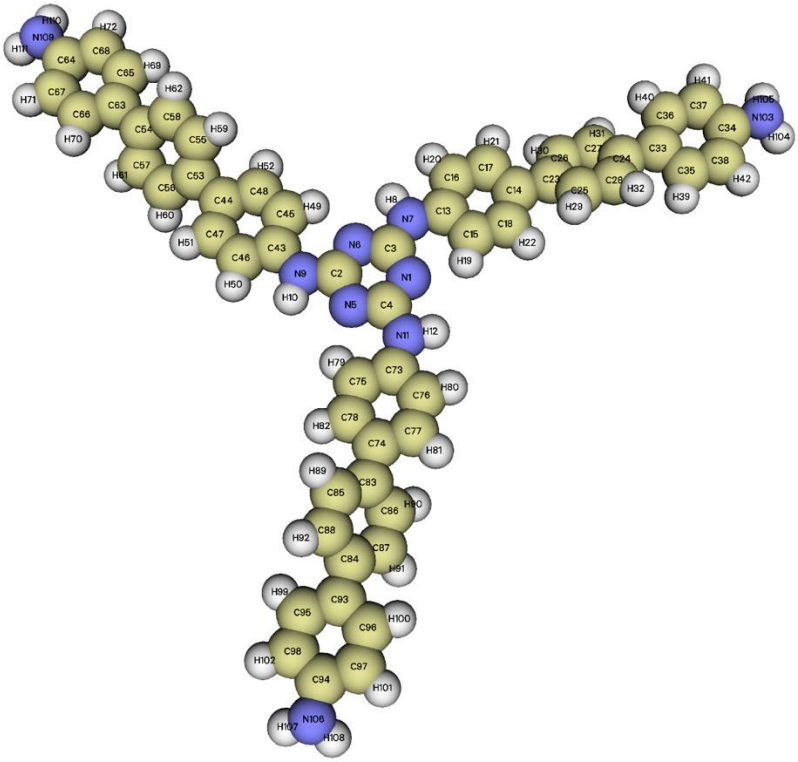

Figure S13. Amino-terminated fragment of **DAPT-CTP** (fragment 1) with numbered atoms for orbital composition analysis.

Table S1. Atom contribution to HOMO amplitude in the amino-terminated fragment of DAPT-CTP (fragment 1).

Contributions after normalization:

HOMO

Atom	1(N) :	0.290 %
Atom	2(C) :	0.237 %
Atom	3(C) :	0.230 %
Atom	4(C) :	0.230 %
Atom	5(N) :	0.307 %
Atom	6(N) :	0.306 %
Atom	7(N) :	1.462 %
Atom	8(H) :	0.105 %
Atom	9(N) :	1.504 %

Atom 10(H) : 0.108 %

Atom 11(N) : 1.465 %

Atom 12(H) : 0.106 %

Atom 13(C) : 1.282 %

Atom 14(C) : 1.408 %

Atom 15(C) : 0.694 %

Atom 16(C) : 0.712 %

Atom 17(C) : 0.712 %

Atom 18(C) : 0.802 %

Atom 19(H) : 0.055 %

Atom 20(H) : 0.050 %

Atom 21(H) : 0.057 %

Atom 22(H) : 0.065 %

Atom 23(C) : 1.922 %

Atom 24(C) : 1.829 %

Atom 25(C) : 0.839 %

Atom 26(C) : 0.833 %

Atom 27(C) : 1.128 %

Atom 28(C) : 1.122 %

Atom 29(H) : 0.064 %

Atom 30(H) : 0.063 %

Atom 31(H) : 0.093 %

Atom 32(H) : 0.093 %

Atom 33(C) : 3.100 %

Atom 34(C) : 2.561 %

Atom 35(C) : 1.256 %

Atom 36(C) : 1.255 %

Atom 37(C) : 1.761 %

Atom 38(C) : 1.753 %

Atom 39(H) : 0.090 %

Atom 40(H) : 0.088 %

Atom 41(H) : 0.131 %

Atom 42(H) : 0.129 %

Atom 43(C) : 1.326 %

Atom 44(C) : 1.454 %

Atom 45(C) : 0.715 %

Atom 46(C) : 0.734 %

Atom 47(C) : 0.738 %

Atom 48(C) : 0.831 %

Atom 49(H) : 0.057 %

Atom 50(H) : 0.051 %

Atom 51(H) : 0.059 %

Atom 52(H) : 0.067 %

Atom 53(C) : 1.997 %

Atom 54(C) : 1.898 %

Atom 55(C) : 0.870 %

Atom 56(C) : 0.864 %

Atom 57(C) : 1.173 %

Atom 58(C) : 1.167 %

Atom 59(H) : 0.067 %

Atom 60(H) : 0.066 %

Atom 61(H) : 0.096 %

Atom 62(H) : 0.097 %

Atom 63(C) : 3.233 %

Atom 64(C) : 2.671 %

Atom 65(C) : 1.309 %

Atom 66(C) : 1.307 %

Atom 67(C) : 1.838 %

Atom 68(C) : 1.830 %

Atom 69(H) : 0.093 %

Atom 70(H) : 0.092 %

Atom 71(H) : 0.137 %

Atom 72(H) : 0.135 %

Atom 73(C) : 1.283 %

Atom 74(C) : 1.409 %
Atom 75(C) : 0.694 %
Atom 76(C) : 0.712 %
Atom 77(C) : 0.712 %
Atom 78(C) : 0.804 %
Atom 79(H) : 0.055 %
Atom 80(H) : 0.050 %
Atom 81(H) : 0.057 %
Atom 82(H) : 0.065 %
Atom 83(C) : 1.925 %
Atom 84(C) : 1.832 %
Atom 85(C) : 0.841 %
Atom 86(C) : 0.835 %
Atom 87(C) : 1.130 %
Atom 88(C) : 1.124 %
Atom 89(H) : 0.065 %
Atom 90(H) : 0.063 %
Atom 91(H) : 0.093 %
Atom 92(H) : 0.094 %
Atom 93(C) : 3.108 %
Atom 94(C) : 2.567 %
Atom 95(C) : 1.259 %
Atom 96(C) : 1.257 %
Atom 97(C) : 1.765 %
Atom 98(C) : 1.758 %
Atom 99(H) : 0.090 %
Atom 100(H) : 0.089 %
Atom 101(H) : 0.132 %
Atom 102(H) : 0.129 %
Atom 103(N) : 4.140 %
Atom 104(H) : 0.345 %
Atom 105(H) : 0.352 %

Atom 106(N) : 4.151 %

Atom 107(H) : 0.346 %

Atom 108(H) : 0.353 %

Atom 109(N) : 4.320 %

Atom 110(H) : 0.360 %

Atom 111(H) : 0.368 %

Table S2. Atom contribution to LUMO amplitude in the amino-terminated fragment of **DAPT-CTP** (fragment 1)

LUMO

Contributions after normalization:

Atom 1(N) : 1.306 %

Atom 2(C) : 0.931 %

Atom 3(C) : 4.840 %

Atom 4(C) : 5.214 %

Atom 5(N) : 3.537 %

Atom 6(N) : 3.500 %

Atom 7(N) : 1.090 %

Atom 8(H) : 0.072 %

Atom 9(N) : 0.104 %

Atom 10(H) : 0.034 %

Atom 11(N) : 1.309 %

Atom 12(H) : 0.096 %

Atom 13(C) : 3.534 %

Atom 14(C) : 3.375 %

Atom 15(C) : 1.651 %

Atom 16(C) : 1.296 %

Atom 17(C) : 2.229 %

Atom 18(C) : 1.553 %

Atom 19(H) : 0.192 %

Atom 20(H) : 0.115 %

Atom 21(H) : 0.251 %

Atom 22(H) : 0.160 %

Atom 23(C) : 3.063 %

Atom 24(C) : 3.133 %

Atom 25(C) : 1.754 %

Atom 26(C) : 1.787 %

Atom 27(C) : 1.226 %

Atom 28(C) : 1.263 %

Atom 29(H) : 0.189 %

Atom 30(H) : 0.201 %

Atom 31(H) : 0.128 %

Atom 32(H) : 0.133 %

Atom 33(C) : 0.921 %

Atom 34(C) : 0.959 %

Atom 35(C) : 0.810 %

Atom 36(C) : 0.807 %

Atom 37(C) : 0.256 %

Atom 38(C) : 0.257 %

Atom 39(H) : 0.091 %

Atom 40(H) : 0.090 %

Atom 41(H) : 0.019 %

Atom 42(H) : 0.019 %

Atom 43(C) : 0.107 %

Atom 44(C) : 0.137 %

Atom 45(C) : 0.072 %

Atom 46(C) : 0.113 %

Atom 47(C) : 0.039 %

Atom 48(C) : 0.199 %

Atom 49(H) : 0.043 %

Atom 50(H) : 0.016 %

Atom 51(H) : 0.003 %

Atom 52(H) : 0.025 %

Atom 53(C) : 0.112 %

Atom 54(C) : 0.112 %

Atom 55(C) : 0.068 %

Atom 56(C) : 0.061 %

Atom 57(C) : 0.049 %

Atom 58(C) : 0.041 %

Atom 59(H) : 0.009 %

Atom 60(H) : 0.007 %

Atom 61(H) : 0.005 %

Atom 62(H) : 0.004 %

Atom 63(C) : 0.033 %

Atom 64(C) : 0.034 %

Atom 65(C) : 0.029 %

Atom 66(C) : 0.029 %

Atom 67(C) : 0.009 %

Atom 68(C) : 0.009 %

Atom 69(H) : 0.003 %

Atom 70(H) : 0.003 %

Atom 71(H) : 0.001 %

Atom 72(H) : 0.001 %

Atom 73(C) : 4.626 %

Atom 74(C) : 4.769 %

Atom 75(C) : 2.000 %

Atom 76(C) : 2.002 %

Atom 77(C) : 2.523 %

Atom 78(C) : 2.724 %

Atom 79(H) : 0.198 %

Atom 80(H) : 0.200 %

Atom 81(H) : 0.272 %

Atom 82(H) : 0.298 %

Atom 83(C) : 4.340 %

Atom 84(C) : 4.440 %

Atom 85(C) : 2.511 %

Atom 86(C) : 2.506 %
Atom 87(C) : 1.765 %
Atom 88(C) : 1.762 %
Atom 89(H) : 0.277 %
Atom 90(H) : 0.274 %
Atom 91(H) : 0.185 %
Atom 92(H) : 0.185 %
Atom 93(C) : 1.305 %
Atom 94(C) : 1.359 %
Atom 95(C) : 1.147 %
Atom 96(C) : 1.144 %
Atom 97(C) : 0.363 %
Atom 98(C) : 0.364 %
Atom 99(H) : 0.129 %
Atom 100(H) : 0.128 %
Atom 101(H) : 0.026 %
Atom 102(H) : 0.028 %
Atom 103(N) : 0.422 %
Atom 104(H) : 0.050 %
Atom 105(H) : 0.050 %
Atom 106(N) : 0.598 %
Atom 107(H) : 0.071 %
Atom 108(H) : 0.071 %
Atom 109(N) : 0.015 %
Atom 110(H) : 0.002 %
Atom 111(H) : 0.002 %

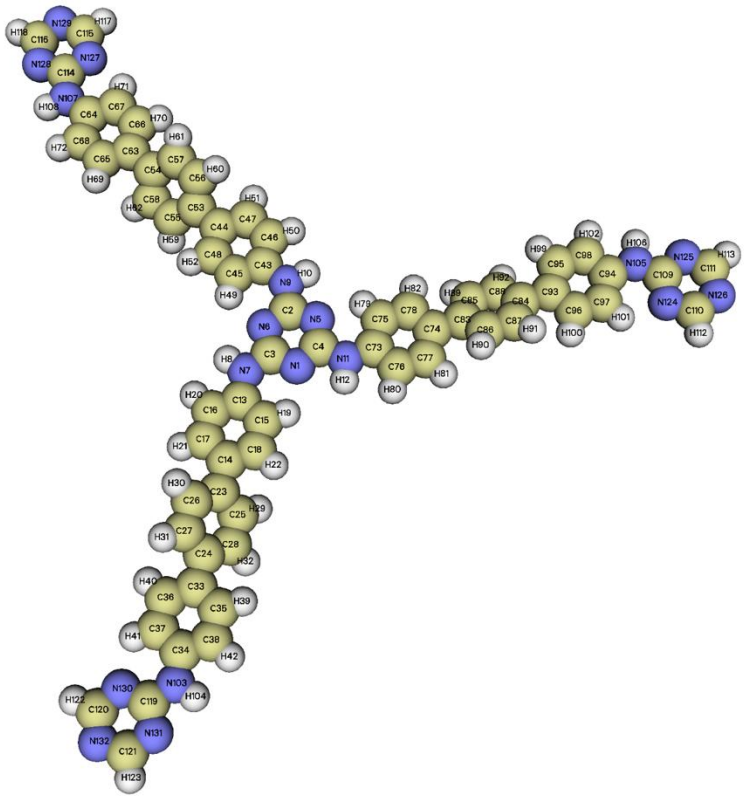

Figure S14. Triazine-terminated fragment of DAPT-CTP (fragment 2) with numbered atoms for orbital composition analysis.

Table S3. Atom contribution to HOMO amplitude in the triazine-terminated fragment of DAPT-CTP (fragment 2).

HOMO

Contributions after normalization:

Atom	1(N) :	0.632 %
Atom	2(C) :	0.500 %
Atom	3(C) :	0.496 %
Atom	4(C) :	0.485 %
Atom	5(N) :	0.642 %
Atom	6(N) :	0.671 %
Atom	7(N) :	3.195 %
Atom	8(H) :	0.229 %
Atom	9(N) :	3.223 %
Atom	10(H) :	0.231 %

Atom 11(N) : 3.128 %

Atom 12(H) : 0.224 %

Atom 13(C) : 2.481 %

Atom 14(C) : 2.848 %

Atom 15(C) : 1.486 %

Atom 16(C) : 1.536 %

Atom 17(C) : 1.188 %

Atom 18(C) : 1.349 %

Atom 19(H) : 0.119 %

Atom 20(H) : 0.108 %

Atom 21(H) : 0.086 %

Atom 22(H) : 0.100 %

Atom 23(C) : 2.094 %

Atom 24(C) : 2.160 %

Atom 25(C) : 1.197 %

Atom 26(C) : 1.191 %

Atom 27(C) : 0.958 %

Atom 28(C) : 0.954 %

Atom 29(H) : 0.097 %

Atom 30(H) : 0.095 %

Atom 31(H) : 0.073 %

Atom 32(H) : 0.072 %

Atom 33(C) : 1.495 %

Atom 34(C) : 1.413 %

Atom 35(C) : 0.807 %

Atom 36(C) : 0.895 %

Atom 37(C) : 0.668 %

Atom 38(C) : 0.691 %

Atom 39(H) : 0.065 %

Atom 40(H) : 0.073 %

Atom 41(H) : 0.052 %

Atom 42(H) : 0.047 %

Atom 43(C) : 2.500 %

Atom 44(C) : 2.872 %

Atom 45(C) : 1.497 %

Atom 46(C) : 1.549 %

Atom 47(C) : 1.197 %

Atom 48(C) : 1.362 %

Atom 49(H) : 0.120 %

Atom 50(H) : 0.109 %

Atom 51(H) : 0.086 %

Atom 52(H) : 0.101 %

Atom 53(C) : 2.112 %

Atom 54(C) : 2.179 %

Atom 55(C) : 1.207 %

Atom 56(C) : 1.201 %

Atom 57(C) : 0.966 %

Atom 58(C) : 0.963 %

Atom 59(H) : 0.098 %

Atom 60(H) : 0.096 %

Atom 61(H) : 0.073 %

Atom 62(H) : 0.072 %

Atom 63(C) : 1.510 %

Atom 64(C) : 1.427 %

Atom 65(C) : 0.816 %

Atom 66(C) : 0.904 %

Atom 67(C) : 0.675 %

Atom 68(C) : 0.698 %

Atom 69(H) : 0.066 %

Atom 70(H) : 0.073 %

Atom 71(H) : 0.052 %

Atom 72(H) : 0.048 %

Atom 73(C) : 2.418 %

Atom 74(C) : 2.778 %

Atom 75(C) : 1.450 %
Atom 76(C) : 1.500 %
Atom 77(C) : 1.157 %
Atom 78(C) : 1.315 %
Atom 79(H) : 0.117 %
Atom 80(H) : 0.106 %
Atom 81(H) : 0.083 %
Atom 82(H) : 0.098 %
Atom 83(C) : 2.036 %
Atom 84(C) : 2.101 %
Atom 85(C) : 1.165 %
Atom 86(C) : 1.159 %
Atom 87(C) : 0.930 %
Atom 88(C) : 0.926 %
Atom 89(H) : 0.094 %
Atom 90(H) : 0.092 %
Atom 91(H) : 0.071 %
Atom 92(H) : 0.070 %
Atom 93(C) : 1.450 %
Atom 94(C) : 1.371 %
Atom 95(C) : 0.784 %
Atom 96(C) : 0.868 %
Atom 97(C) : 0.647 %
Atom 98(C) : 0.670 %
Atom 99(H) : 0.063 %
Atom 100(H) : 0.071 %
Atom 101(H) : 0.050 %
Atom 102(H) : 0.046 %
Atom 103(N) : 1.186 %
Atom 104(H) : 0.085 %
Atom 105(N) : 1.150 %
Atom 106(H) : 0.082 %

Atom 107(N) : 1.199 %

Atom 108(H) : 0.086 %

Atom 109(C) : 0.235 %

Atom 110(C) : 0.067 %

Atom 111(C) : 0.082 %

Atom 112(H) : 0.004 %

Atom 113(H) : 0.005 %

Atom 114(C) : 0.245 %

Atom 115(C) : 0.070 %

Atom 116(C) : 0.086 %

Atom 117(H) : 0.004 %

Atom 118(H) : 0.005 %

Atom 119(C) : 0.242 %

Atom 120(C) : 0.069 %

Atom 121(C) : 0.085 %

Atom 122(H) : 0.004 %

Atom 123(H) : 0.005 %

Atom 124(N) : 0.274 %

Atom 125(N) : 0.279 %

Atom 126(N) : 0.306 %

Atom 127(N) : 0.286 %

Atom 128(N) : 0.291 %

Atom 129(N) : 0.319 %

Atom 130(N) : 0.283 %

Atom 131(N) : 0.288 %

Atom 132(N) : 0.315 %

Table S4. Atom contribution to LUMO amplitude in the triazine-terminated fragment of **DAPT-CTP** (fragment 2)

LUMO

Contributions after normalization:

Atom 1(N) : 0.523 %

Atom 2(C) : 0.417 %

Atom 3(C) : 1.714 %

Atom 4(C) : 2.202 %

Atom 5(N) : 1.342 %

Atom 6(N) : 1.566 %

Atom 7(N) : 0.392 %

Atom 8(H) : 0.026 %

Atom 9(N) : 0.063 %

Atom 10(H) : 0.016 %

Atom 11(N) : 0.606 %

Atom 12(H) : 0.044 %

Atom 13(C) : 1.535 %

Atom 14(C) : 1.445 %

Atom 15(C) : 0.607 %

Atom 16(C) : 0.521 %

Atom 17(C) : 1.067 %

Atom 18(C) : 0.794 %

Atom 19(H) : 0.067 %

Atom 20(H) : 0.044 %

Atom 21(H) : 0.118 %

Atom 22(H) : 0.084 %

Atom 23(C) : 2.288 %

Atom 24(C) : 2.273 %

Atom 25(C) : 1.068 %

Atom 26(C) : 1.082 %

Atom 27(C) : 1.157 %

Atom 28(C) : 1.179 %

Atom 29(H) : 0.111 %

Atom 30(H) : 0.117 %

Atom 31(H) : 0.123 %

Atom 32(H) : 0.126 %

Atom 33(C) : 1.914 %

Atom 34(C) : 1.872 %

Atom 35(C) : 1.118 %

Atom 36(C) : 1.098 %

Atom 37(C) : 0.808 %

Atom 38(C) : 0.771 %

Atom 39(H) : 0.121 %

Atom 40(H) : 0.118 %

Atom 41(H) : 0.079 %

Atom 42(H) : 0.074 %

Atom 43(C) : 0.137 %

Atom 44(C) : 0.165 %

Atom 45(C) : 0.063 %

Atom 46(C) : 0.077 %

Atom 47(C) : 0.059 %

Atom 48(C) : 0.173 %

Atom 49(H) : 0.019 %

Atom 50(H) : 0.010 %

Atom 51(H) : 0.006 %

Atom 52(H) : 0.020 %

Atom 53(C) : 0.253 %

Atom 54(C) : 0.251 %

Atom 55(C) : 0.120 %

Atom 56(C) : 0.118 %

Atom 57(C) : 0.132 %

Atom 58(C) : 0.126 %

Atom 59(H) : 0.014 %

Atom 60(H) : 0.012 %

Atom 61(H) : 0.014 %

Atom 62(H) : 0.013 %

Atom 63(C) : 0.211 %

Atom 64(C) : 0.206 %

Atom 65(C) : 0.123 %

Atom 66(C) : 0.121 %

Atom 67(C) : 0.089 %

Atom 68(C) : 0.085 %

Atom 69(H) : 0.013 %

Atom 70(H) : 0.013 %

Atom 71(H) : 0.009 %

Atom 72(H) : 0.008 %

Atom 73(C) : 2.574 %

Atom 74(C) : 2.601 %

Atom 75(C) : 0.986 %

Atom 76(C) : 0.969 %

Atom 77(C) : 1.613 %

Atom 78(C) : 1.705 %

Atom 79(H) : 0.092 %

Atom 80(H) : 0.091 %

Atom 81(H) : 0.175 %

Atom 82(H) : 0.186 %

Atom 83(C) : 4.141 %

Atom 84(C) : 4.114 %

Atom 85(C) : 1.940 %

Atom 86(C) : 1.948 %

Atom 87(C) : 2.115 %

Atom 88(C) : 2.117 %

Atom 89(H) : 0.205 %

Atom 90(H) : 0.205 %

Atom 91(H) : 0.226 %

Atom 92(H) : 0.227 %

Atom 93(C) : 3.474 %

Atom 94(C) : 3.397 %

Atom 95(C) : 2.028 %

Atom 96(C) : 1.989 %

Atom 97(C) : 1.468 %

Atom 98(C) : 1.399 %

Atom 99(H) : 0.219 %
Atom 100(H) : 0.213 %
Atom 101(H) : 0.144 %
Atom 102(H) : 0.134 %
Atom 103(N) : 0.538 %
Atom 104(H) : 0.036 %
Atom 105(N) : 0.976 %
Atom 106(H) : 0.065 %
Atom 107(N) : 0.059 %
Atom 108(H) : 0.004 %
Atom 109(C) : 3.841 %
Atom 110(C) : 0.779 %
Atom 111(C) : 2.240 %
Atom 112(H) : 0.063 %
Atom 113(H) : 0.263 %
Atom 114(C) : 0.233 %
Atom 115(C) : 0.047 %
Atom 116(C) : 0.136 %
Atom 117(H) : 0.004 %
Atom 118(H) : 0.016 %
Atom 119(C) : 2.115 %
Atom 120(C) : 0.429 %
Atom 121(C) : 1.232 %
Atom 122(H) : 0.035 %
Atom 123(H) : 0.144 %
Atom 124(N) : 1.852 %
Atom 125(N) : 0.958 %
Atom 126(N) : 2.589 %
Atom 127(N) : 0.112 %
Atom 128(N) : 0.058 %
Atom 129(N) : 0.157 %
Atom 130(N) : 1.019 %

Atom 131(N) : 0.527 %

Atom 132(N) : 1.425 %

a)

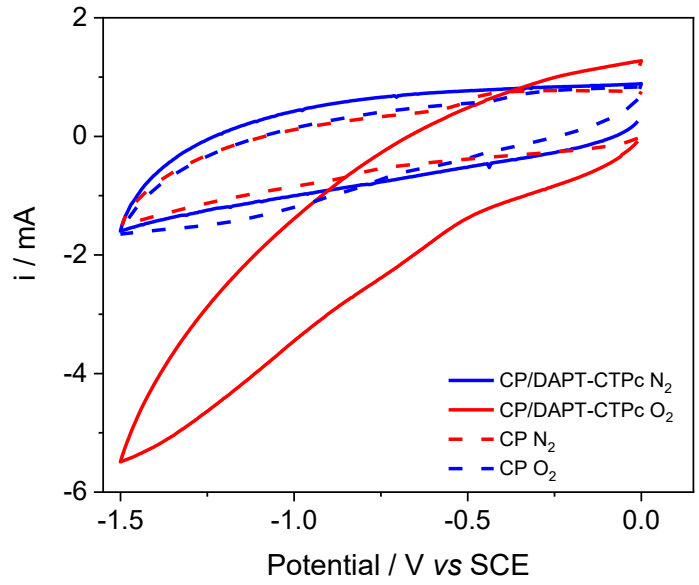

b)

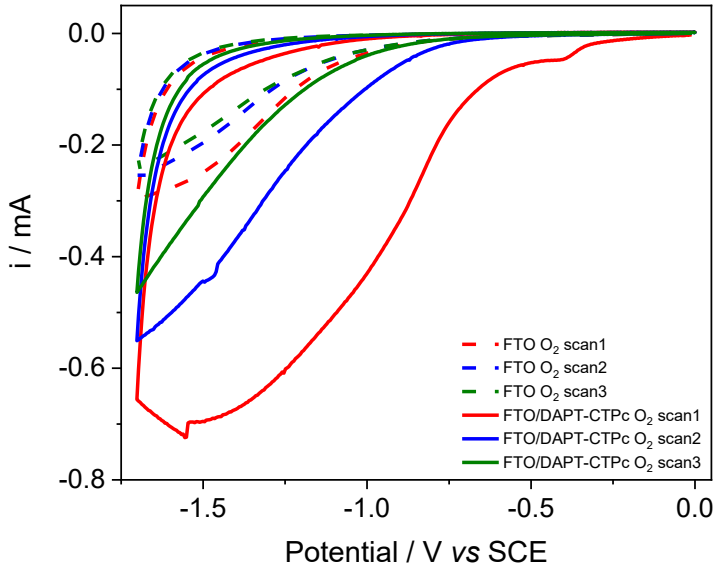

Figure S15. Cyclic voltammetry of CP/**DAPT-CTP$_c$** (a) and FTO/**DAPT-CTP$_c$** (b) in $CH_3CN/LiClO_4$ 0.1M under O_2 and N_2 atmosphere.

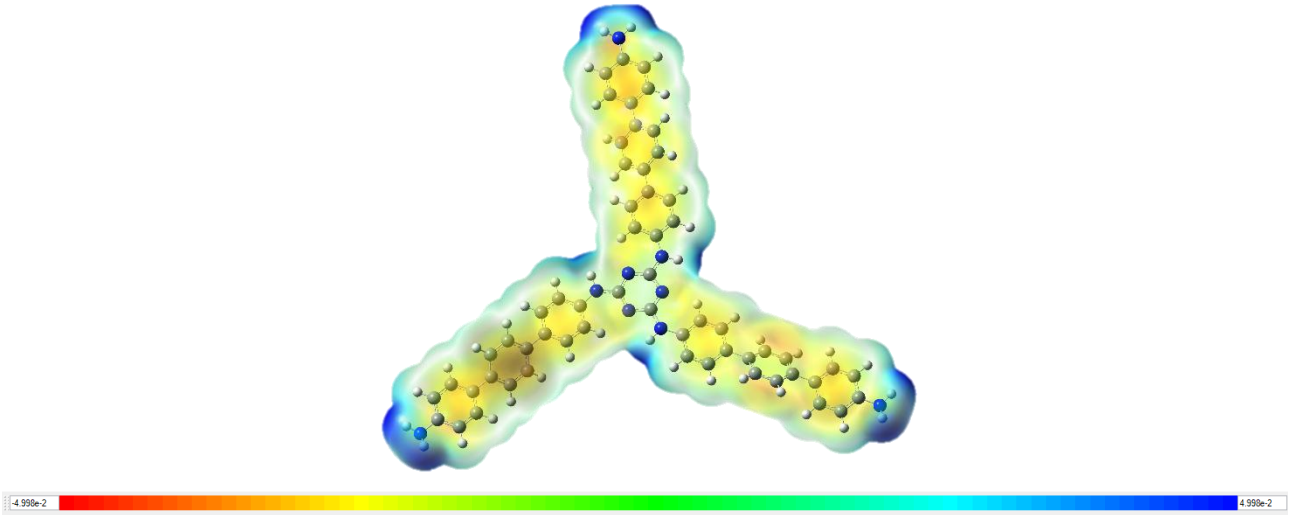

Figure S16. Electrostatic potential map projected on the total electronic density of amino-terminated fragment of **DAPT-CTP** (fragment 1).

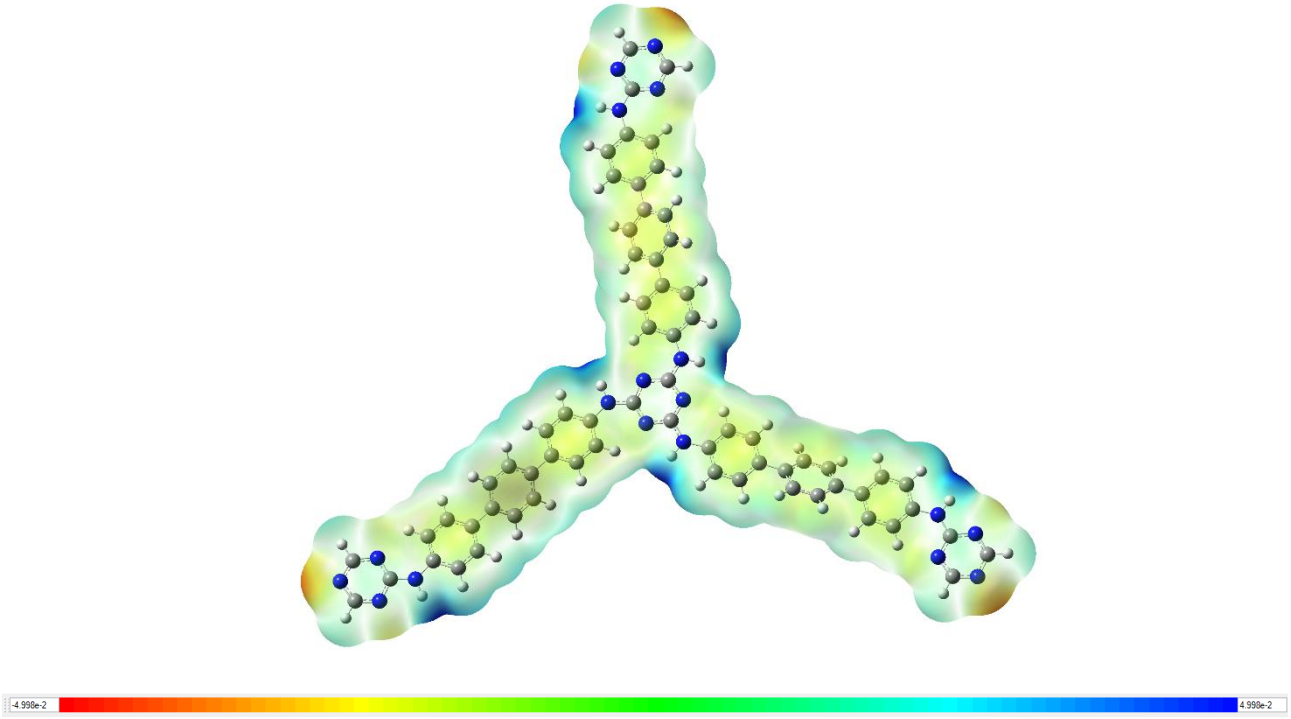

Figure S17. Electrostatic potential map projected on the total electronic density of a triazine terminated fragment of **DAPT-CTP** (fragment 2).

2.4 Experimental procedures for the photochemical reactions

2.4.1 General procedure A for the selective oxidation of Sulfides to Sulfoxides (2a-2l)

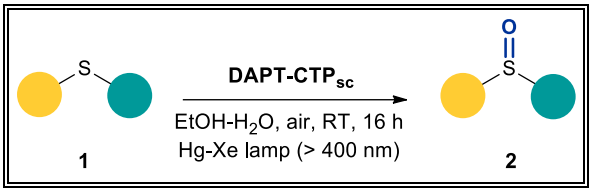

Scheme S1. Synthesis of sulfoxides **2**

In a glass vial, a mixture of sulfide **1** (0.2 mmol) and **DAPT-CTP$_{sc}$** (0.04 mmol) in 1 mL of EtOH-H_2O (see **Table S3** for the composition of hydroalcoholic mixture) was irradiated with a 200 W Hg-Xe lamp equipped with a 400 nm long-pass filter at a distance of 5 cm, and stirred under air atmosphere (balloon) at room temperature for 16 hours (24 h for **1g** and **1h**). At the end of the process, the reaction mixture was filtered and subsequently washed with ethyl acetate (5 mL). The mixture was diluted with water (5 mL) and extracted with ethyl acetate (3 × 5 mL). The organic layers were combined, dried over anhydrous Na_2SO_4 and concentrated under reduced pressure. The residue, when necessary, was purified by flash chromatography on silica gel with the suitable elution system to afford the desired product **2**.

2.4.2 Procedure B for the selective oxidation of Sulfide 1m to Sulfoxide 2m

In a glass vial, a mixture of **1m** (0.2 mmol), **DAPT-CTP$_{sc}$** (0.04 mmol) in 1 mL of EtOH-H_2O (1:2) was irradiated with a 200 W Hg-Xe lamp equipped with a 400 nm long-pass filter at a distance of 5 cm, and stirred under air atmosphere (balloon) at room temperature for 24 hours. At the end of the process, the reaction mixture was filtered and subsequently washed with EtOH. The mixture was concentrated in vacuo and then lyophilized to afford the desired product **2m**.

2.4.3 General procedure C for the cross-dehydrogenative coupling between Aryl Glycine and Indoles

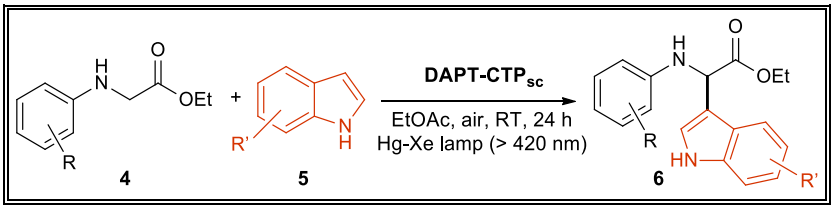

Scheme S2. Synthesis of NPAAs **6**

In a glass vial, a mixture of aryl glycine **4** (0.13 mmol), indole **5** (0.1 mmol) and **DAPT-CTP$_{sc}$** (0.02 mmol) in 1 mL of ethyl acetate was irradiated with a 200 W Hg-Xe lamp equipped with a 420 nm long-pass filter at a distance of 5 cm, and stirred under air atmosphere (balloon) at room temperature for 24 hours. At the end of the process, the reaction mixture was filtered and subsequently washed with ethyl acetate (5 mL). The mixture was concentrated under reduced pressure and purified by flash chromatography on silica gel with the suitable elution system to afford the desired product **6**.

2.5 Setup of the batch photoreactor and spectrum of Hg-Xe lamp

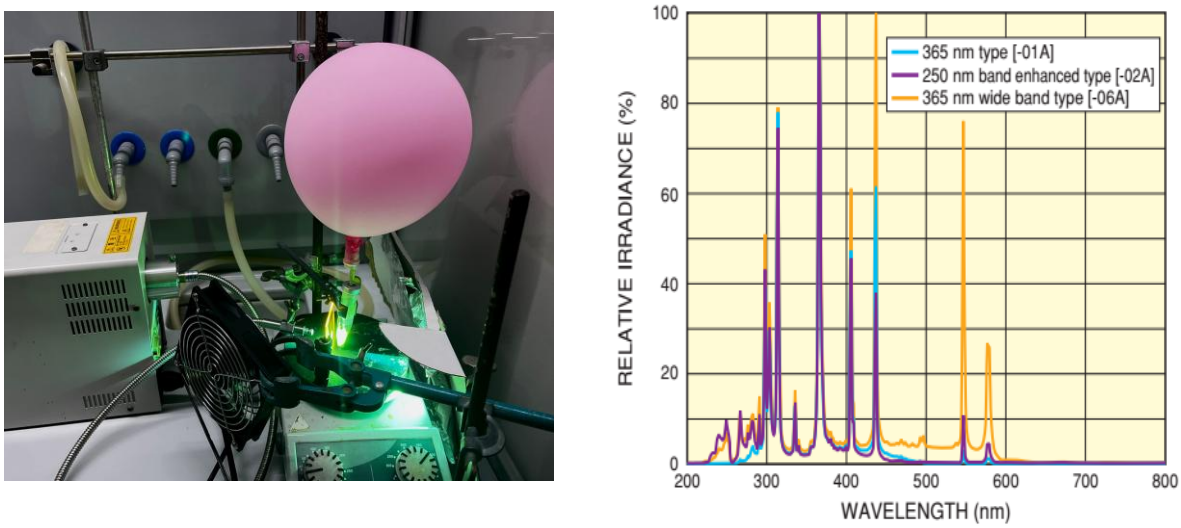

Figure S18. Left: Batch photoreactor setup; Right: Spectrum of Hg-Xe lamp (orange line).

2.6 Recycle experiment

In a glass vial, a mixture of aryl glycine **4** (0.13 mmol), indole **5** (0.1 mmol) and **DAPT-CTP$_{sc}$** (0.02 mmol) in 1 mL of ethyl acetate was irradiated with a 200 W Hg-Xe lamp equipped with a 420 nm long-pass filter at a distance of 5 cm, and stirred under air atmosphere (balloon) at room temperature for 24 hours. At the end of the process, the catalyst previously used was filtered, subsequently washed with ethyl acetate (5 mL) and centrifuged at 10000 rpm for 10 min. Finally, after removing the supernatant, the recyclable **DAPT-CTP$_{sc}$** was dried under vacuum and directly reused for the next reaction cycle without any further purification. FT-IR analysis of recycled **DAPT-CTP$_{sc}$** after 5 runs (Figure S19) confirmed its chemical stability.

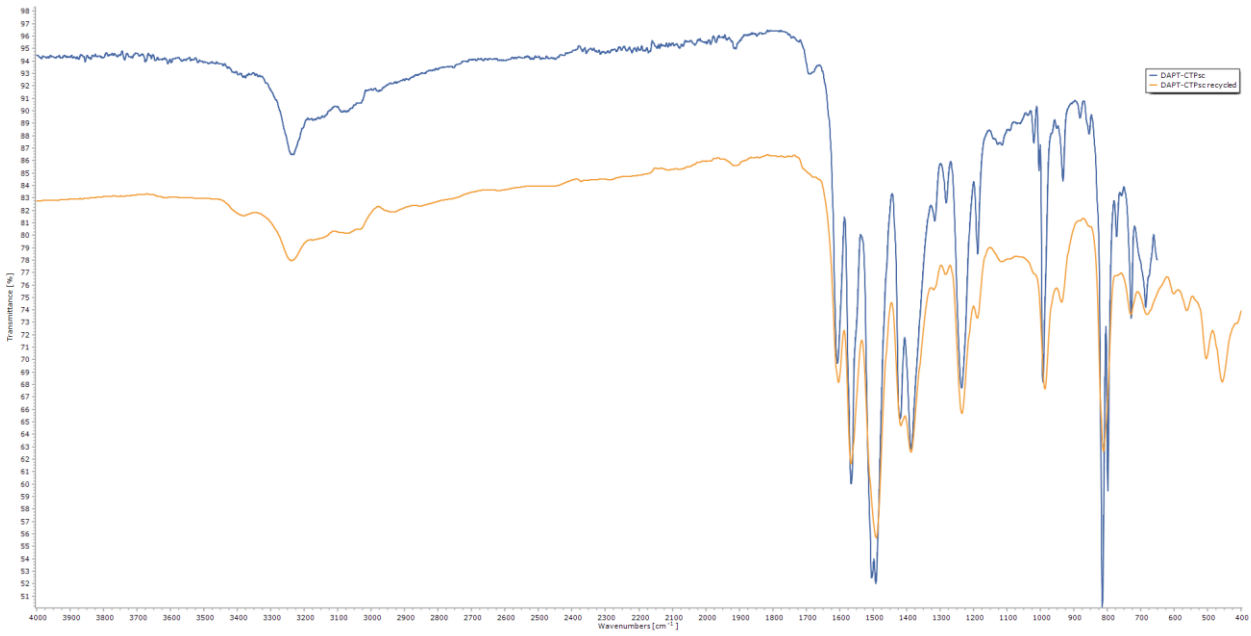

Figure S19. ATR-FTIR spectra of **DAPT-CTP$_{sc}$** and recycled (5 runs) **DAPT-CTP$_{sc}$**.

2.7 Quenching experiments

2.7.1 Procedure for the selective oxidation of 1a to 2a with different additives

In a glass vial, a mixture of **1a** (0.2 mmol), **DAPT-CTP$_{sc}$** (0.04 mmol) and **additive** (0.2 mmol) in 1 mL of EtOH-H_2O (1:1) was irradiated with a 200 W Hg-Xe lamp equipped with a 400 nm long-pass filter at a distance of 5 cm, and stirred under air atmosphere (balloon) at room temperature for 16 hours. At the end of the process, the reaction mixture was filtered and subsequently washed with ethyl acetate (5 mL). The mixture was diluted with water (5 mL) and extracted with ethyl acetate (3 × 5 mL). The organic layers were combined, dried over anhydrous Na_2SO_4 and concentrated under reduced pressure. The yield of **2a** was determined by ^{1}H NMR of the crude reaction mixture with ethylene carbonate as external standard (**Table S5**).

Table S5

Additive	Yield 2a (%)
-	> 95
p-benzoquinone	< 5
NaN_3	20
KI	8
Triethylamine	18

2.7.2 Procedure for the cross-dehydrogenative coupling between 4a and 5a with different additives

In a glass vial, a mixture of **4a** (0.13 mmol), **5a** (0.1 mmol), **DAPT-CTP$_{sc}$** (0.02 mmol) and **additive** (0.1 mmol) in 1 mL of ethyl acetate was irradiated with a 200 W Hg-Xe lamp equipped with a 420 nm long-pass filter at a distance of 5 cm, and stirred under air atmosphere (balloon) at room temperature for 24 hours. At the end of the process, the reaction mixture was filtered, subsequently washed with ethyl acetate (5 mL) and concentrated under reduced pressure. The yield of **6aa** was determined by ^{1}H NMR of the crude reaction mixture with durene as external standard (**Table S6**).

Table S6

Additive	Yield 6aa (%)
-	74
p-benzoquinone	55
NaN_3	< 5
KI	25

2.8 Experimental procedures for the synthesis of standard sulfones

2.8.1 General procedure D for the selective oxidation of Sulfides to Sulfones (3a-3l)

In a 10 mL vial, sulfide **1** (0.36 mmol) was solubilized in 5 mL of DCM. Then *meta*-Chloroperbenzoic acid (MCPBA) (1.11 mmol) was added to the solution and stirred vigorously for 16 hours. The solution was then diluted with DCM (10 mL) and washed with an aqueous NaOH solution (0.5 M, 3 × 15 mL). The organic layer was dried over anhydrous Na_2SO_4 and concentrated under reduced pressure. The residue, when necessary, was purified by chromatography on silica gel with the suitable elution system to afford the desired sulfone **3**.

2.8.2 Procedure E for the selective oxidation of Sulfide 1m to Sulfone 3m

In a 10 mL vial, **1m** (0.36 mmol) was solubilized in 5 mL of water. Then *meta*-Chloroperbenzoic acid (MCPBA) (1.11 mmol) was added to the solution and stirred vigorously for 16 hours. The solution was then diluted with water (10 mL) and washed with DCM (1 × 15 mL). The aqueous layer was lyophilized to afford the desired sulfone **3m**.

2.9 Experimental procedures for the synthesis of starting materials of the CDC reaction

2.9.1 General procedure F for the preparation of Aryl Glycines (4) [4]

In a two-neck round-bottom flask under an argon atmosphere, a mixture of the desired aniline (10 mmol), ethyl chloroacetate (1.3 g, 12 mmol), and sodium acetate (0.82 g, 10 mmol) in anhydrous ethanol (10 mL) was refluxed (oil bath) for 24 h. Then water was added (15 mL), and the aqueous layer was extracted three times with ethyl acetate. The organic layer was dried with anhydrous Na_2SO_4, filtered, and concentrated under reduced pressure. The residue was purified by chromatography on silica gel to give the final product **4**.

2.9.2 Procedure G for the preparation of 1-Benzyl-1H-indole (5g) [4]

In a two-neck round-bottom flask under an argon atmosphere was prepared a mixture of indole (1.17 g, 10 mmol), benzyl bromide (1.78 mL, 15 mmol), and sodium hydride (0.29 g, 12 mmol) in anhydrous dimethylformamide (10 mL) at 0 °C. The mixture was warmed to room temperature and reacted for 24 h. After 24 h, a solution of a saturated $NaHCO_3$ solution (15 mL) was added and the aqueous layer was extracted three times with diethyl ether (3 × 10 mL). The organic layer was dried with anhydrous Na_2SO_4, filtered, and concentrated under reduced pressure. The crude product was purified by chromatography on silica gel to give the final product **5g**.

2.10 Optimization of sulfides solubility in EtOH-H_2O mixture

Table S7[a]

Entry	Sulfide	EtOH : H_2O ratio
1	Thioanisole (**1a**)	1 : 1
2	4-fluoro-thioanisole (**1b**)	1 : 1
3	4-chloro-thioanisole (**1c**)	3 : 1
4	4-bromo-thioanisole (**1d**)	9 : 1
5	4-methoxy-thioanisole (**1e**)	3 : 1
6	3-methoxy-thioanisole (**1f**)	3 : 1
7	2-methoxy-thioanisole (**1g**)	3 : 1
8	2-chloro-thioanisole (**1h**)	3 : 1

9	4-methylthio-benzaldehyde (**1i**)	1 : 1
10	Allyl phenyl sulfide (**1j)**	3 : 1
11	Benzyl methyl sulfide (**1k**)	3 : 1
12	Pentamethylene sulfide (**1l**)	1 : 1
13	L-methionine (**1m**)	1 : 2

[a] Concentration = 0.2 M.

2.11 Selective sulfide oxidation in continuous-flow

2.11.1 Procedure H for the selective oxidation of Albendazole to Ricobendazole in continuous-flow

SETUP A: Omnifit column (6.6 mm × 100 mm) was packed with **DAPT-CTP$_{sc}$** (300 mg) and **glass beads** (4.9 g, 425−600 μm diameter). Hg-Xe lamp was positioned at a distance of 7 cm from a 400 nm long-pass filter and 15 cm from the resulting reactor **R$_1$-DAPT-CTP$_{sc}$** (Figure S20a).

SETUP B: Omnifit column (6.6 mm × 100 mm) was packed with **DAPT-CTP$_{sc}$** (150 mg) and **glass beads** (4.9 g, 425−600 μm diameter). The resulting reactor **R$_2$-DAPT-CTP$_{sc}$** was placed inside a custom-made photoreactor system (Figure S20b, S20c), irradiated by a LED array (6 × 10 W each, λ = 418 nm). An integrated cooling system (Figure S20c) was assembled for cooling the reactor (2 fans, back and front) and the LEDs (2 fans on the left of the heat sinks).

Albendazole (159 mg, 0.6 mmol) and ethylene carbonate (Internal Standard, 53 mg, 0.6 mmol) were dissolved in 12 mL of DMSO and the solution was pumped at 5 µL min^{-1} by an HPLC pump. Concurrently, air was pumped through a mass flow controller at a flow rate of 50 µL min^{-1} (Figure S20a, S20b). After a mixing stage, the resulting air-liquid segmented flow reached the photoreactor. The reactor outsream was finally collected in different fractions and concentrated under reduced pressure. The conversion of **Albendazole** and the production of **Ricobendazole** were monitored by sampling the crude every 30 minutes via ^{1}H NMR with ethylene carbonate as internal standard.

SETUP A: Steady state (88% yield) was reached after 120 minutes

SETUP B: Steady state (93% yield) was reached after 120 minutes and the reaction outcome was monitored for a total time of 120 h (12 consecutive runs of 10 h each).

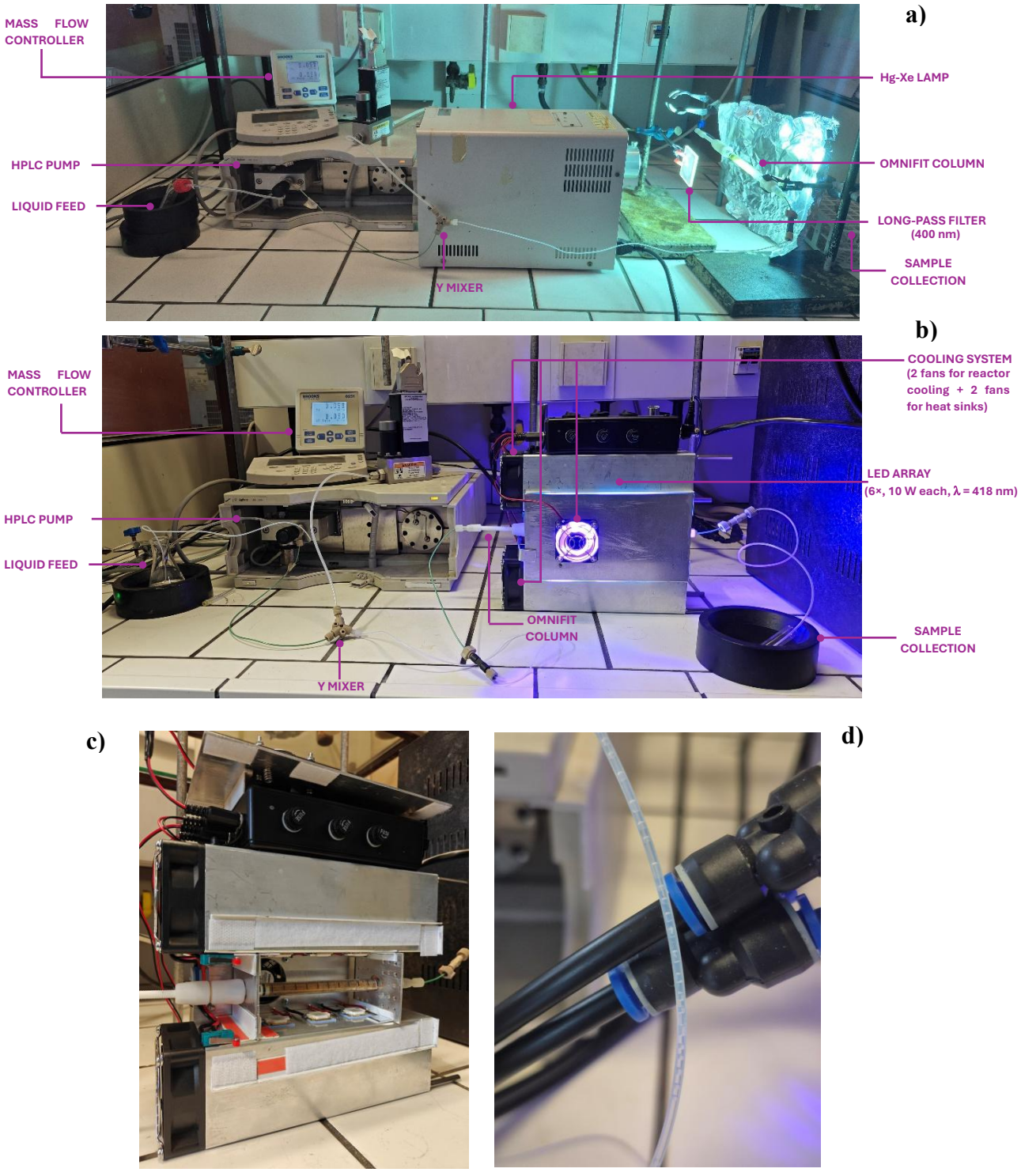

Figure S20. Continuous flow Setup A (a); Continuous flow Setup B (b); Photoreactor Setup B details and Omnifit column packed with **DAPT-CTP$_{sc}$** and glass beads (c); Gas-Liquid segmented flow (d).

2 Characterization data

(Methylsulfinyl)benzene (**2a**) [5]

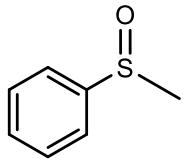

By following General Procedure A, **2a** (26 mg, 0.18 mmol, 92% yield) was obtained as a pale yellow oil after column chromatography on silica gel (100% EtOAc). ^{1}H NMR (400 MHz, $CDCl_3$) δ = 7.66-7.64 (m, 2H), 7.56-7.49 (m, 3H), 2.73 (s, 3H). ^{13}C NMR (101 MHz, $CDCl_3$) δ = 145.7, 131.0, 129.3, 123.5, 44.0.

(Methylsulfonyl)benzene **(3a)** [5]

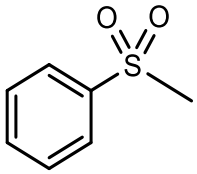

By following General Procedure D, **3a** (55 mg, 0.35 mmol, 98% yield) was obtained as a white amorphous solid. No further purification was needed. ^{1}H NMR (300 MHz, $CDCl_3$) δ = 7.97-7.94 (m, 2H), 7.71-7.56 (m, 3H), 3.10 (s, 3H). ^{13}C NMR (101 MHz, $CDCl_3$) δ = 140.5, 133.7, 129.3, 127.3, 44.5.

1-fluoro-4-(methylsulfinyl)benzene **(2b)** [6]

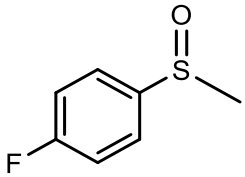

By following General Procedure A, **2b** (29 mg, 0.18 mmol, 91% yield) was obtained as a yellow oil. No further purification was needed. ^{1}H NMR (400 MHz, $CDCl_3$) δ = 7.71-7.62 (m, 2H), 7.28-7.19 (m, 2H), 2.72 (s, 3H). ^{13}C NMR (101 MHz, $CDCl_3$) δ = 164.3 (d, J = 250.0 Hz), 141.1 (d, J = 3.0 Hz), 125.8 (d, J = 9.0 Hz), 116.7 (d, J = 23.0 Hz), 44.2. ^{19}F NMR (376 MHz, $CDCl_3$) δ = -108.6 (m).

1-fluoro-4-(methylsulfonyl)benzene **(3b)** [7]

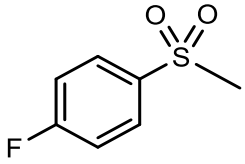

By following General Procedure D, **3b** (59 mg, 0.34 mmol, 94% yield) was obtained as a white amorphous solid. No further purification were needed. ^{1}H NMR (300 MHz, $CDCl_3$) δ = 8.00-7.95 (m, 2H), 7.28-7.22 (m,

2H), 3.10 (s, 3H). ^{13}C NMR (101 MHz, CDCl3) δ = 165.7 (d, *J* = 250.0 Hz), 136.6 (d, *J* = 3.0 Hz), 130.2 (d, *J* = 9.0 Hz), 116.7 (d, *J* = 23.0 Hz), 44.6. ^{19}F NMR (376 MHz, $CDCl_3$) δ = -103.5 (m).

1-chloro-4-(methylsulfinyl)benzene **(2c)** [5]

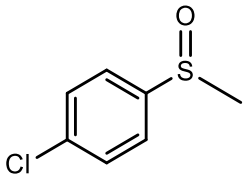

By following General Procedure A, **2c** (31 mg, 0.18 mmol, 91% yield) was obtained as a colourless oil after column chromatography on silica gel (100% EtOAc). ^{1}H NMR (400 MHz, $CDCl_3$) *δ* = 7.63-7.58 (m, 2H), 7.54-7.49 (m, 2H), 2.73 (s, 3H). ^{13}C NMR (101 MHz, $CDCl_3$) *δ* = 144.3, 137.2, 129.6, 124.9, 44.1.

1-chloro-4-(methylsulfonyl)benzene **(3c)** [5]

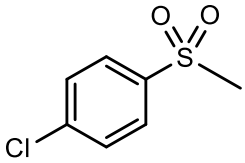

By following General Procedure D, **3c** (67 mg, 0.35 mmol, 98% yield) was obtained as a yellow oil. No further purification was needed. ^{1}H NMR (300 MHz, $CDCl_3$) δ = 7.91-7.87 (m, 2H), 7.68-7.53 (m, 2H), 3.10 (s, 3H). ^{13}C NMR (101 MHz, $CDCl_3$) δ = 140.3, 138.9, 129.6, 128.8, 44.4.

1-bromo-4-(methylsulfinyl)benzene **(2d)** [6]

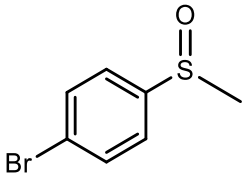

By following General Procedure A, **2d** (39 mg, 0.18 mmol, 91% yield) was obtained as a yellow amorphous solid after column chromatography on silica gel (100% EtOAc). ^{1}H NMR (400 MHz, $CDCl_3$) *δ* = 7.75-7.63 (m, 2H), 7.60-7.48 (m, 2H), 2.72 (s, 3H). ^{13}C NMR (101 MHz, $CDCl_3$) *δ* = 144.9, 132.6, 125.4, 125.1, 44.0.

1-bromo-4-(methylsulfonyl)benzene **(3d)** [8]

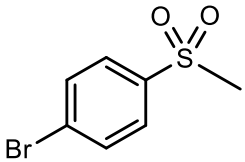

By following General Procedure D, **3d** (83 mg, 0.35 mmol, 98% yield) was obtained as a white amorphous solid. No further purification was needed. ^{1}H NMR (300 MHz, $CDCl_3$) δ = 7.83-7.80 (m, 2H), 7.73-7.70 (m, 2H), 3.10 (s, 3H). ^{13}C NMR (101 MHz, $CDCl_3$) δ = 139.5, 132.7, 129.1, 129.0, 44.5.

1-methoxy-4-(methylsulfinyl)benzene **(2e)** [5]

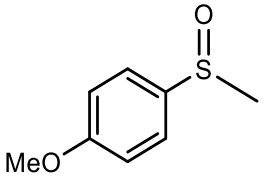

By following General Procedure A, **2e** (30 mg, 0.17 mmol, 88% yield) was obtained as a white amorphous solid after column chromatography on silica gel (100% EtOAc). ^{1}H NMR (400 MHz, $CDCl_3$) δ = 7.57 (d, J = 8.6 Hz, 2H), 7.05 (d, J = 8.6 Hz, 2H), 3.85 (s, 3H), 2.70 (s, 3H). ^{13}C NMR (101 MHz, $CDCl_3$) δ = 162.2, 136.7, 125.4, 114.8, 55.5, 44.0.

1-methoxy-4-(methylsulfonyl)benzene **(3e)** [5]

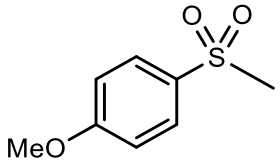

By following General Procedure D, **3e** (55 mg, 0.29 mmol, 98% yield) was obtained as a white amorphous solid. No further purification was needed. ^{1}H NMR (400 MHz, $CDCl_3$) δ = 7.95-7.86 (m, 2H), 7.13-7.05 (m, 2H), 3.90 (s, 3H) 3.10 (s, 3H). ^{13}C NMR (101 MHz, $CDCl_3$) δ = 163.7, 132.3, 129.5, 114.5, 55.7, 44.8.

1-methoxy-3-(methylsulfinyl)benzene **(2f)** [9]

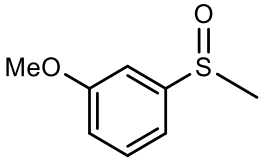

By following General Procedure A, **2f** (29 mg, 0.17 mmol, 85% yield) was obtained as a white amorphous solid after column chromatography on silica gel (70% EtOAc in cyclohexane). ^{1}H NMR (400 MHz, $CDCl_3$) δ = 7.41 (t, J = 7.9 Hz, 1H), 7.26 (dd, J = 2.6, 1.6 Hz, 1H), 7,13 (ddd, J = 7.9, 1.6, 0.9 Hz, 1H), 7.0 (ddd, J = 8.3, 2.6, 0.9 Hz, 1H), 3.86 (s, 3H), 2.70 (s, 3H). ^{13}C NMR (101 MHz, $CDCl_3$) δ = 160.5, 147.1, 130.3, 117.5, 115.5, 107.9, 55.6, 44.0.

1-methoxy-3-(methylsulfonyl)benzene **(3f)** [8]

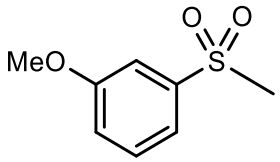

By following General Procedure D, **3f** (66 mg, 0.35 mmol, 98% yield) was obtained as a white amorphous solid. No further purification were needed. ^{1}H NMR (300 MHz, $CDCl_3$) δ = 7.53-7.42 (m, 3H), 7.18-7.14 (m, 1H), 3.87 (s, 3H), 3.10 (s, 3H). ^{13}C NMR (101 MHz, $CDCl_3$) δ = 160.1, 141.7, 130.5, 120.1, 119.4, 111.8, 55.7, 44.4.

1-methoxy-2-(methylsulfinyl)benzene **(2g)** [6]

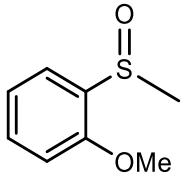

By following General Procedure A, **2g** (26 mg, 0.15 mmol, 77% yield) was obtained as a colourless oil after column chromatography on silica gel (70% EtOAc in cyclohexane). ^{1}H NMR (400 MHz, $CDCl_3$) δ = 7.83-7.82 (m, 1H), 7.47-7.44 (m, 1H), 7,21-7.18 (m, 1H), 6.92 (d, J = 8.2 Hz, 1H), 3.90 (s, 3H), 2.77 (s, 3H). ^{13}C NMR (101 MHz, $CDCl_3$) δ = 154.8, 132.0, 132.0, 124.7, 121.7, 110.6, 55.7, 41.1.

1-methoxy-2-(methylsulfonyl)benzene **(3g)** [10]

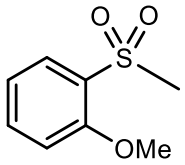

By following General Procedure D, **3g** (63 mg, 0.34 mmol, 95% yield) was obtained as a white amorphous solid. No further purification was needed. ^{1}H NMR (300 MHz, $CDCl_3$) δ = 7.98-7.95 (dd, J = 1.7 Hz, 1H), 7.62-7.56 (m, 1H), 7,12-7.05 (m, 2H), 4.05 (s, 3H), 3.21 (s, 3H). ^{13}C NMR (101 MHz, $CDCl_3$) δ = 157.2, 135.5, 129.7, 128.3, 120.7, 112.3, 56.3, 42.9.

1-chloro-2-(methylsulfinyl)benzene **(2h)** [5]

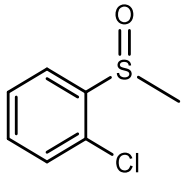

By following General Procedure A, **2h** (19 mg, 0.11 mmol, 55% yield) was obtained as a colourless oil after column chromatography on silica gel (30% EtOAc in cyclohexane). ^{1}H NMR (400 MHz, $CDCl_3$) δ = 7.96 (d, J = 7.9 Hz, 1H), 7.56-7.53 (m, 1H), 7.47-7.44 (m, 1H), 7.40 (dd, J = 7.9 Hz, 1H), 2.83 (s, 3H). ^{13}C NMR (101 MHz, $CDCl_3$) δ = 143.6, 131.9, 129.8, 129.7, 128.1, 125.3, 41.6.

1-chloro-2-(methylsulfonyl)benzene **(3h)** [5]

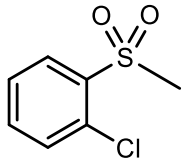

By following General Procedure D, **3h** (66 mg, 0.35 mmol, 96% yield) was obtained as a colourless oil. No further purification were needed. ^{1}H NMR (300 MHz, $CDCl_3$) δ = 8.17-8.14 (m, 1H), 7.59-7.56 (m, 2H), 7.50-7.45 (m, 1H), 3.27 (s, 3H). ^{13}C NMR (101 MHz, $CDCl_3$) δ = 137.9, 134.7, 132.4, 131.8, 130.7, 127.4, 42.6.

4-(methylsulfinyl)benzaldehyde **(2i)** [6]

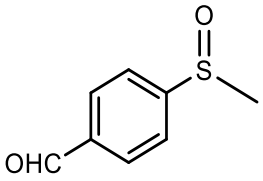

By following General Procedure A, **2i** (30 mg, 0.18 mmol, 90% yield) was obtained as a yellow amorphous solid after column chromatography on silica gel (100% EtOAc). ^{1}H NMR (400 MHz, $CDCl_3$) δ = 10.10 (s, 1H), 8.16-7.96 (m, 2H), 7,99-7.75 (m, 2H), 2.81 (s, 3H). ^{13}C NMR (101 MHz, $CDCl_3$) δ = 191.1, 152.5, 138.1, 130.4, 124.1, 43.8.

4-(methylsulfonyl)benzaldehyde **(3i)** [11]

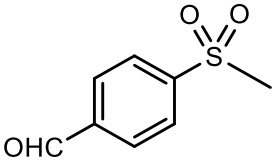

By following General Procedure D, **3i** (65 mg, 0.35 mmol, 98% yield) was obtained as a yellow amorphous solid. No further purification were needed. ^{1}H NMR (300 MHz, $CDCl_3$) δ = 10.13 (s, 1H), 8.14-8.06 (m, 4H), 3.10 (s, 3H). ^{13}C NMR (101 MHz, $CDCl_3$) δ = 190.6, 145.3, 139.6, 130.4, 128.2, 44.3.

(Allylsulfinyl)benzene **(2j)**

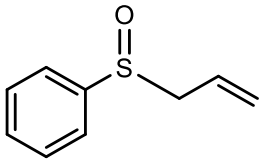

By following General Procedure A, **2k** (23 mg, 0.14 mmol, 70% yield) was obtained as a colourless oil after column chromatography on silica gel (20% EtOAc in cyclohexane). ^{1}H NMR (400 MHz, CD_3OD) δ = 7.70-7.64 (m, 2H), 7.62-7.56 (m, 3H), 5.70 (ddt, *J* = 17.0, 10.2, 7.5 Hz, 1H), 5.33 (d, *J* = 10.2 Hz, 1H), 5.25 (d, *J* = 17.0 Hz, 1H), 3.70 (dd, *J* = 12.8, 7.5 Hz, 1H), 3.60 (dd, *J* = 12.8, 7.5 Hz, 1H). ^{13}C NMR (101 MHz, CD_3OD) *δ* = 141.7, 131.2, 129.0, 125.1, 124.2, 123.1, 59.6.

(Allylsulfonyl)benzene **(3j)**

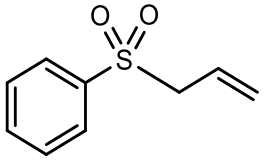

By following General Procedure D, **3k** (61 mg, 0.33 mmol, 93% yield) was obtained as a colourless oil after column chromatography on silica gel (10% EtOAc in cyclohexane). ^{1}H NMR (400 MHz, CD_3OD) δ = 7.95-7.90 (m, 2H), 7.76-7.69 (m, 1H), 7,66-7.61 (m, 2H), 5.80 (ddt, *J* = 17.2, 10.3, 7.2 Hz, 1H), 5.33 (d, *J* = 10.3 Hz, 1H), 5.25 (d, *J* = 17.0 Hz, 1H), 4.00 (d, *J* = 7.2 Hz, 2H). ^{13}C NMR (101 MHz, CD_3OD) δ = 138.4, 133.6, 128.8, 128.1, 124.9, 123.5, 59.9.

((Methylsulfinyl)methyl)benzene **(2k)**

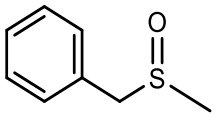

By following General Procedure A, **2l** (22 mg, 0.14 mmol, 72% yield) was obtained as a white amorphous solid after column chromatography on silica gel (20% EtOAc in cyclohexane). ^{1}H NMR (400 MHz, CD_3OD) δ = 7.46-7.35 (m, 5H), 4.05 (d, *J* = 12.8 Hz, 1H), 4.15 (d, *J* = 12.8 Hz, 1H), 2.60 (s, 3H). ^{13}C NMR (101 MHz, CD_3OD) *δ* = 130.1, 130.0, 128.4, 128.1, 58.6, 35.8.

((Methylsulfonyl)methyl)benzene **(3k)**

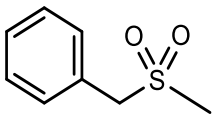

By following General Procedure D, **3l** (59 mg, 0.34 mmol, 97% yield) was obtained as a white amorphous solid after column chromatography on silica gel (30% EtOAc in cyclohexane). ^{1}H NMR (400 MHz, CD_3OD) δ = 7.53-7.48 (m, 5H), 4.48 (s, 2H), 2.90 (s, 3H). ^{13}C NMR (101 MHz, CD_3OD) δ = 131.2, 130.0, 129.0, 127.8, 38.6, 37.5.

Tetrahydro-2H-thiopyran 1-oxide **(2l)**

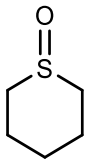

By following General Procedure B, **2m** (16 mg, 0.13 mmol, 67% yield) was obtained as a colourless oil. No further purification were needed. ^{1}H NMR (400 MHz, CD_3OD) δ = 3.00-2.95 (m, 2H), 2.83-2.80 (m, 2H), 2.25-2.21 (m, 2H), 1.71-1.59 (m, 4H). ^{13}C NMR (101 MHz, CD_3OD) δ =72.4, 63.0, 23.8, 18.2.

Tetrahydro-2H-thiopyran 1,1-dioxide **(3l)** [12]

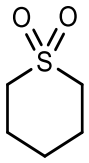

By following General Procedure E, **3m** (29 mg, 0.22 mmol, 60% yield) was obtained as a colourless oil. No further purification were needed. ^{1}H NMR (400 MHz, $CDCl_3$) δ = 3.00-2.97 (m, 4H), 2.15-2.10 (m, 4H), 1.66-1.60 (m, 2H). ^{13}C NMR (101 MHz, $CDCl_3$) δ = 48.8, 24.6, 19.1.

(S)-2-amino-4-(methylsulfinyl)butanoic acid **(2m)** [13]

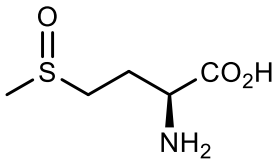

By following General Procedure B, **2n** (21 mg, 0.13 mmol, 64% yield) was obtained as a white amorphous solid. No further purification were needed. ^{1}H NMR (400 MHz, D_2O) δ = 3.79-3.74 (m, 1H), 2.95-2.91 (m, 2H), 2.65 (s, 3H, CH_3), 2.26-2.18 (m, 2H). ^{13}C NMR (101 MHz, D_2O) δ = 173.1, 53.3, 48.2, 36.5, 23.7.

(S)-2-amino-4-(methylsulfonyl)butanoic acid **(3m)** [14]

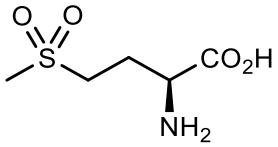

By following General Procedure E, **3n** (49 mg, 0.27 mmol, 75% yield) was obtained as a white amorphous solid. No further purification was needed. ^{1}H NMR (400 MHz, D_2O) δ = 3.80 (m, 1H), 3.36-3.32 (m, 2H), 3.04 (s, 3H), 2.35-2.26 (m, 2H). ^{13}C NMR (101 MHz, D_2O) δ = 172.8, 53.5, 49.8, 40.2, 23.1.

Ethyl phenylglycinate **(4a)** [4]

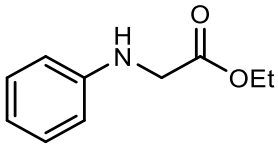

By following General Procedure F, **4a** (1.15 g, 6.4 mmol, 64% yield) was obtained as a yellow amorphous solid after column chromatography on silica gel (20% EtOAc in cyclohexane). ^{1}H NMR (300 MHz, $CDCl_3$) δ = 7.20 (t, *J* = 8.2 Hz, 2H), 6.75 (t, *J* = 8.2 Hz, 1H), 6.62 (d, *J* = 8.2 Hz, 2H), 4.19−4.33 (m, 3H, CH_2 and NH), 3.90 (s, 2H), 1.30 (t, J = 7.3 Hz, 3H). ^{13}C NMR (101 MHz, $CDCl_3$) δ = 171.0, 146.8, 129.3, 118.4, 113.2, 61.3, 46.0, 14.2.

Ethyl (4-fluorophenyl)glycinate **(4b)** [4]

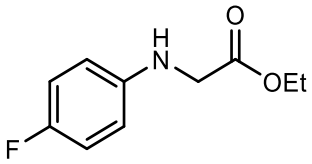

By following General Procedure F, **4b** (1.24 g, 6.3 mmol, 63% yield) was obtained as a yellow amorphous solid after column chromatography on silica gel (15% EtOAc in cyclohexane). ^{1}H NMR (300 MHz, $CDCl_3$) δ = 6.90 (t, *J* = 8.8 Hz, 2H), 6.55 (dd, *J* = 8.8 Hz, 2H), 4.24 (q, *J* = 7.1 Hz, 2H), 4.17 (s, 1H), 3.86 (d, *J* = 5.3 Hz, 2H), 1.29 (t, *J* = 7.1 Hz, 3H). ^{13}C NMR (101 MHz, $CDCl_3$) δ = 171.0, 157.4, 143.4, 115.9, 115.6, 113.9, 113.8, 61.3, 46.4, 14.2. ^{19}F NMR (376 MHz, $CDCl_3$) δ = −127.2.

Ethyl (4-chlorophenyl)glycinate **(4c)** [4]

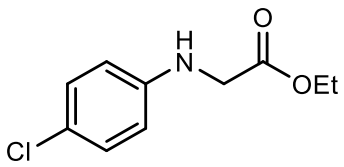

By following General Procedure F, **4c** (1.30 g, 6.1 mmol, 61% yield) was obtained as a white amorphous solid after column chromatography on silica gel (20% EtOAc in cyclohexane). ^{1}H NMR (300 MHz, $CDCl_3$) δ = 7.14

(d, J = 8.9 Hz, 2H), 6.53 (d, J = 8.9 Hz, 2H), 4.25 (q, J = 7.1 Hz, 2H), 3.87 (d, J = 5.5 Hz, 2H), 1.30 (t, J = 7.1 Hz, 3H). ^{13}C NMR (101 MHz, $CDCl_3$) δ = 170.8, 145.5, 129.1, 122.8, 114.0, 61.4, 45.8, 14.12.

Ethyl p-tolylglycinate **(4d)** [4]

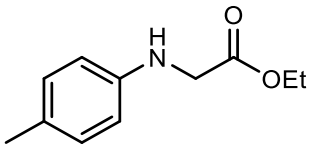

By following General Procedure F, **4d** (1.31 g. 6.8 mmol, 68% yield) was obtained as a yellow amorphous solid after column chromatography on silica gel (20% EtOAc in cyclohexane). ^{1}H NMR (300 MHz, $CDCl_3$) δ = 7.00 (d, J = 8.4 Hz, 2H, Ar), 6.54 (d, J = 8.4 Hz, 2H), 4.79 (s, 1H), 4.23 (q, J = 7.1 Hz, 2H), 3.88 (s, 2H), 2.24 (s, 3H), 1.29 (t, J = 7.1 Hz, 3H). ^{13}C NMR (101 MHz, $CDCl_3$) δ = 171.0, 144.15, 129.8, 128.1, 113.7, 61.3, 46.5, 20.4, 14.2.

Ethyl (4-methoxyphenyl)glycinate **(4e)** [4]

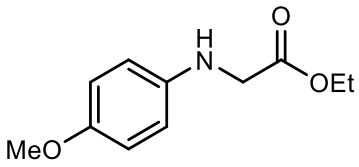

By following General Procedure F, **4e** (1.48 g, 7.1 mmol, 71% yield) was obtained as a yellow amorphous solid after column chromatography on silica gel (20% EtOAc in cyclohexane). ^{1}H NMR (300 MHz, $CDCl_3$) δ = 6.79 (d, J = 8.9 Hz, 2H), 6.59 (d, J = 8.9 Hz, 2H), 4.23 (q, J = 7.1 Hz, 2H), 4.02 (s, 1H), 3.86 (s, 2H), 3.75 (s, 3H), 1.29 (t, J = 7.1 Hz, 3H). ^{13}C NMR (101 MHz, $CDCl_3$) δ = 171.3, 152.6, 141.2, 114.9, 114.3, 61.2, 55.7, 46.8, 14.2.

Ethyl (2-fluorophenyl)glycinate **(4f)** [4]

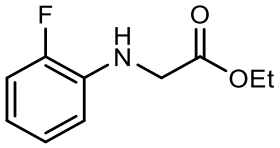

By following General Procedure F, **4f** (1.43 g, 7.3 mmol, 73% yield) was obtained as a white amorphous solid after column chromatography on silica gel (20% EtOAc in cyclohexane). ^{1}H NMR (300 MHz, $CDCl_3$) δ = 6.99 (t, J = 8.4 Hz, 2H), 6.72−6.63 (m, 1H), 6.59 (t, J = 8.4 Hz, 1H), 4.52 (s, 1H), 4.25 (q, J = 7.1 Hz, 2H), 3.93 (d, J = 5.6 Hz, 2H), 1.31 (t, J = 7.1, 3H). ^{13}C NMR (101 MHz, $CDCl_3$) δ = 170.6, 124.5, 117.6, 117.6, 114.7, 114.5, 112.2, 61.4, 45.5, 14.1. ^{19}F NMR (376 MHz, $CDCl_3$) δ = −127.19 to −127.50 (m).

1-benzyl-1H-indole **(5g)** [4]

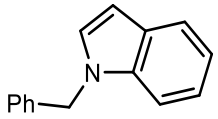

By following General Procedure G, **5g** (1.29 g, 6.2 mmol, 62% yield) was obtained as a pale red oil after column chromatography on silica gel (10% EtOAc in cyclohexane). ^{1}H NMR (300 MHz, $CDCl_3$) δ = 7.66 (d, *J* = 7.1 Hz, 1H), 7.35−7.22 (m, 5H), 7.19 (dd, *J* = 7.1, 1.3 Hz, 1H), 7.16−7.05 (m, 4H), 6.56 (dd, *J* = 3.1, 0.8 Hz, 1H), 5.34 (s, 2H). ^{13}C NMR (101 MHz, $CDCl_3$) δ = 137.5, 136.3, 128.7, 128.2, 127.6, 126.7, 121.7, 121.0, 119.5, 109.7, 101.7, 50.1, 29.7.

Ethyl 2-(1H-indol-3-yl)-2-(phenylamino)acetate **(6aa)** [4]

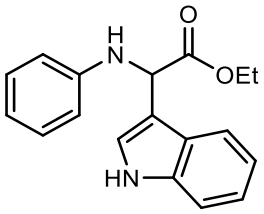

By following General Procedure C, **6aa** (21 mg, 0.072 mmol, 72% yield) was obtained as a white amorphous solid after column chromatography on silica gel (20% EtOAc in cyclohexane). ^{1}H NMR (300 MHz, $CDCl_3$) δ = 8.13 (s, 1H), 7.84 (d, *J* = 8.0 Hz, 1H), 7.39 (d, *J* = 8.0 Hz, 1H), 7.25−7.11 (m, 5H), 6.72 (t, *J* = 7.5 Hz, 1H), 6.64 (d, *J* = 7.5 Hz, 2H), 5.40 (d, *J* = 5.5 Hz, 1H), 4.77 (s, 1H), 4.32−4.06 (m, 2H), 1.22 (t, *J* = 7.1 Hz, 3H). ^{13}C NMR (101 MHz, $CDCl_3$) δ = 172.5, 146.5, 136.5, 129.2, 125.8, 123.0, 122.5, 120.0, 119.6, 118.0, 113.3, 112.7, 111.3, 61.6, 54.2, 14.1.

Ethyl (E)-2-(1H-indol-3-yl)-2-(phenylimino)acetate **(7)** [4]

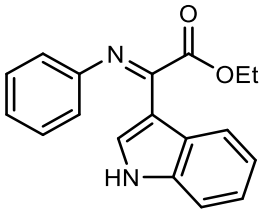

By following General Procedure C, byproduct **7** (1 mg, 0.004 mmol, 4% yield) was isolated as a white amorphous solid after column chromatography on silica gel (20% EtOAc in cyclohexane). ^{1}H NMR (300 MHz, $CDCl_3$) δ = 8.55 (dd, *J* = 3.0 Hz, 1H), 8.48 (s, 1H), 7.66 (d, *J* = 3.0 Hz, 1H), 7.46 – 7.39 (m, 1H), 7.35 – 7.27 (m, 4H), 7.15 – 7.07 (m, 1H), 6.99 (d, *J* = 7.3 Hz, 2H), 4.08 (q, *J* = 7.1 Hz, 2H), 0.94 (t, *J* = 7.1 Hz, 3H). ^{13}C NMR (101 MHz, $CDCl_3$) δ = 165.1, 155.8, 151.4, 136.8, 130.0, 129.3, 128.7, 125.3, 124.1, 124.0, 123.1, 122.2, 120.1, 113.7, 111.3, 61.2, 13.7.

Ethyl 2,2-di(1H-indol-3-yl)acetate **(8)** [4]

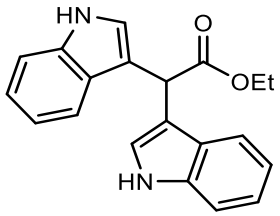

By following General Procedure C, byproduct **8** (2 mg, 0.005 mmol, 5% yield) was isolated as a white amorphous solid after column chromatography on silica gel (20% EtOAc in cyclohexane). ^{1}H NMR (300 MHz, $CDCl_3$) δ = 8.03 (s, 2H), 7.65 (d, *J* = 7.9 Hz, 2H), 7.37 (d, *J* = 7.9 Hz, 2H), 7.23 – 7.13 (m, 4H), 7.13 – 7.05 (m, 2H), 5.51 (s, 1H), 4.22 (q, *J* = 7.1 Hz, 2H), 1.27 (s, *J* = 7.1 Hz, 3H). ^{13}C NMR (101 MHz, $CDCl_3$) δ = 173.2, 136.3, 126.7, 123.2, 122.1, 119.5, 113.87, 111.12, 61.02, 40.66, 14.24, 1.00.

Ethyl 2-[(4-fluorophenyl)amino]-2-(1H-indol-3-yl)acetate **(6ba)** [4]

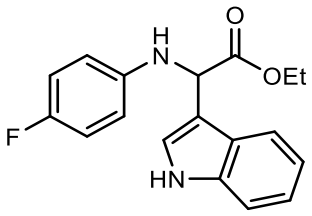

By following General Procedure C, **6ba** (24 mg, 0.076 mmol, 76% yield) was obtained as a white amorphous solid after column chromatography on silica gel (20% EtOAc in cyclohexane). ^{1}H NMR (400 MHz, $CDCl_3$) δ = 8.15 (s, 1H), 7.82 (d, *J* = 8.0 Hz, 1H), 7.39 (d, *J* = 7.2 Hz, 1H), 7.25−7.13 (m, 3H), 6.85 (t, *J* = 8.9 Hz, 2H), 6.60−6.57 (dd, *J* = 8.9, 4.4 Hz, 2H), 5.33 (s, 1H), 4.65 (s, 1H), 4.30−4.05 (m, 2H), 1.22 (t, *J* = 7.1 Hz, 3H). ^{13}C NMR (101 MHz, $CDCl_3$) δ = 172.4, 136.5, 125.8, 123.0, 122.6, 120.1, 119.5, 115.8, 115.5, 114.3, 114.3, 112.6, 111.4, 61.6, 54.8, 14.1. ^{19}F NMR (376 MHz, $CDCl_3$) δ = −127.25 to −127.34 (m).

Ethyl 2-[(4-chlorophenyl)amino]-2-(1H-indol-3-yl)acetate **(6ca)** [4]

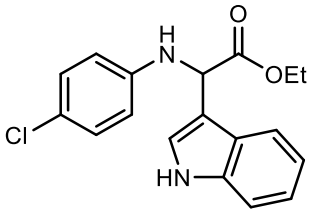

By following General Procedure C, **6ca** (24 mg, 0.074 mmol, 74% yield) was obtained as a white amorphous solid after column chromatography on silica gel (20% EtOAc in cyclohexane). ^{1}H NMR (400 MHz, acetone-d6) δ = 10.33 (s, 1H), 7.79 (d, *J* = 9.1 Hz, 1H), 7.50−7.36 (m, 2H), 7.17−7.05 (m, 4H), 6.79 (d, *J* = 9.1 Hz, 2H), 5.68 (d, *J* = 7.2 Hz, 1H), 5.45 (d, *J* = 7.2 Hz, 1H), 4.28−4.01 (m, 2H), 1.18 (t, *J* = 7.1 Hz, 3H). ^{13}C NMR (101 MHz, acetone-d6) δ = 172.0, 146.5, 128.7, 126.1, 124.0, 123.9, 121.8, 121.1, 119.3, 119.3, 114.5, 111.6, 111.6, 60.8, 54.1, 13.6.

Ethyl 2-(1H-indol-3-yl)-2-(p-tolylamino)acetate **(6da)** [4]

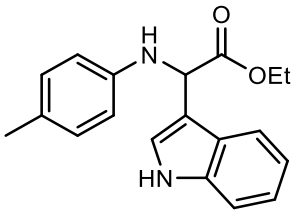

By following General Procedure C, **6da** (22 mg, 0.071 mmol, 71% yield) was obtained as a white amorphous solid after column chromatography on silica gel (20% EtOAc in cyclohexane). ^{1}H NMR (300 MHz, acetone-d6) δ = 10.29 (s, 1H), 7.78 (d, *J* = 7.9 Hz, 1H), 7.41 (dd, *J* = 6.0, 1.8 Hz, 2H), 7.20−6.98 (m, 2H), 6.92 (d, *J* = 8.1 Hz, 2H), 6.73−6.61 (m, 2H), 5.41 (d, *J* = 7.6 Hz, 1H), 5.24 (d, *J* = 7.6 Hz, 1H), 4.25−3.99 (m, 2H), 2.16 (s, 3H), 1.16 (t, *J* = 7.1 Hz, 3H). ^{13}C NMR (101 MHz, acetone-d6) δ = 172.5, 145.4, 136.9, 129.4, 126.2, 126.0, 123.9, 121.8, 119.4, 119.2, 113.4, 112.0, 111.6, 60.6, 54.3, 19.6, 13.7.

Ethyl 2-(1H-indol-3-yl)-2-[(4-methoxyphenyl)amino]acetate **(6ea)** [4]

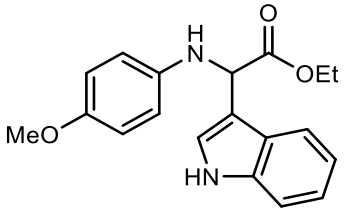

By following General Procedure C, **6ea** (23 mg, 0.07 mmol, 70% yield) was obtained as a white amorphous solid after column chromatography on silica gel (20% EtOAc in cyclohexane). ^{1}H NMR (300 MHz, $CDCl_3$) δ = 8.13 (s, 1H), 7.83 (d, *J* = 7.8 Hz, 1H), 7.38 (d, *J* = 7.7 Hz, 1H), 7.28−7.22 (m, 3H), 7.22−7.11 (m, 1H), 6.80−6.68 (m, 2H), 6.66−6.56 (m, 2H), 5.33 (s, 1H), 4.32−4.06 (m, 2H), 3.72 (s, 3H), 1.22 (t, *J* = 7.1 Hz, 3H). ^{13}C NMR (101 MHz, $CDCl_3$) δ = 172.7, 152.5, 140.8, 136.4, 131.6, 125.8, 123.0, 122.5, 120.0, 119.6, 114.8, 112.9, 111.3, 61.5, 55.7, 55.2, 14.1.

Ethyl 2-[(2-fluorophenyl)amino]-2-(1H-indol-3-yl)acetate **(6fa)** [4]

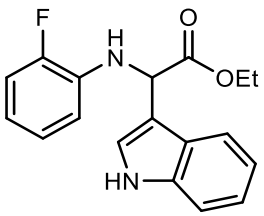

By following General Procedure C, **6fa** (19 mg, 0.062 mmol, 62% yield) was obtained as a white amorphous solid after column chromatography on silica gel (20% EtOAc in cyclohexane). ^{1}H NMR (300 MHz, $CDCl_3$) δ = 8.15 (s, 1H), 7.84 (d, *J* = 7.9 Hz, 1H), 7.39 (d, *J* = 7.9 Hz, 1H), 7.29−7.26 (m, 1H), 7.22−7.15 (m, 2H), 7.02−6.94 (m, 1H), 6.90 (t, *J* = 7.9 Hz, 1H), 6.68−6.58 (m, 2H), 5.41 (d, *J* = 6.4 Hz, 1H), 5.03 (s, 1H), 4.33−4.08

(m, 2H), 1.22 (t, *J* = 7.1 Hz, 3H). ^{13}C NMR (101 MHz, $CDCl_3$) δ = 172.0, 136.5, 125.7, 124.4, 123.0, 122.6, 120.1, 119.5, 117.5, 117.4, 114.7, 114.5, 112.9, 112.4, 111.3, 61.6, 54.0, 14.1. ^{19}F NMR (376 MHz, $CDCl_3$) δ = −135.45 to −135.56 (m).

Ethyl 2-(6-fluoro-1H-indol-3-yl)-2-(phenylamino)acetate **(6ab)** [4]

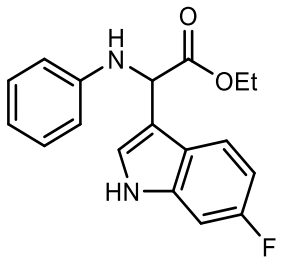

By following General Procedure C, **6ab** (25 mg, 0.08 mmol, 80% yield) was obtained as a white amorphous solid after column chromatography on silica gel (20% EtOAc in cyclohexane). ^{1}H NMR (300 MHz, $CDCl_3$) δ = 8.11 (s, 1H), 7.75 (dd, *J* = 8.7, 5.3 Hz, 1H), 7.22 (d, *J* = 2.5 Hz, 1H), 7.14 (t, *J* = 7.6 Hz, 2H), 7.06 (dd, *J* = 9.5, 2.5 Hz, 1H), 6.97−6.87 (m, 1H), 6.72 (t, *J* = 7.3 Hz, 1H), 6.63 (d, *J* = 7.6 Hz, 2H), 5.35 (d, *J* = 4.7 Hz, 1H), 4.76 (d, *J* = 4.1 Hz, 1H), 4.32−4.02 (m, 2H), 1.22 (t, *J* = 7.1 Hz, 3H). ^{13}C NMR (101 MHz, $CDCl_3$) δ = 172.6, 146.7, 129.6, 123.6, 120.9, 120.8, 118.5, 113.7, 113.3, 109.4, 109.1, 98.2, 97.8, 62.0, 54.6, 14.5. ^{19}F NMR (376 MHz, $CDCl_3$) δ = −120.37 (td, *J* = 9.5, 5.3 Hz).

Ethyl 2-(6-chloro-1H-indol-3-yl)-2-(phenylamino)acetate **(6ac)** [4]

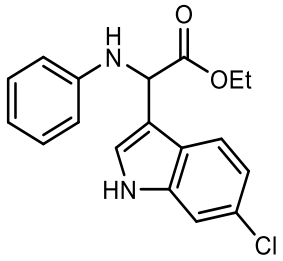

By following General Procedure C, **6ac** (23 mg, 0.072 mmol, 72% yield) was obtained as a white amorphous solid after column chromatography on silica gel (20% EtOAc in cyclohexane). ^{1}H NMR (300 MHz, $CDCl_3$) δ = 8.11 (s, 1H), 7.75 (d, *J* = 8.5 Hz, 1H), 7.37 (d, *J* = 1.7 Hz, 1H), 7.24 (d, *J* = 2.6 Hz, 1H), 7.18−7.10 (m, 3H), 6.72 (t, *J* = 7.4 Hz, 1H), 6.62 (d, *J* = 7.4 Hz, 2H), 5.35 (d, *J* = 5.7 Hz, 1H), 4.78 (d, *J* = 5.7 Hz, 1H), 4.32−4.05 (m, 2H), 1.21 (t, *J* = 7.1 Hz, 3H). ^{13}C NMR (101 MHz, $CDCl_3$) δ = 172.3, 146.4, 136.9, 129.3, 124.5, 123.7, 123.1, 120.9, 120.7, 118.3, 113.5, 113.2, 111.3, 61.8, 54.2, 14.2.

Ethyl 2-(6-methyl-1H-indol-3-yl)-2-(phenylamino)acetate **(6ad)** [4]

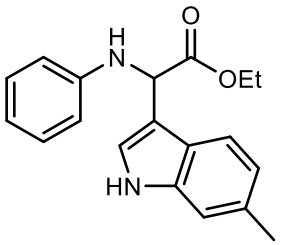

By following General Procedure C, **6ad** (17 mg, 0.055 mmol, 55% yield) was obtained as a white amorphous solid after column chromatography on silica gel (20% EtOAc in cyclohexane). ^{1}H NMR (300 MHz, $CDCl_3$) δ = 8.00 (s, 1H), 7.71 (d, *J* = 8.2 Hz, 1H), 7.17 (d, *J* = 2.5 Hz, 2H), 7.13 (d, *J* = 8.2 Hz, 2H), 7.01 (d, *J* = 8.2 Hz, 1H), 6.71 (t, *J* = 7.4 Hz, 1H), 6.63 (d, *J* = 7.4 Hz, 2H), 5.35 (s, 1H), 4.75 (s, 1H), 4.34− 4.04 (m, 2H), 2.47 (s, 3H), 1.22 (t, *J* = 7.1 Hz, 3H). ^{13}C NMR (101 MHz, $CDCl_3$) δ = 172.9, 146.9, 137.3, 132.8, 129.5, 124.0, 122.7, 122.2, 119.6, 118.3, 113.7, 112.9, 111.6, 61.9, 54.7, 22.0, 14.5.

Ethyl 2-(6-methoxy-1H-indol-3-yl)-2-(phenylamino)acetate **(6ae)** [4]

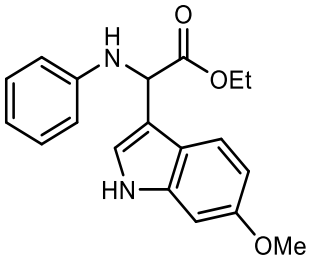

By following General Procedure C, **6ae** (16 mg, 0.051 mmol, 51% yield) was obtained as a white amorphous solid after column chromatography on silica gel (20% EtOAc in cyclohexane). ^{1}H NMR (300 MHz, $CDCl_3$) δ = 7.98 (s, 1H), 7.70 (d, *J* = 8.5 Hz, 1H), 7.17− 7.10 (m, 3H), 6.88−6.79 (m, 2H), 6.71 (t, *J* = 7.4 Hz, 1H), 6.63 (d, *J* = 7.4 Hz, 2H), 5.34 (d, *J* = 6.2 Hz, 1H), 4.75 (d, *J* = 6.2 Hz, 1H), 4.33−4.05 (m, 2H), 3.85 (s, 3H), 1.22 (t, *J* = 7.1 Hz, 3H). ^{13}C NMR (101 MHz, $CDCl_3$) δ = 172.5, 156.8, 146.5, 137.3, 129.2, 121.8, 120.3, 120.1, 118.0, 113.3, 112.7, 110.1, 94.7, 61.5, 55.6, 54.3, 14.1.

Ethyl 2-(1-methyl-1H-indol-3-yl)-2-(phenylamino)acetate **(6af)** [4]

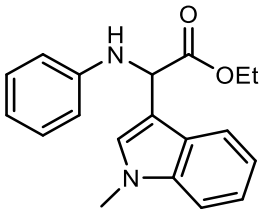

By following General Procedure C, **6af** (20 mg, 0.065 mmol, 65% yield) was obtained as a white amorphous solid after column chromatography on silica gel (20% EtOAc in cyclohexane). ^{1}H NMR (300 MHz, $CDCl_3$) δ = 7.82 (d, *J* = 7.9 Hz, 1H), 7.31 (t, *J* = 6.8 Hz, 2H), 7.20 − 7.09 (m, 4H), 6.72 (t, *J* = 7.7 Hz, 1H), 6.64 (d, *J* = 7.7 Hz, 2H), 5.37 (d, *J* = 6.1 Hz 1H), 4.74 (d, *J* = 6.1 Hz, 1H), 4.36−4.03 (m, 2H), 3.75 (s, 3H), 1.22 (t, *J* = 7.1

Hz, 3H). ^{13}C NMR (101 MHz, $CDCl_3$) δ =172.6, 146.5, 129.2, 127.6, 126.3, 122.0, 119.6, 119.5, 117.9, 113.3, 110.9, 109.5, 61.5, 54.2, 32.9, 14.1.

Ethyl 2-(1-benzyl-1H-indol-3-yl)-2-(phenylamino)acetate **(6ag)** [4]

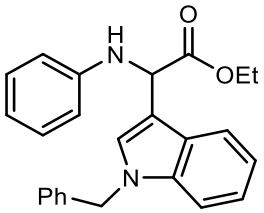

By following General Procedure C, **6ag** (28 mg, 0.074 mmol, 74% yield) was obtained as a white amorphous solid after column chromatography on silica gel (20% EtOAc in cyclohexane). ^{1}H NMR (300 MHz, $CDCl_3$) δ = 7.84 (d, *J* = 6.9 Hz, 1H), 7.27 (d, *J* = 6.9 Hz, 4H), 7.22− 7.10 (m, 5H), 7.07 (dd, *J* = 6.9, 2.2 Hz, 2H), 6.72 (t, *J* = 7.4 Hz, 1H), 6.65 (d, *J* = 7.4 Hz, 2H), 5.39 (d, *J* = 6.2 Hz, 1H), 5.27 (s, 2H), 4.74 (d, *J* = 6.2 Hz, 1H), 4.33−4.05 (m, 2H), 1.21 (t, *J* = 7.1 Hz, 3H). ^{13}C NMR (101 MHz, $CDCl_3$) δ = 172.0, 146.0, 136.4, 136.3, 128.6, 128.2, 127.1, 126.6, 126.2, 126.0, 121.7, 119.2, 119.2, 117.5, 112.8, 111.0, 109.4, 60.9, 53.7, 49.6, 13.5.

Ricobendazole [15]

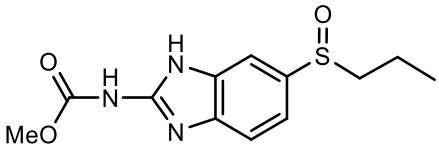

By following General Procedure H, the collected crude reaction mixture was purified by column chromatography on silica gel (30% EtOAc in cyclohexane). **Ricobendazole** was obtained as a white amorphous solid. ^{1}H NMR (400 MHz, DMSO-d_6) δ = 11.83 (s, 2H), 7.69-7.68 (m, 1H), 7.53 (d, *J* = 8.2 Hz, 1H), 7.30 (dd, *J* = 8.2, 1.6 Hz, 1H), 3.76 (s, 3H), 2.89-2.76 (m, 2H), 1.68-1.49 (m, 2H), 0.98 (t, *J* = 7.4 Hz, 3H). ^{13}C NMR (101 MHz, DMSO-d_6) δ = 154.7, 148.7, 136.8, 117.5, 114.8, 110.5, 58.5, 53.2, 53.0, 15.8, 13.5, 13.3.

3 Comparison of different triazine-based photocatalysts in the aerobic oxidation of sulfides

Table S8

Entry	Catalyst	Light Source	Solvent	Oxidant	Yield (%)	Ref
1	Q-COF-T	Xe Lamp (300 W)	CH_3CN	O_2	53-100[a]	[16]
2	COF-TZ-2	Blue Led (460 nm)	CH_3OH	O_2	80-92[a]	[17]
3	TTT-COF	Blue Led (460 nm)	C_2H_5OH	O_2	72-94[a]	[18]
4	CTF-HUST-D2	Blue Led (4 × 3W)	CH_3OH	Air	80-89[a]	[19]
5	TPDH-PTBA	Blue Led (450 nm)	CH_3OH	O_2	88-97[a,b]	[20]
6	DPhBTBT-CTF	Blue Led (2 × 30W)	CH_3CN	O_2	> 99[a,b]	[21]
7	HEP-FL	Blue Led (20 W, 450 nm)	H_2O	O_2	88-98[b]	[22]
8	A-CTP-DPA	Xe lamp (300 W ,>420 nm)	CH_3CN	O_2	54-96[a]	[23]
9	Am-COF-T	Xe lamp (300 W)	CH_3CN	O_2	45-99[a]	[24]
10	COF-NUST-31	Blue Light (30 W,460 nm)	CH_3CN	O_2	79-97[b]	[25]
11	TpTAPT-COF	Blue Led (4 × 3W, 460 nm)	CH_3OH	O_2	7-92[a]	[26]
12	p-TCT	Compact Fluor. Lamp (26 W)	CH_3OH	Air	93-98[c]	[27]
13	DAPT-CTP_{sc}	Hg-Xe lamp (200 W, >400 nm)	C_2H_5OH-H_2O	Air	64-92[c]	This work

[a]Determined by GC analysis. [b]Determined by ^{1}HNMR analysis. [c]Isolated yield.

5. References

[1] Frisch, M. J.; Trucks, G. W.; Schlegel, H. B.; Scuseria, G. E.; Robb, M. A.; Cheeseman, J. R.; Scalmani, G.; Barone, V.; Petersson, G. A.; Nakatsuji, H.; Li, X.; Caricato, M.; Marenich, A. V.; Bloino, J.; Janesko, B. G.; Gomperts, R.; Mennucci, B.; Hratchian, H. P.; Ortiz, J. V.; Izmaylov, A. F.; Sonnenberg, J. L.; Williams; Ding, F.; Lipparini, F.; Egidi, F.; Goings, J.; Peng, B.; Petrone, A.; Henderson, T.; Ranasinghe, D.; Zakrzewski, V. G.; Gao, J.; Rega, N.; Zheng, G.; Liang, W.; Hada, M.; Ehara, M.; Toyota, K.; Fukuda, R.; Hasegawa, J.; Ishida, M.; Nakajima, T.; Honda, Y.; Kitao, O.; Nakai, H.; Vreven, T.; Throssell, K.; Montgomery Jr., J. A.; Peralta, J. E.; Ogliaro, F.; Bearpark, M. J.; Heyd, J. J.; Brothers, E. N.; Kudin, K. N.; Staroverov, V. N.; Keith, T. A.; Kobayashi, R.; Normand, J.; Raghavachari, K.; Rendell, A. P.; Burant, J. C.; Iyengar, S. S.; Tomasi, J.; Cossi, M.; Millam, J. M.; Klene, M.; Adamo, C.; Cammi, R.; Ochterski, J. W.; Martin, R. L.; Morokuma, K.; Farkas, O.; Foresman, J. B.; Fox, D. J. Gaussian 16 Rev. C.01, 2016.

[2] Lu, T.; Chen, F. Multiwfn: A Multifunctional Wavefunction Analyzer. *J. Comput. Chem.* **2012**, *33* (5), 580–592. https://doi.org/10.1002/jcc.22885.

[3] Zhao, R.; Niu, C.; Aly Aboud, M. F.; Shakir, I.; Yu, C.; Xu, Y. Monomer-Dependent Synthesis of Secondary Amine-Linked Triazine-Based Two-Dimensional Polymers Nanosheets. *Sci. China Chem.* **2020**, *63* (7), 966–972. https://doi.org/10.1007/s11426-020-9720-1.

[4] Poletti, L.; Ragno, D.; Bortolini, O.; Presini, F.; Pesciaioli, F.; Carli, S.; Caramori, S.; Molinari, A.; Massi, A.; Di Carmine, G. Photoredox Cross-Dehydrogenative Coupling of *N* -Aryl Glycines Mediated by Mesoporous Graphitic Carbon Nitride: An Environmentally Friendly Approach to the Synthesis of Non-Proteinogenic α-Amino Acids (NPAAs) Decorated with Indoles. *J. Org. Chem.* **2022**, *87* (12), 7826–7837. https://doi.org/10.1021/acs.joc.2c00474.

[5] Yang, C.; Jin, Q.; Zhang, H.; Liao, J.; Zhu, J.; Yu, B.; Deng, J. Tetra-(Tetraalkylammonium)Octamolybdate Catalysts for Selective Oxidation of Sulfides to Sulfoxides with Hydrogen Peroxide. *Green Chem.* **2009**, *11* (9), 1401. https://doi.org/10.1039/b912521n.

[6] Niu, K.-K.; Luan, T.-X.; Cui, J.; Liu, H.; Xing, L.-B.; Li, P.-Z. Red-Light-Based Effective Photocatalysis of a Photosensitive Covalent Organic Framework Triggered Singlet Oxygen. *ACS Catal.* **2024**, *14* (4), 2631–2641. https://doi.org/10.1021/acscatal.3c05454.

[7] Yuan, G.; Zheng, J.; Gao, X.; Li, X.; Huang, L.; Chen, H.; Jiang, H. Copper-Catalyzed Aerobic Oxidation and Cleavage/Formation of C–S Bond: A Novel Synthesis of Aryl Methyl Sulfones from Aryl Halides and DMSO. *Chem. Commun.* **2012**, *48* (60), 7513. https://doi.org/10.1039/c2cc32964f.

[8] Shavnya, A.; Coffey, S. B.; Smith, A. C.; Mascitti, V. Palladium-Catalyzed Sulfination of Aryl and Heteroaryl Halides: Direct Access to Sulfones and Sulfonamides. *Org. Lett.* **2013**, *15* (24), 6226–6229. https://doi.org/10.1021/ol403072r.

[9] Izquierdo, F.; Chartoire, A.; Nolan, S. P. Direct S-Arylation of Unactivated Arylsulfoxides Using [Pd(IPr*)(Cin)Cl]. *ACS Catal.* **2013**, *3* (10), 2190–2193. https://doi.org/10.1021/cs400533e.

[10] Bhadra, S.; Dzik, W. I.; Goossen, L. J. Decarboxylative Etherification of Aromatic Carboxylic Acids. *J. Am. Chem. Soc.* **2012**, *134* (24), 9938–9941. https://doi.org/10.1021/ja304539j.

[11] Huang, H.; Li, X.; Yu, C.; Zhang, Y.; Mariano, P. S.; Wang, W. Visible-Light-Promoted Nickel- and Organic-Dye-Cocatalyzed Formylation Reaction of Aryl Halides and Triflates and Vinyl Bromides with Diethoxyacetic Acid as a Formyl Equivalent. *Angew. Chem. Int. Ed.* **2017**, *56* (6), 1500–1505. https://doi.org/10.1002/anie.201610108.

[12] Voutyritsa, E.; Triandafillidi, I.; Kokotos, C. Green Organocatalytic Oxidation of Sulfides to Sulfoxides and Sulfones. *Synthesis* **2016**, *49* (04), 917–924. https://doi.org/10.1055/s-0036-1588315.

[13] Oonishi, T.; Kawahara, T.; Arakawa, Y.; Minagawa, K.; Imada, Y. Greener Preparation of 5-Ethyl-4a-hydroxyisoalloxazine and Its Use for Catalytic Aerobic Oxygenations. *Eur. J. Org. Chem.* **2019**, *2019* (8), 1791–1795. https://doi.org/10.1002/ejoc.201801865.

[14] Madduluri, V. K.; Baig, N.; Chander, S.; Murugesan, S.; Sah, A. K. Mo(VI) Complex Catalysed Synthesis of Sulfones and Their Modification for Anti-HIV Activities. *Catal. Commun.* **2020**, *137*, 105931. https://doi.org/10.1016/j.catcom.2020.105931.

[15] Diprima, D.; Gemoets, H.; Bonciolini, S.; Van Aken, K. Selective and Scalable Oxygenation of Heteroatoms Using the Elements of Nature: Air, Water, and Light. *Beilstein J. Org. Chem.* **2023**, *19*, 1146–1154. https://doi.org/10.3762/bjoc.19.82.

[16] Xue, R.; Liu, Y.-S.; Guo, H.; Yang, W.; Yang, G.-Y. Chemical Conversion of Imine- into Quinoline-Linked Covalent Organic Frameworks for Photocatalytic Oxidation. *J. Colloid Interface Sci.* **2024**, *655*, 709–716. https://doi.org/10.1016/j.jcis.2023.11.078.

[17] Wang, Y.; Zhang, F.; Huang, F.; Dong, X.; Zeng, B.; Gu, X.-K.; Lang, X. Thiazole-Linked Isomeric Covalent Organic Frameworks for Divergent Photocatalysis: Selective Oxidation of Organic Sulfides. *Appl. Catal., B* **2024**, *354*, 124103. https://doi.org/10.1016/j.apcatb.2024.124103.

[18] Wang, Y.; Huang, F.; Sheng, W.; Miao, X.; Li, X.; Gu, X.-K.; Lang, X. Blue Light Photocatalytic Oxidation of Sulfides to Sulfoxides with Oxygen over a Thiazole-Linked 2D Covalent Organic Framework. *Appl. Catal. B* **2023**, *338*, 123070. https://doi.org/10.1016/j.apcatb.2023.123070.

[19] Wang, X.; Zhang, S.; Li, X.; Zhan, Z.; Tan, B.; Lang, X.; Jin, S. Two-Dimensional Crystalline Covalent Triazine Frameworks *via* Dual Modulator Control for Efficient Photocatalytic Oxidation of Sulfides. *J. Mater. Chem. A* **2021**, *9* (30), 16405–16410. https://doi.org/10.1039/D1TA03951B.

[20] Hu, Y.; Ji, Y.; Qiao, Z.; Tong, L. Phenothiazine-Linked Covalent Triazine Frameworks for Enhanced Photocatalytic Aerobic Oxidation Reactions. *Microporous and Mesoporous Mater.* **2023**, *362*, 112767. https://doi.org/10.1016/j.micromeso.2023.112767.

[21] Borrallo-Aniceto, M. C.; Pintado-Sierra, M.; Valverde-González, A.; Díaz, U.; Sánchez, F.; Maya, E. M.; Iglesias, M. Unveiling the Potential of a Covalent Triazine Framework Based on [1]Benzothieno[3,2- *b*][1]Benzothiophene (DPhBTBT-CTF) as a Metal-Free Heterogeneous Photocatalyst. *Green Chem.* **2024**, *26* (4), 1975–1983. https://doi.org/10.1039/D3GC03529H.

[22] Saini, N.; Dhingra, K.; Kumar, A.; Kailasam, K. Molecular Structural Engineering of Donor–Acceptor-Based Porous Organic Polymers for Sulfide Photooxidation in Water: A Sustainable Approach. *Green Chem.* **2024**, *26* (19), 10314–10323. https://doi.org/10.1039/D4GC03255A.

[23] Lan, X.; Wang, J.; Li, Q.; Wang, A.; Zhang, Y.; Yang, X.; Bai, G. Acetylene/Vinylene-Bridged Π-Conjugated Covalent Triazine Polymers for Photocatalytic Aerobic Oxidation Reactions under Visible Light Irradiation. *ChemSusChem* **2022**, *15* (4). https://doi.org/10.1002/cssc.202102455.

[24] Xue, R.; Liu, Y.; Wang, M.; Guo, H.; Yang, W.; Guo, J.; Yang, G. Rational Conversion of Imine Linkages to Amide Linkages in Covalent Organic Frameworks for Photocatalytic Oxidation with Enhanced Photostability. *ChemSusChem* **2024**, *17* (19). https://doi.org/10.1002/cssc.202400732.

[25] Gu, Z.; Wang, J.; Shan, Z.; Wu, M.; Liu, T.; Song, L.; Wang, G.; Ju, X.; Su, J.; Zhang, G. Modulating Electronic Structure of Triazine-Based Covalent Organic Frameworks for Photocatalytic Organic Transformations. *J. Mater. Chem. A* **2022**, *10* (34), 17624–17632. https://doi.org/10.1039/D2TA04541A.

[26] Miao, X.; Zhang, F.; Wang, Y.; Dong, X.; Lang, X. 2D β-Ketoenamine-Linked Triazine Covalent Organic Framework Photocatalysis for Selective Oxidation of Sulfides. *Sustainable Energy Fuels* **2023**, *7* (8), 1963–1973. https://doi.org/10.1039/D3SE00020F.

[27] Luo, J.; Lu, J.; Zhang, J. Carbazole–Triazine Based Donor–Acceptor Porous Organic Frameworks for Efficient Visible-Light Photocatalytic Aerobic Oxidation Reactions. *J. Mater. Chem. A* **2018**, *6* (31), 15154–15161. https://doi.org/10.1039/C8TA05329D.

6. NMR Spectra

^{13}C CP-MAS NMR for DAPT-CTP$_{sc}$

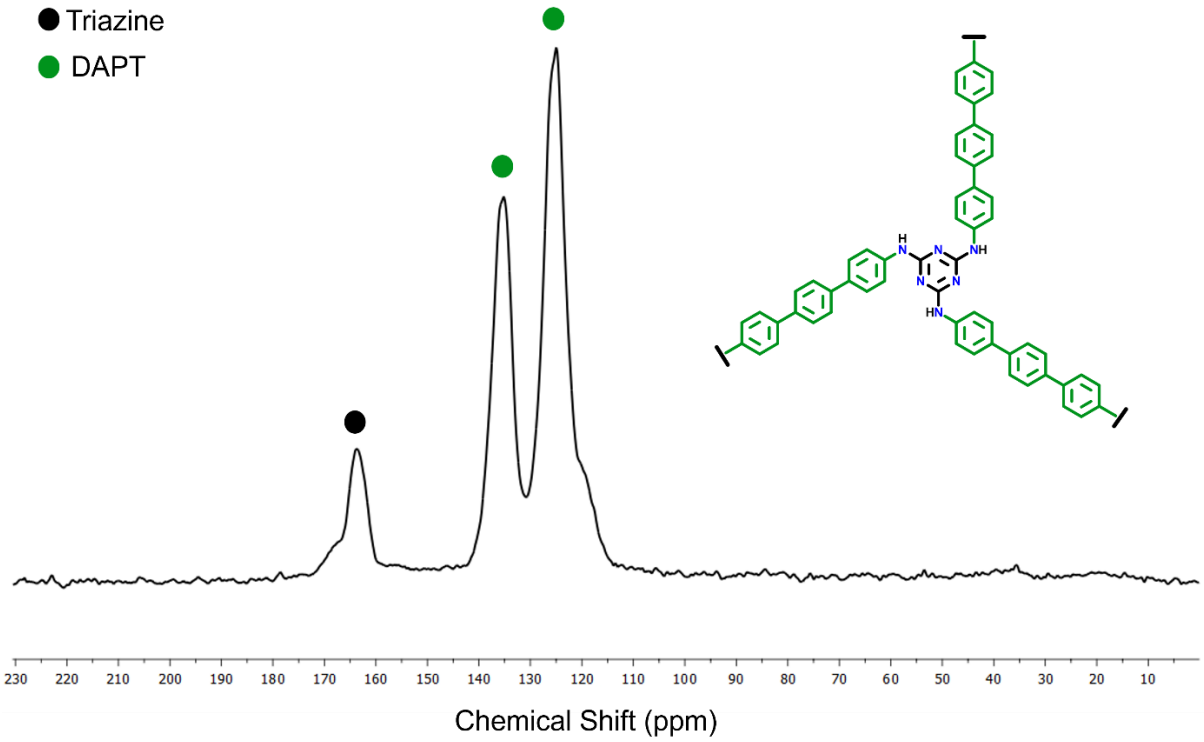

^{1}H-NMR (400 MHz, $CDCl_3$) spectrum of 2a

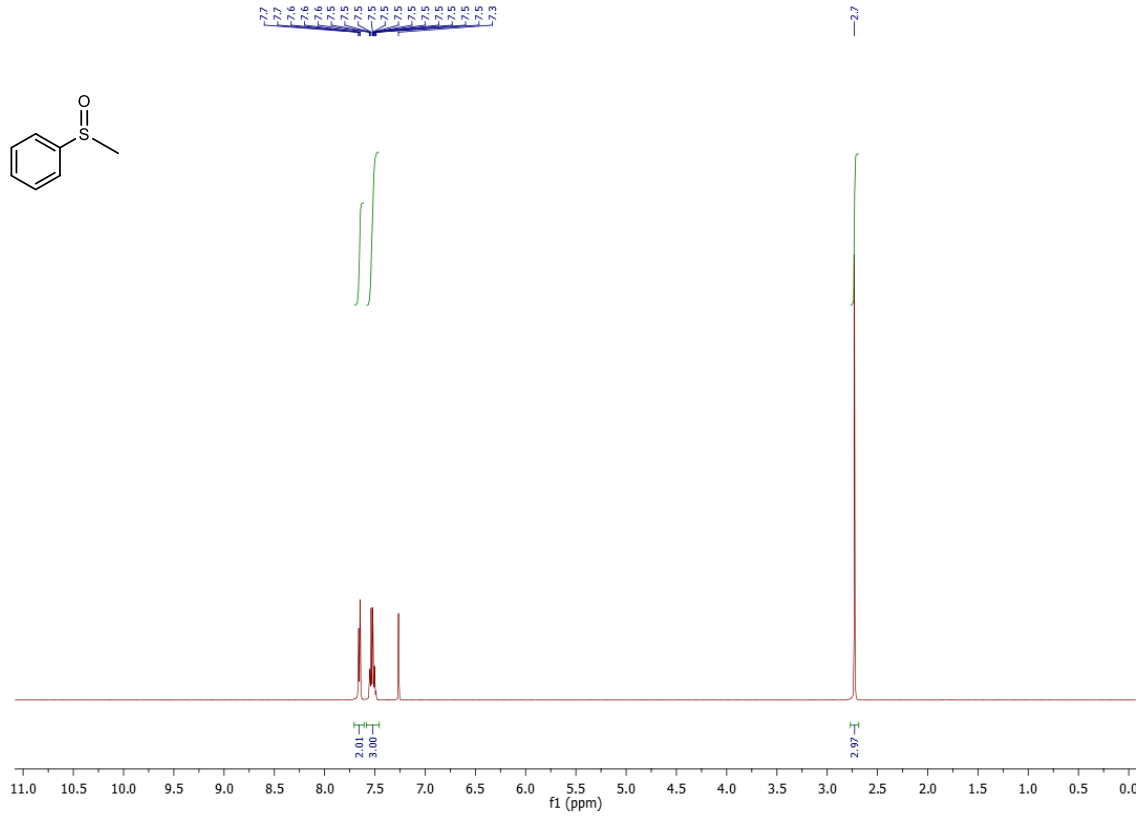

^{13}C-NMR (101 MHz, $CDCl_3$) spectrum of 2a

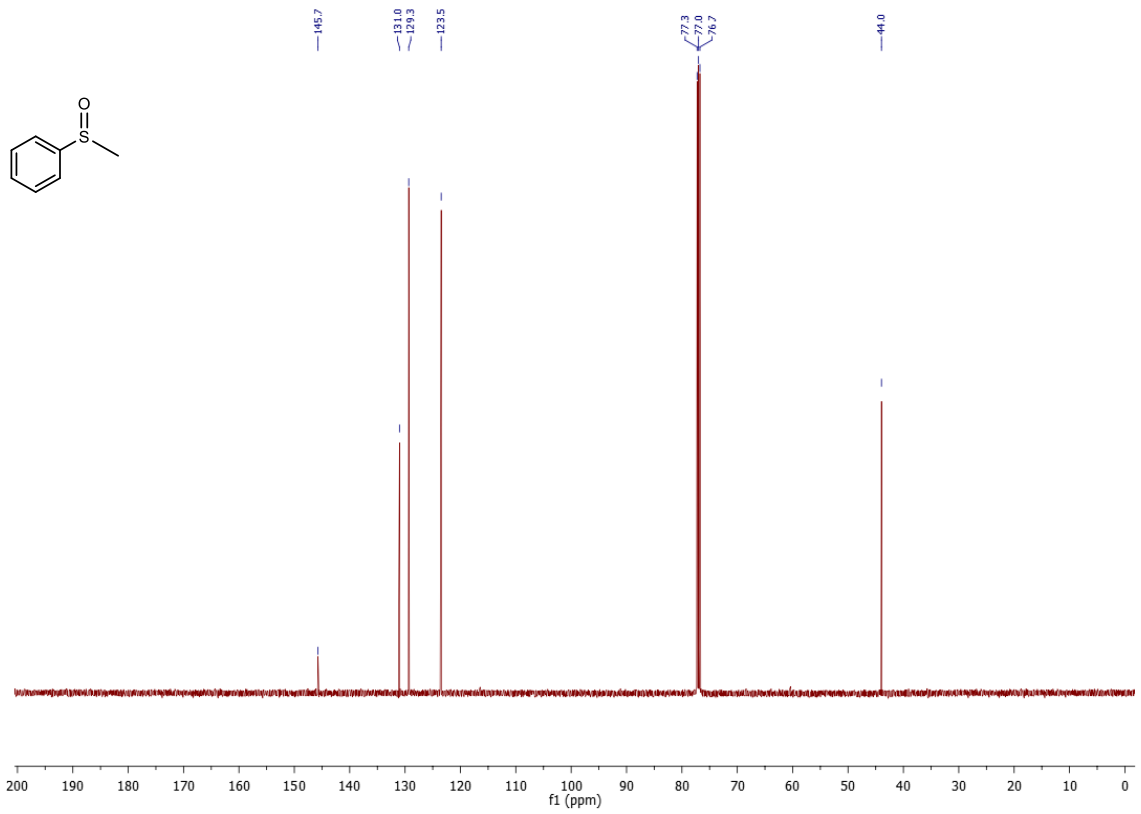

^{1}H-NMR (300 MHz, $CDCl_3$) spectrum of 3a

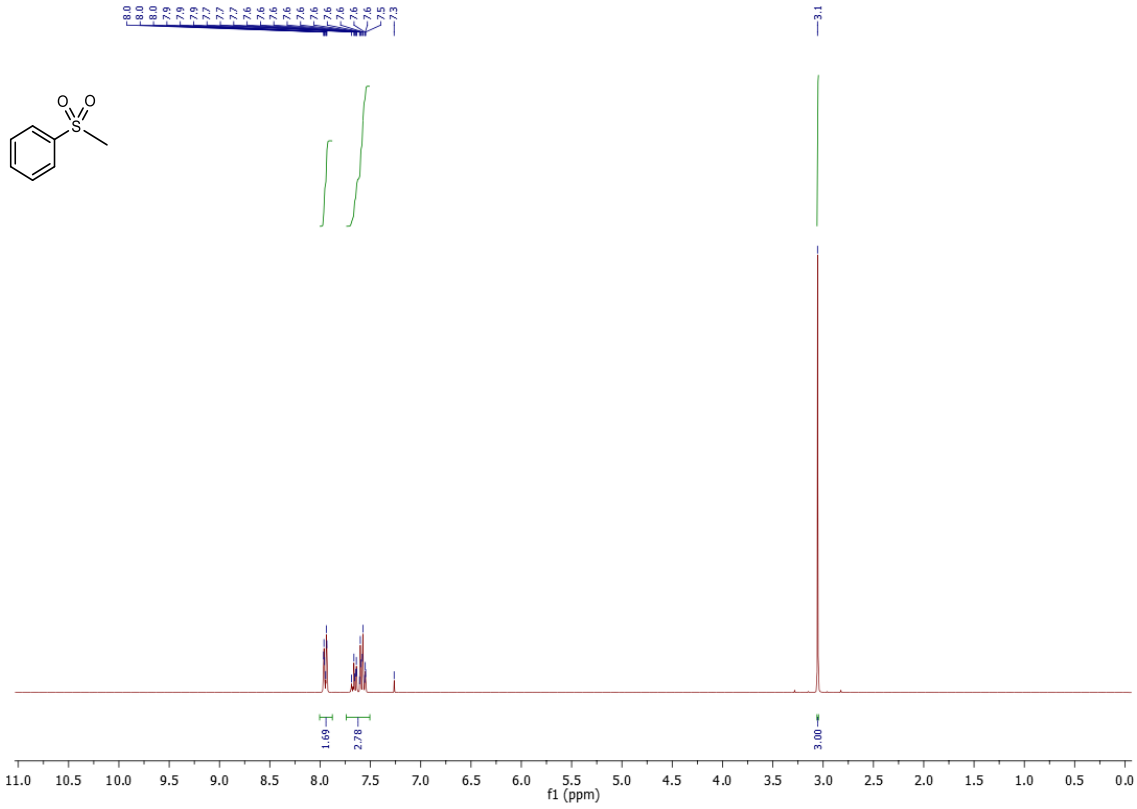

^{13}C-NMR (101 MHz, $CDCl_3$) spectrum of 3a

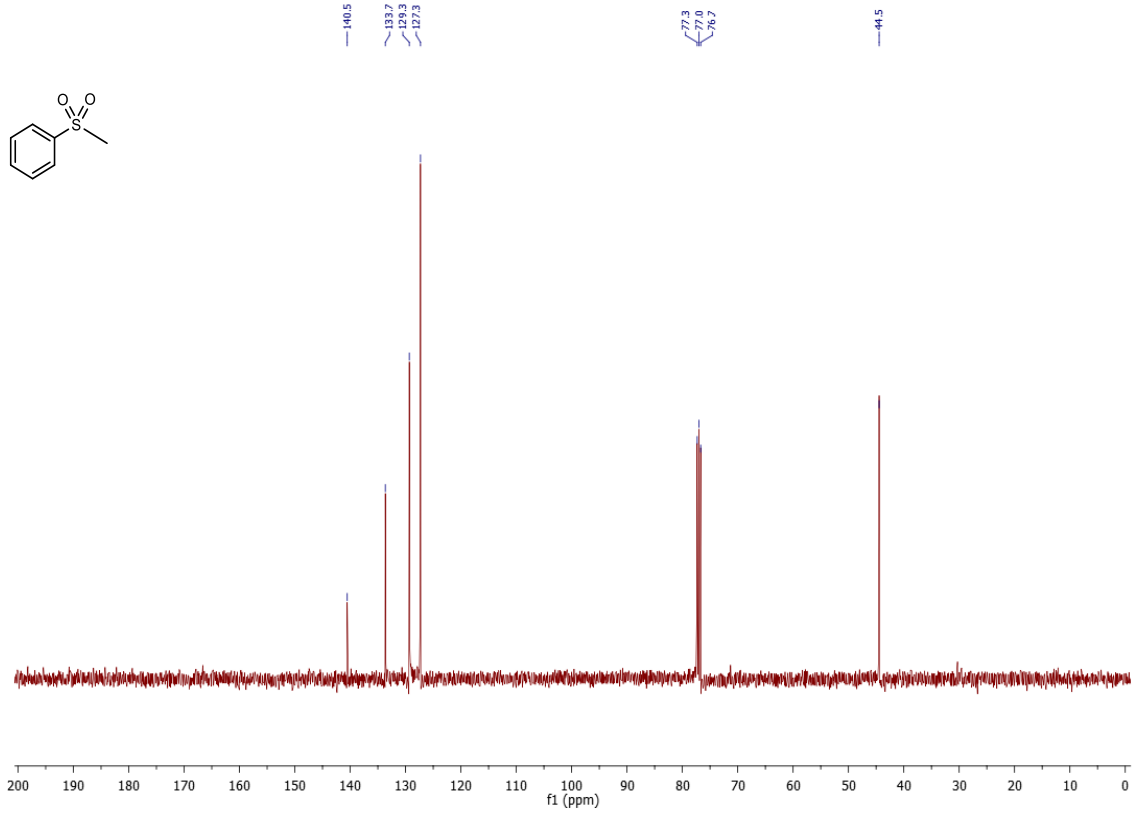

^{1}H-NMR (300 MHz, CD_3OD) spectrum of 2b

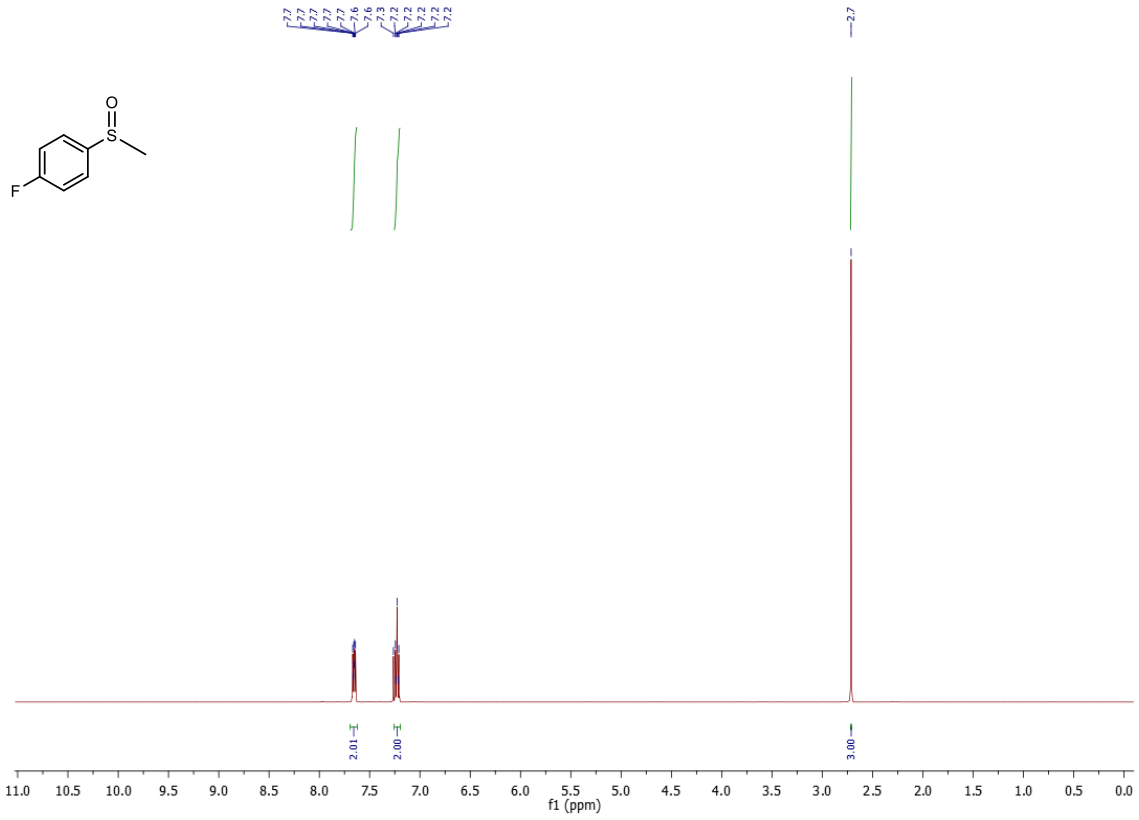

^{13}C-NMR (101 MHz, $CDCl_3$) spectrum of 2b

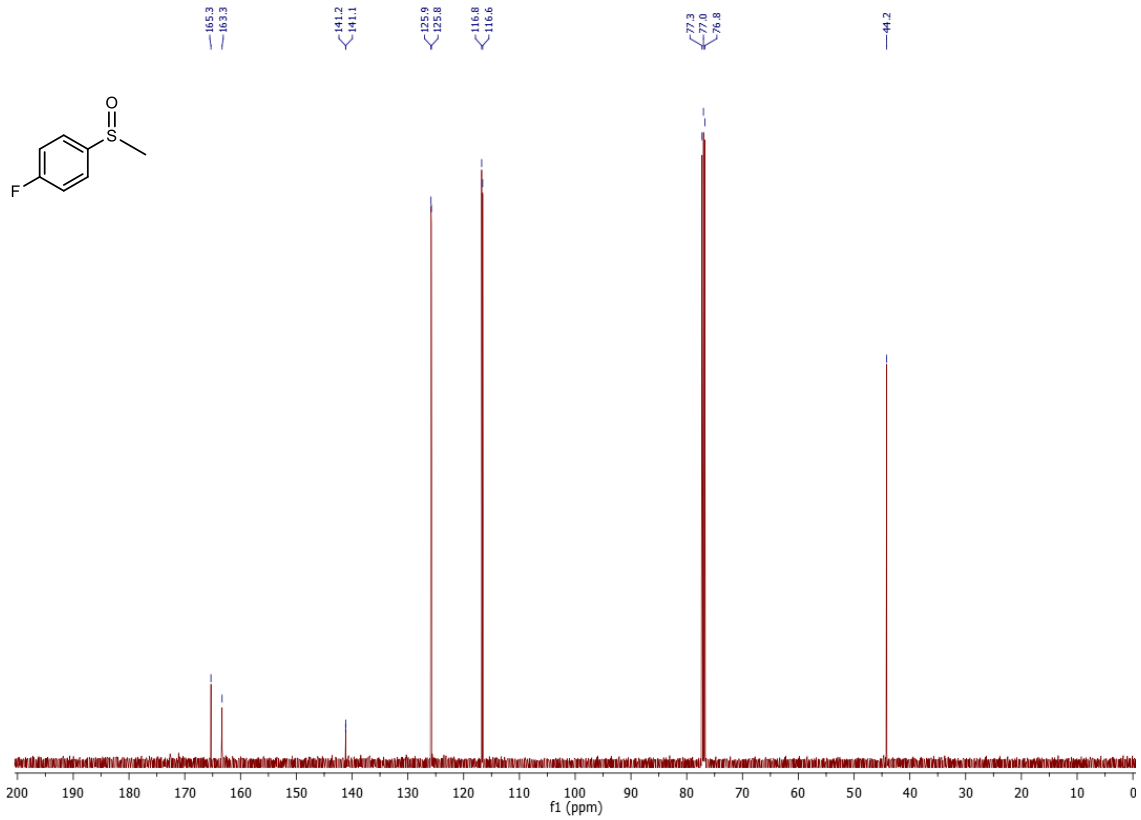

^{19}F-NMR (470 MHz, $CDCl_3$) spectrum of 2b

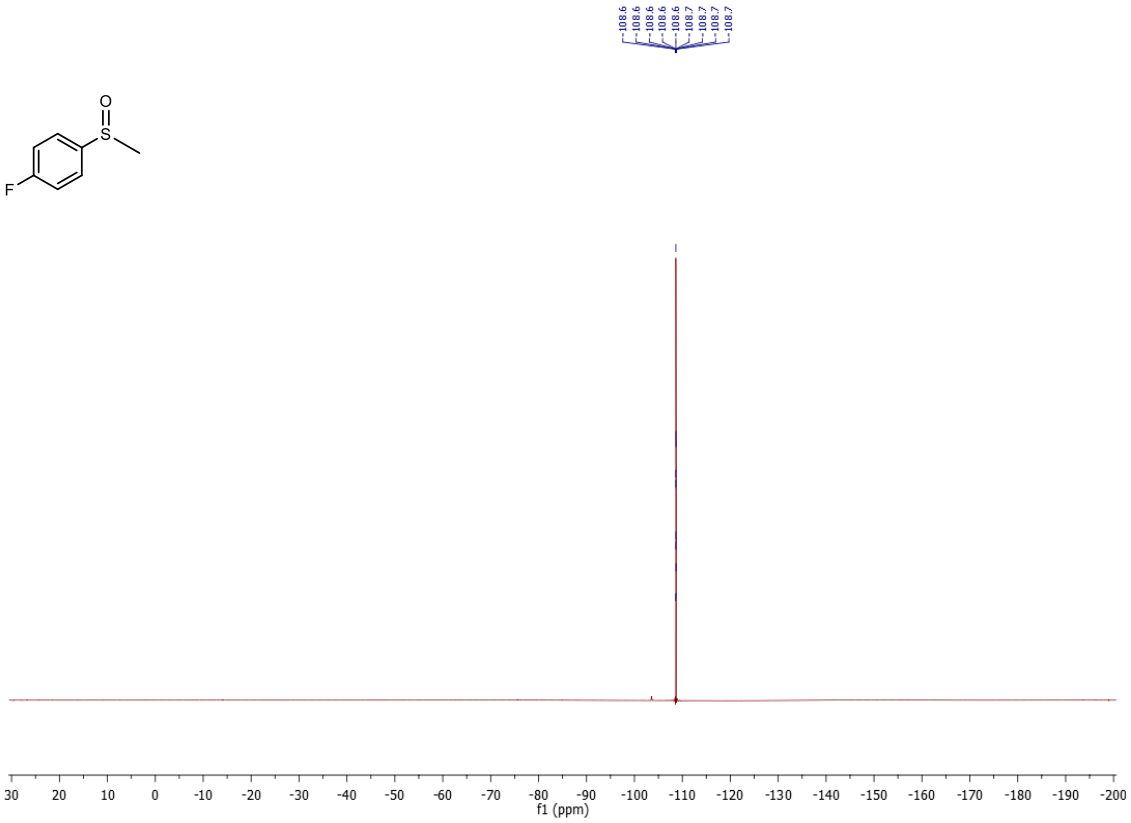

^{1}H-NMR (300 MHz, $CDCl_3$) spectrum of 3b

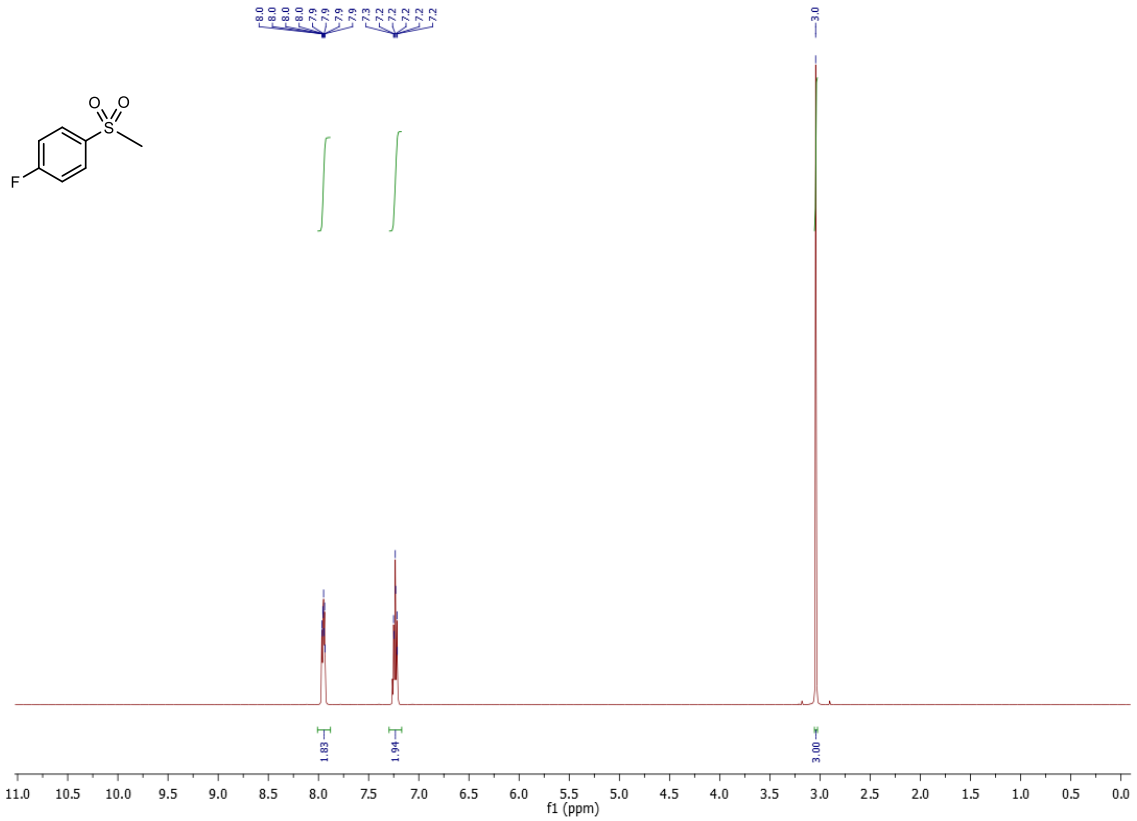

^{13}C-NMR (101 MHz, $CDCl_3$) spectrum of 3b

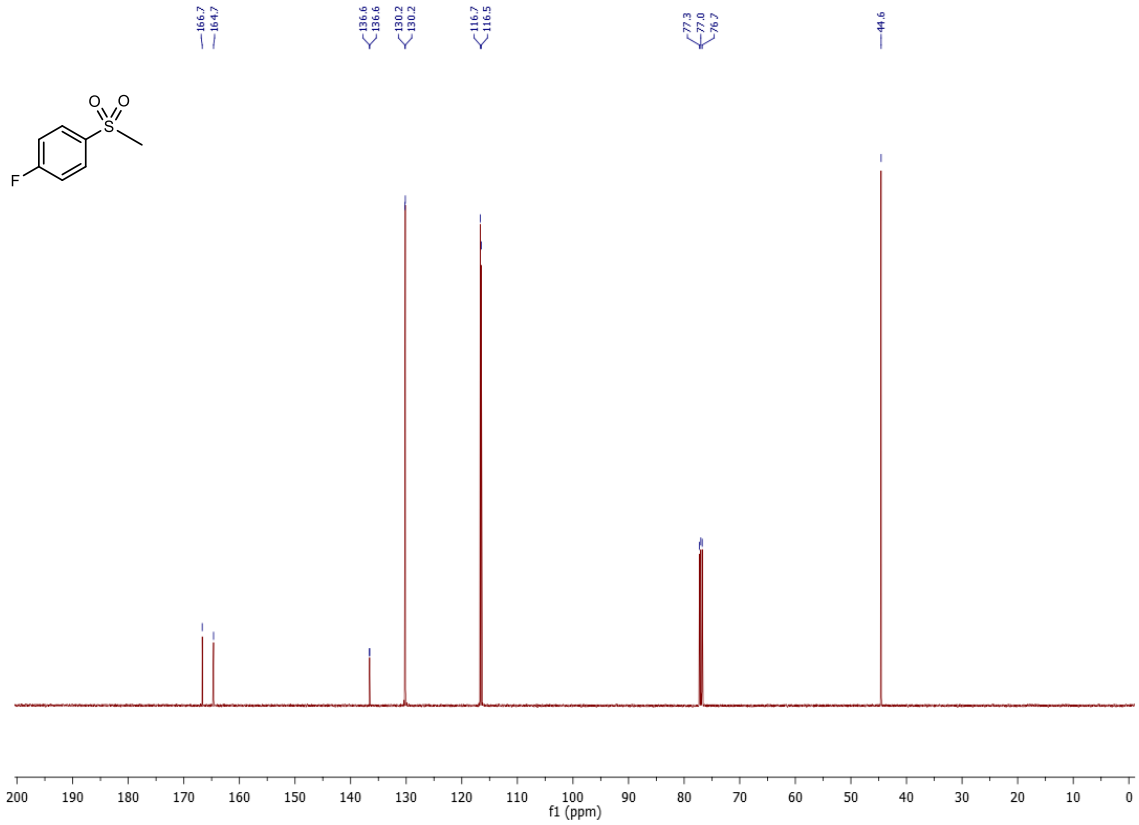

^{19}F-NMR (376 MHz, $CDCl_3$) spectrum of 3b

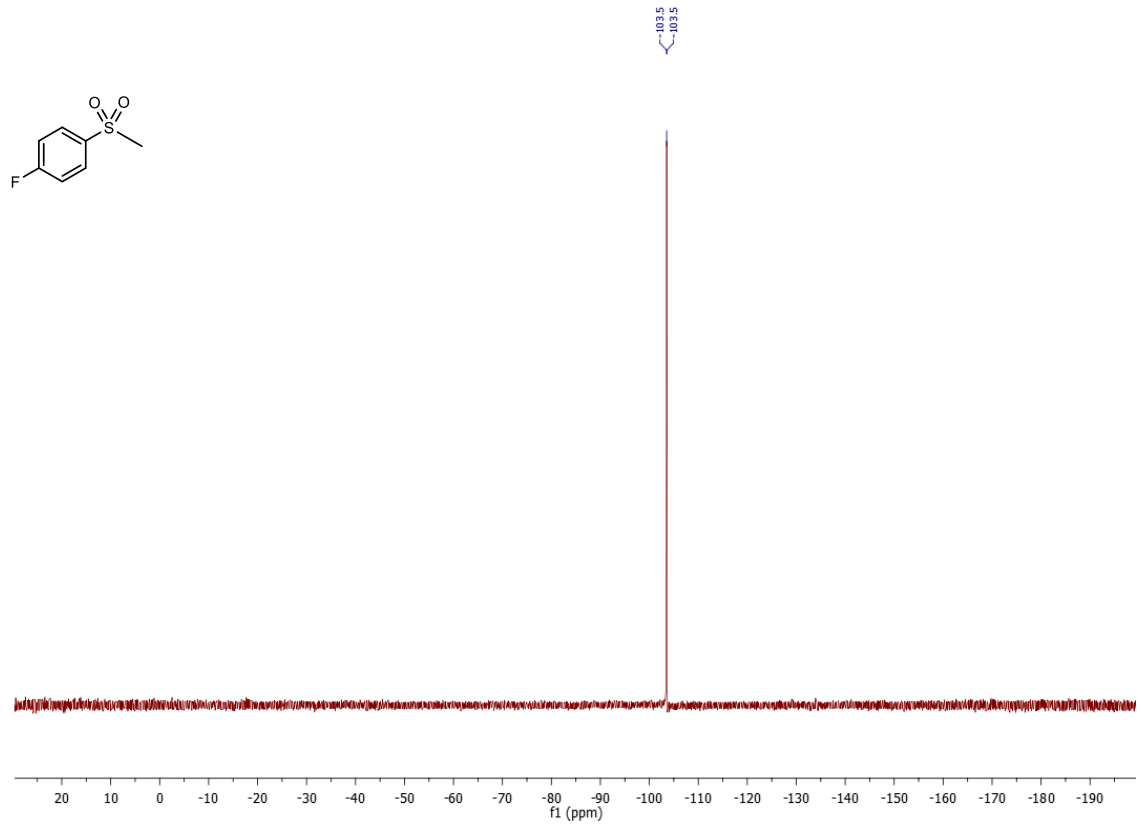

^{1}H-NMR (400 MHz, $CDCl_3$) spectrum of 2c

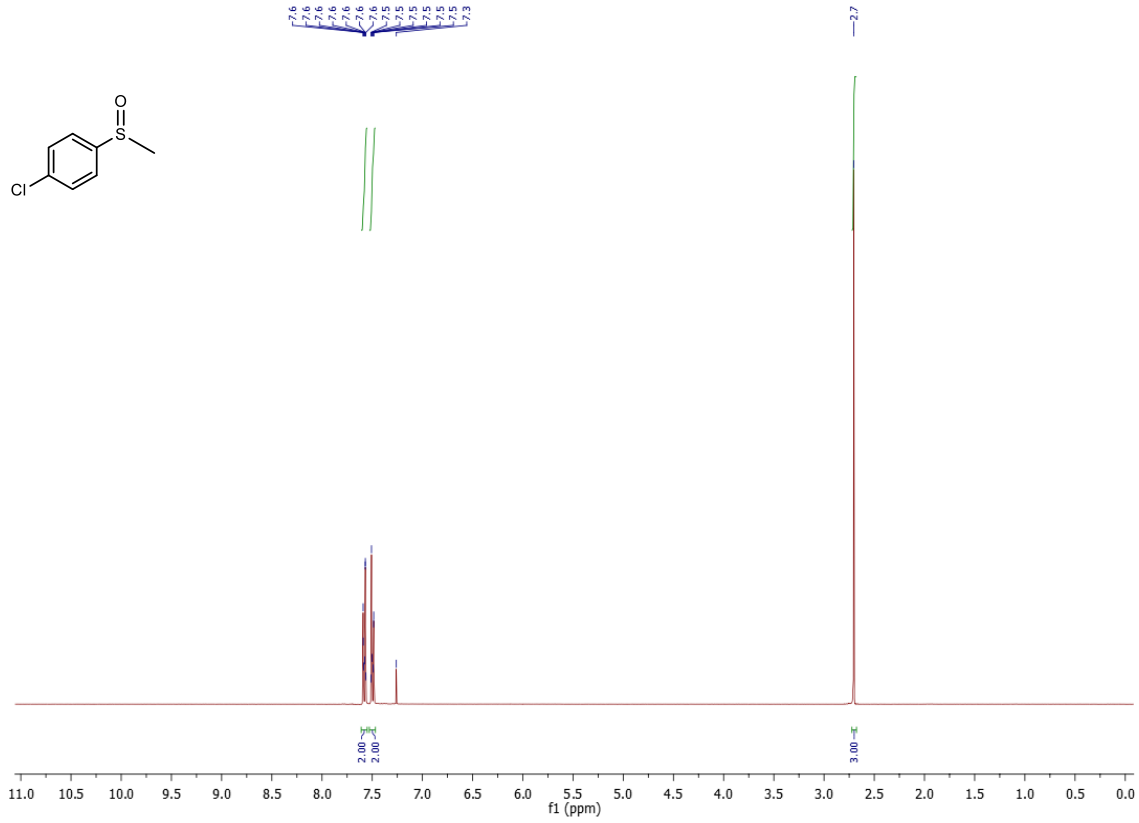

^{13}C-NMR (101 MHz, $CDCl_3$) spectrum of 2c

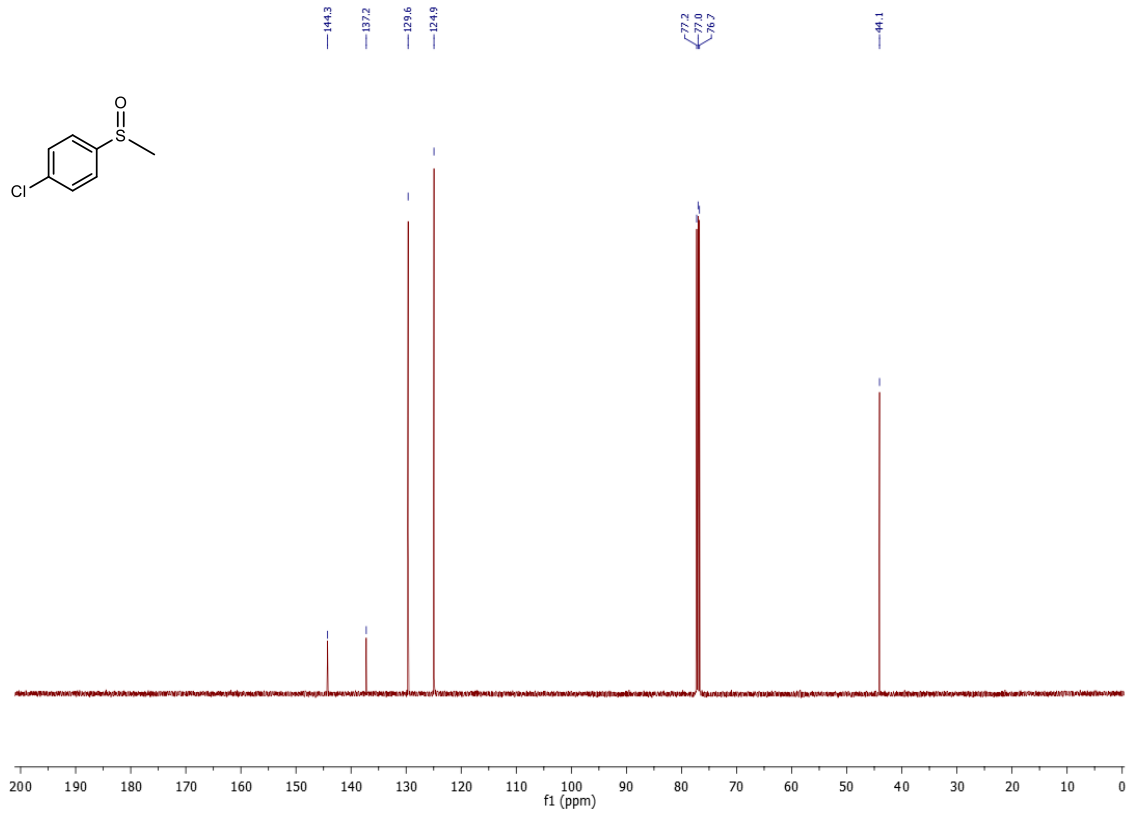

^{1}H-NMR (300 MHz, $CDCl_3$) spectrum of 3c

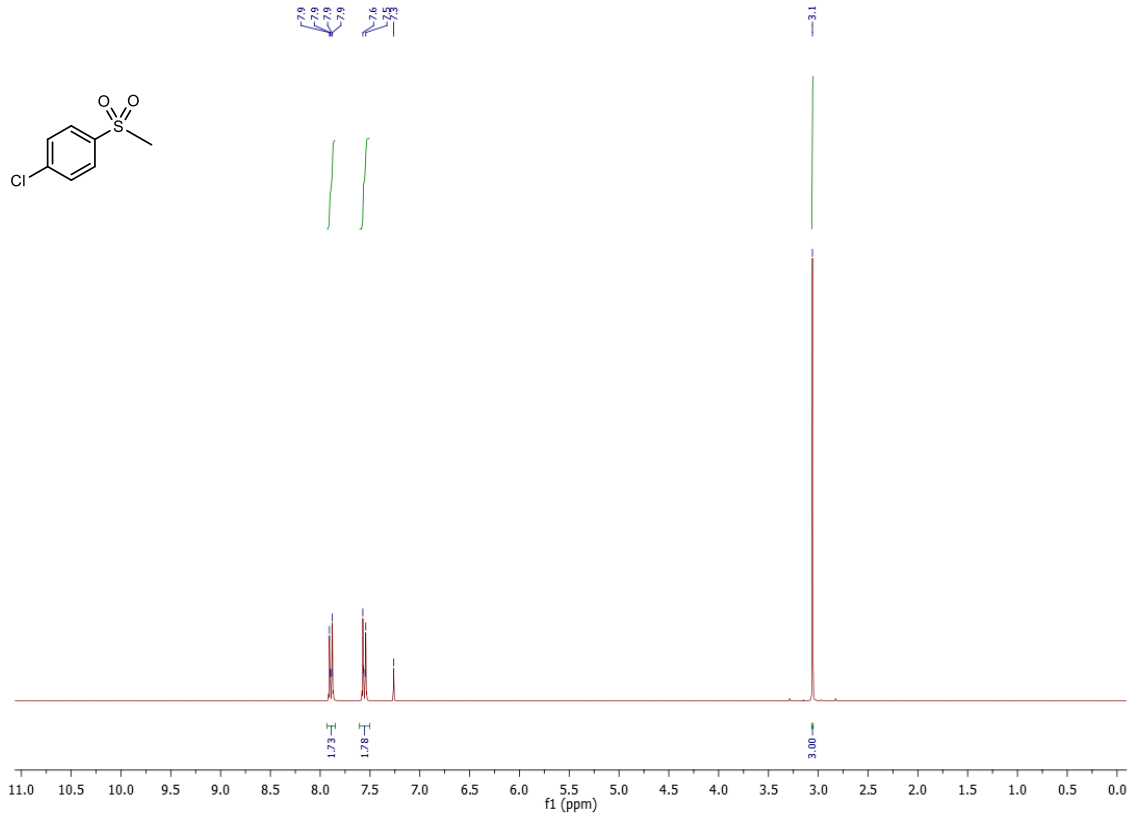

^{13}C-NMR (101 MHz, $CDCl_3$) spectrum of 3c

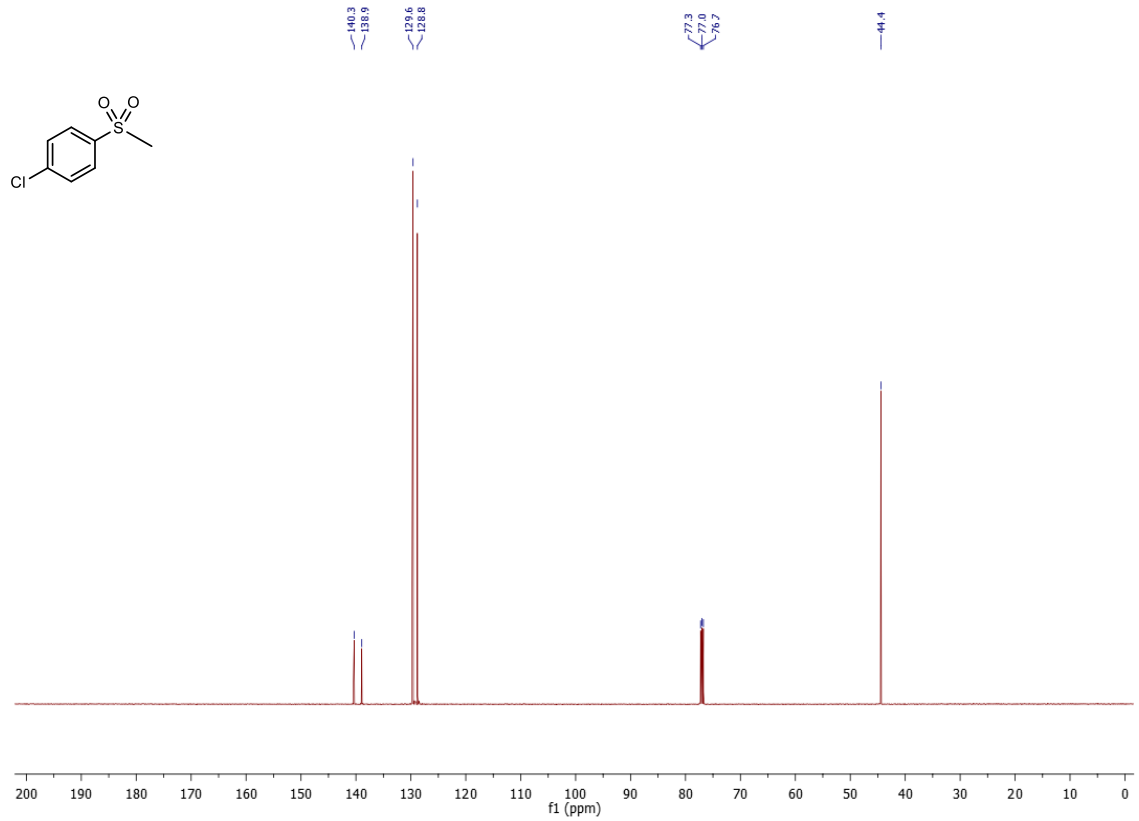

^{1}H-NMR (400 MHz, $CDCl_3$) spectrum of 2d

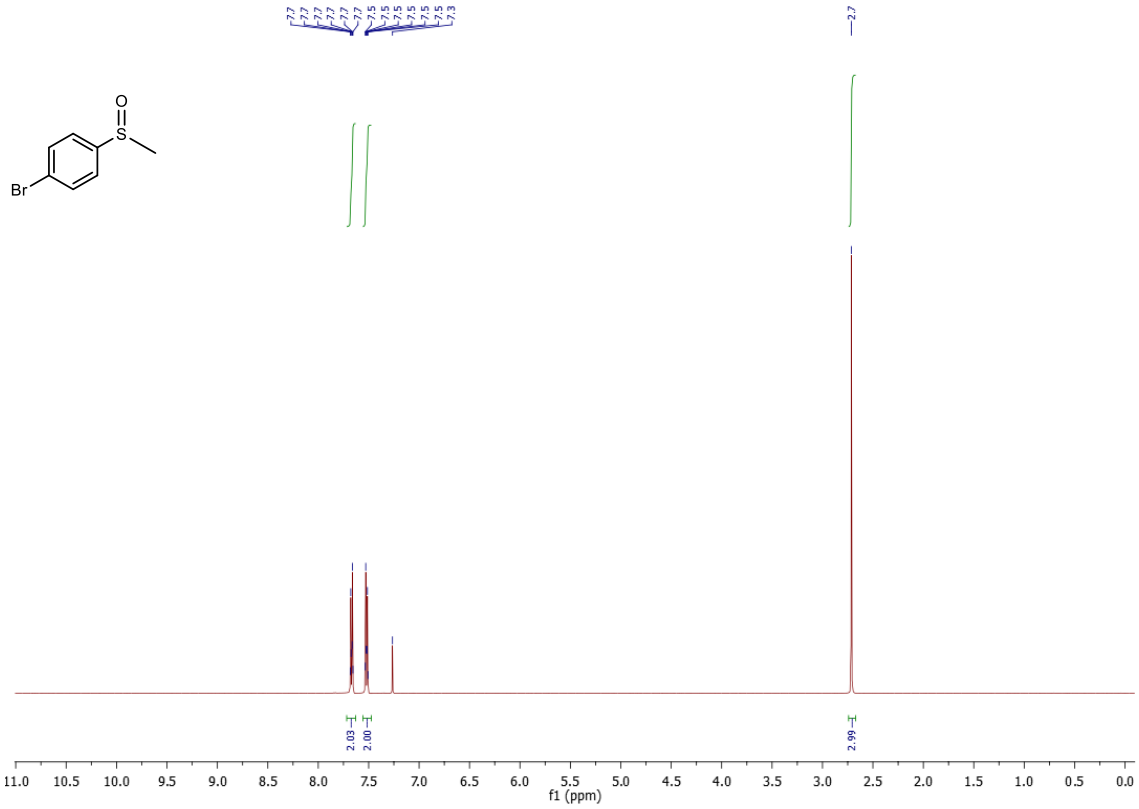

^{13}C-NMR (101 MHz, $CDCl_3$) spectrum of 2d

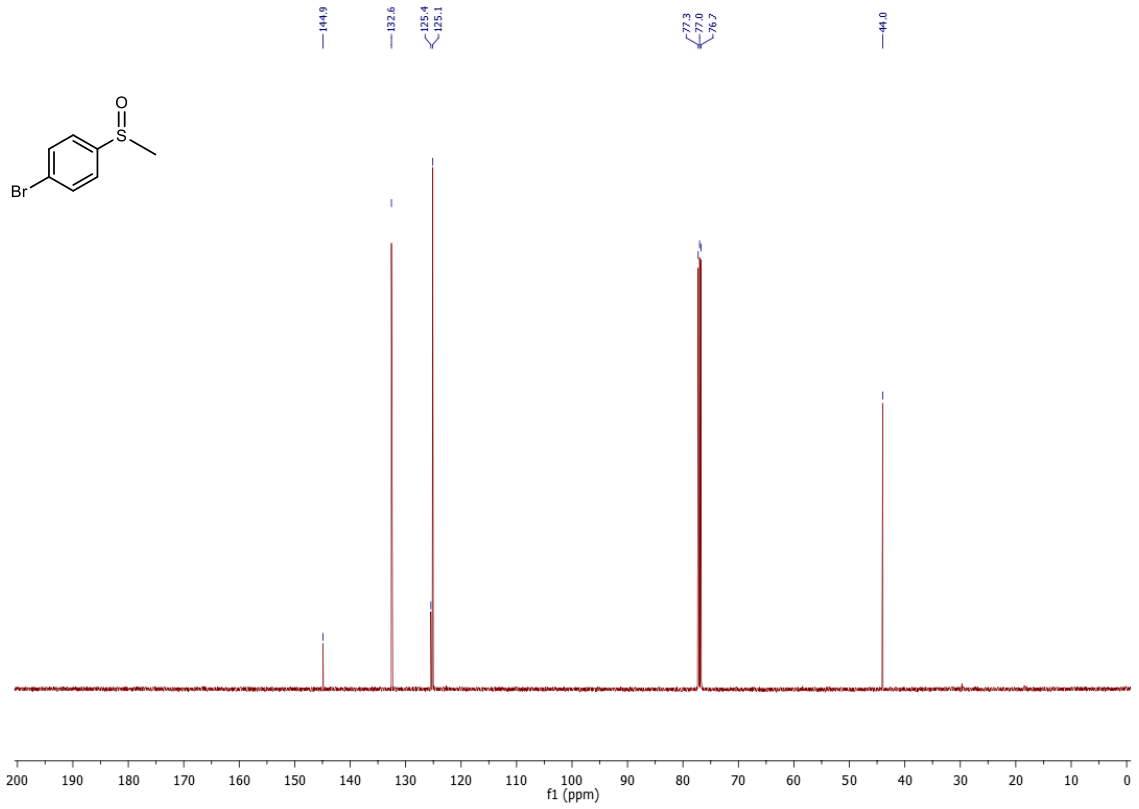

^{1}H-NMR (300 MHz, $CDCl_3$) spectrum of 3d

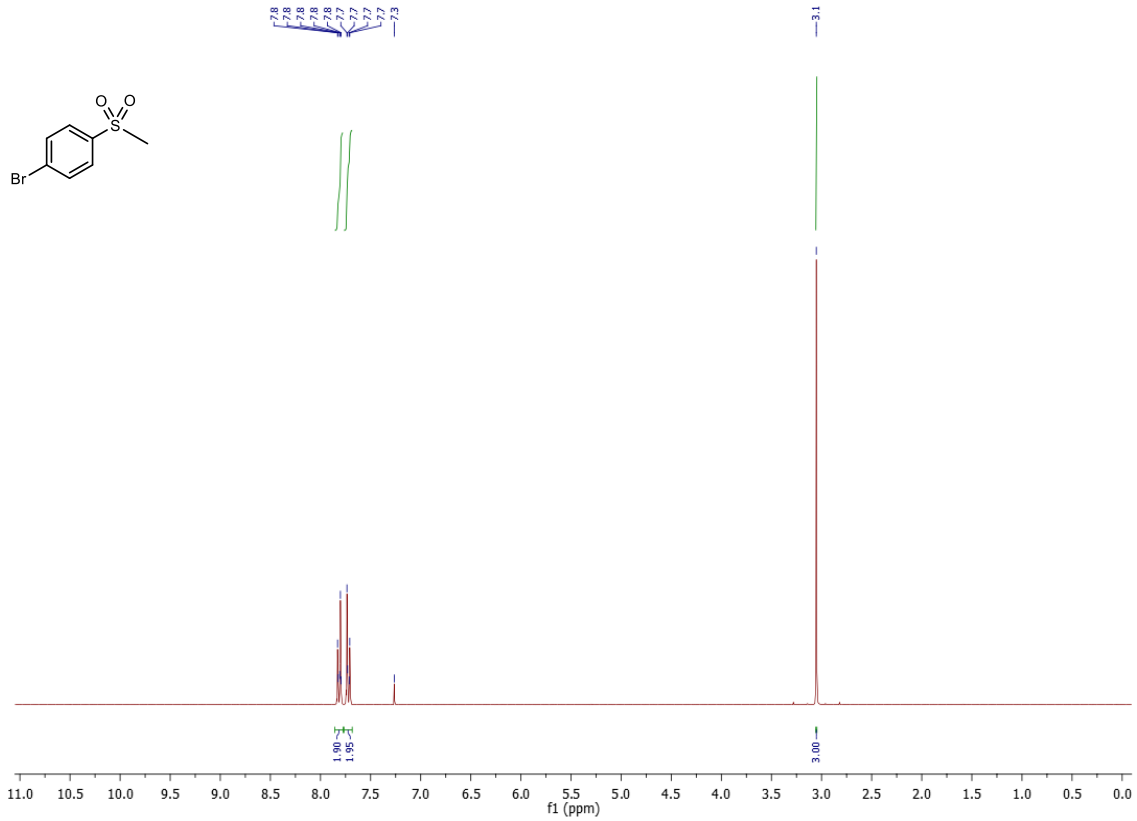

^{13}C-NMR (101 MHz, $CDCl_3$) spectrum of 3d

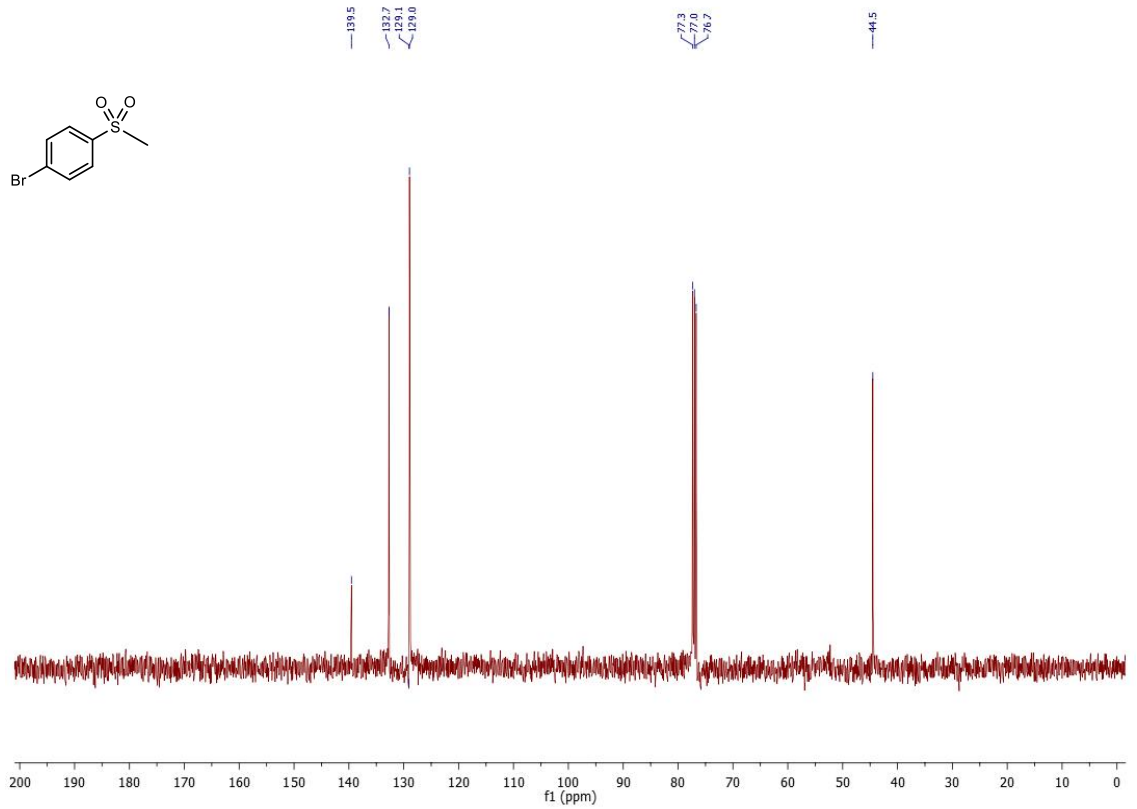

^{1}H-NMR (400 MHz, $CDCl_3$) spectrum of 2e

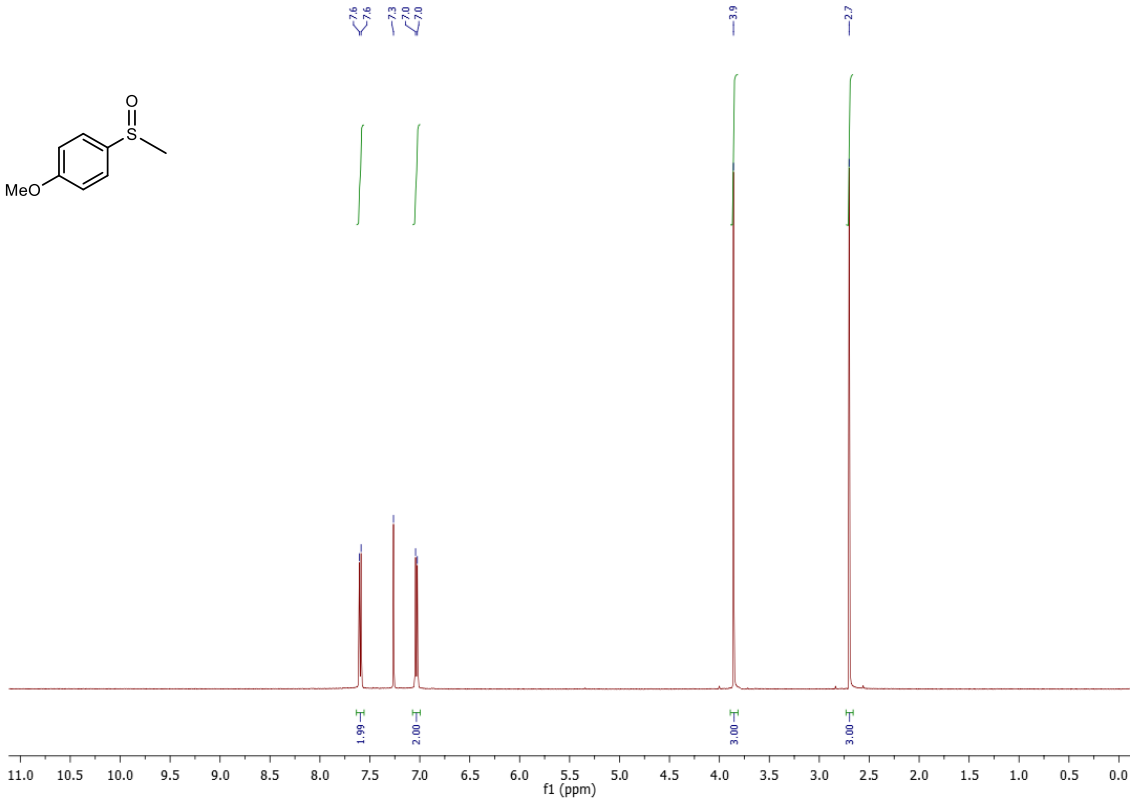

^{13}C-NMR (101 MHz, $CDCl_3$) spectrum of 2e

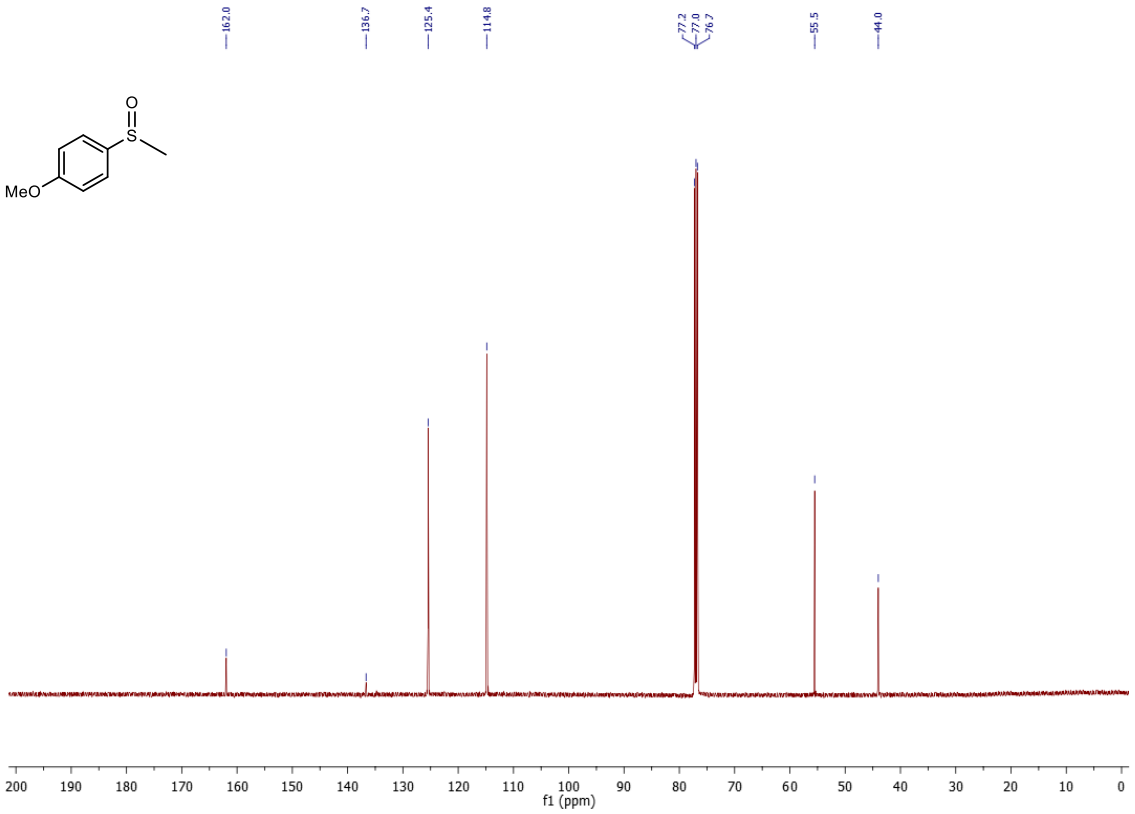

^{1}H-NMR (400 MHz, $CDCl_3$) spectrum of 3e

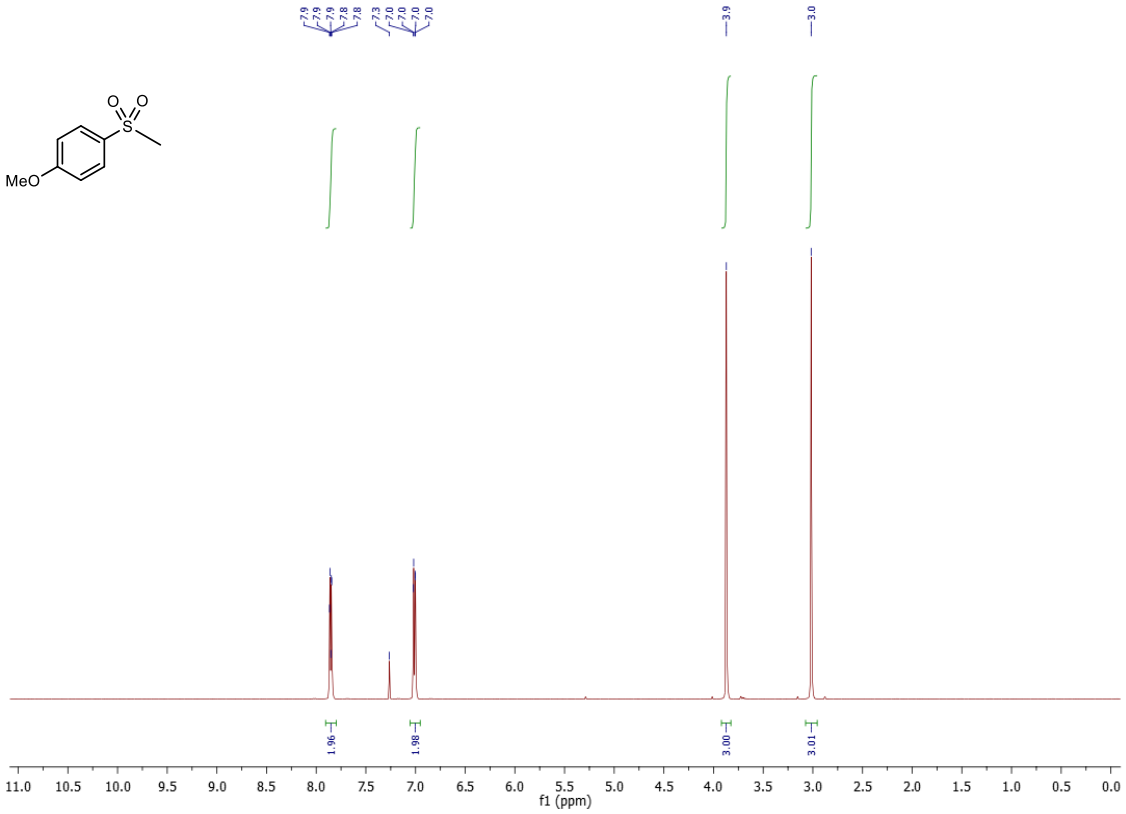

^{13}C-NMR (101 MHz, $CDCl_3$) spectrum of 3e

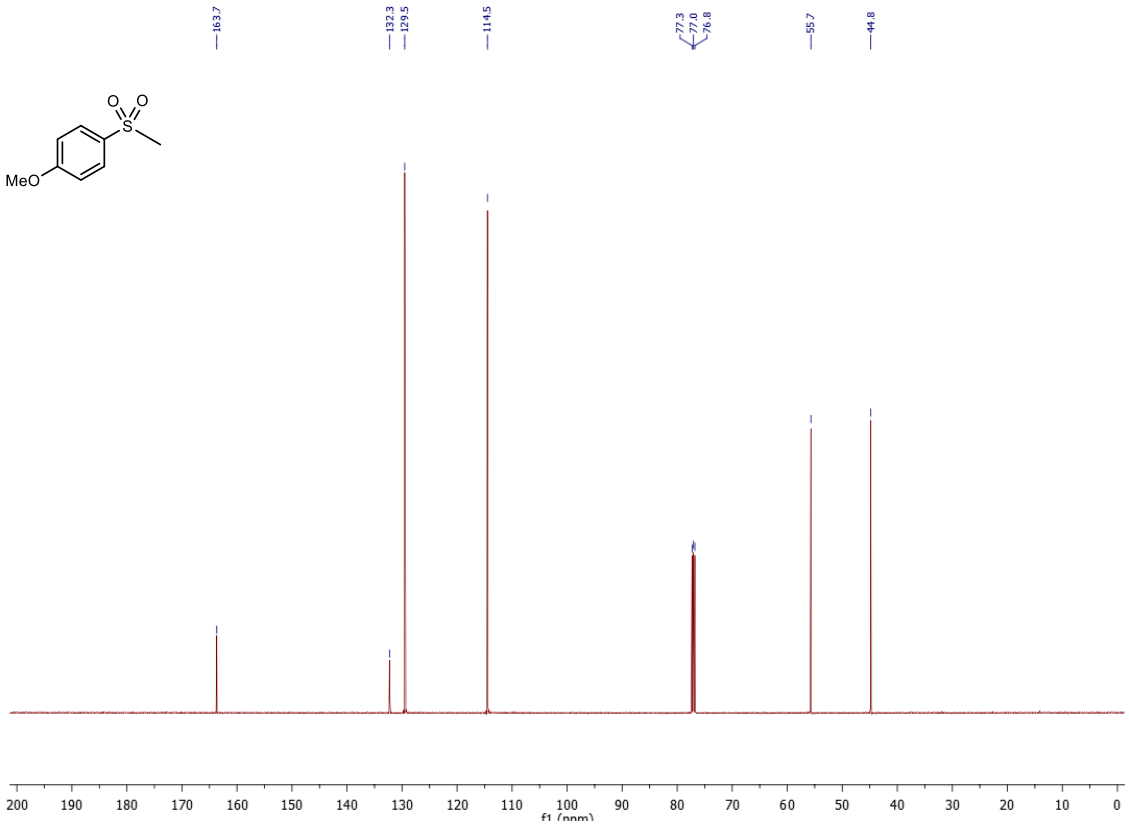

^{1}H-NMR (400 MHz, $CDCl_3$) spectrum of 2f

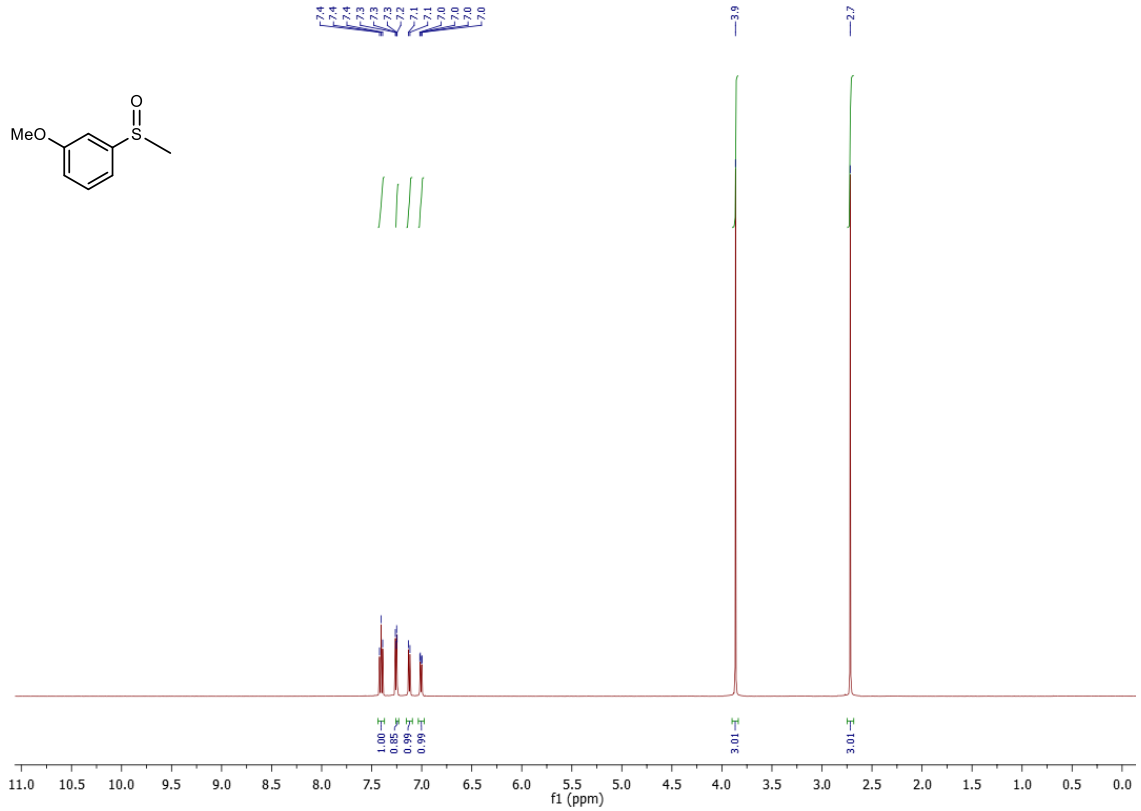

^{13}C-NMR (101 MHz, $CDCl_3$) spectrum of 2f

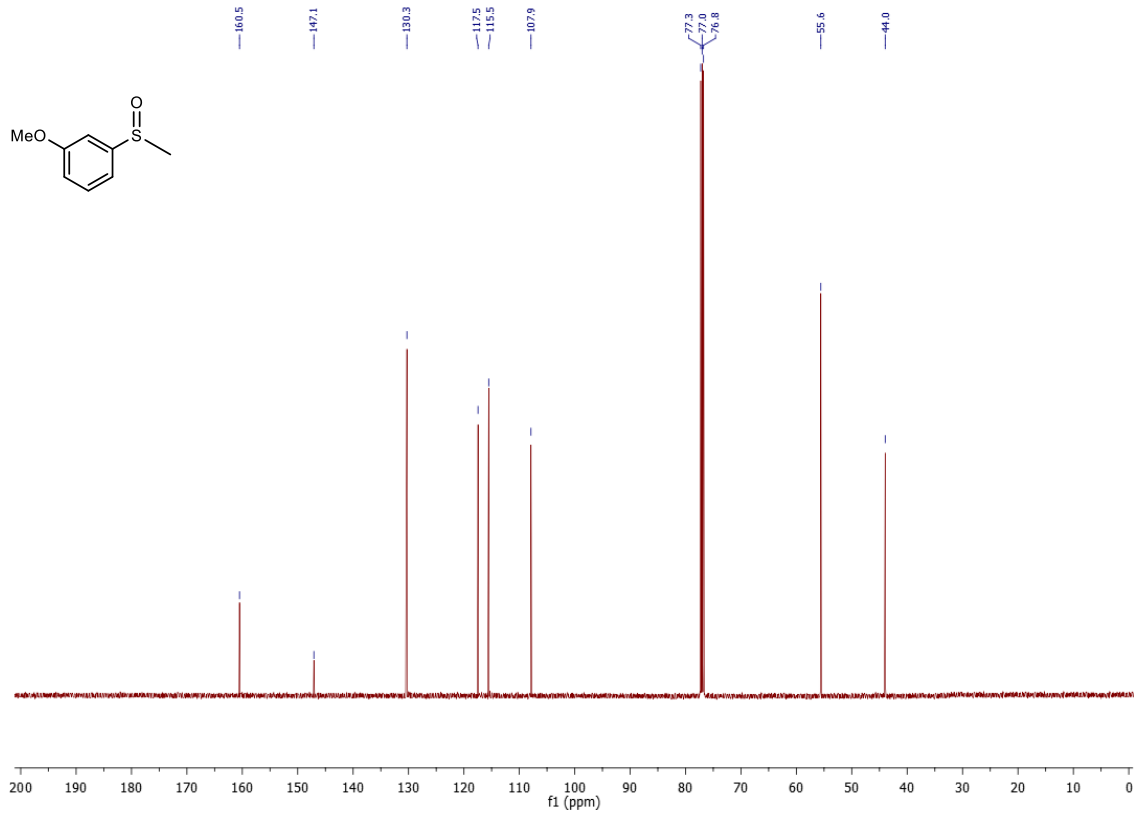

[1]H-NMR (300 MHz, $CDCl_3$) spectrum of 3f

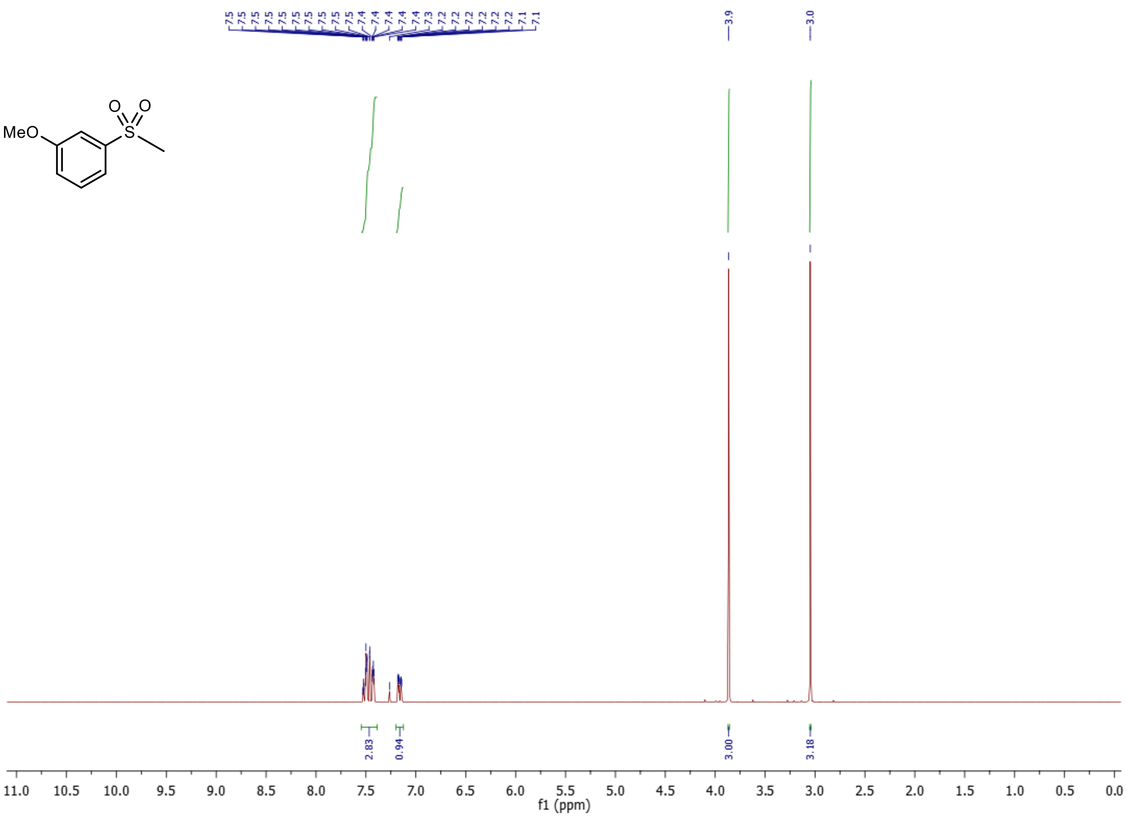

[13]C-NMR (101 MHz, $CDCl_3$) spectrum of 3f

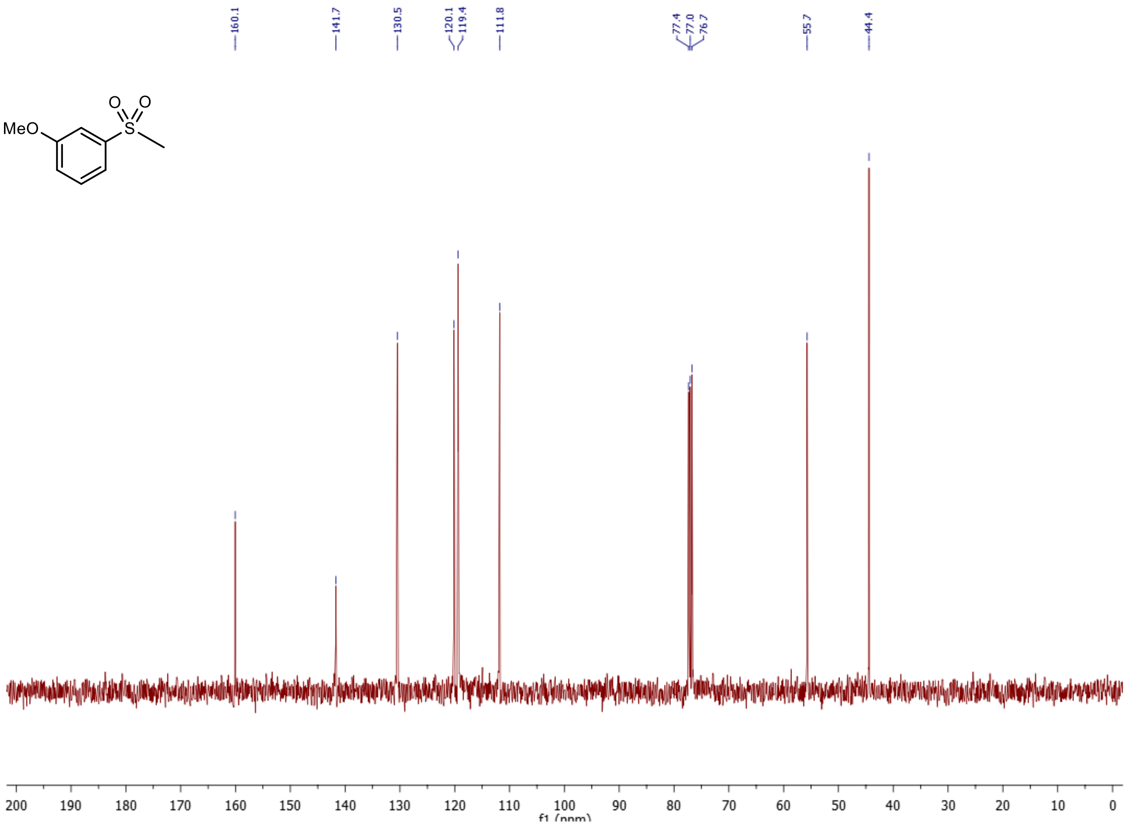

^{1}H-NMR (400 MHz, $CDCl_3$) spectrum of 2g

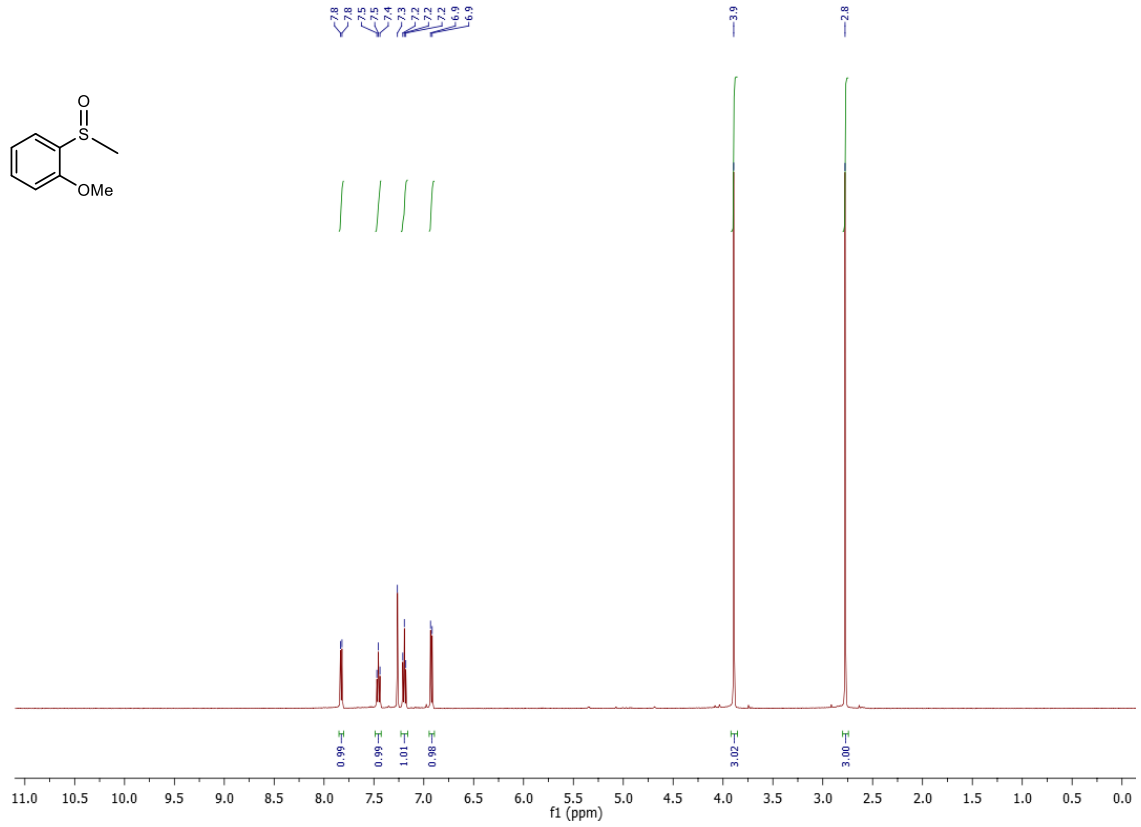

^{13}C-NMR (101 MHz, $CDCl_3$) spectrum of 2g

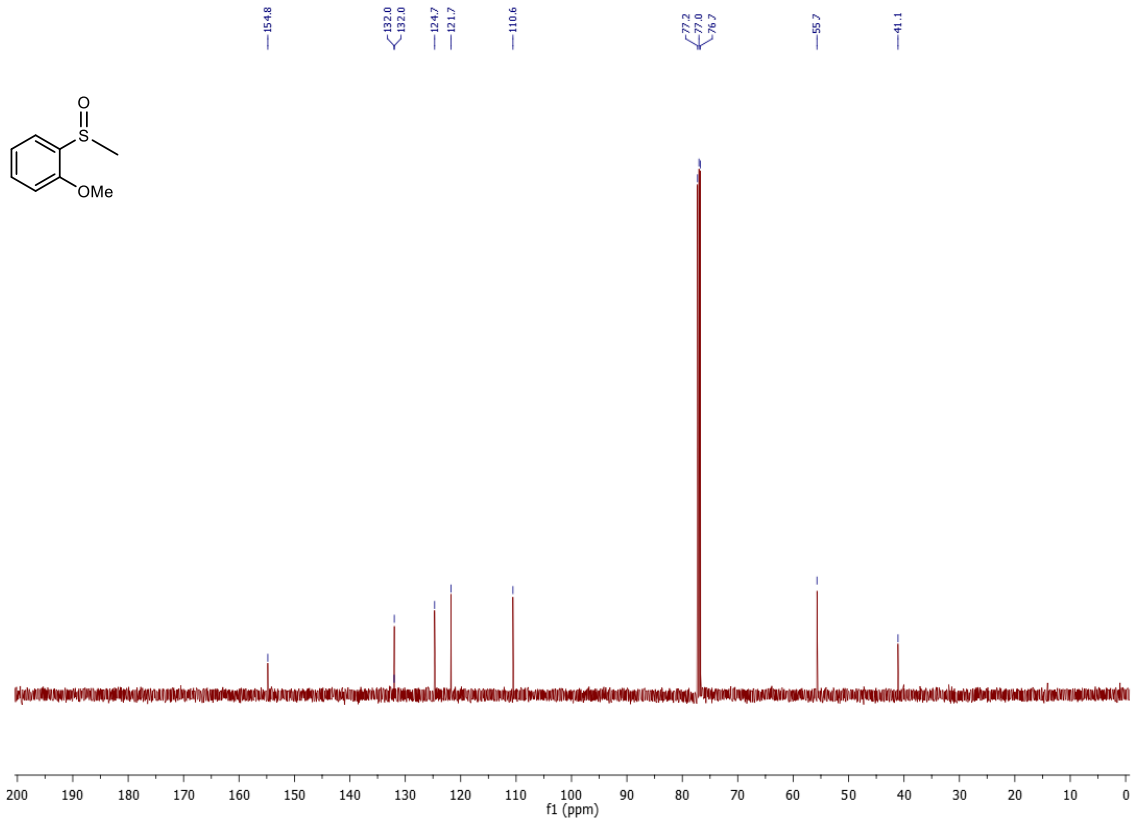

^{1}H-NMR (300 MHz, $CDCl_3$) spectrum of 3g

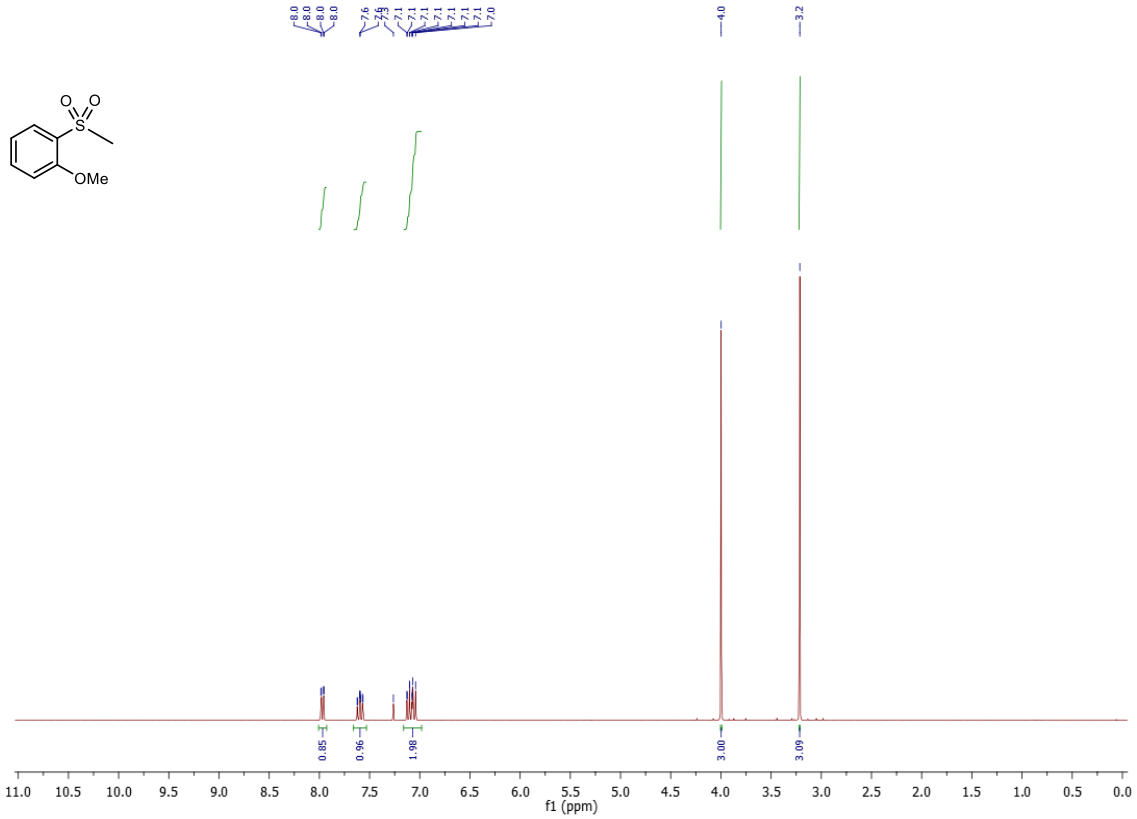

^{13}C-NMR (101 MHz, $CDCl_3$) spectrum of 3g

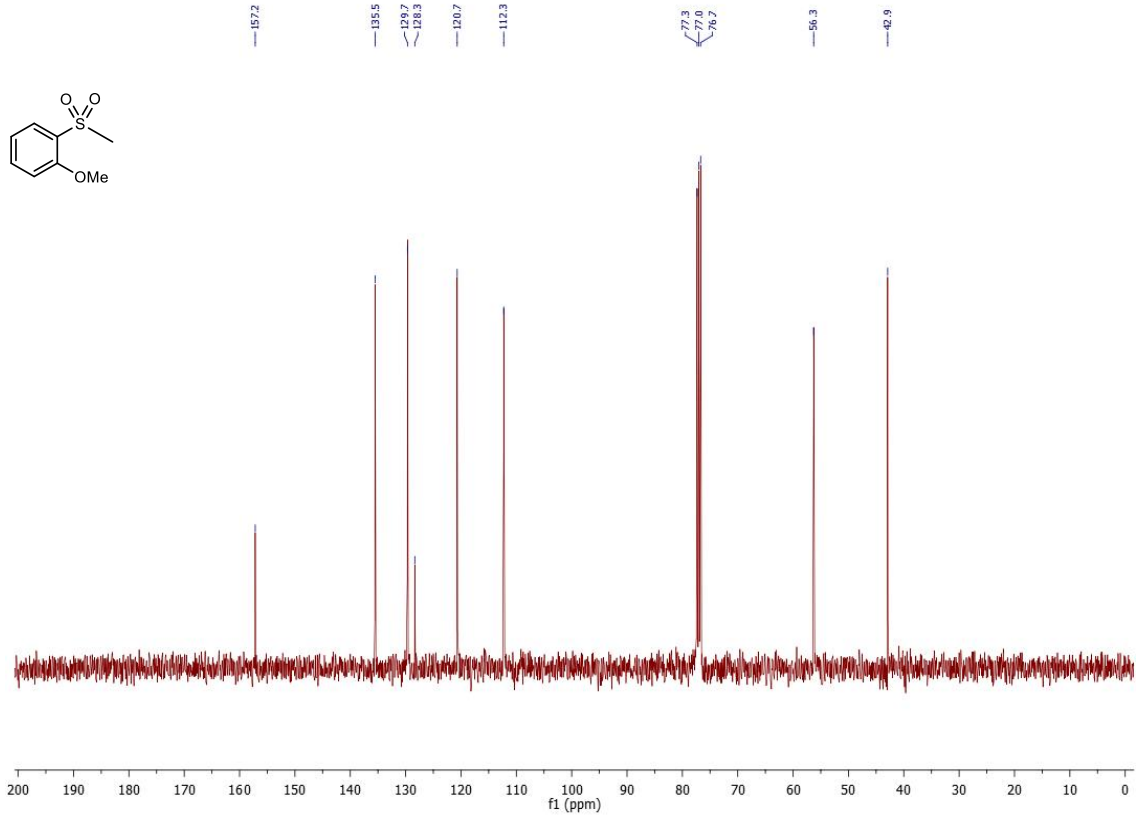

^{1}H-NMR (400 MHz, $CDCl_3$) spectrum of 2h

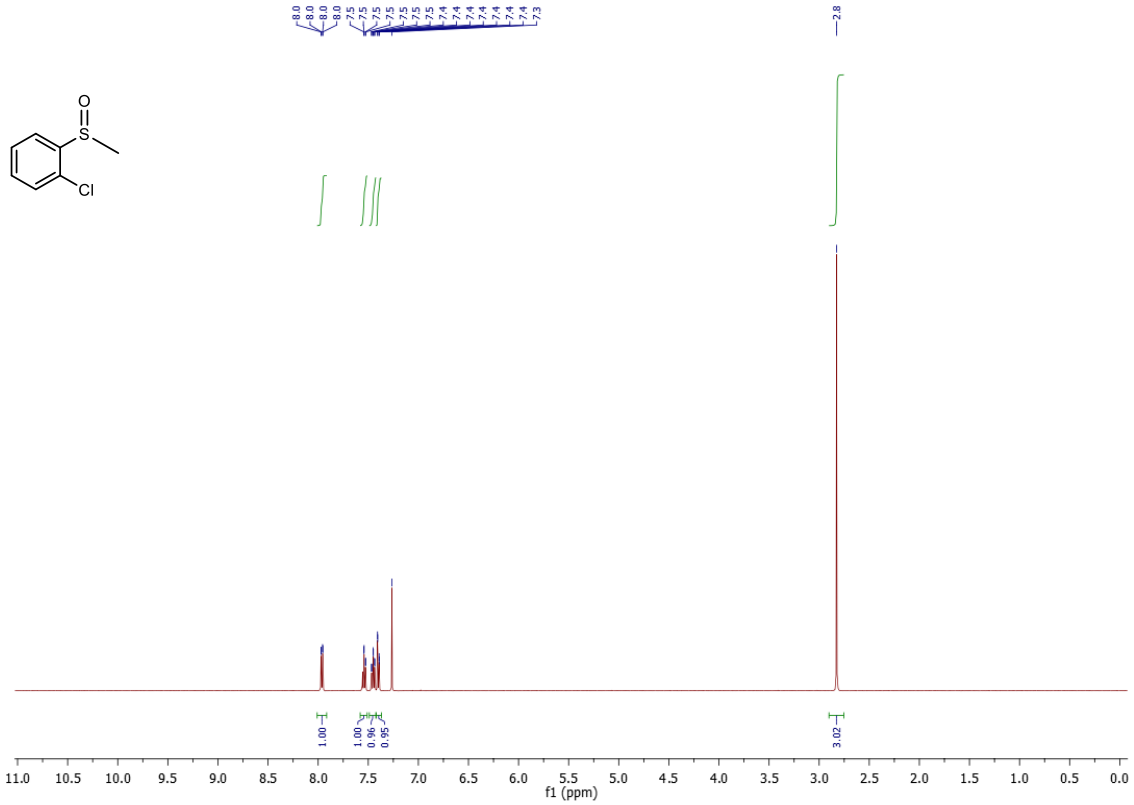

^{13}C-NMR (101 MHz, $CDCl_3$) spectrum of 2h

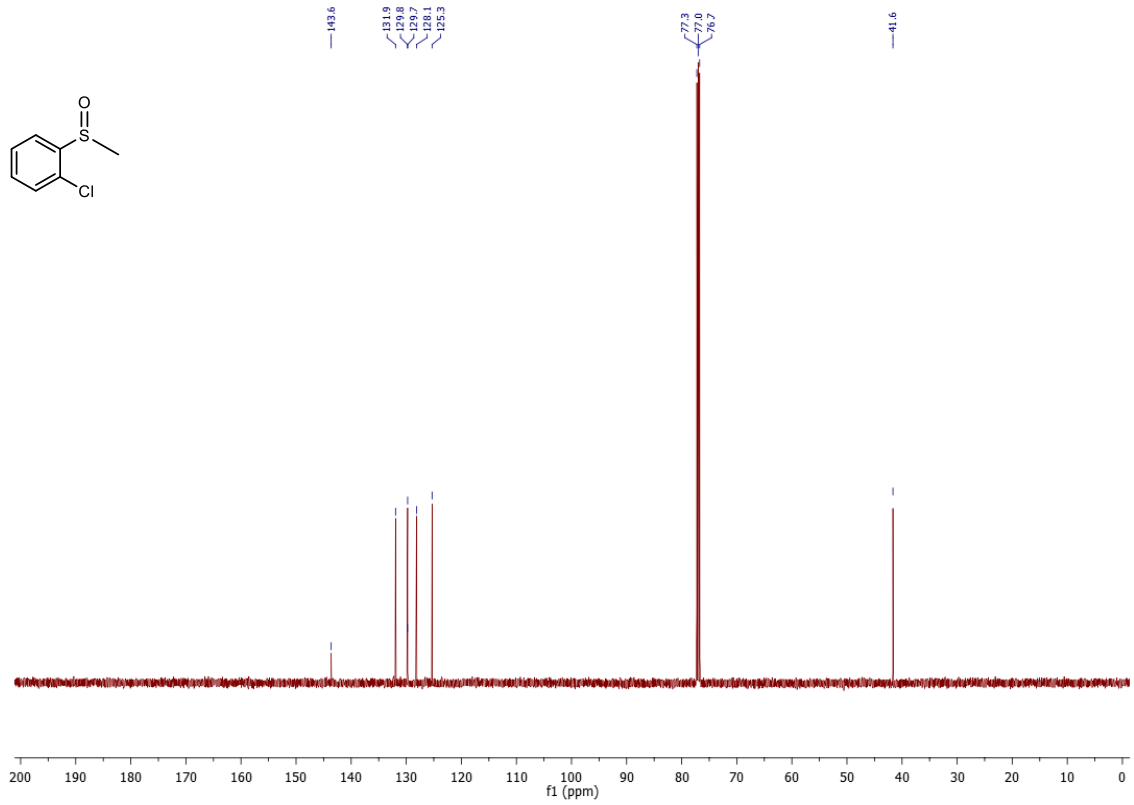

^{1}H-NMR (300 MHz, $CDCl_3$) spectrum of 3h

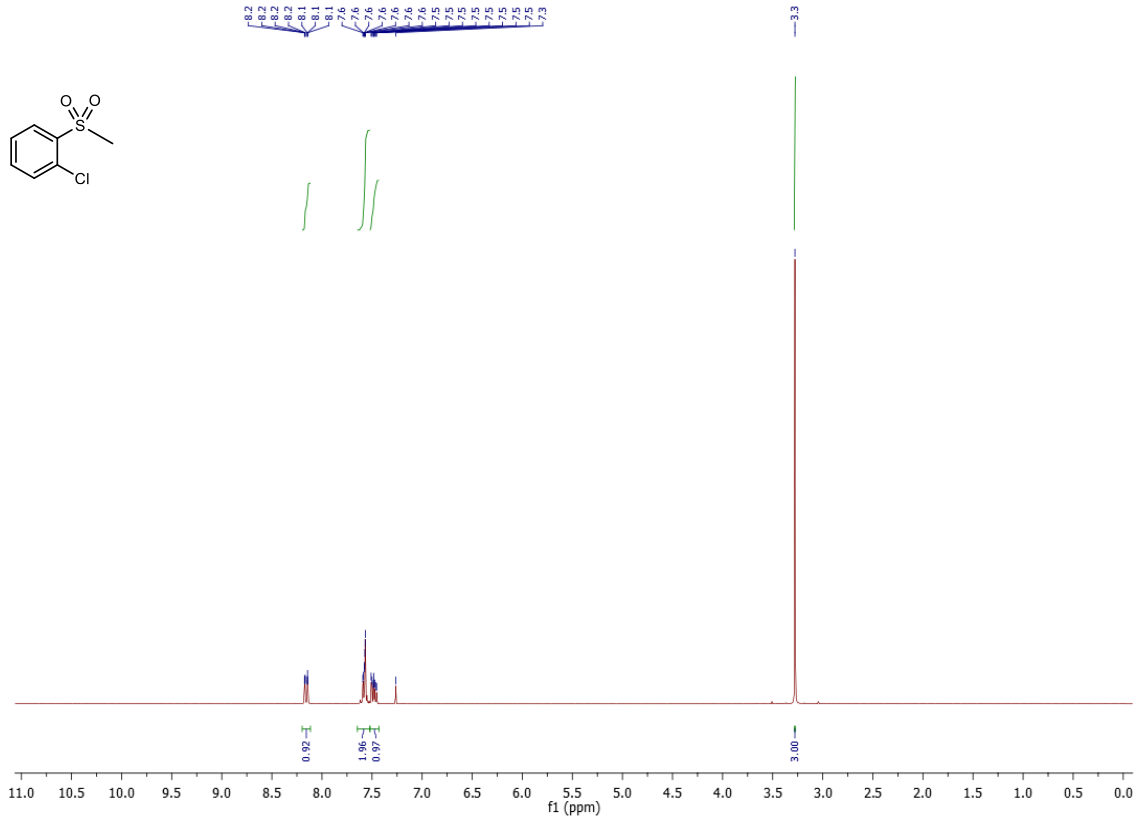

^{13}C-NMR (101 MHz, $CDCl_3$) spectrum of 3h

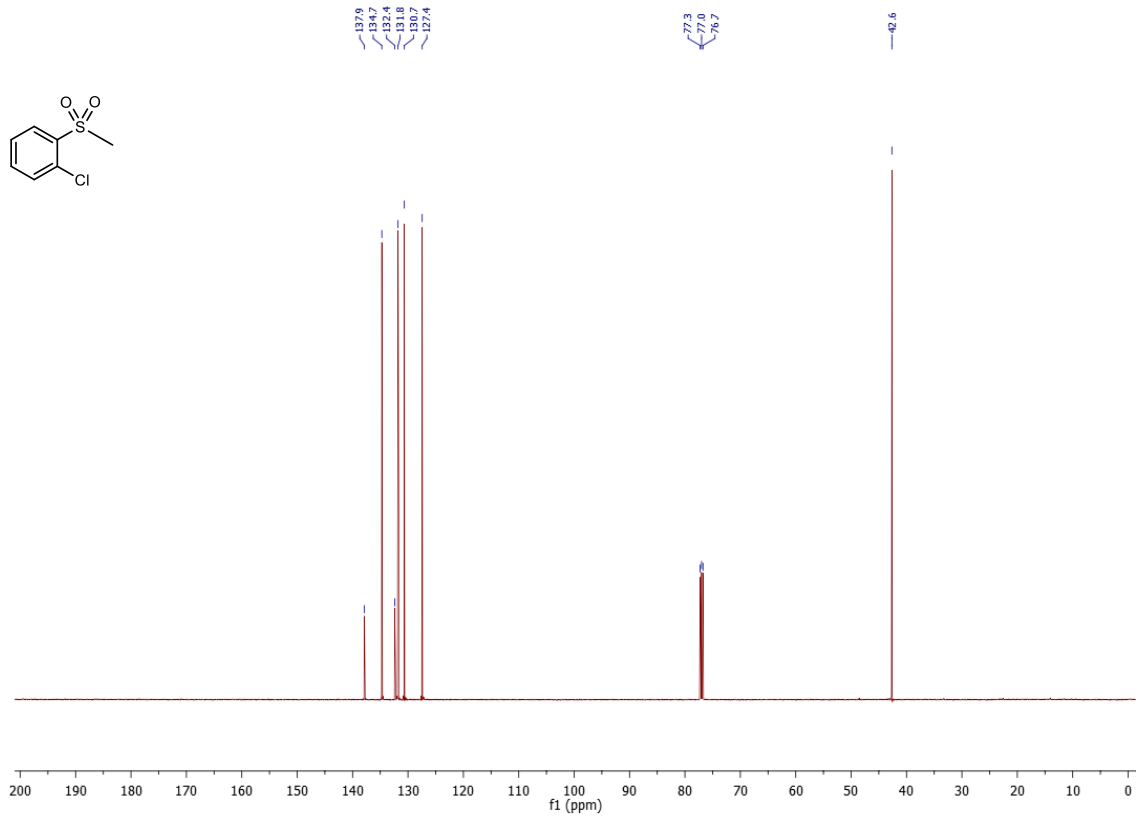

^{1}H-NMR (400 MHz, $CDCl_3$) spectrum of 2i

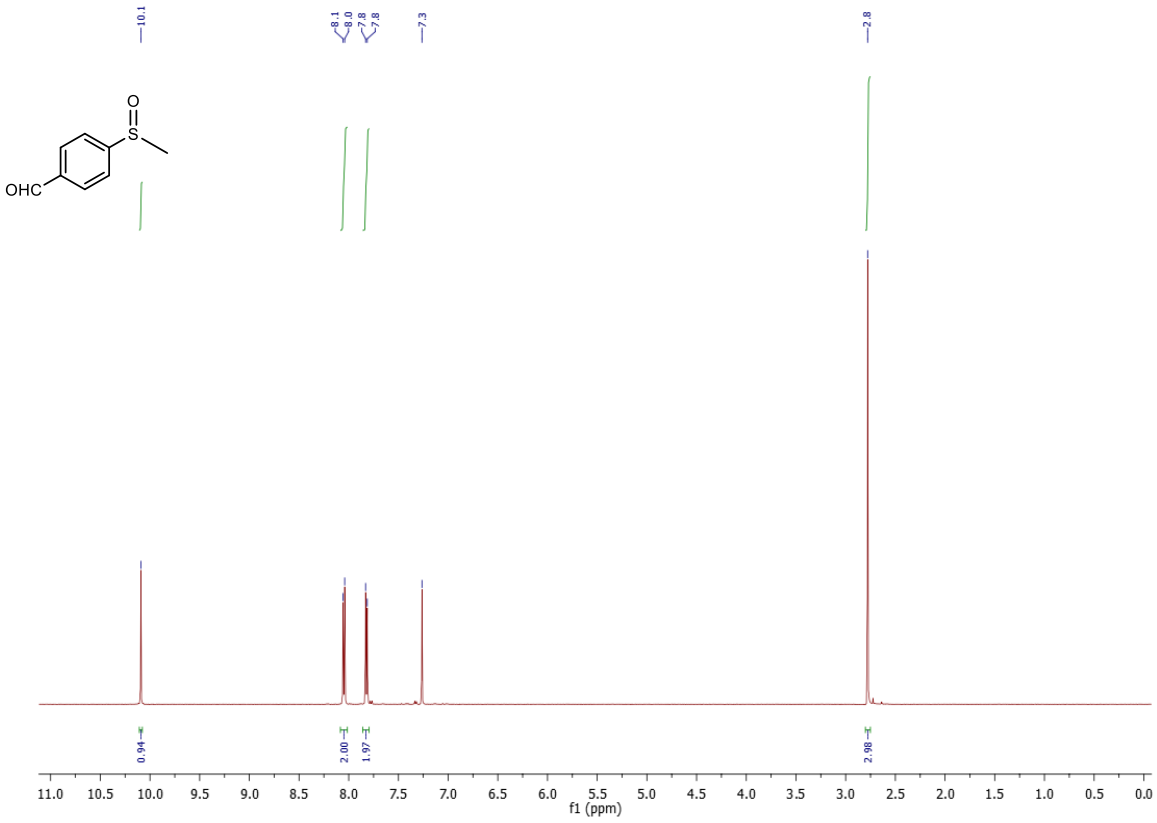

^{13}C-NMR (101 MHz, $CDCl_3$) spectrum of 2i

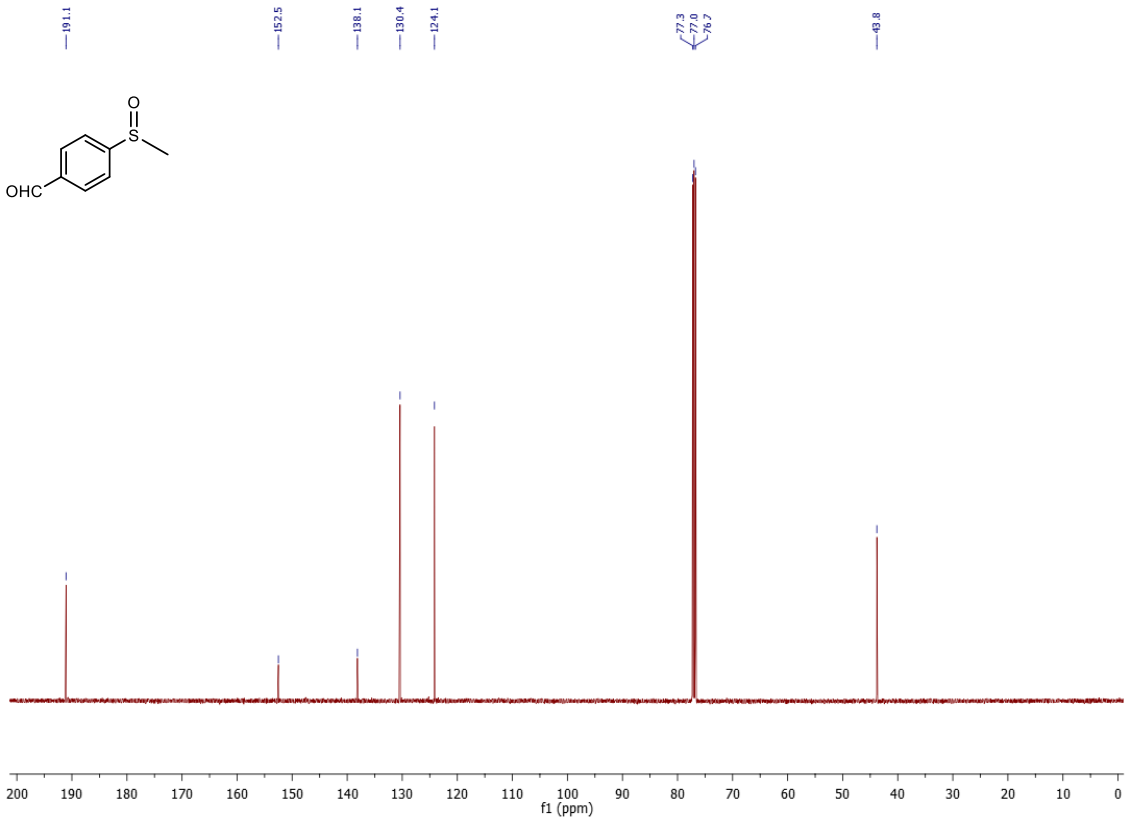

^{1}H-NMR (300 MHz, $CDCl_3$) spectrum of 3i

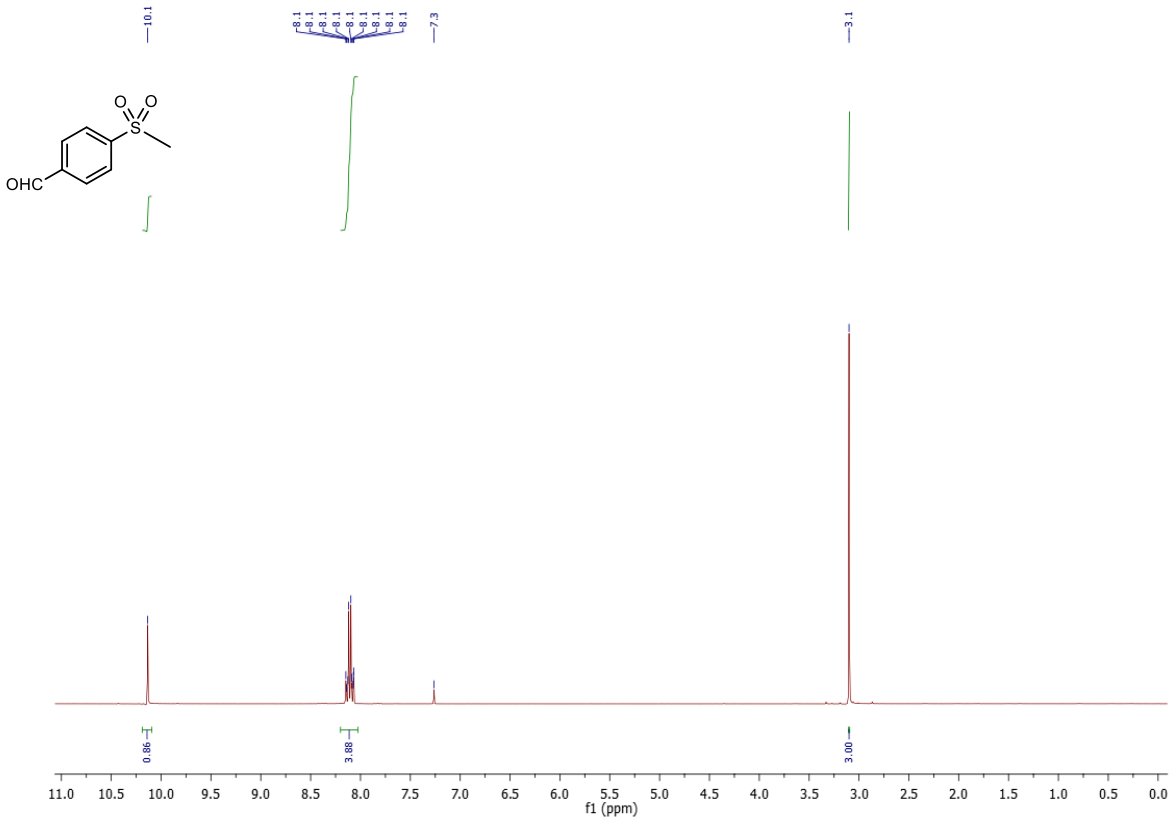

^{13}C-NMR (101 MHz, $CDCl_3$) spectrum of 3i

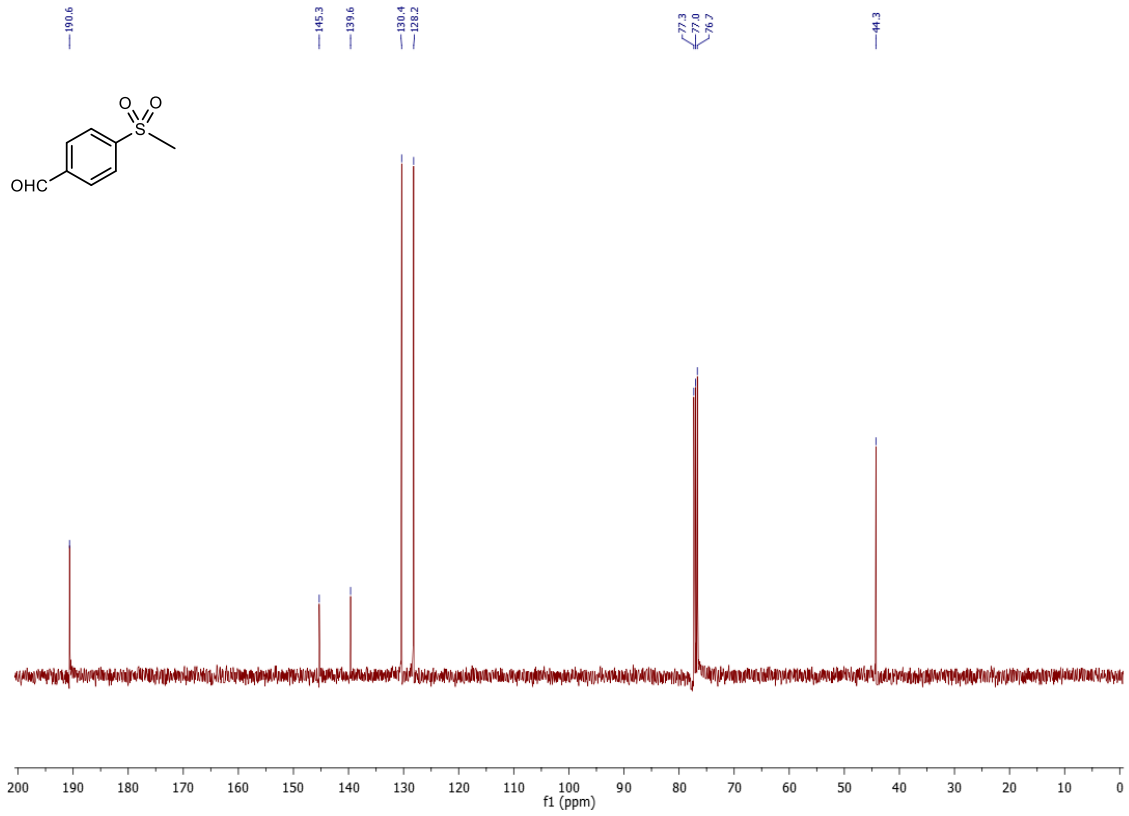

^{1}H-NMR (400 MHz, CD_3OD) spectrum of 2j

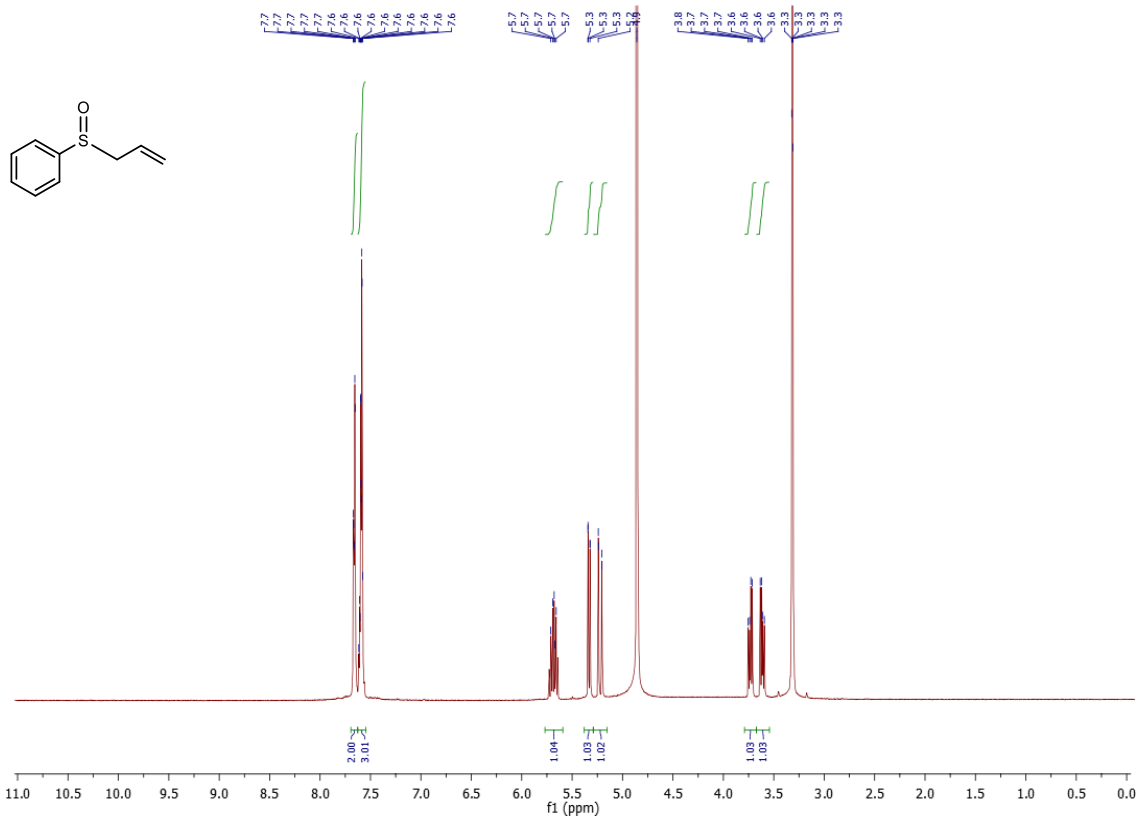

^{13}C-NMR (101 MHz, CD_3OD) spectrum of 2j

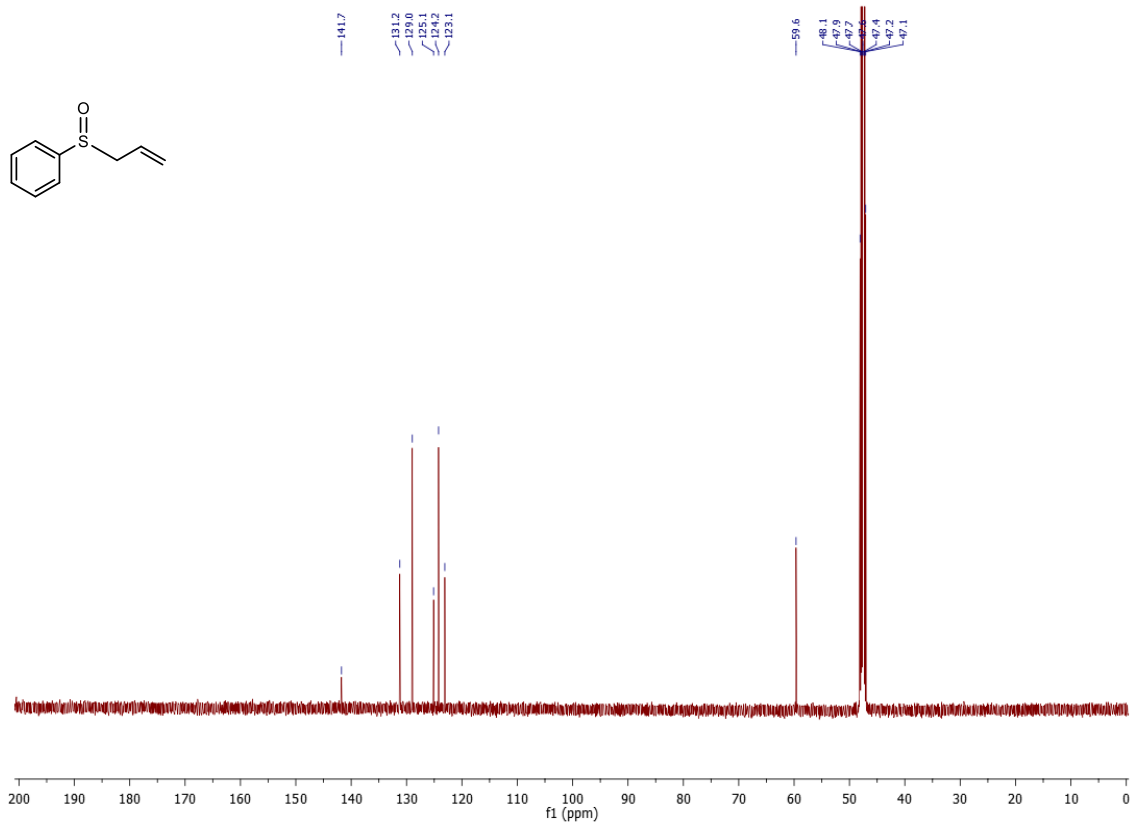

^{1}H-NMR (400 MHz, CD_3OD) spectrum of 3j

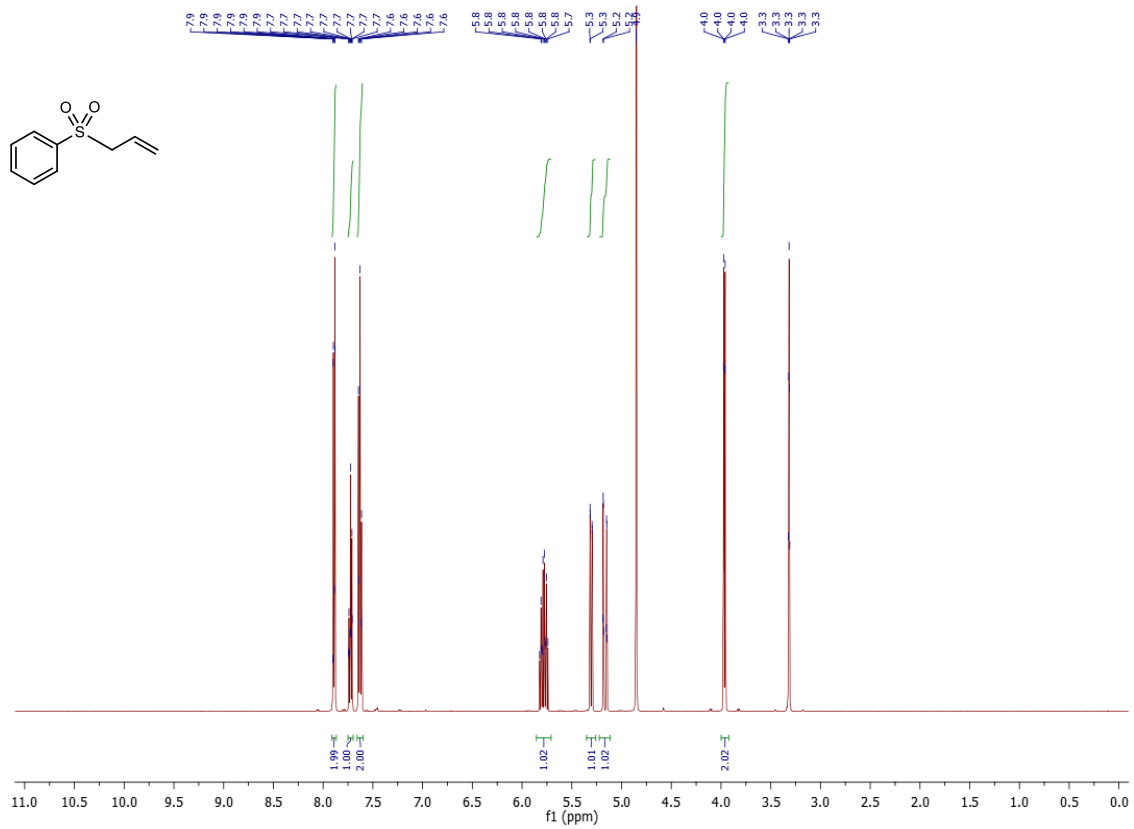

^{13}C-NMR (101 MHz, CD_3OD) spectrum of 3j

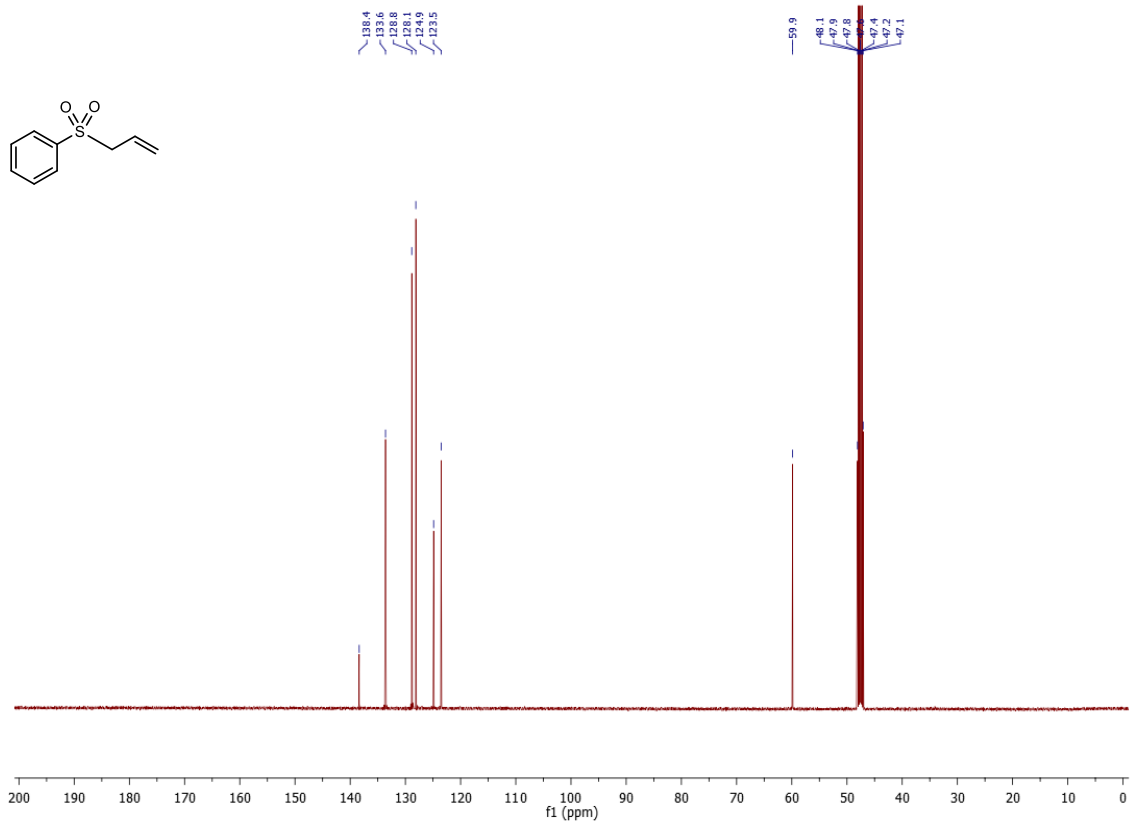

^{1}H-NMR (400 MHz, CD_3OD) spectrum of 2k

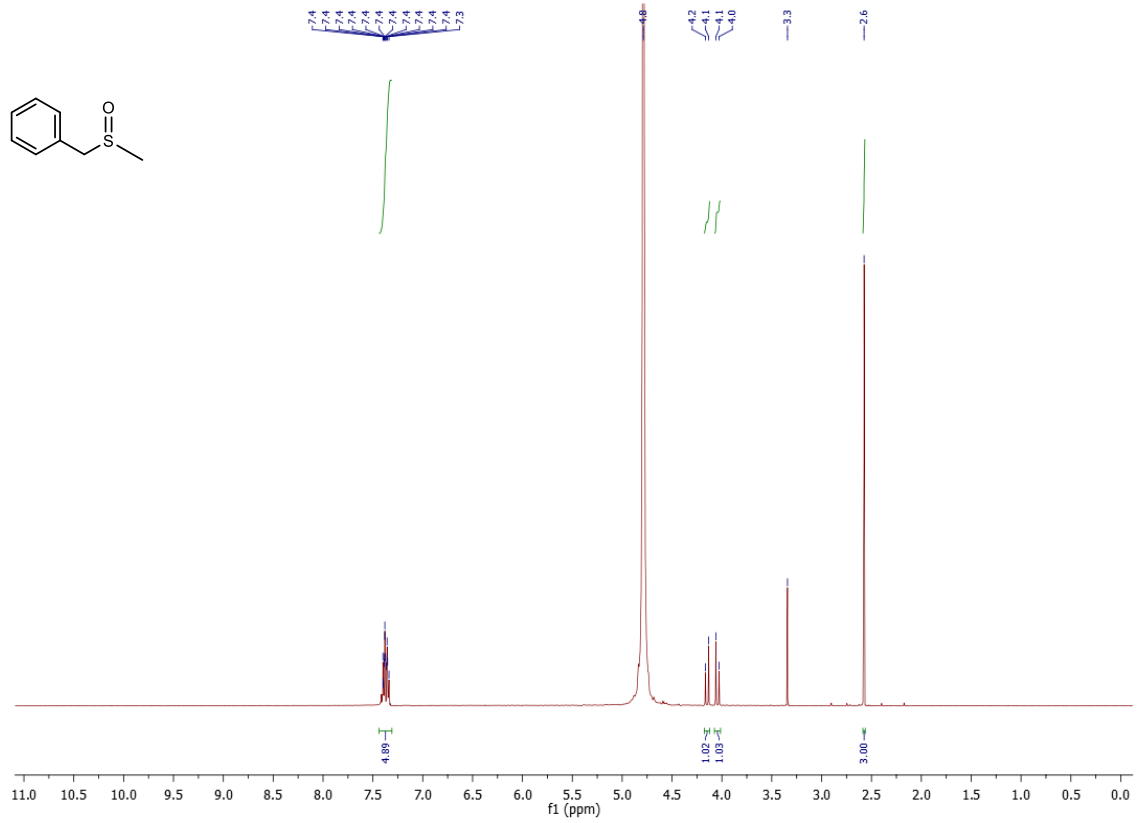

^{13}C-NMR (101 MHz, CD_3OD) spectrum of 2k

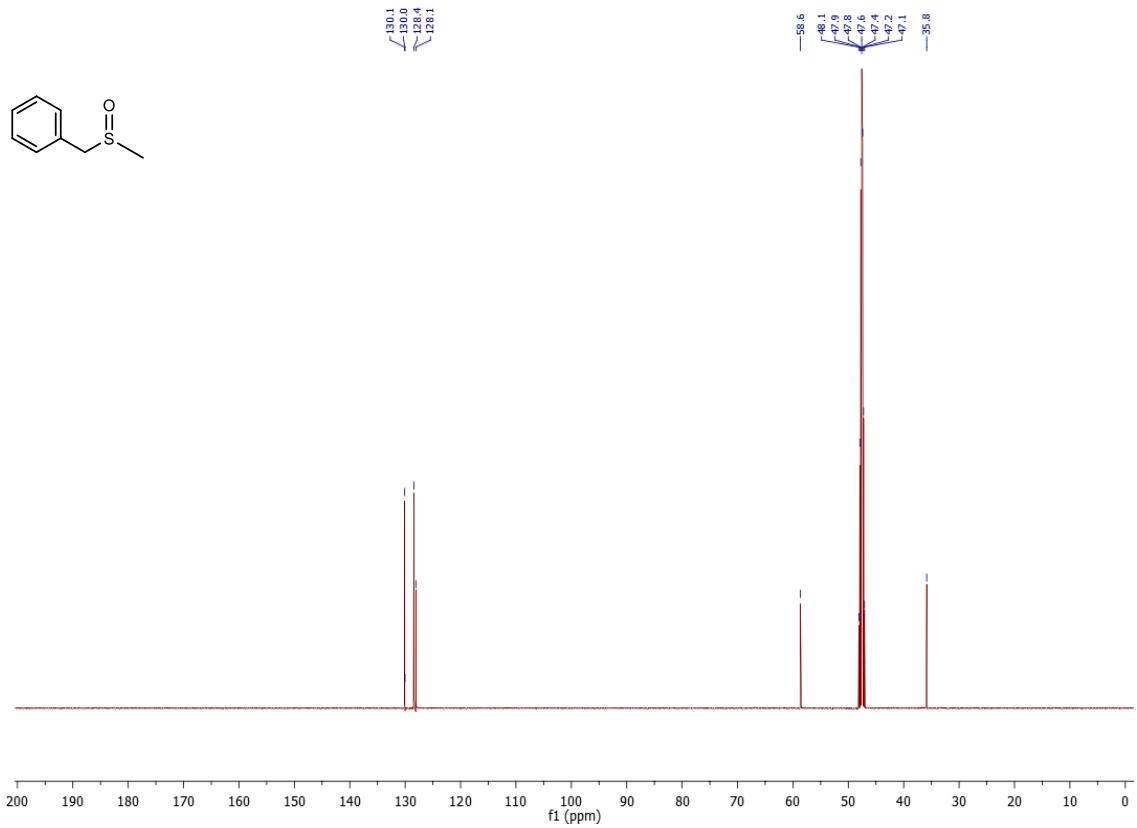

^{1}H-NMR (400 MHz, CD_3OD) spectrum of 3k

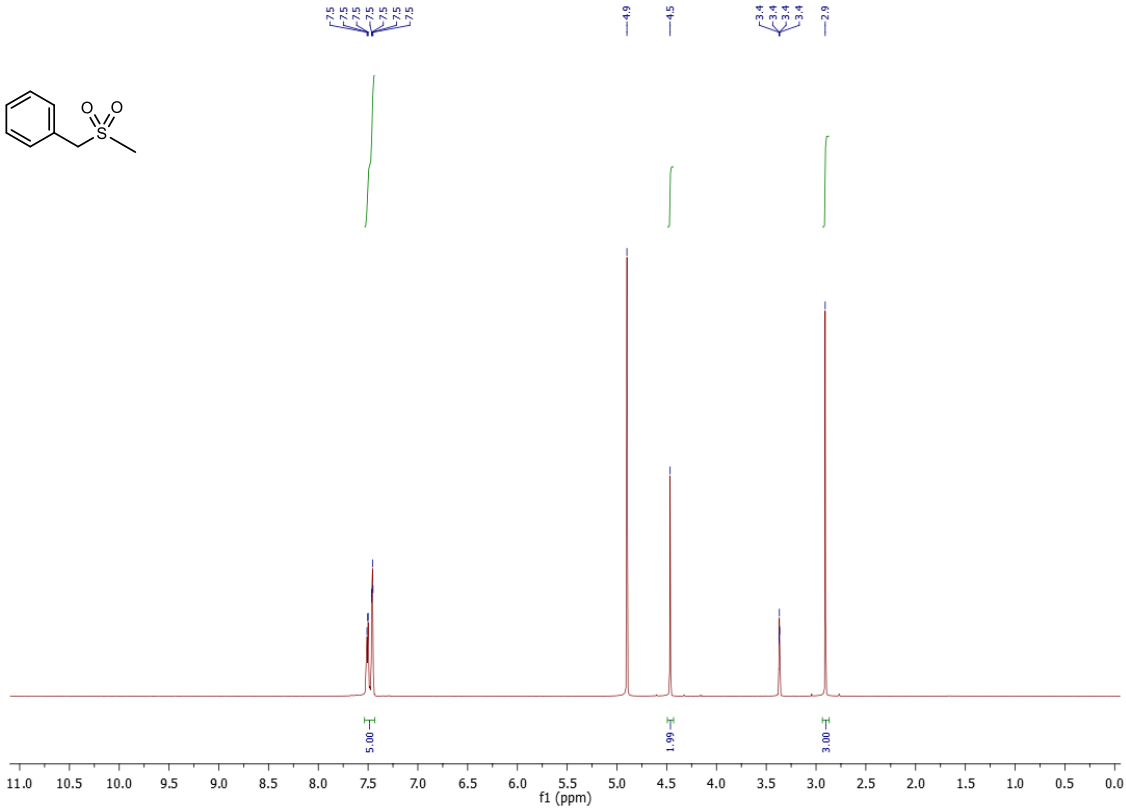

^{13}C-NMR (101 MHz, CD_3OD) spectrum of 3k

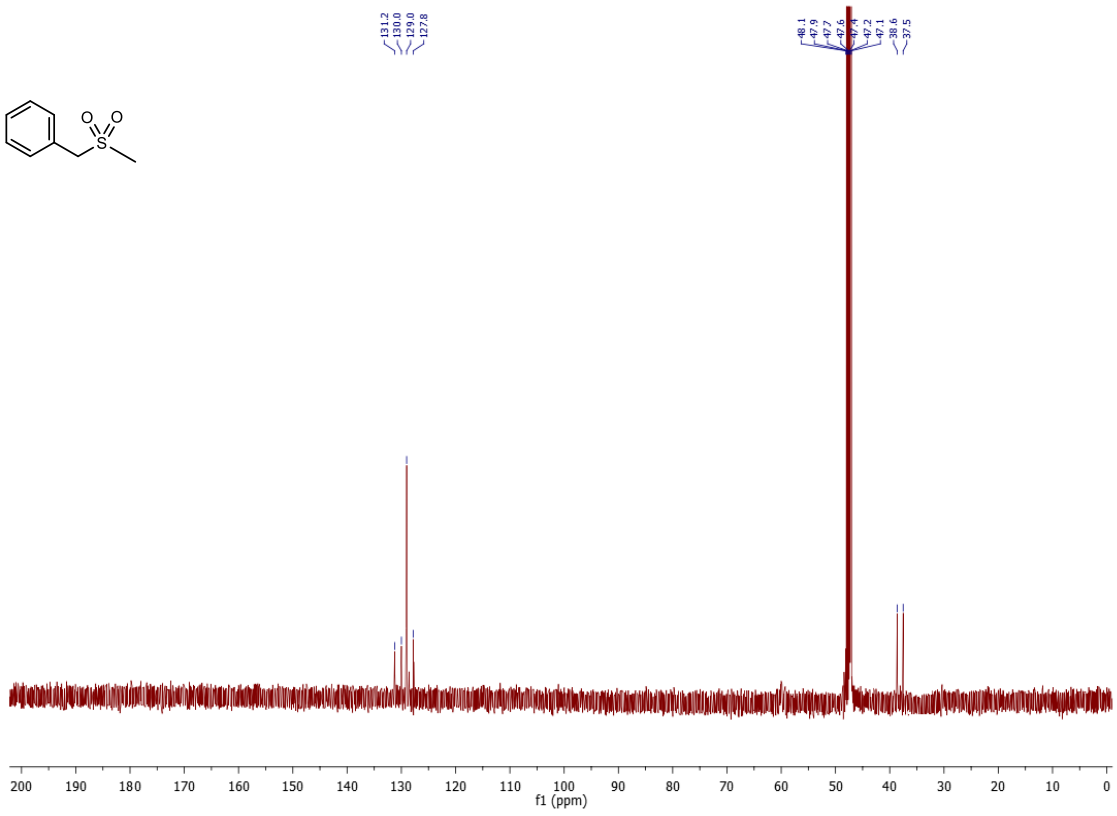

^{1}H-NMR (400 MHz, CD_3OD) spectrum of 2l

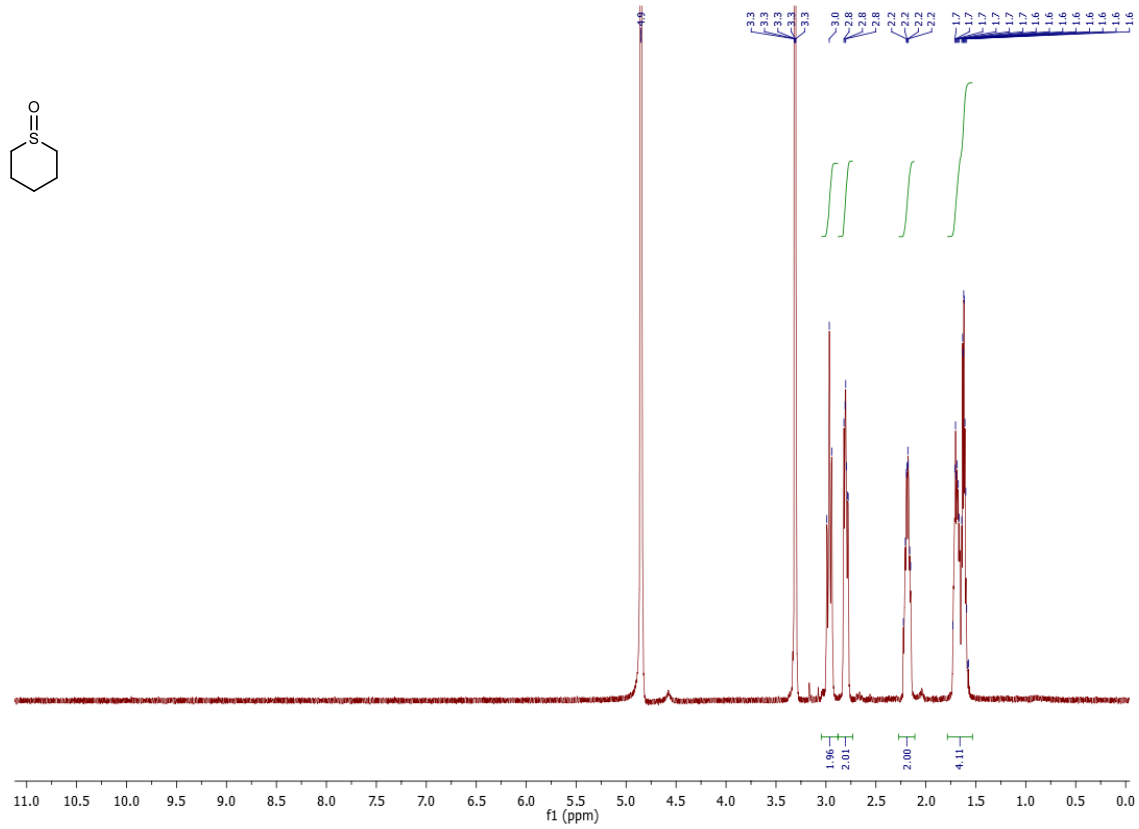

^{13}C-NMR (101 MHz, CD_3OD) spectrum of 2l

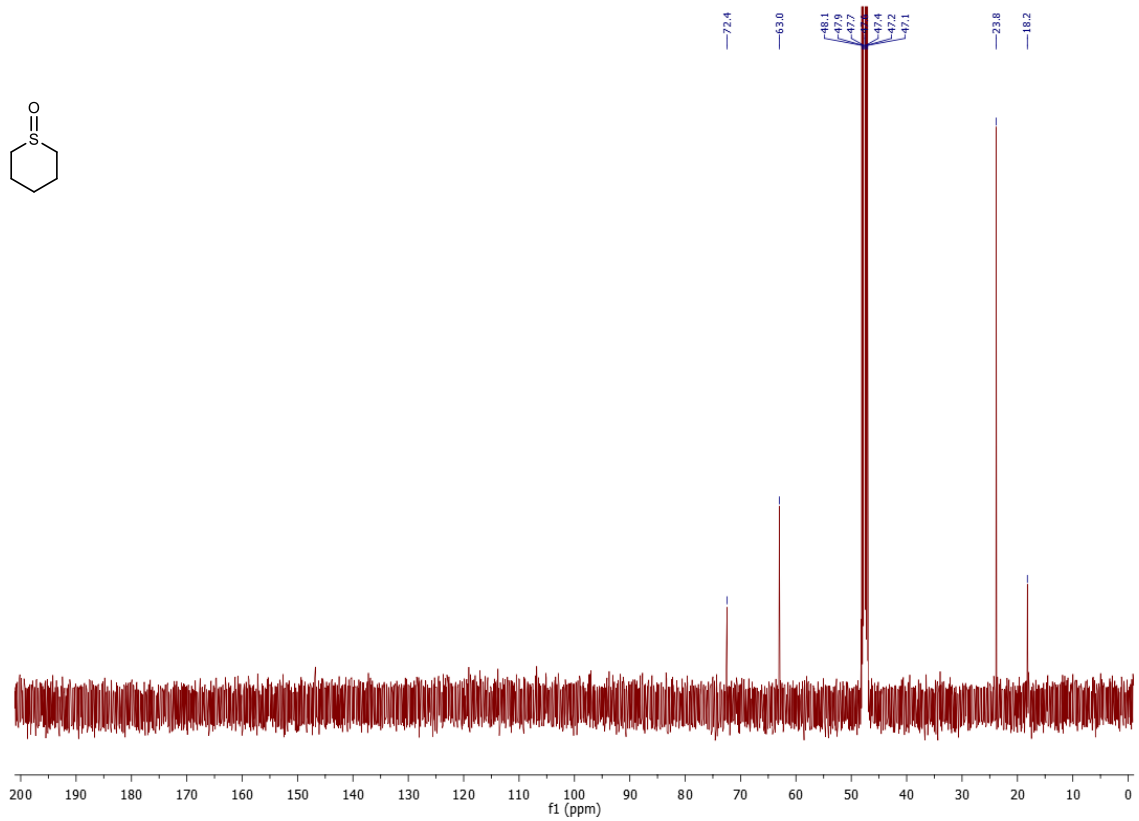

^{1}H-NMR (400 MHz, $CDCl_3$) spectrum of 3l

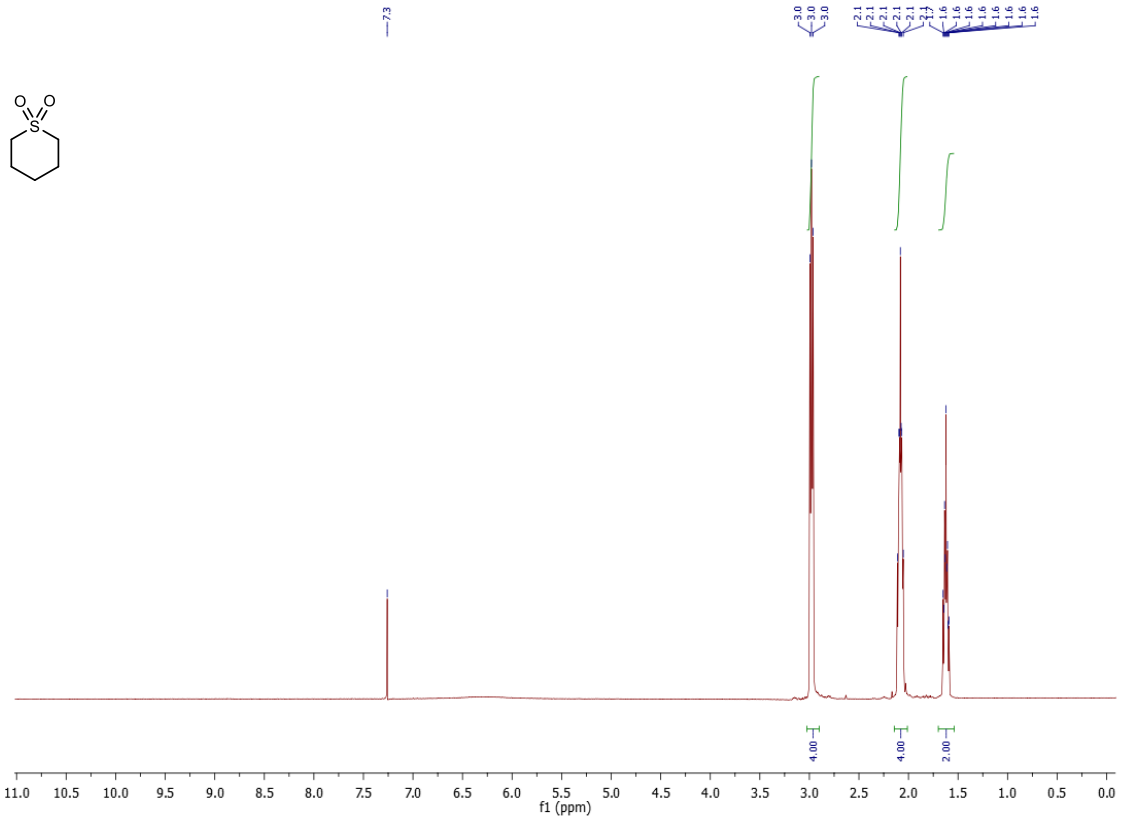

^{13}C-NMR (101 MHz, $CDCl_3$) spectrum of 3l

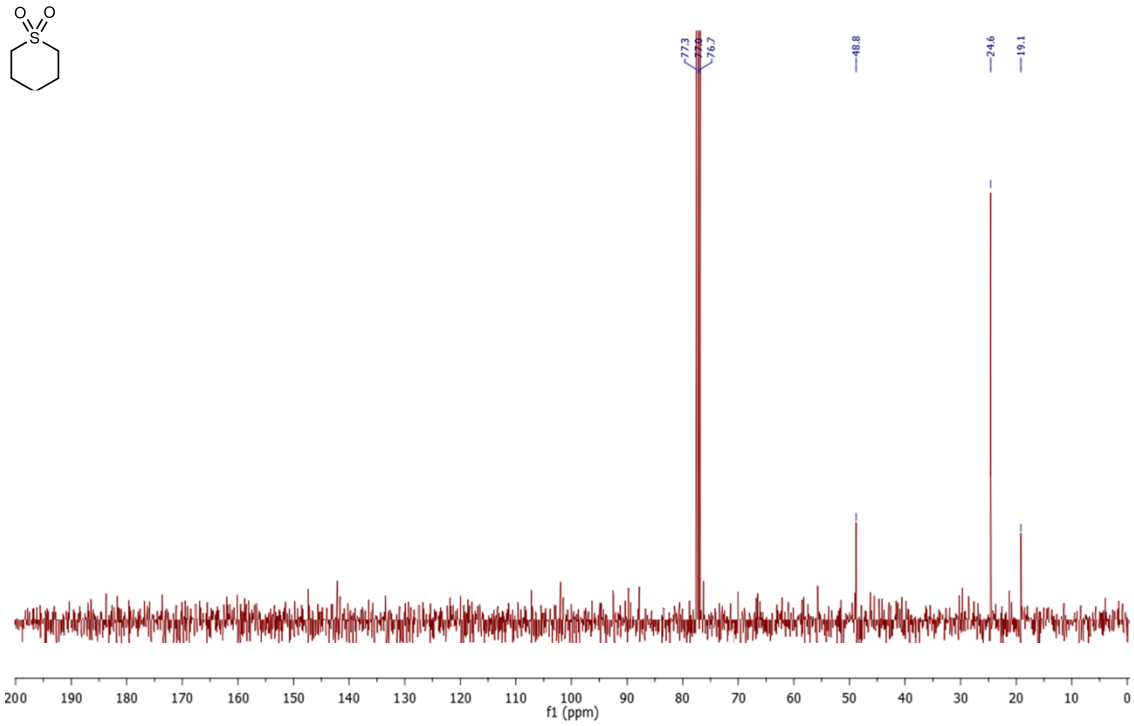

^{1}H-NMR (400 MHz, D_2O) spectrum of 2m

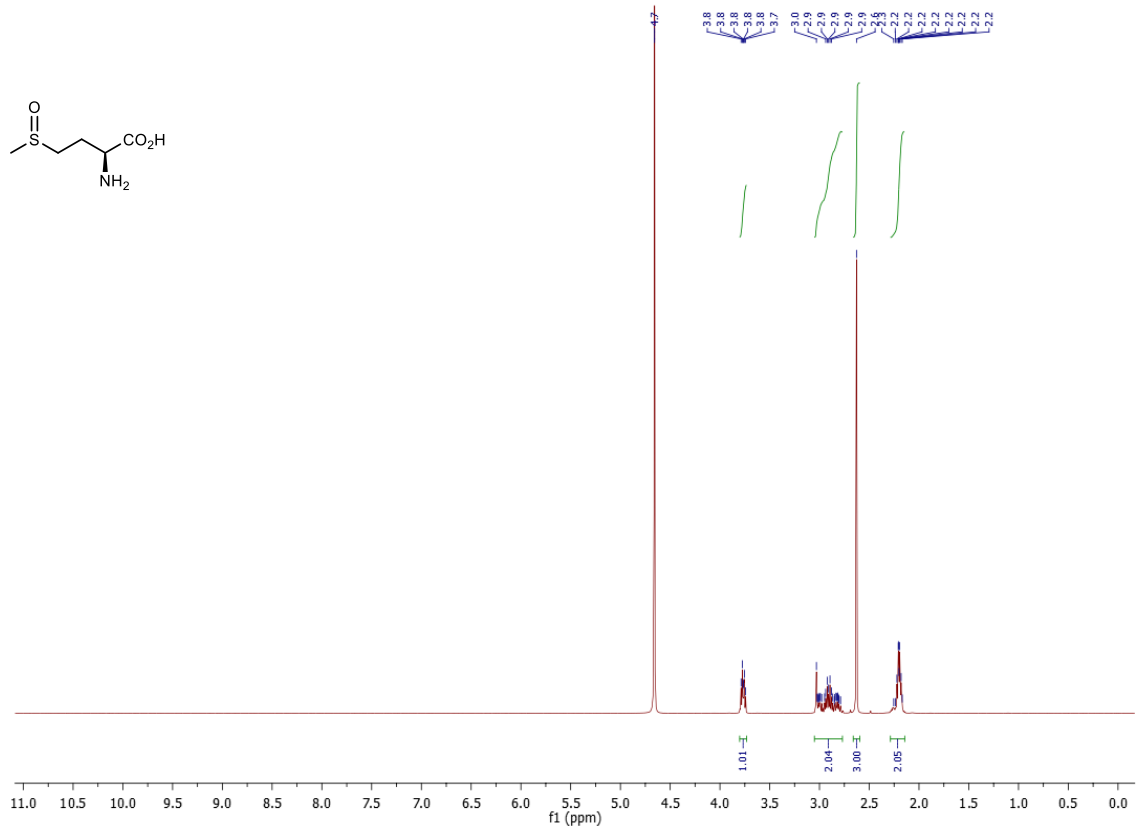

^{13}C-NMR (101 MHz, D_2O) spectrum of 2m

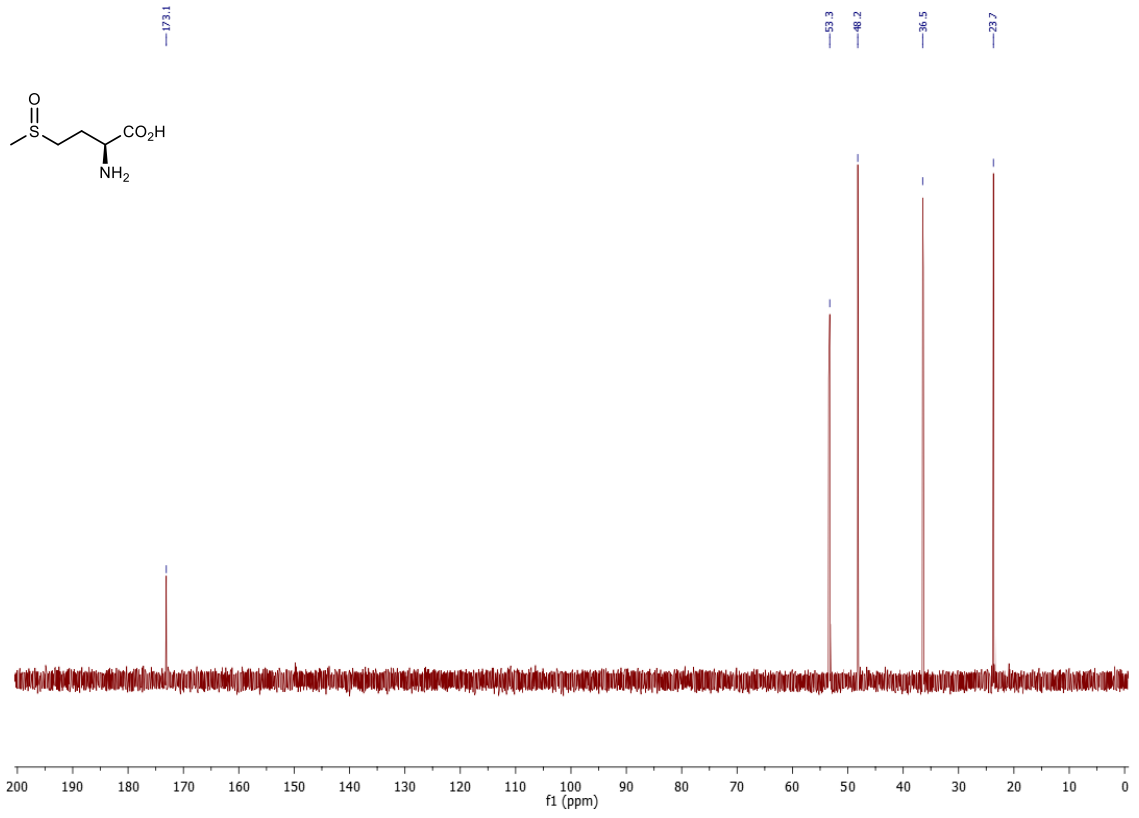

^{1}H-NMR (400 MHz, D_2O) spectrum of 3m

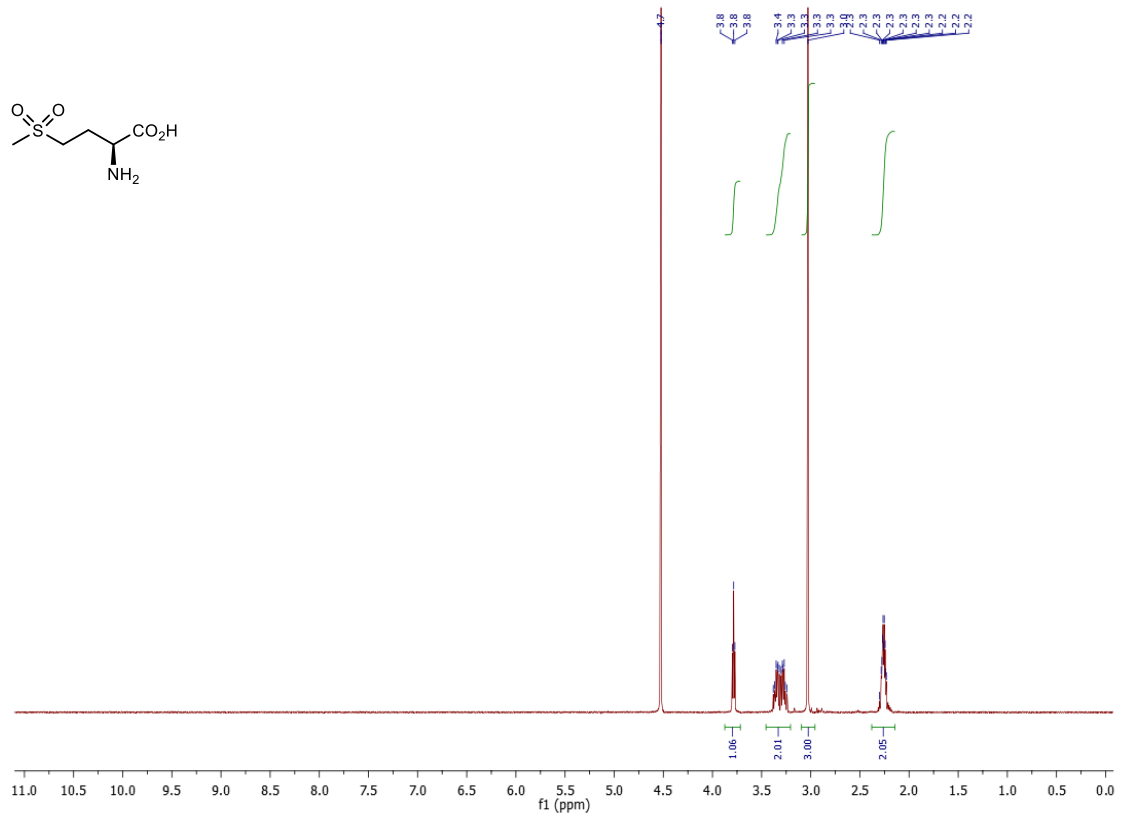

^{13}C-NMR (101 MHz, D_2O) spectrum of 3m

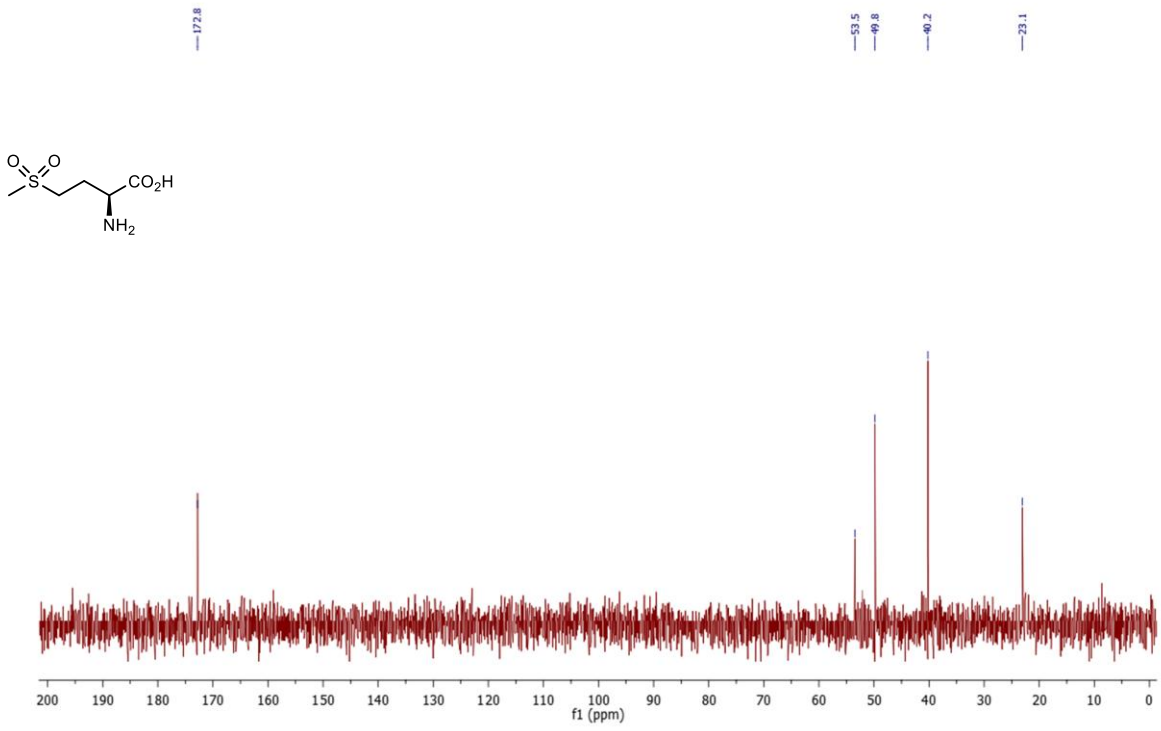

^{1}H-NMR (300 MHz, $CDCl_3$) spectrum of 4a

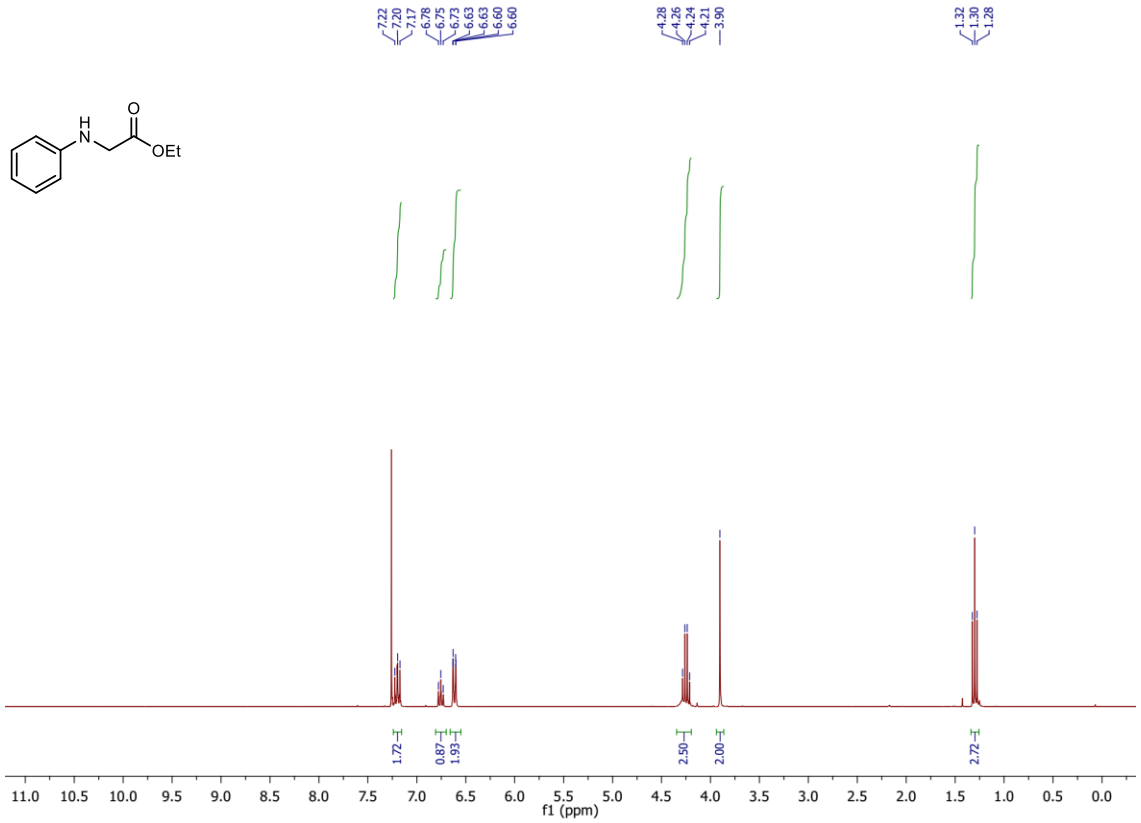

^{13}C-NMR (101 MHz, $CDCl_3$) spectrum of 4a

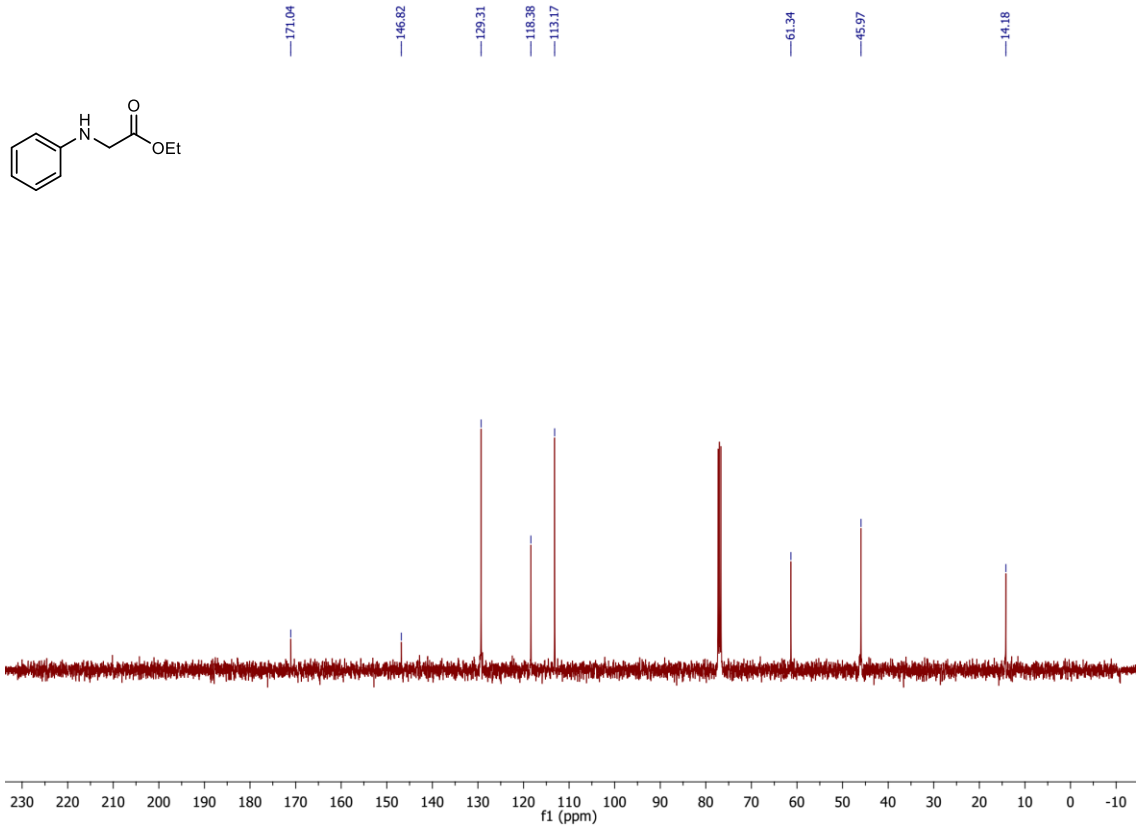

^{1}H-NMR (300 MHz, $CDCl_3$) spectrum of 4b

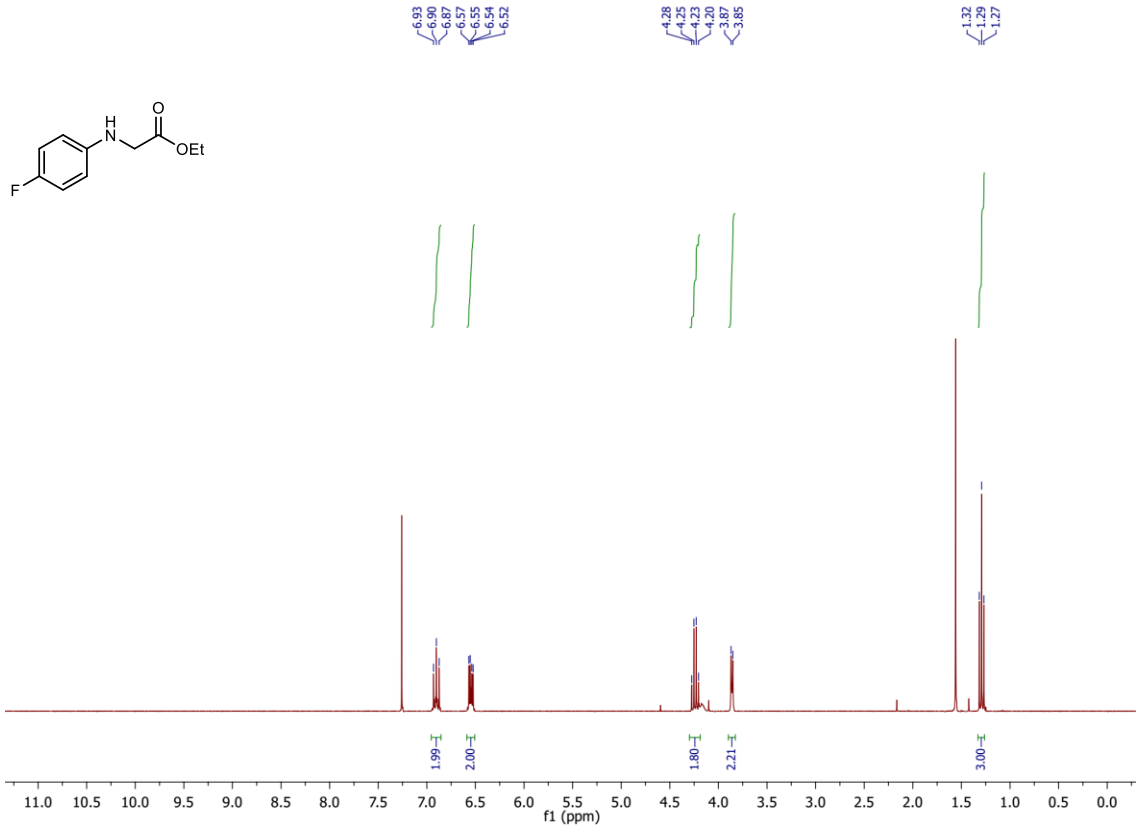

^{13}C-NMR (101 MHz, $CDCl_3$) spectrum of 4b

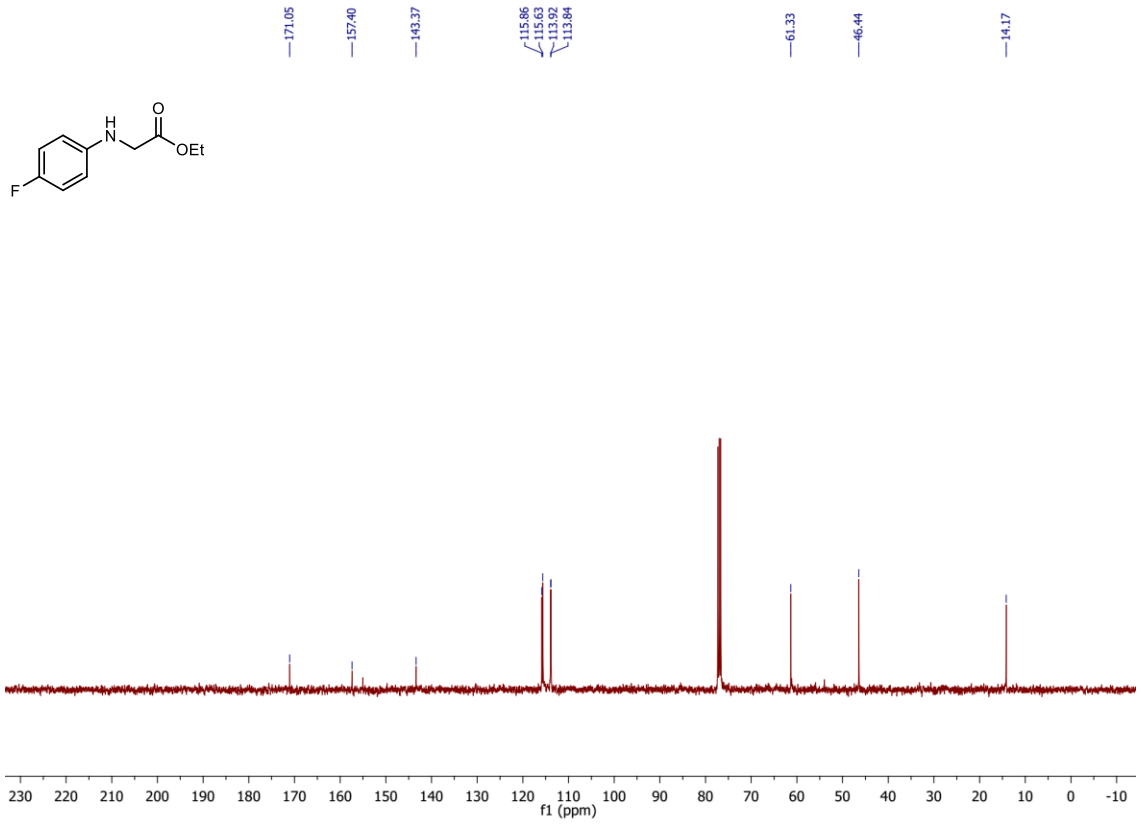

^{19}F-NMR (376 MHz, $CDCl_3$) spectrum of 4b

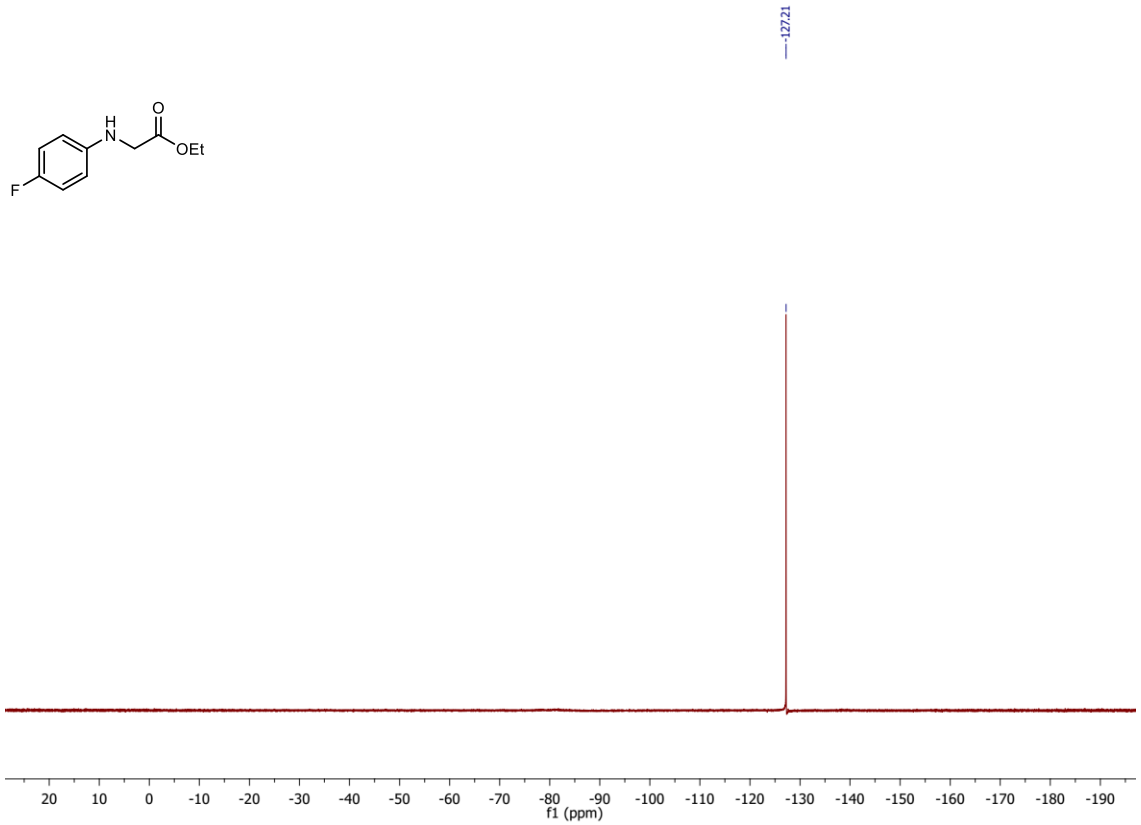

^{1}H-NMR (300 MHz, $CDCl_3$) spectrum of 4c

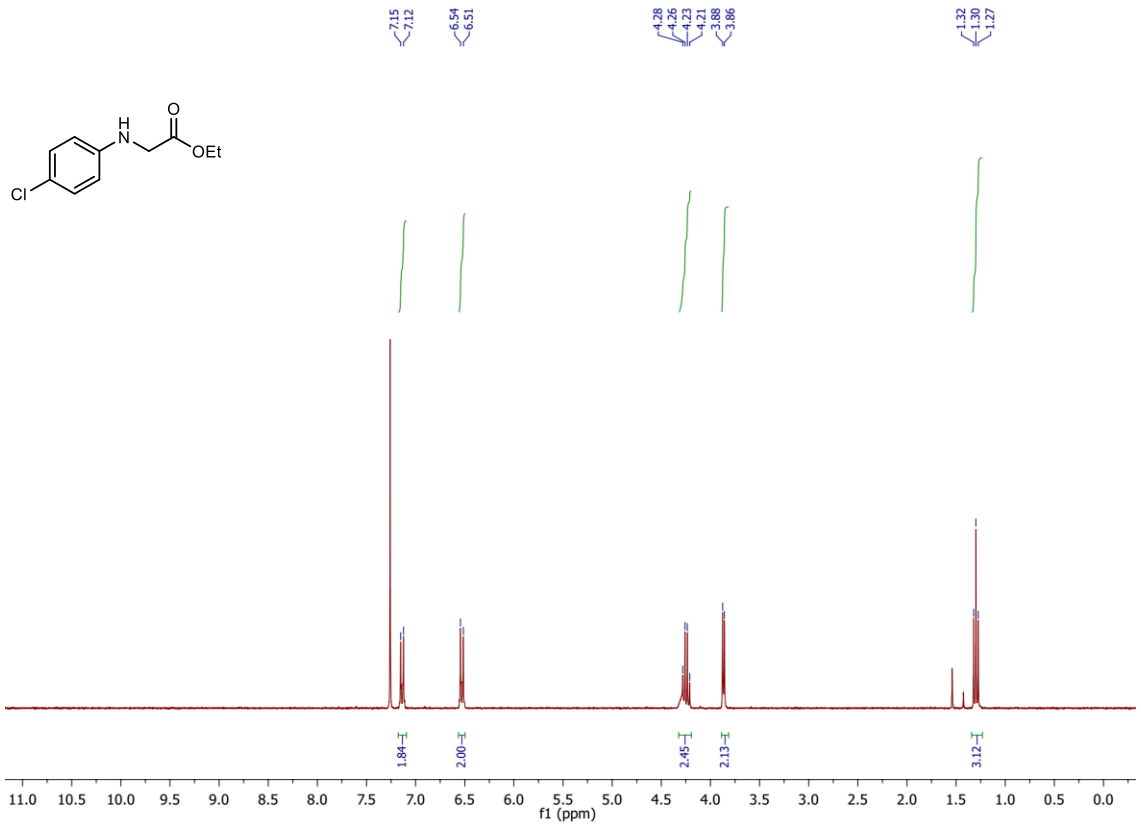

^{13}C-NMR (101 MHz, $CDCl_3$) spectrum of 4c

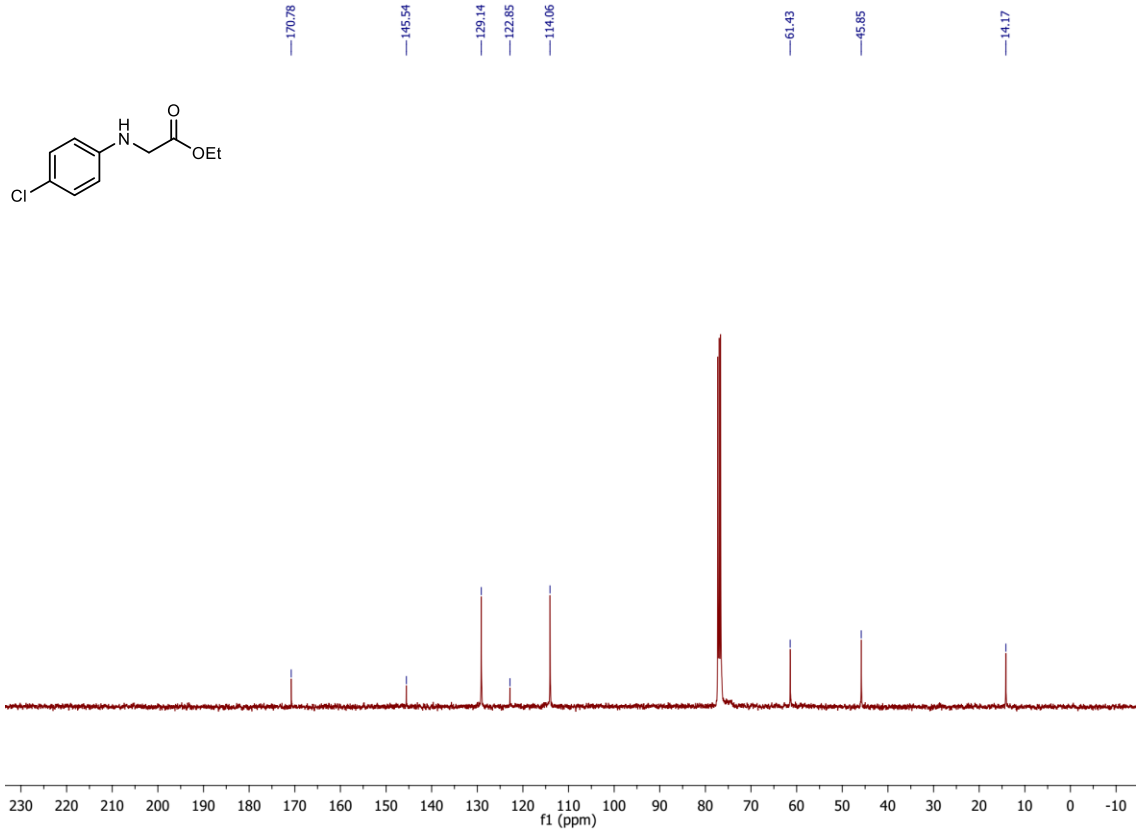

^{1}H-NMR (300 MHz, $CDCl_3$) spectrum of 4d

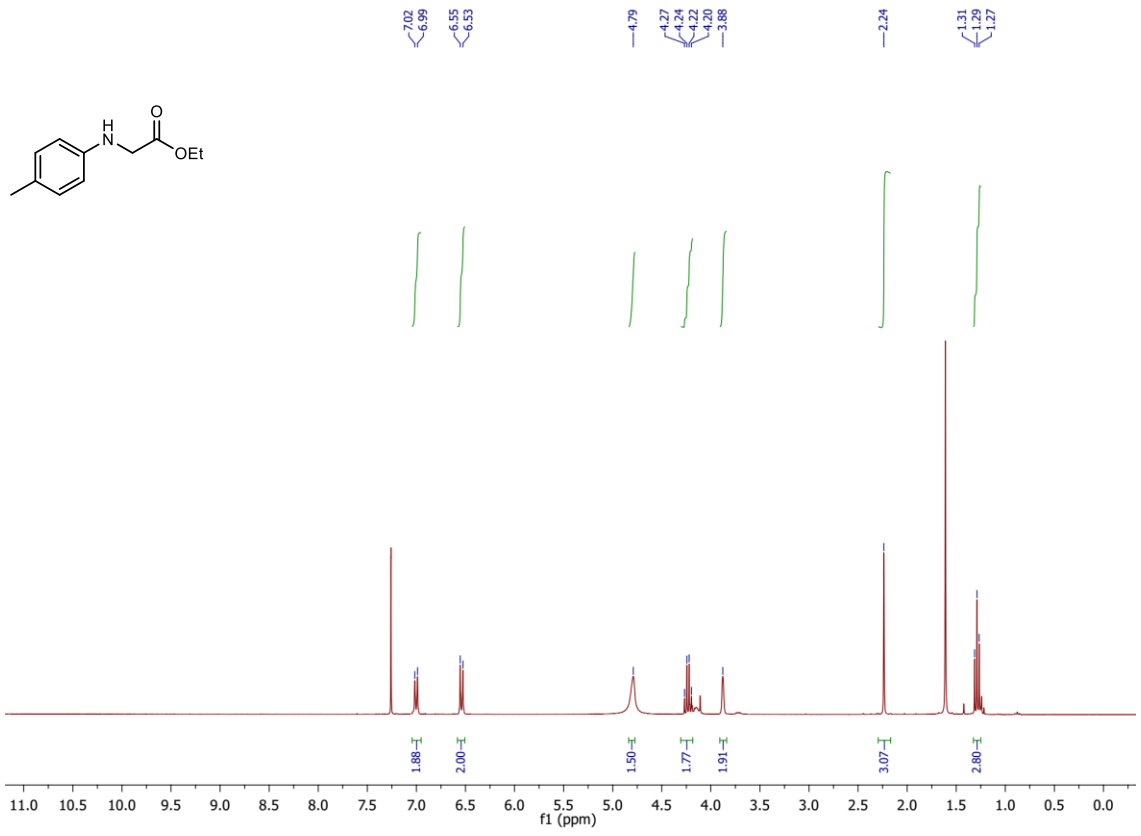

^{13}C-NMR (101 MHz, $CDCl_3$) spectrum of 4d

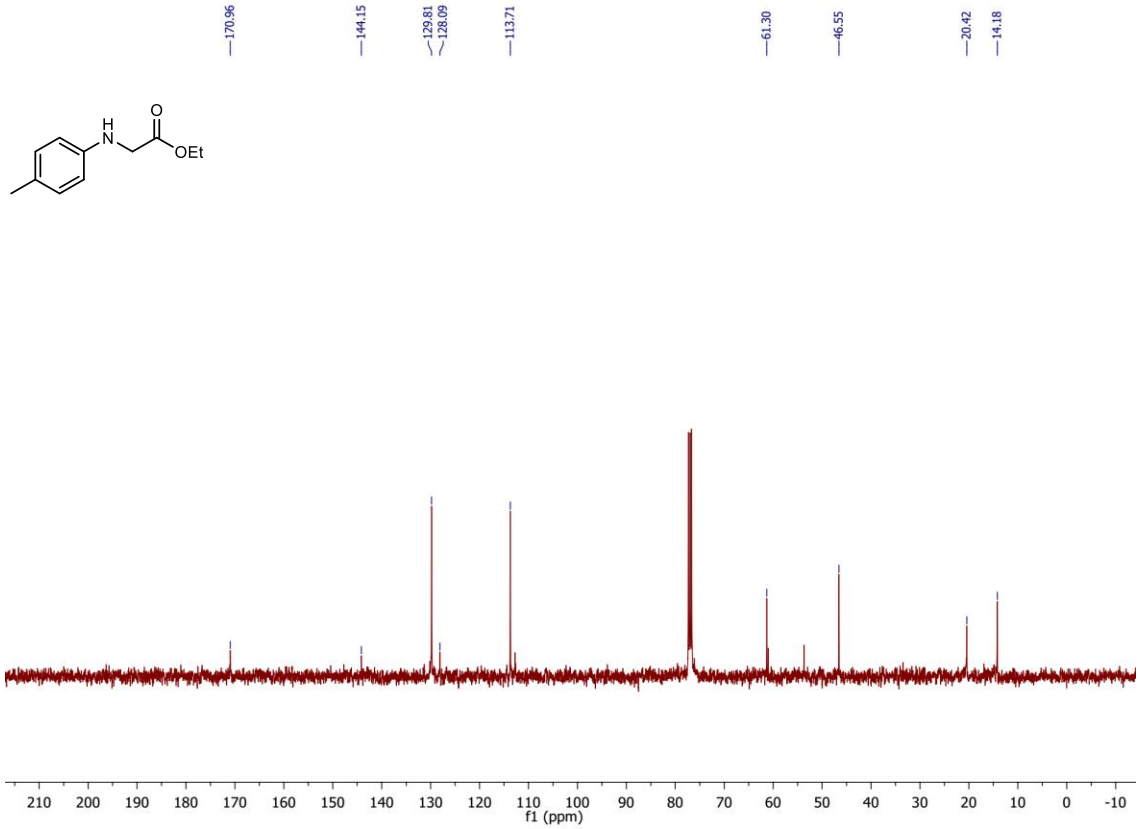

^{1}H-NMR (300 MHz, $CDCl_3$) spectrum of 4e

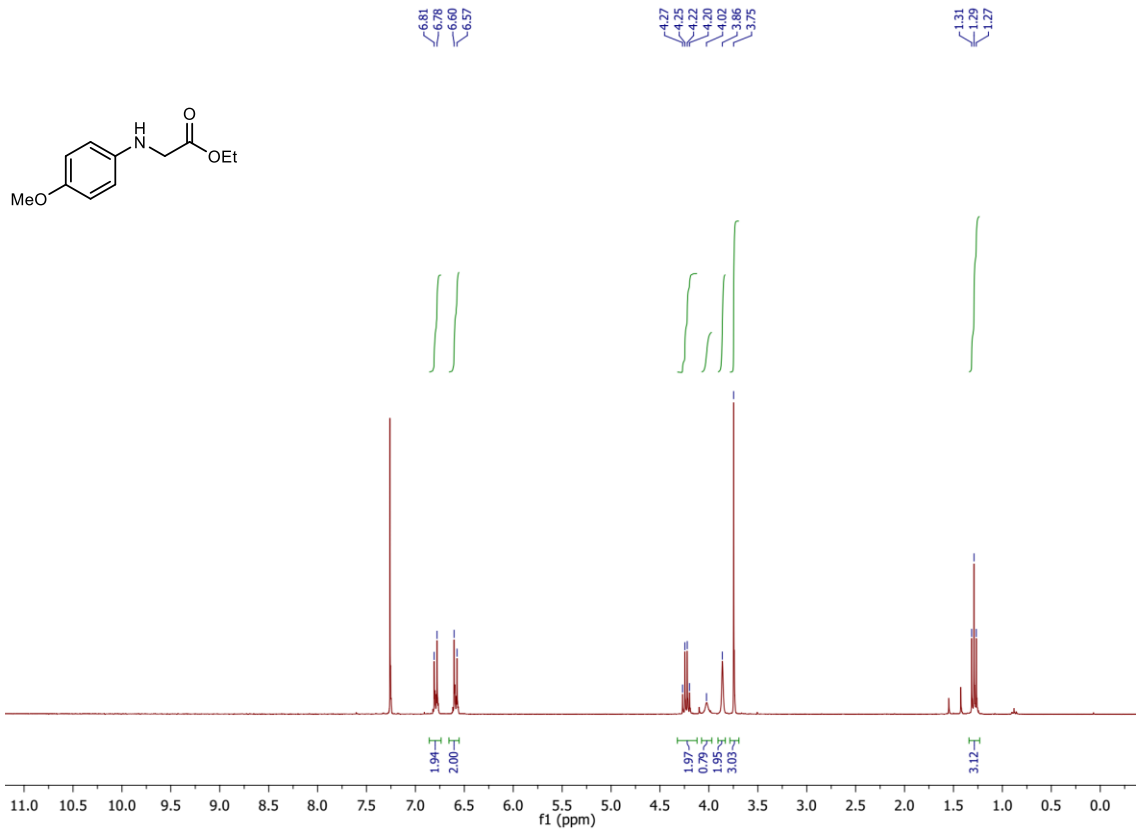

^{13}C-NMR (101 MHz, $CDCl_3$) spectrum of 4e

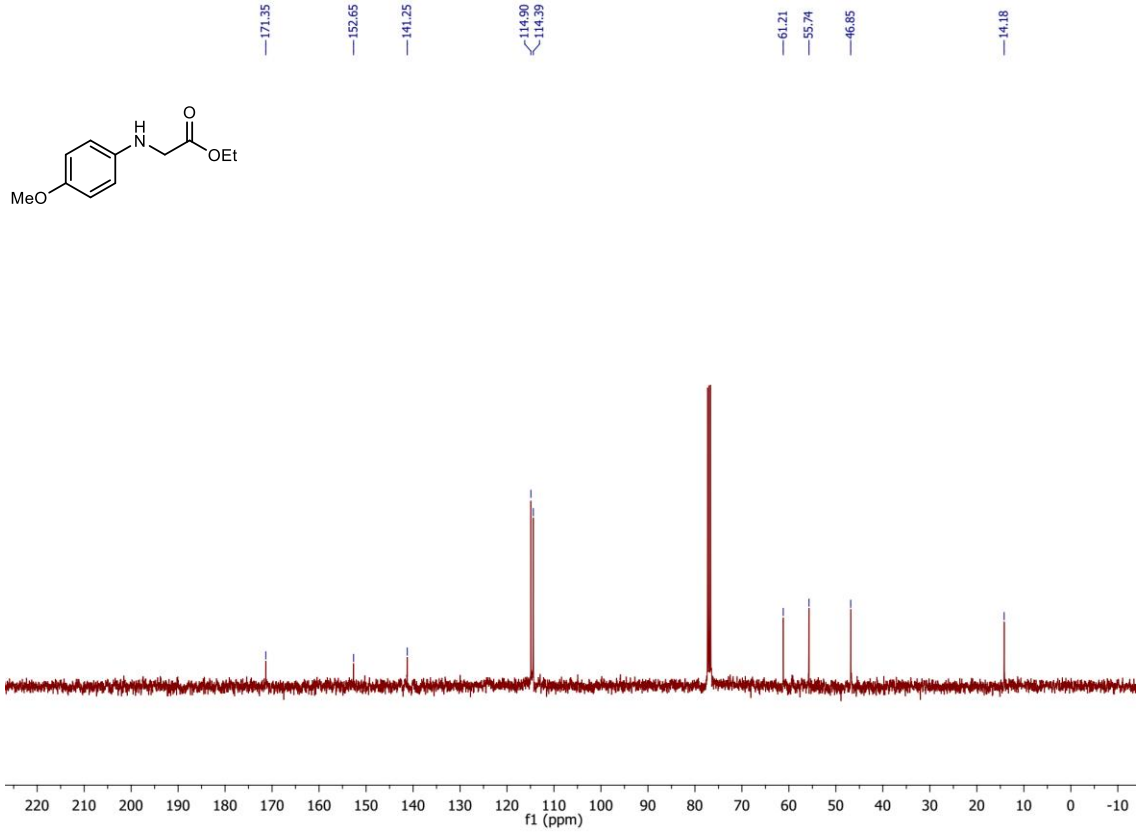

^{1}H-NMR (300 MHz, $CDCl_3$) spectrum of 4f

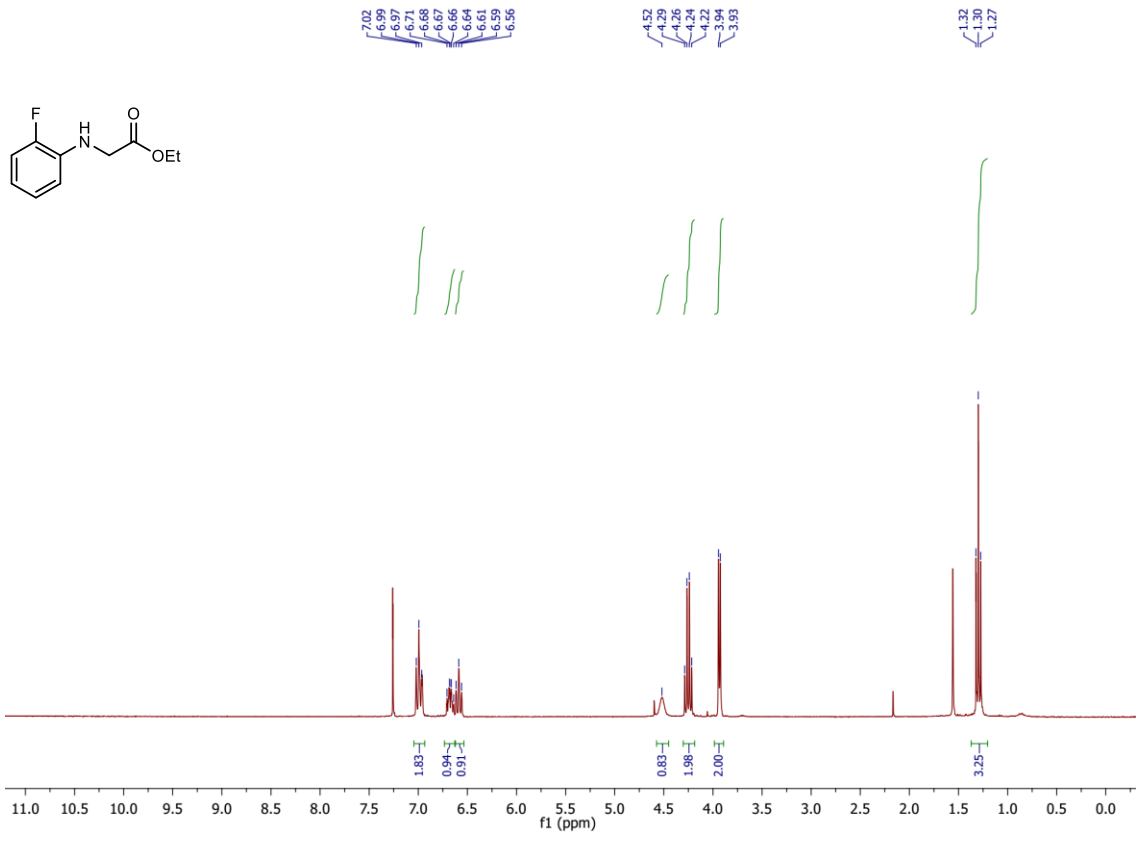

^{13}C-NMR (101 MHz, $CDCl_3$) spectrum of 4f

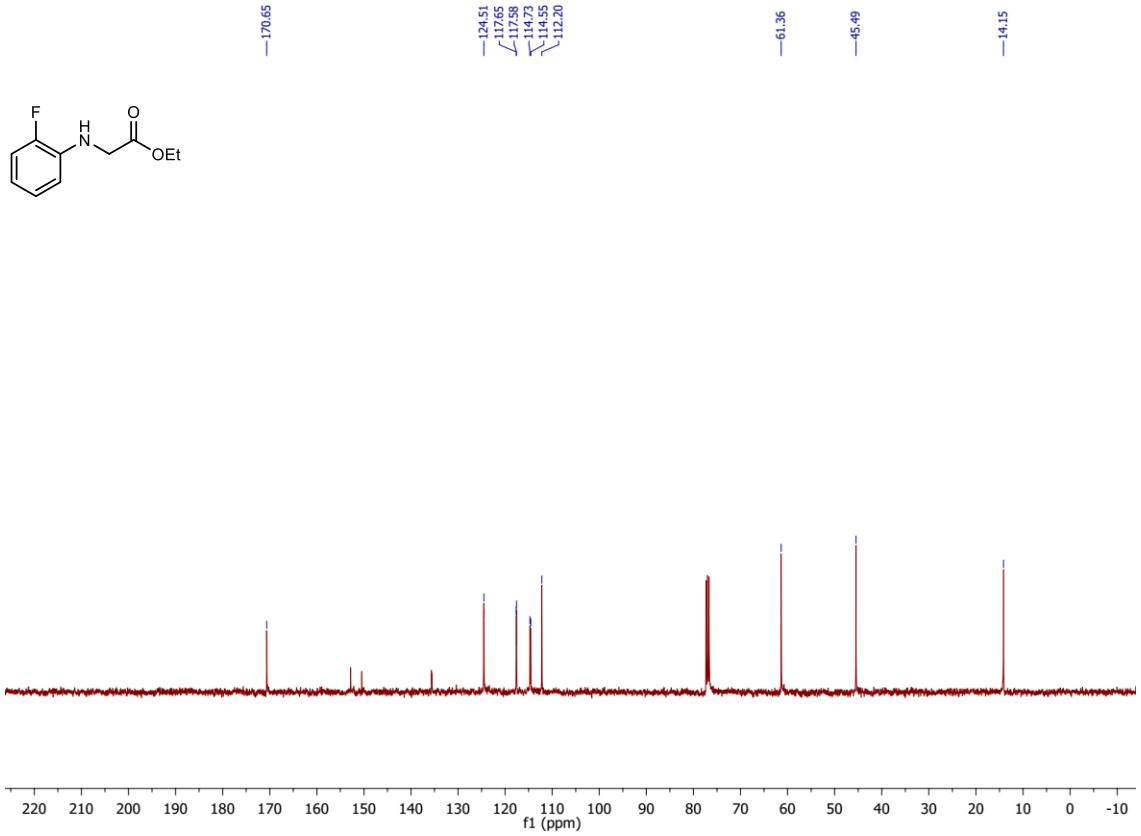

^{19}F-NMR (376 MHz, $CDCl_3$) spectrum of 4f

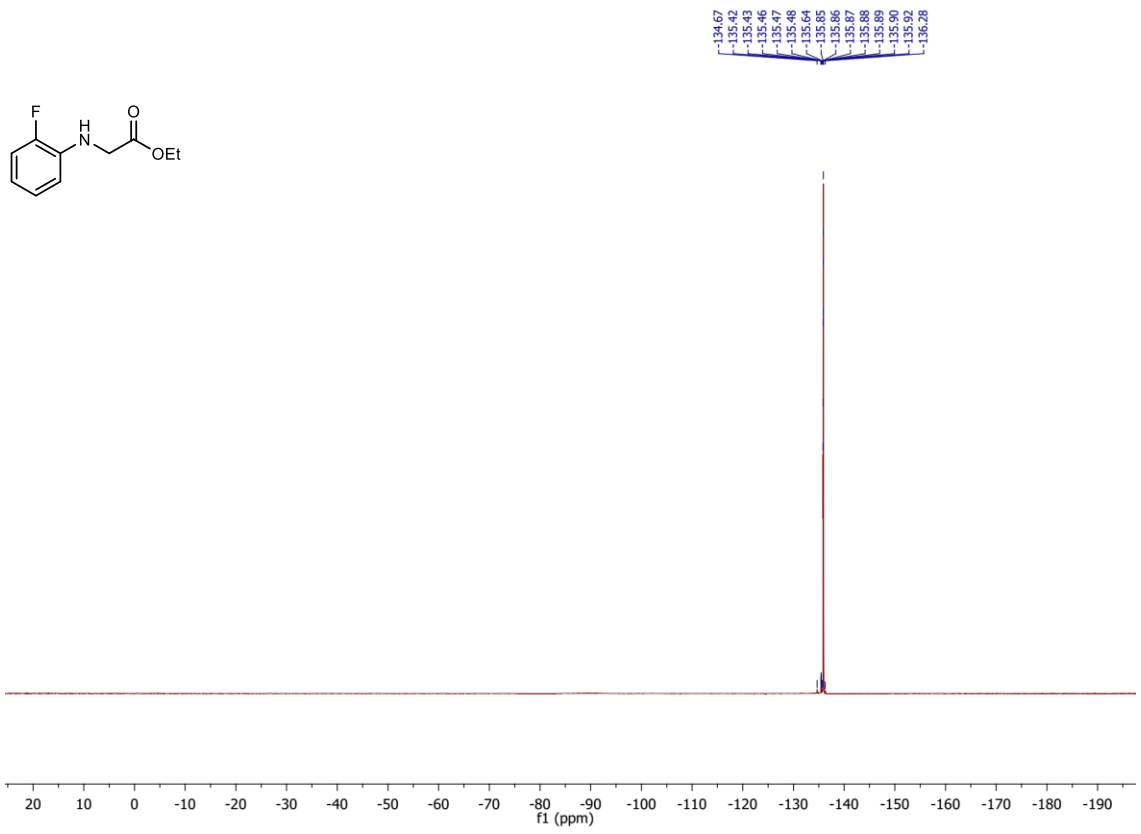

^{1}H-NMR (300 MHz, $CDCl_3$) spectrum of 5g

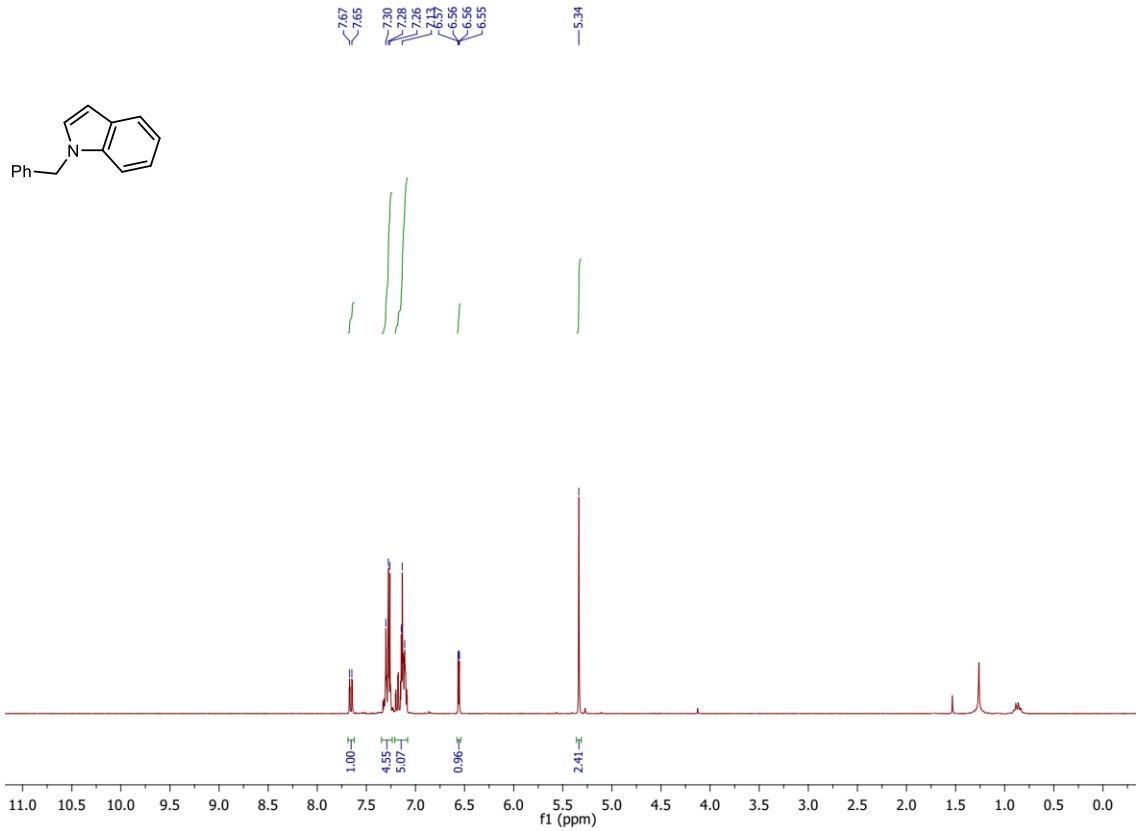

^{13}C-NMR (101 MHz, $CDCl_3$) spectrum of 5g

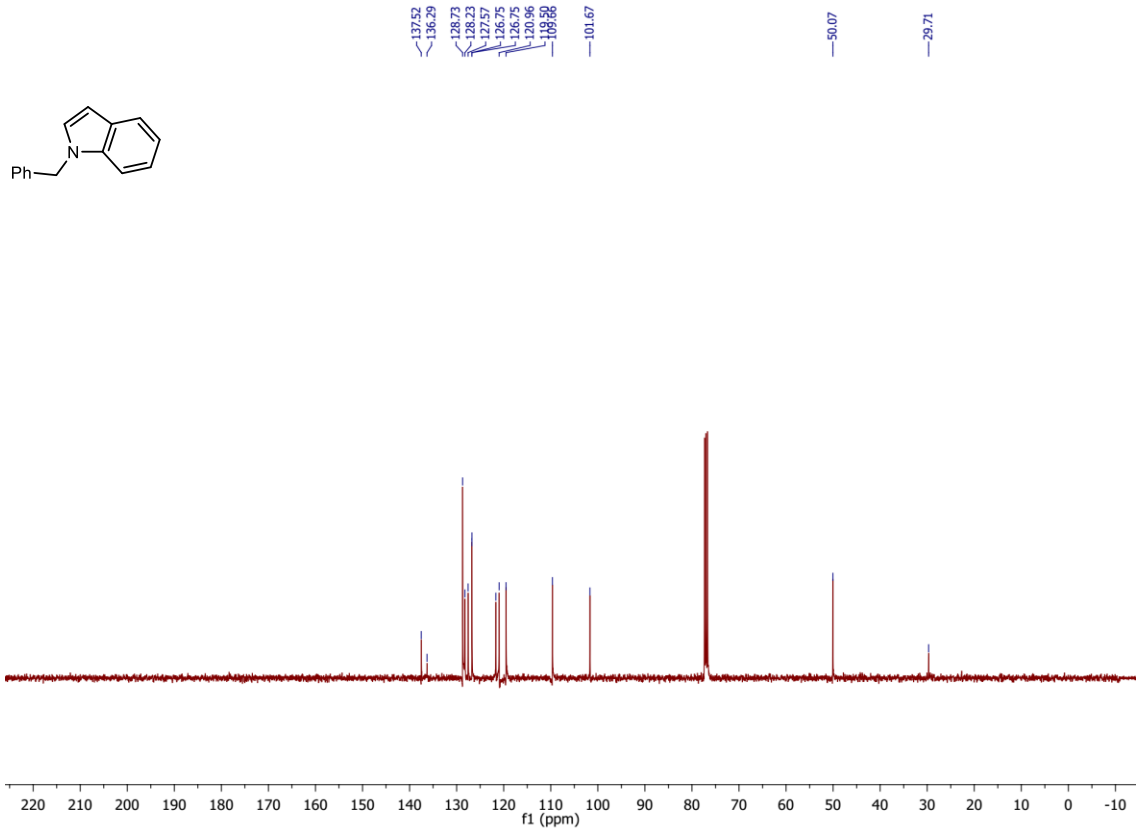

^{1}H-NMR (300 MHz, $CDCl_3$) spectrum of 6aa

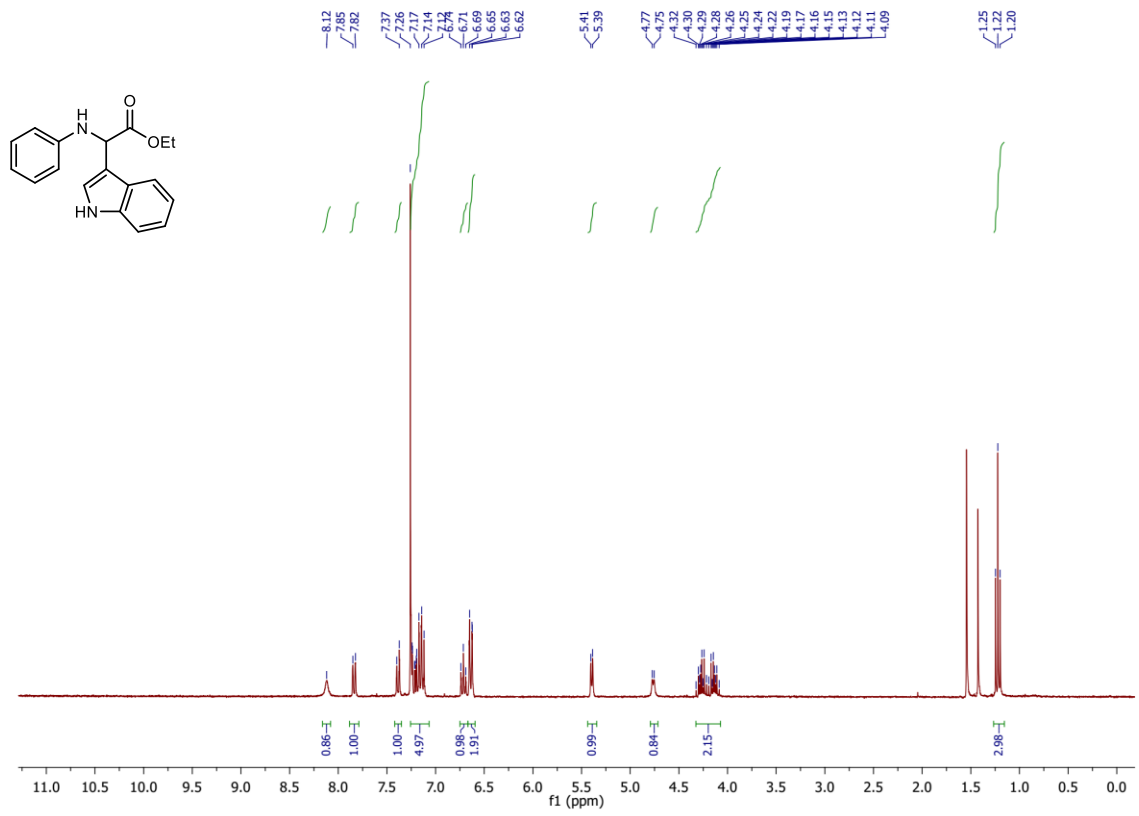

^{13}C-NMR (101 MHz, $CDCl_3$) spectrum of 6aa

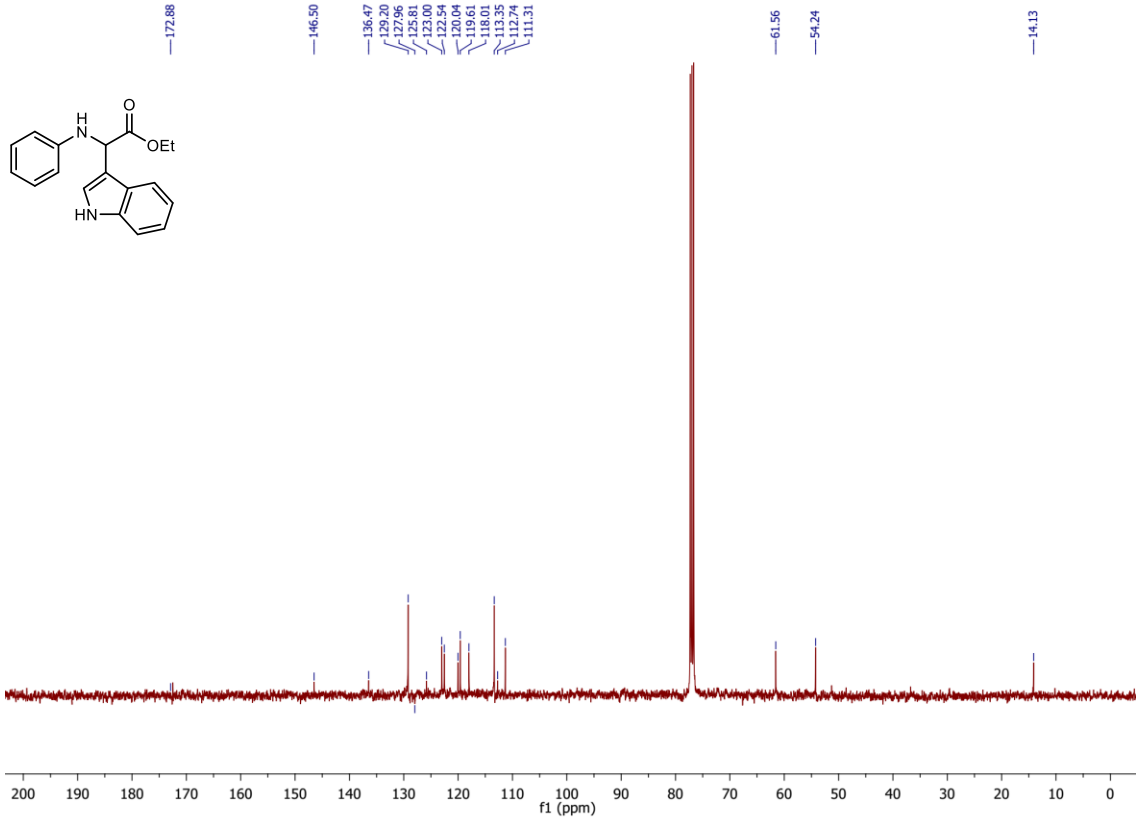

^{1}H-NMR (300 MHz, $CDCl_3$) spectrum of 7

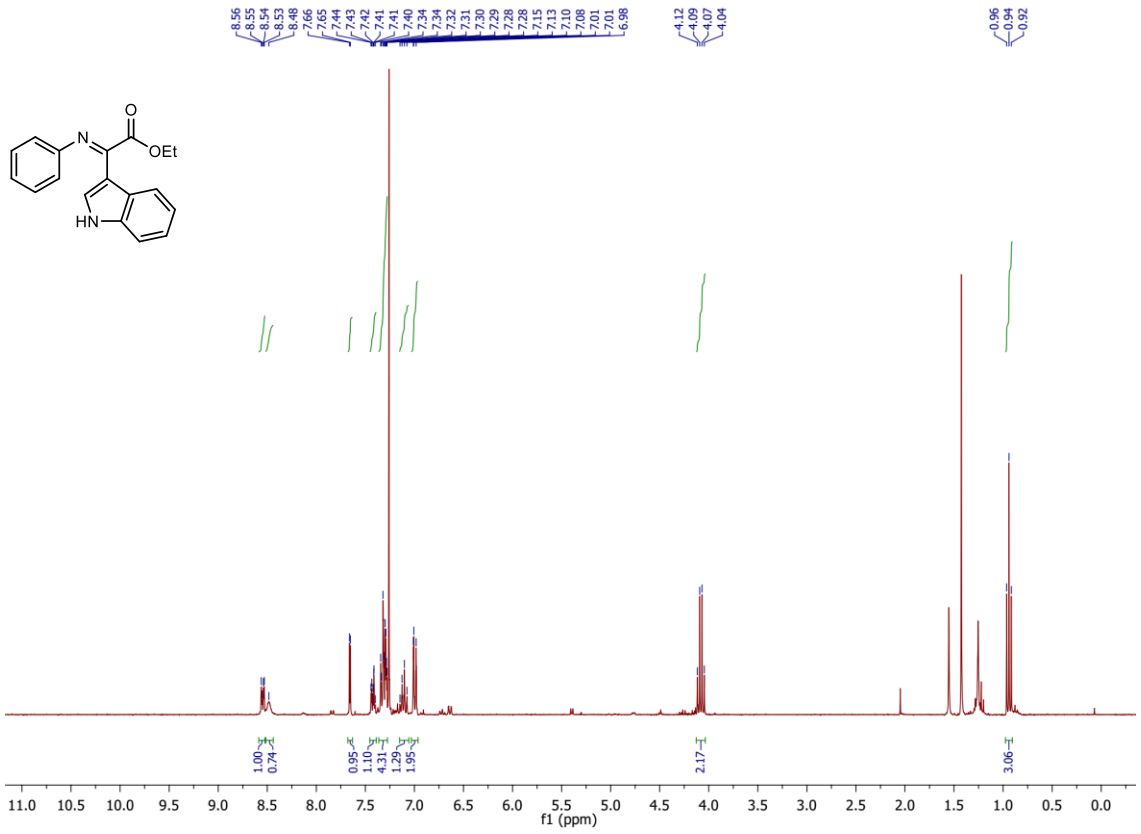

^{13}C-NMR (101 MHz, $CDCl_3$) spectrum of 7

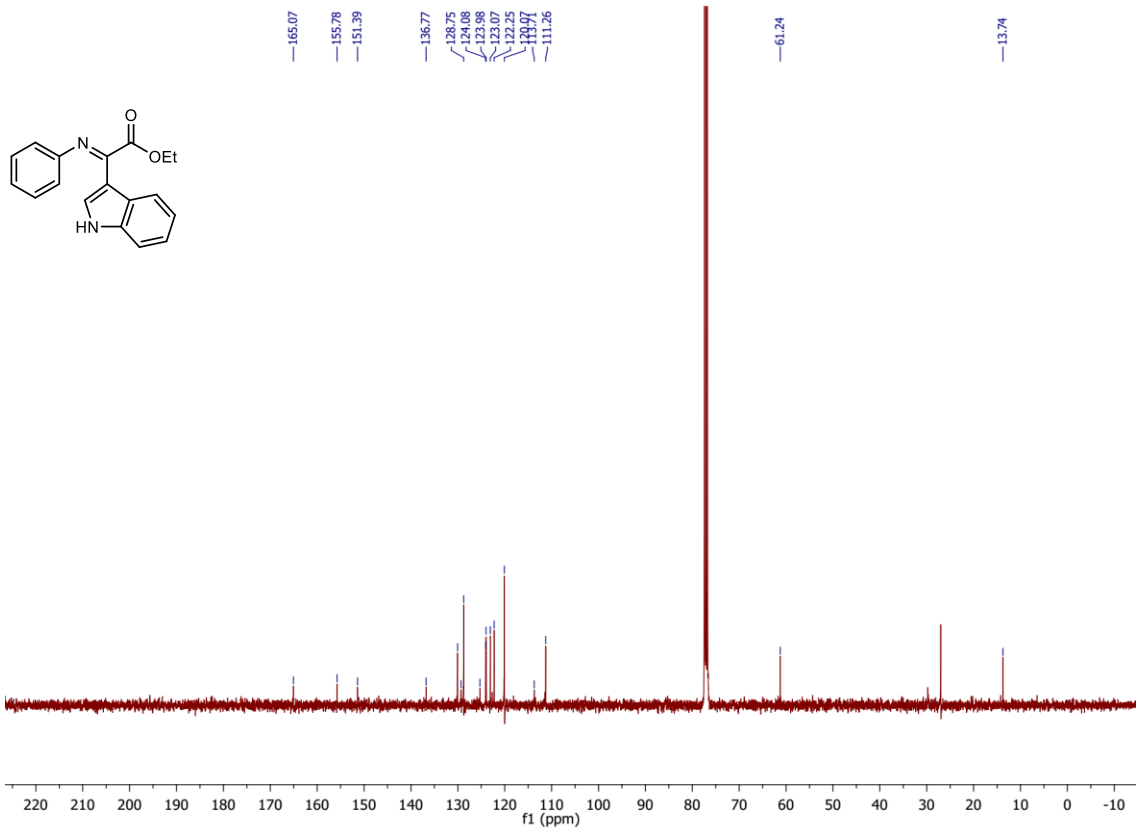

^{1}H-NMR (300 MHz, $CDCl_3$) spectrum of 8

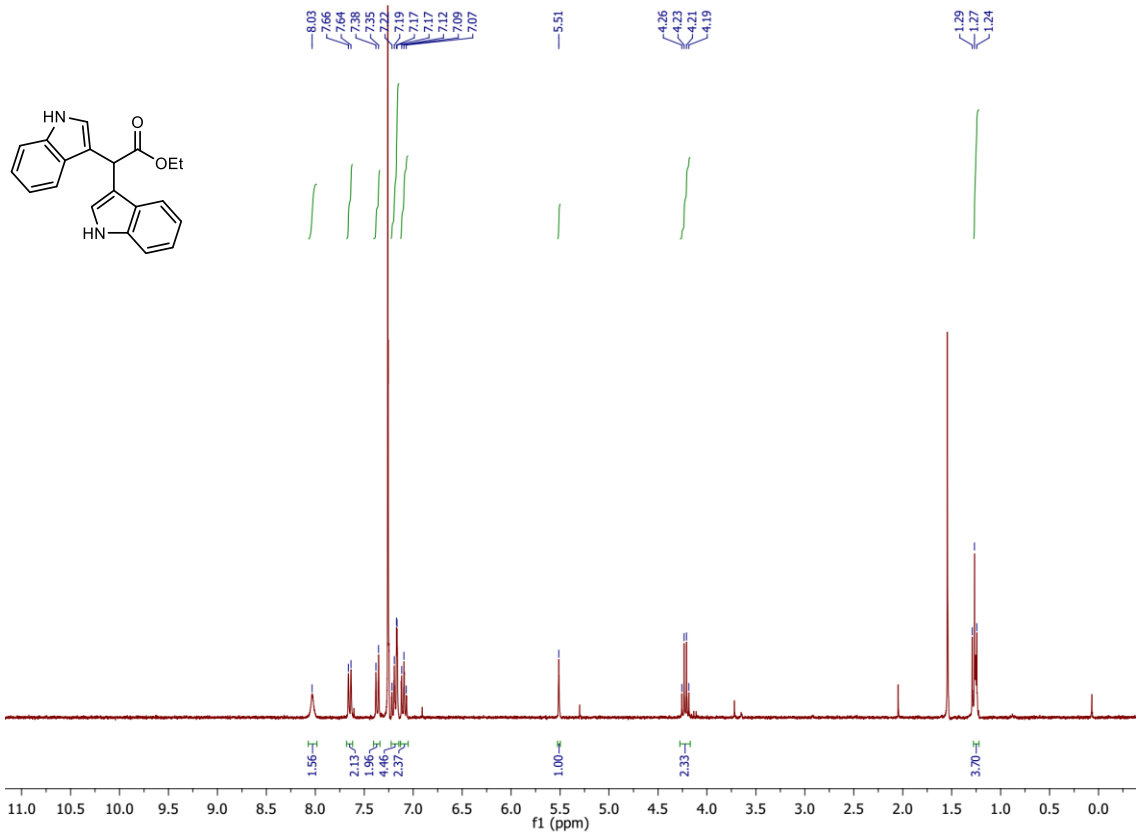

^{13}C-NMR (101 MHz, $CDCl_3$) spectrum of 8

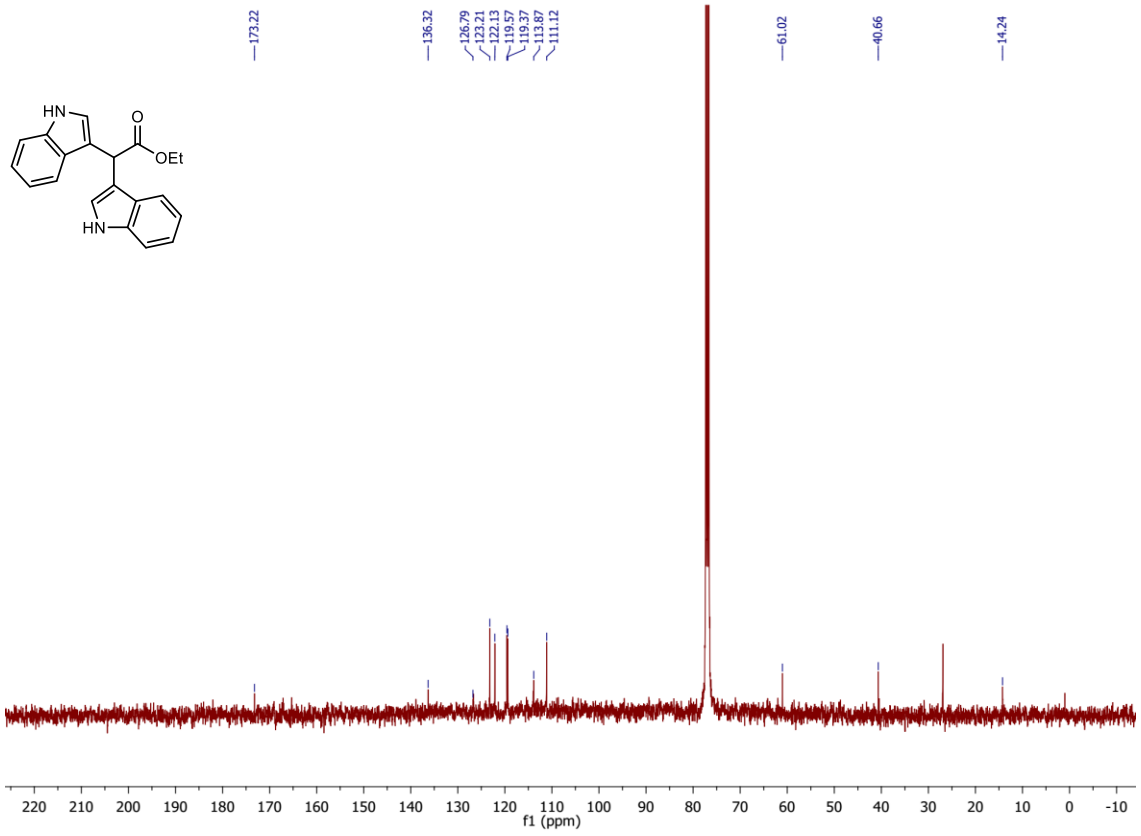

^{1}H-NMR (300 MHz, $CDCl_3$) spectrum of 6ba

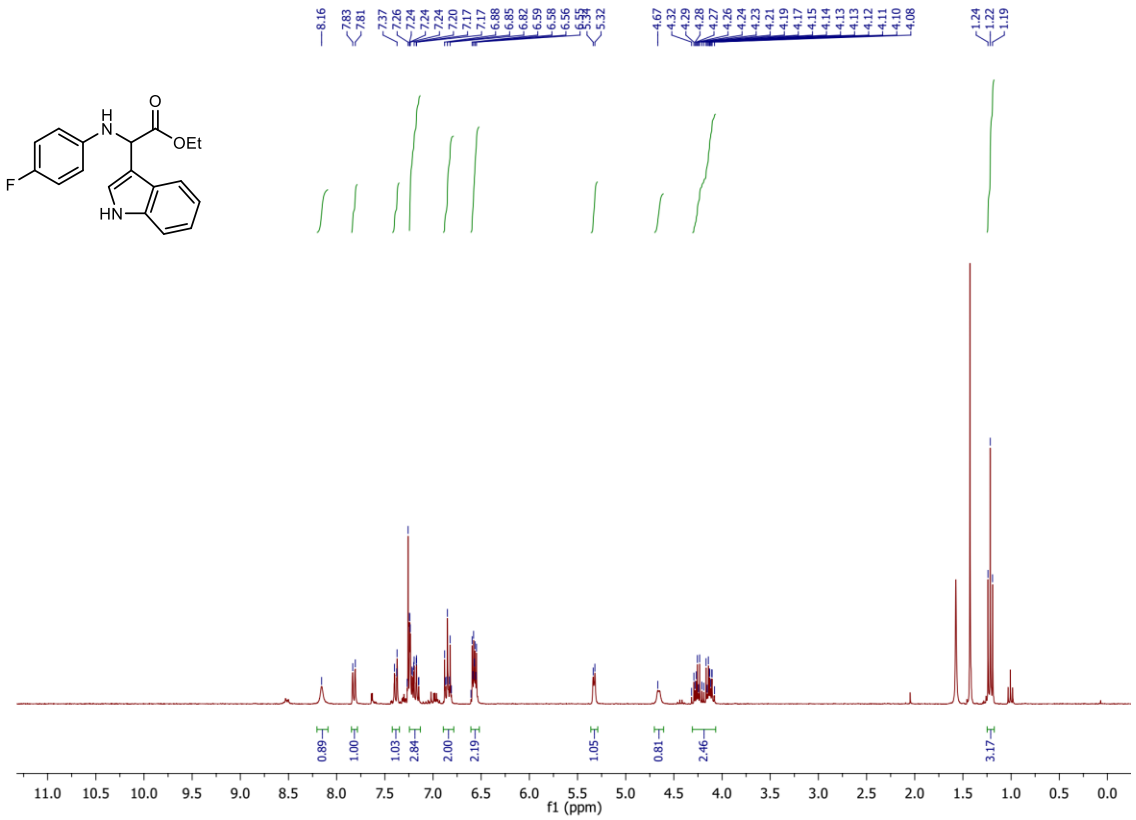

^{13}C-NMR (101 MHz, $CDCl_3$) spectrum of 6ba

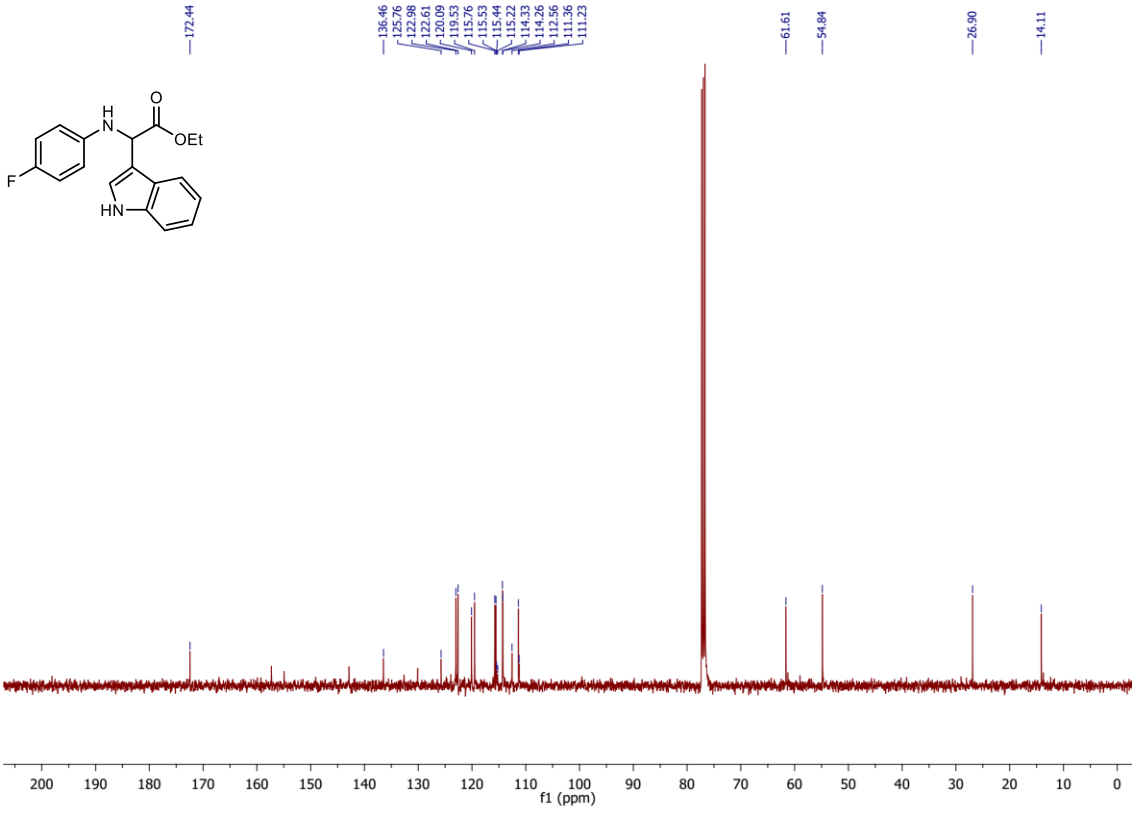

^{19}F-NMR (376 MHz, $CDCl_3$) spectrum of 6ba

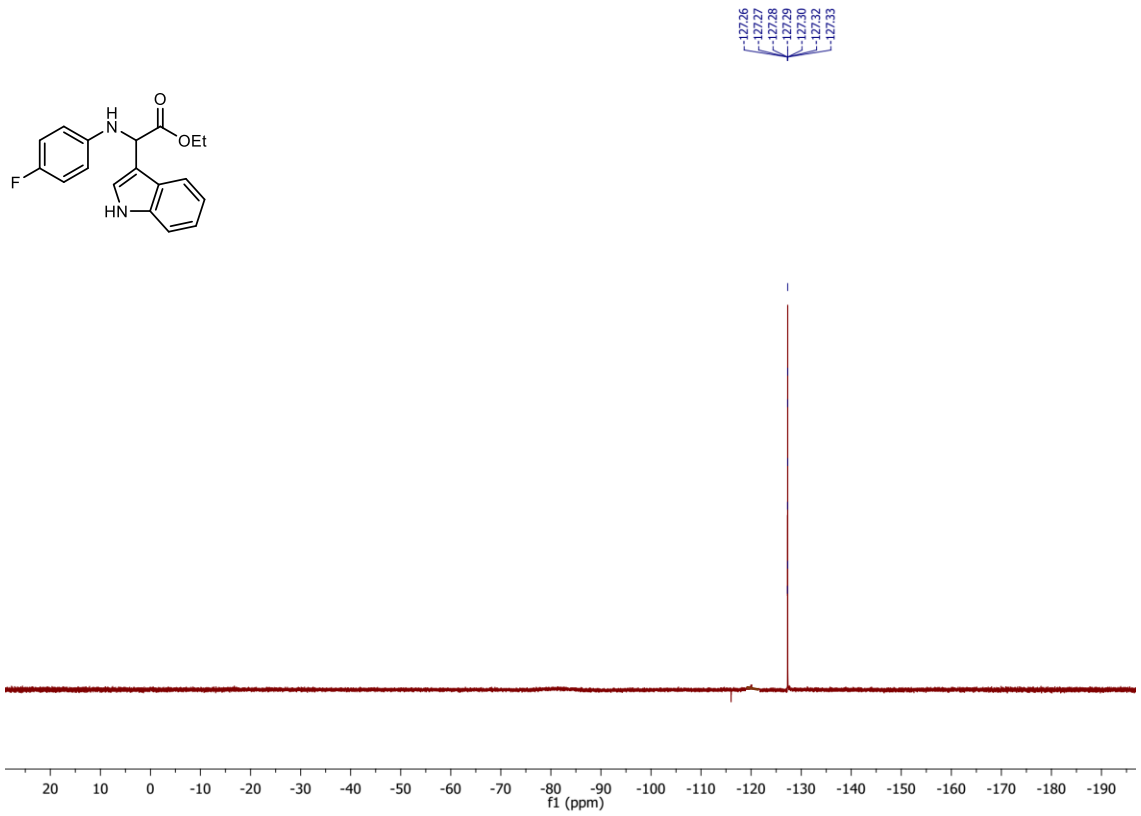

^{1}H-NMR (300 MHz, $CDCl_3$) spectrum of 6ca

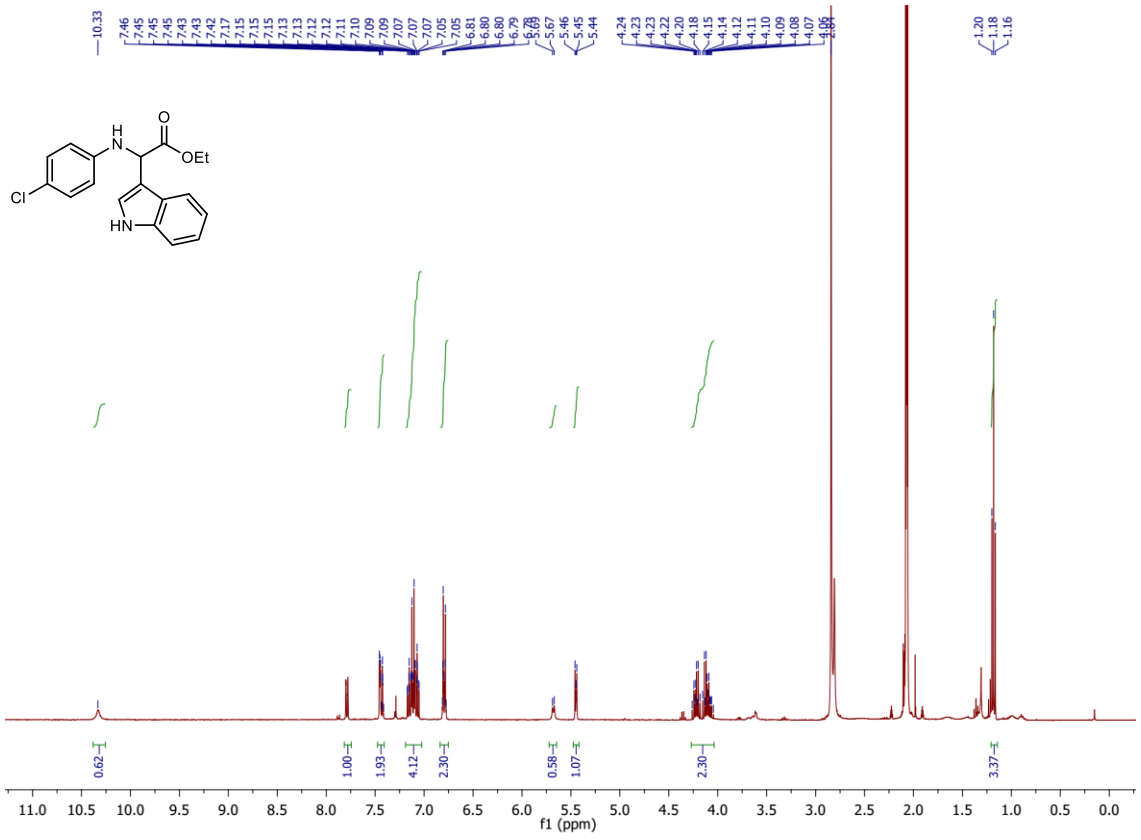

^{13}C-NMR (101 MHz, $CDCl_3$) spectrum of 6ca

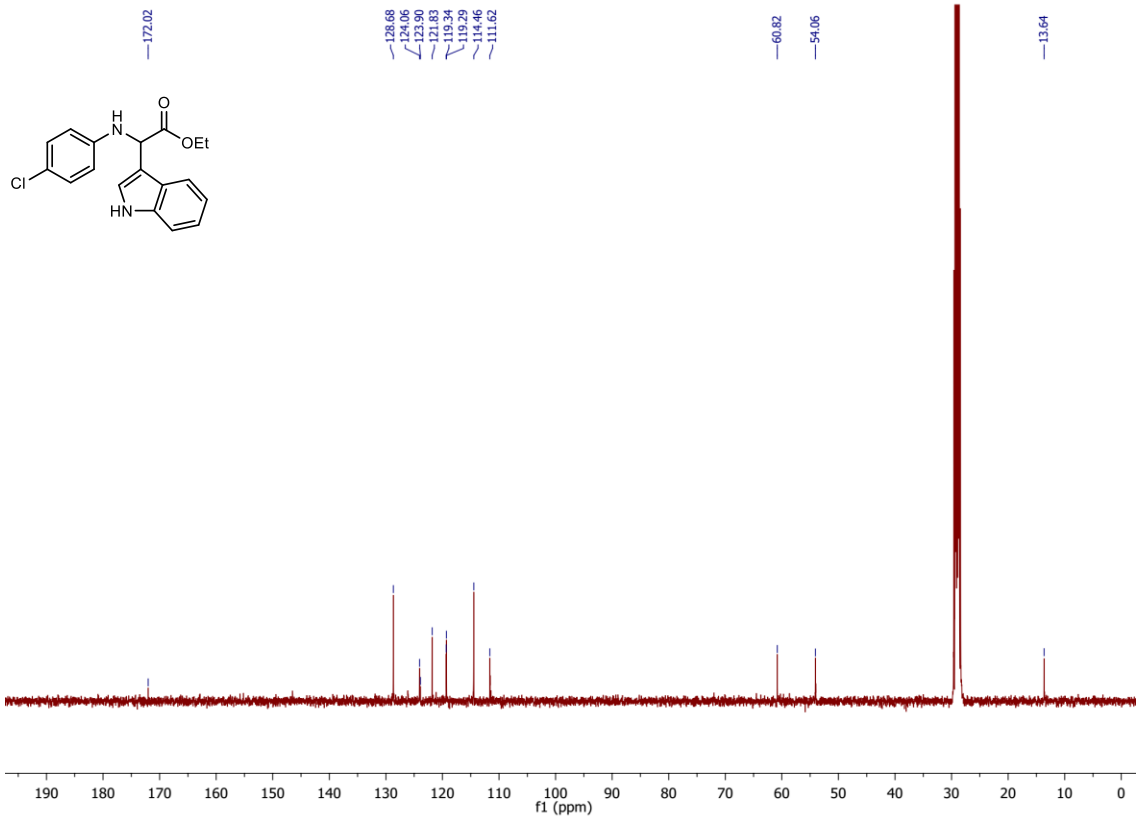

^{1}H-NMR (300 MHz, acetone-D6) spectrum of 6da

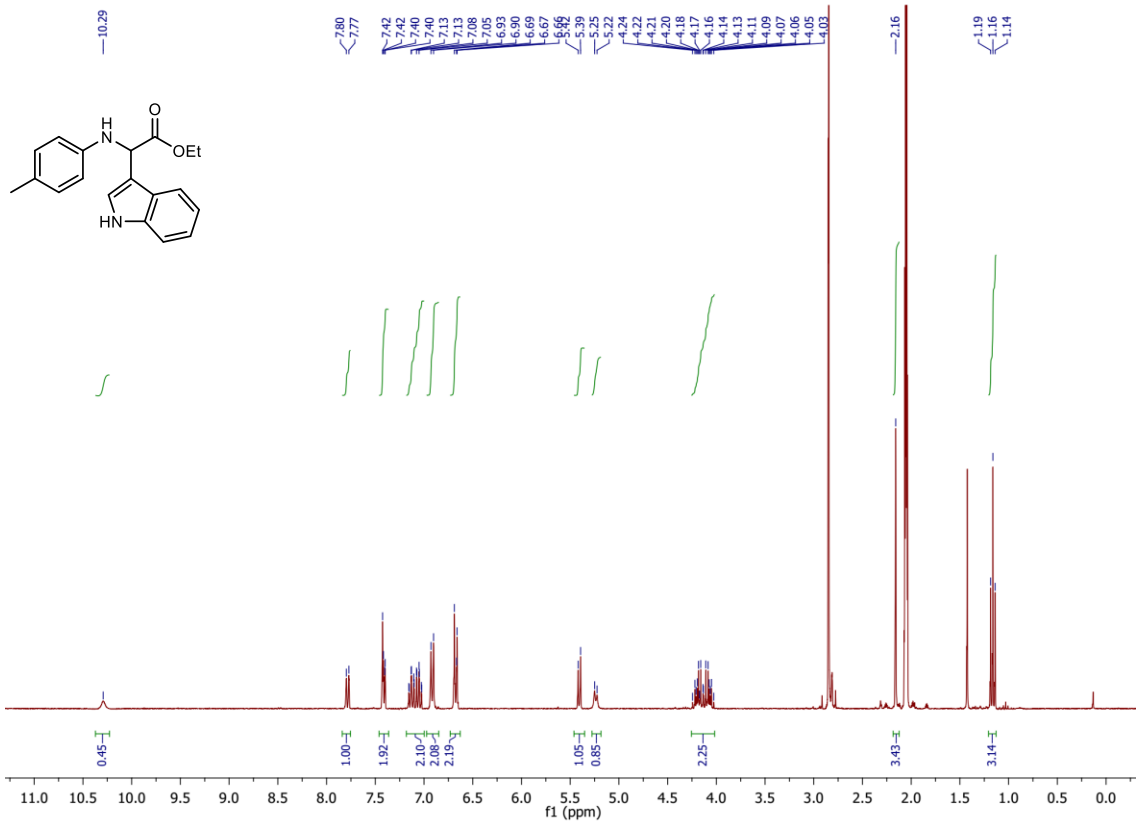

^{13}C-NMR (101 MHz, acetone-D6) spectrum of 6da

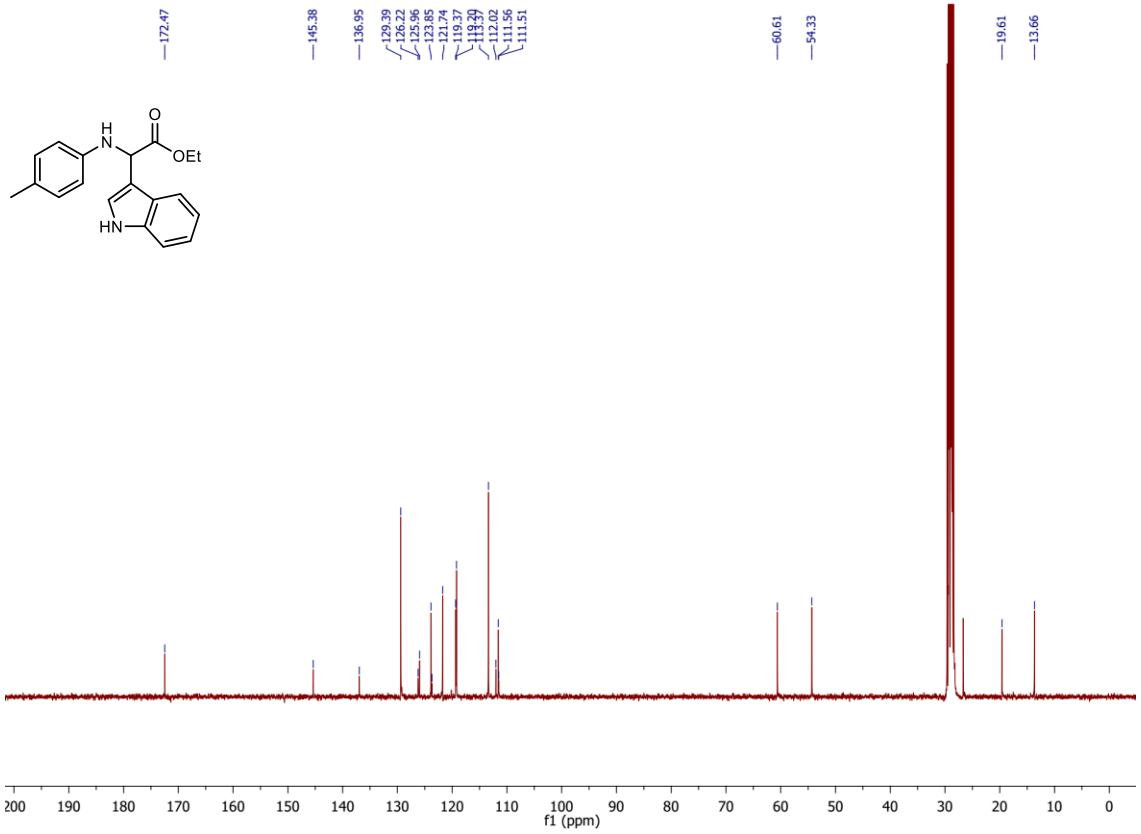

^{1}H-NMR (300 MHz, $CDCl_3$) spectrum of 6ea

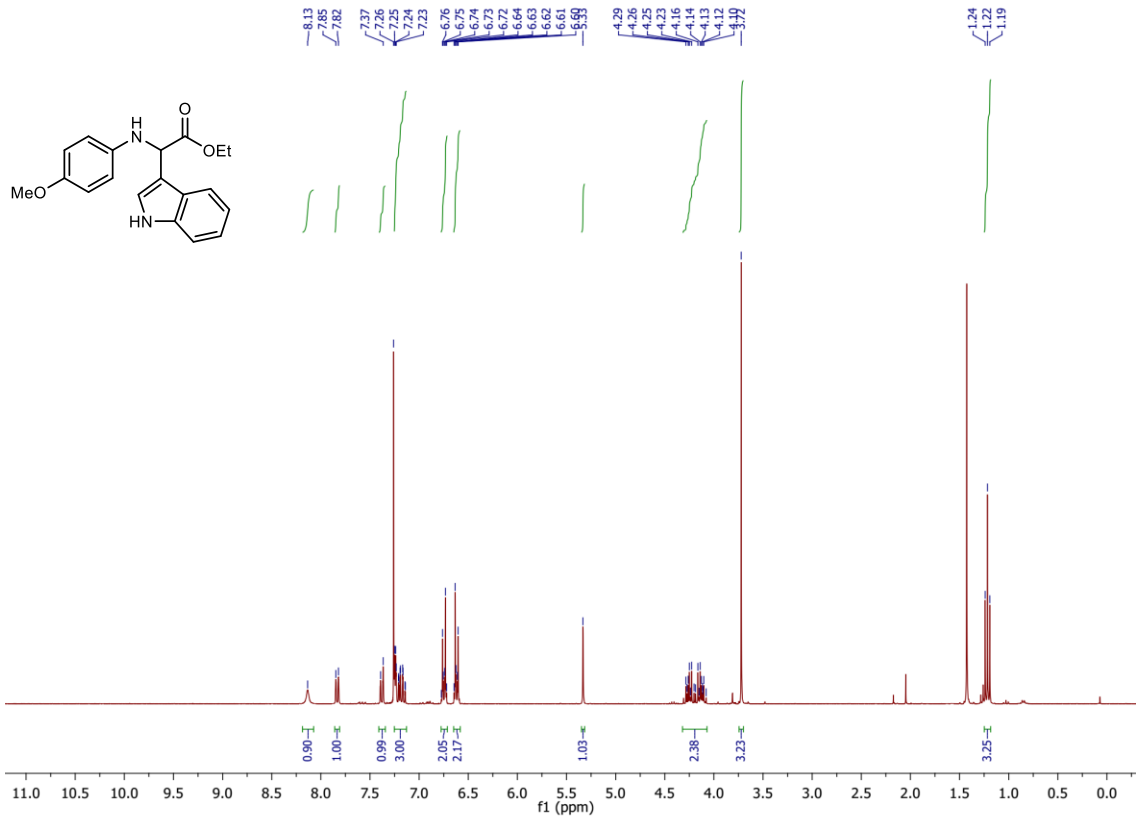

^{13}C-NMR (101 MHz, $CDCl_3$) spectrum of 6ea

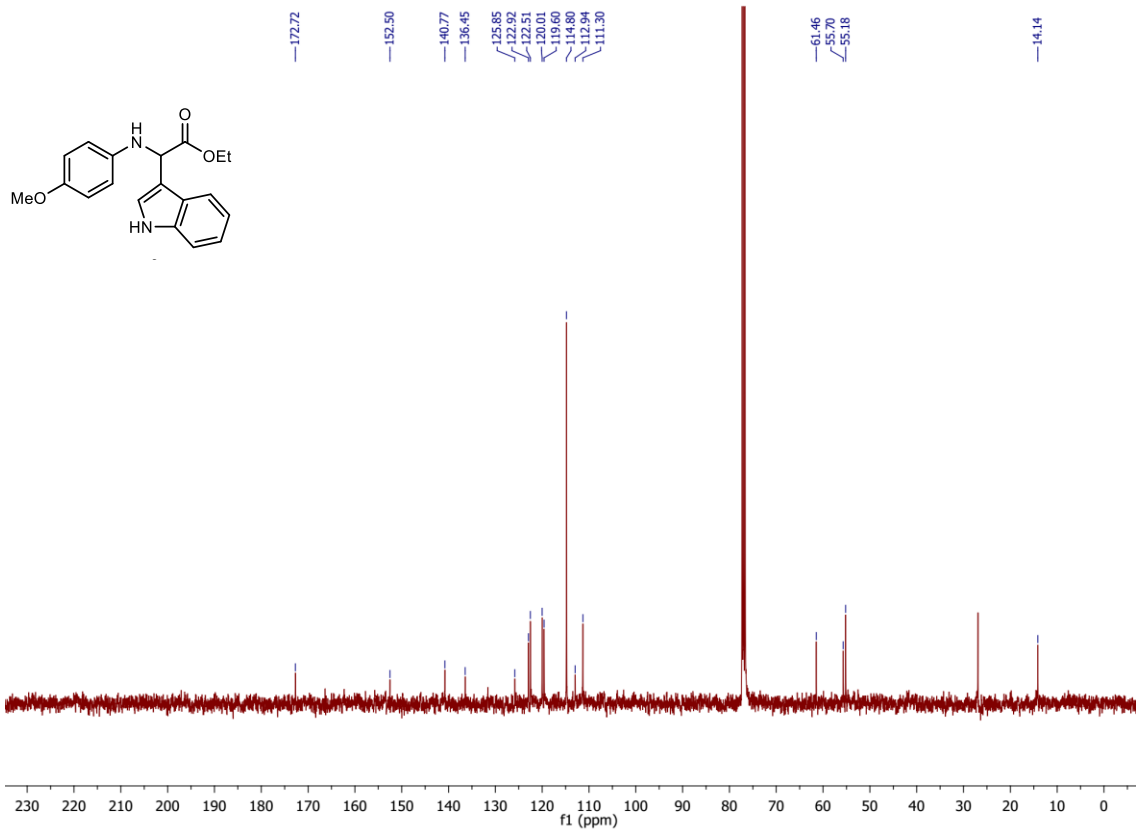

^{1}H-NMR (300 MHz, $CDCl_3$) spectrum of 6fa

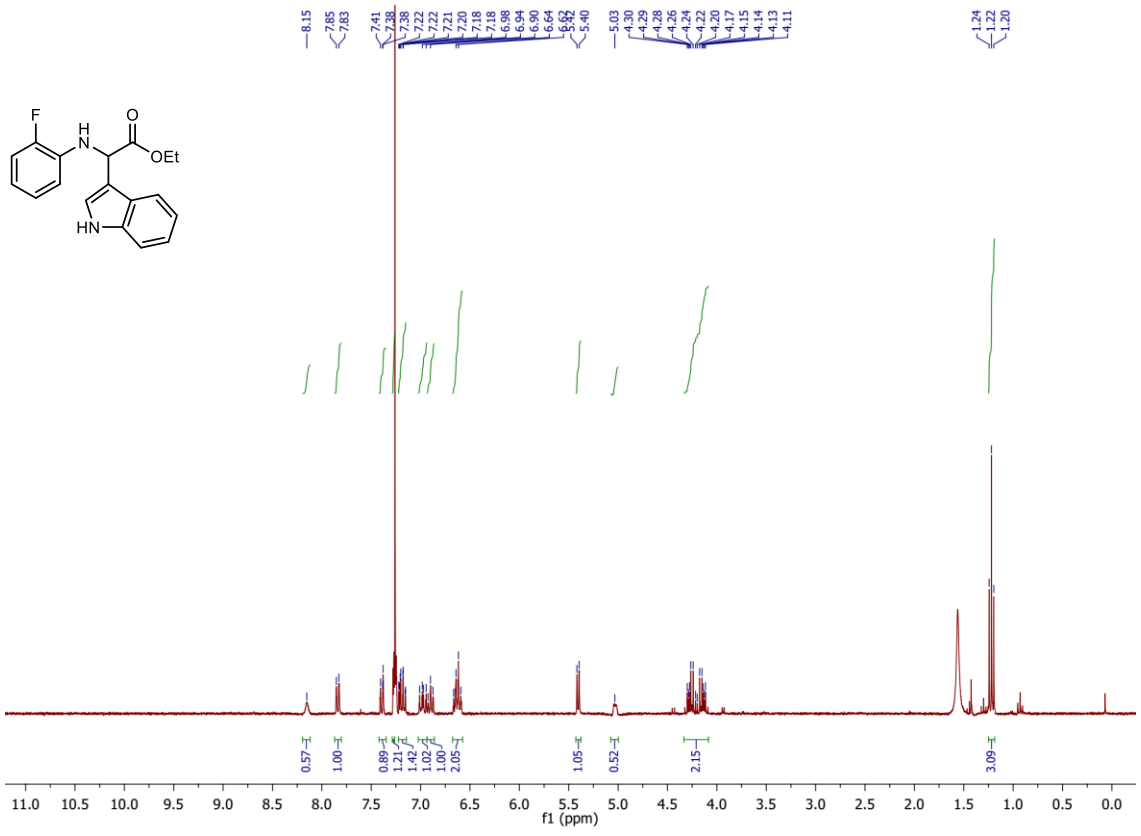

^{13}C-NMR (101 MHz, $CDCl_3$) spectrum of 6fa

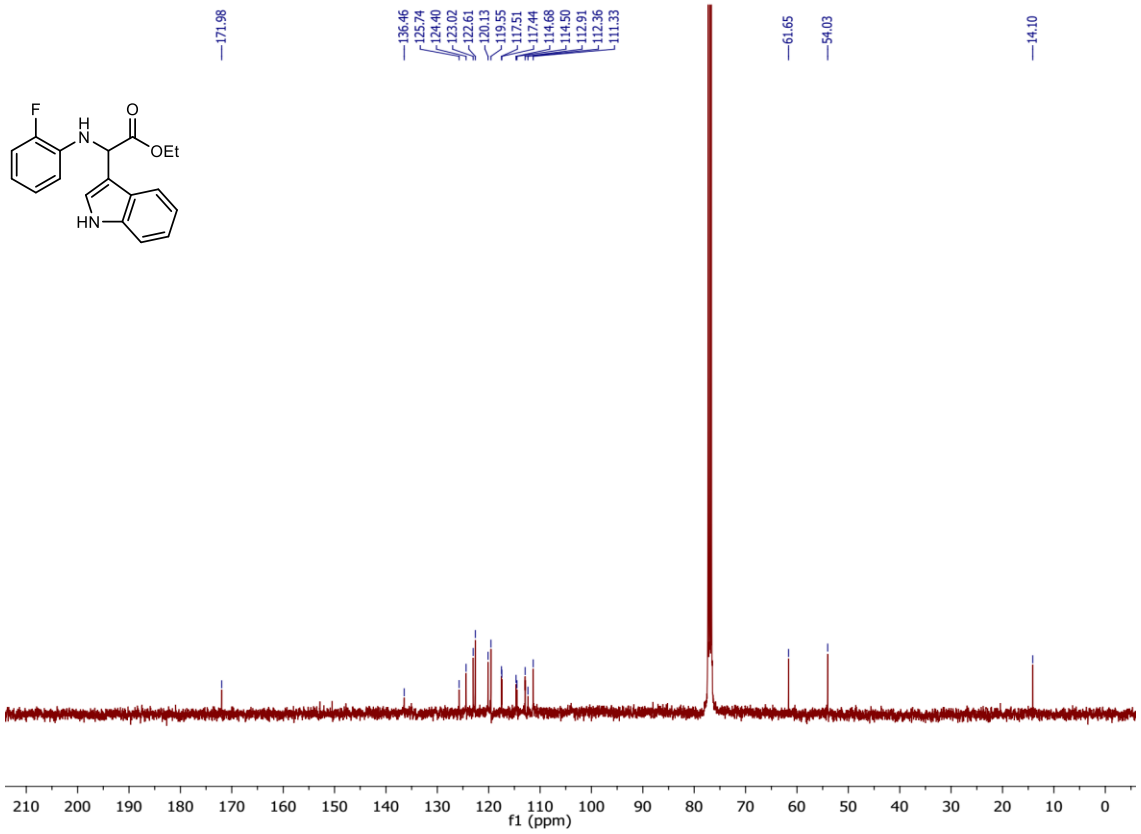

^{19}F-NMR (376 MHz, $CDCl_3$) spectrum of 6fa

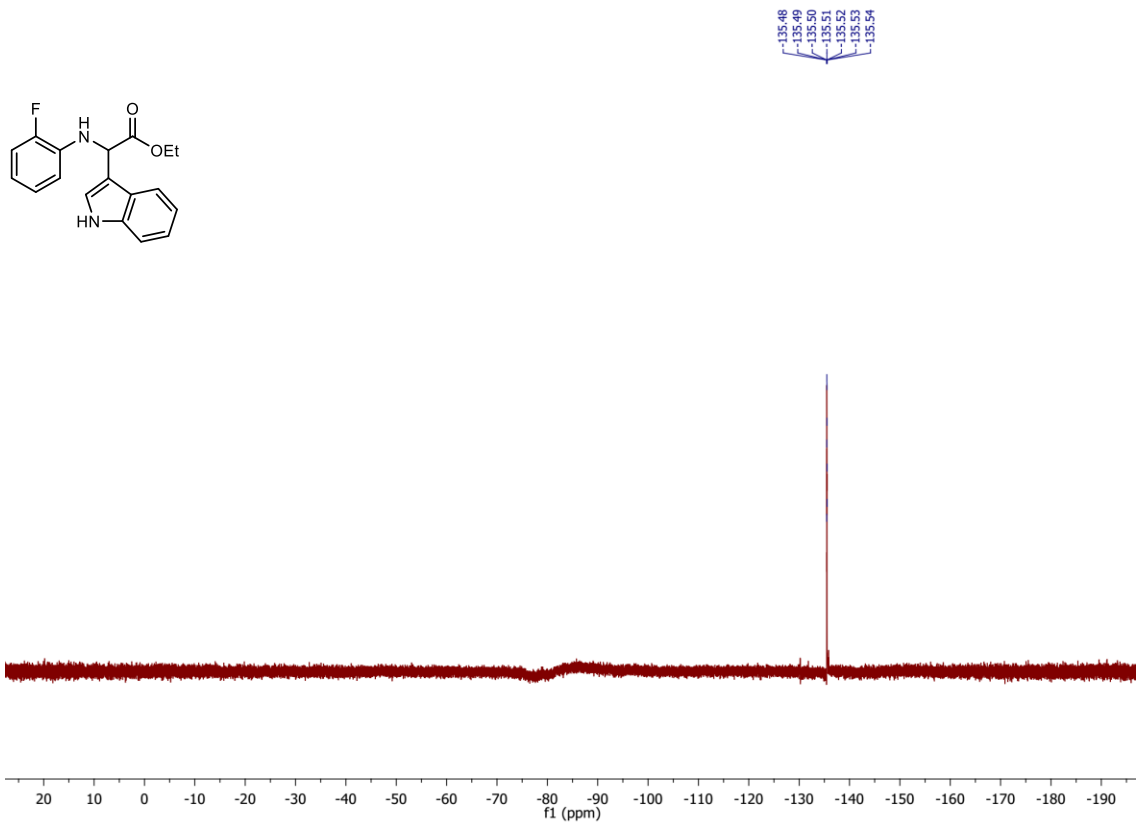

^{1}H-NMR (300 MHz, $CDCl_3$) spectrum of 6ab

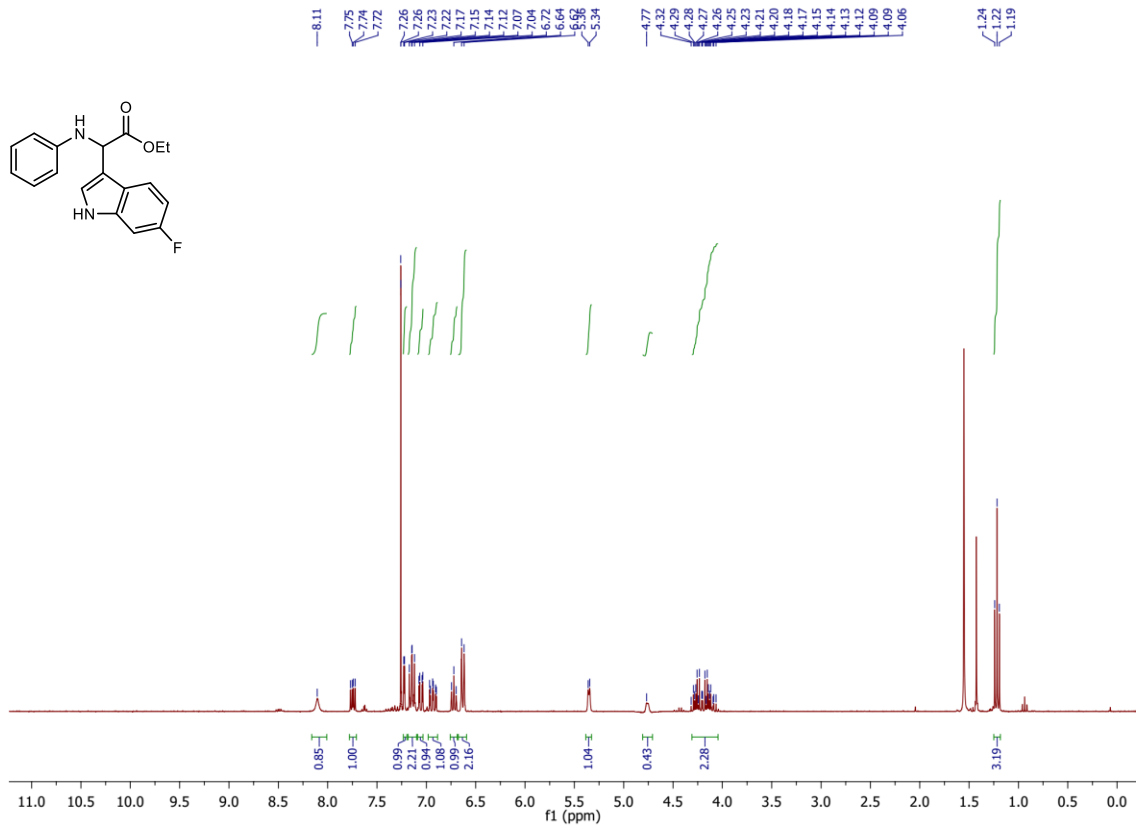

^{13}C-NMR (101 MHz, $CDCl_3$) spectrum of 6ab

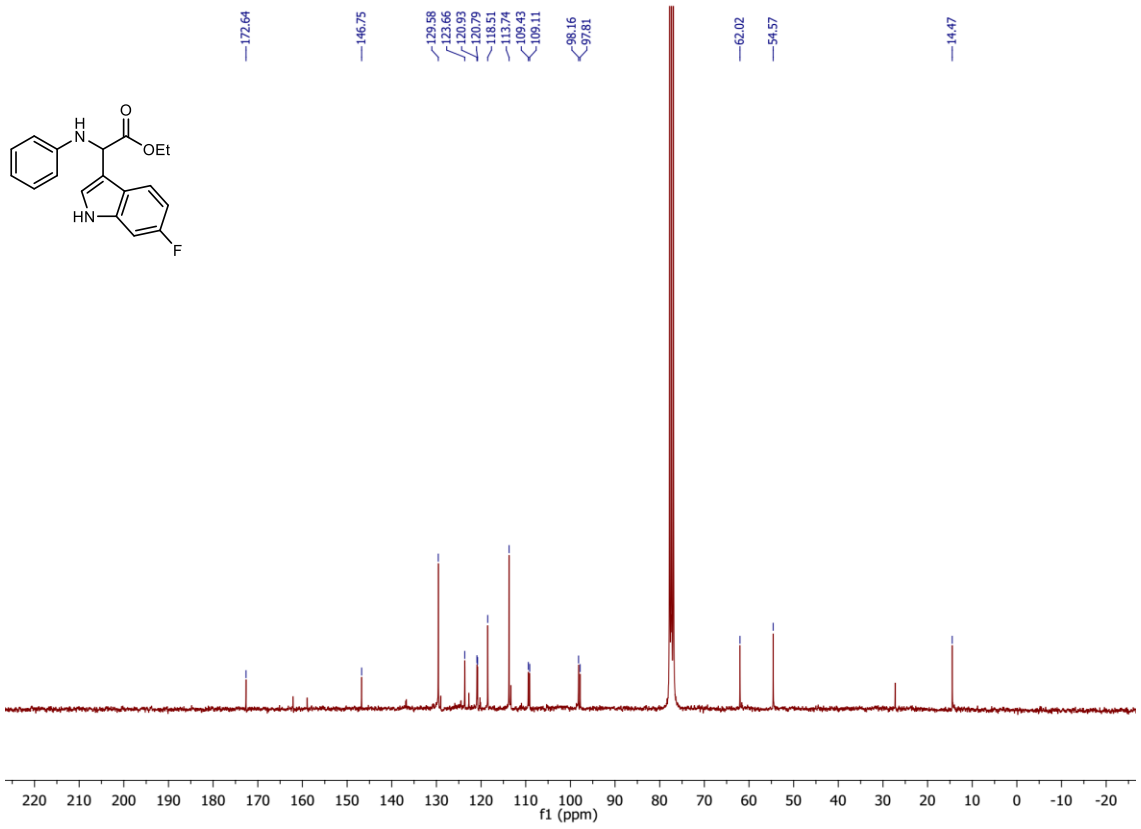

^{19}F-NMR (376 MHz, $CDCl_3$) spectrum of 6ab

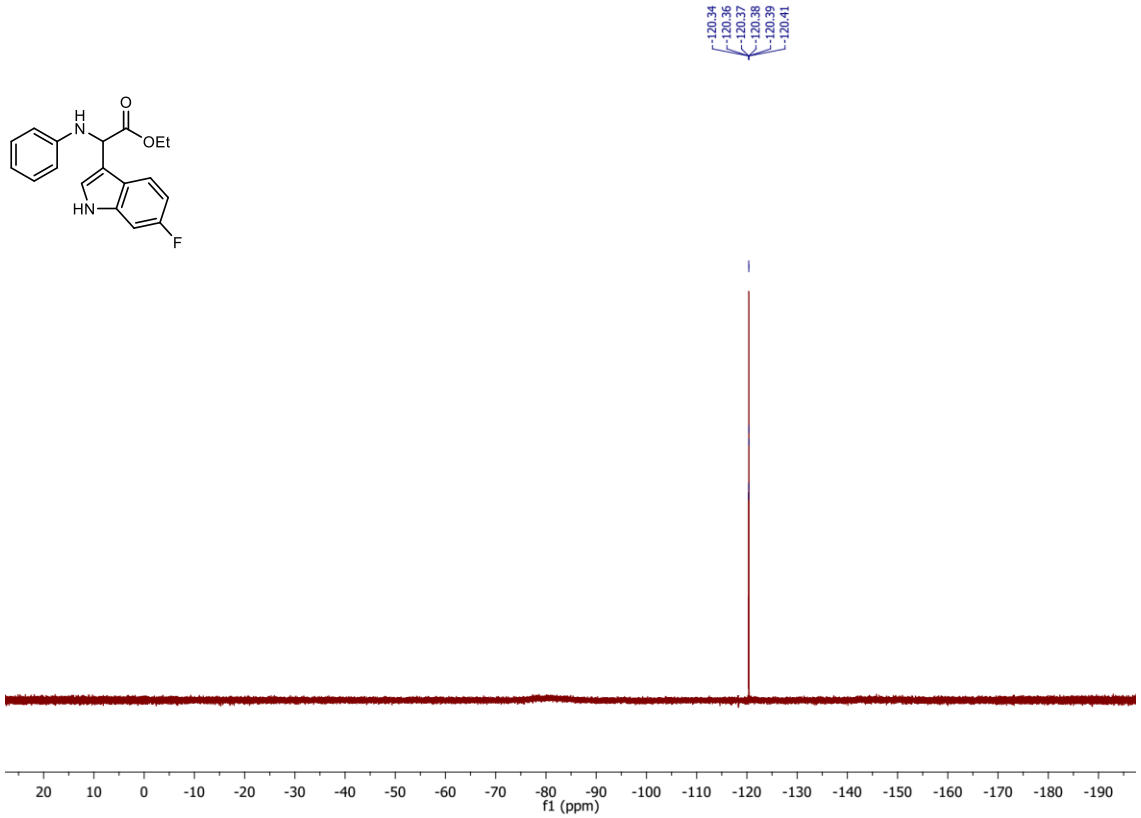

^{1}H-NMR (300 MHz, $CDCl_3$) spectrum of 6ac

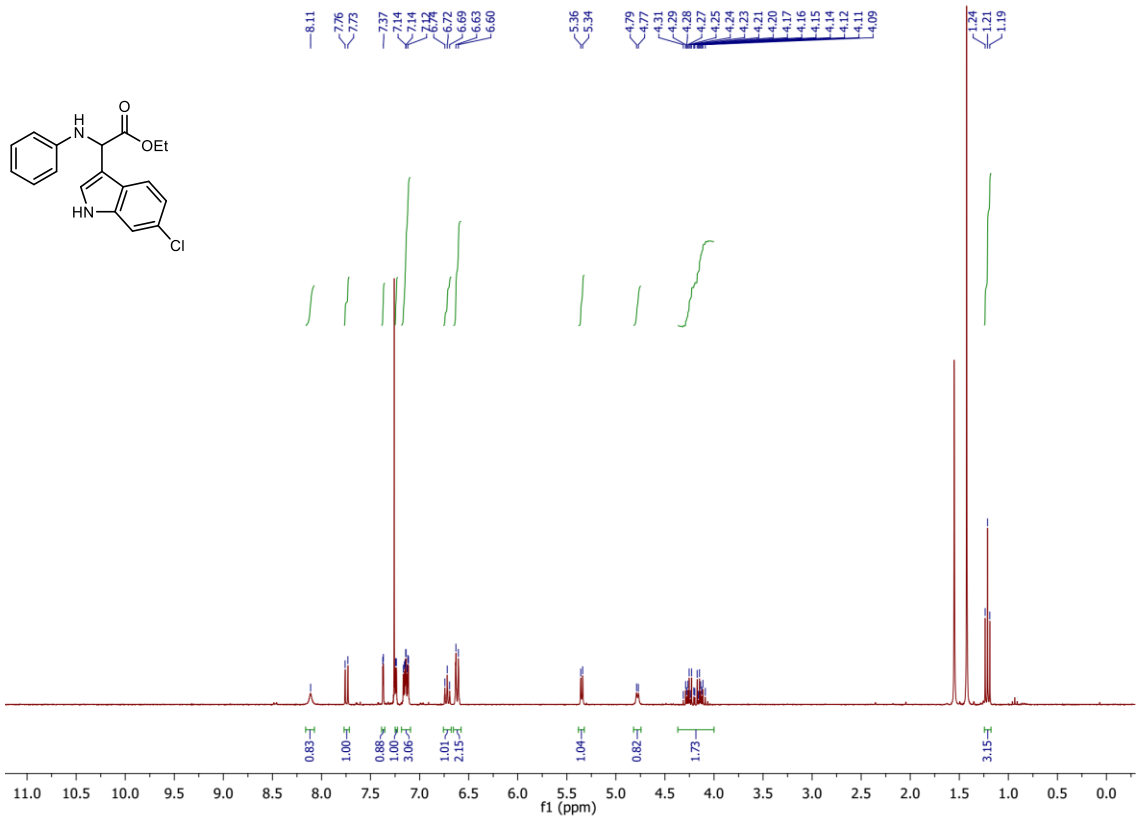

^{13}C-NMR (101 MHz, $CDCl_3$) spectrum of 6ac

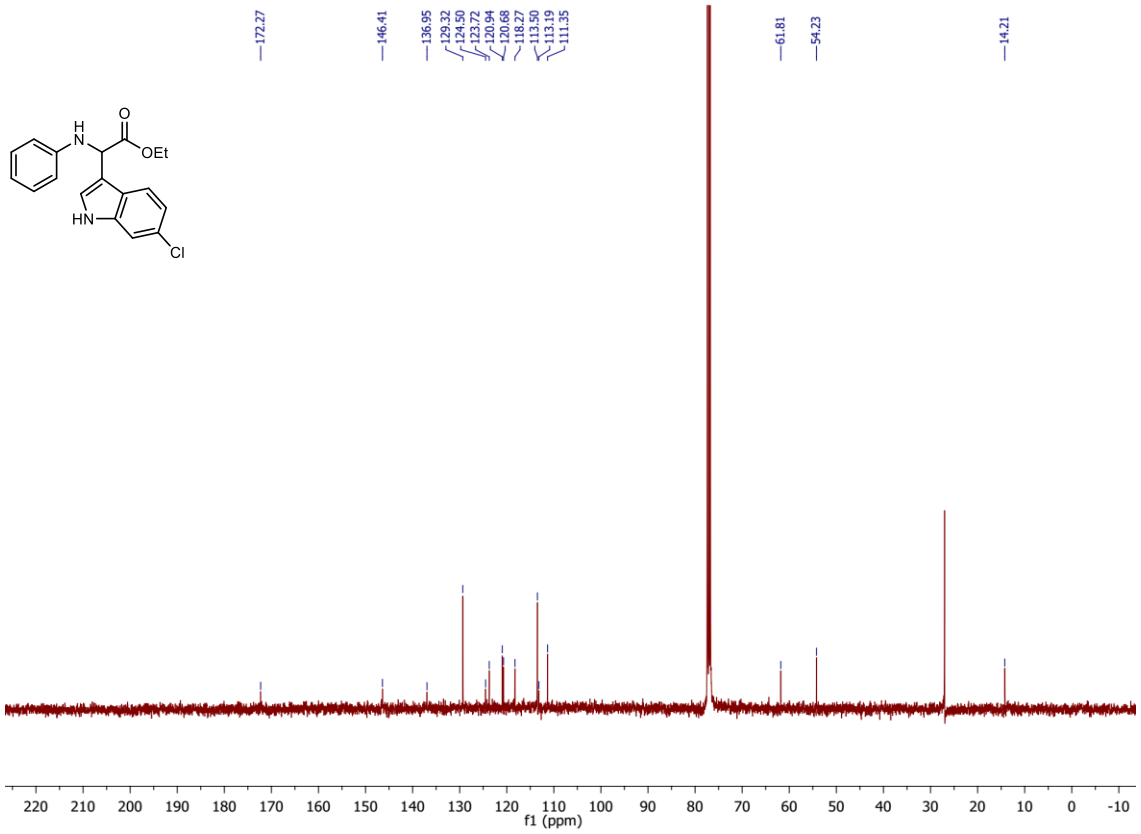

^{1}H-NMR (300 MHz, $CDCl_3$) spectrum of 6ad

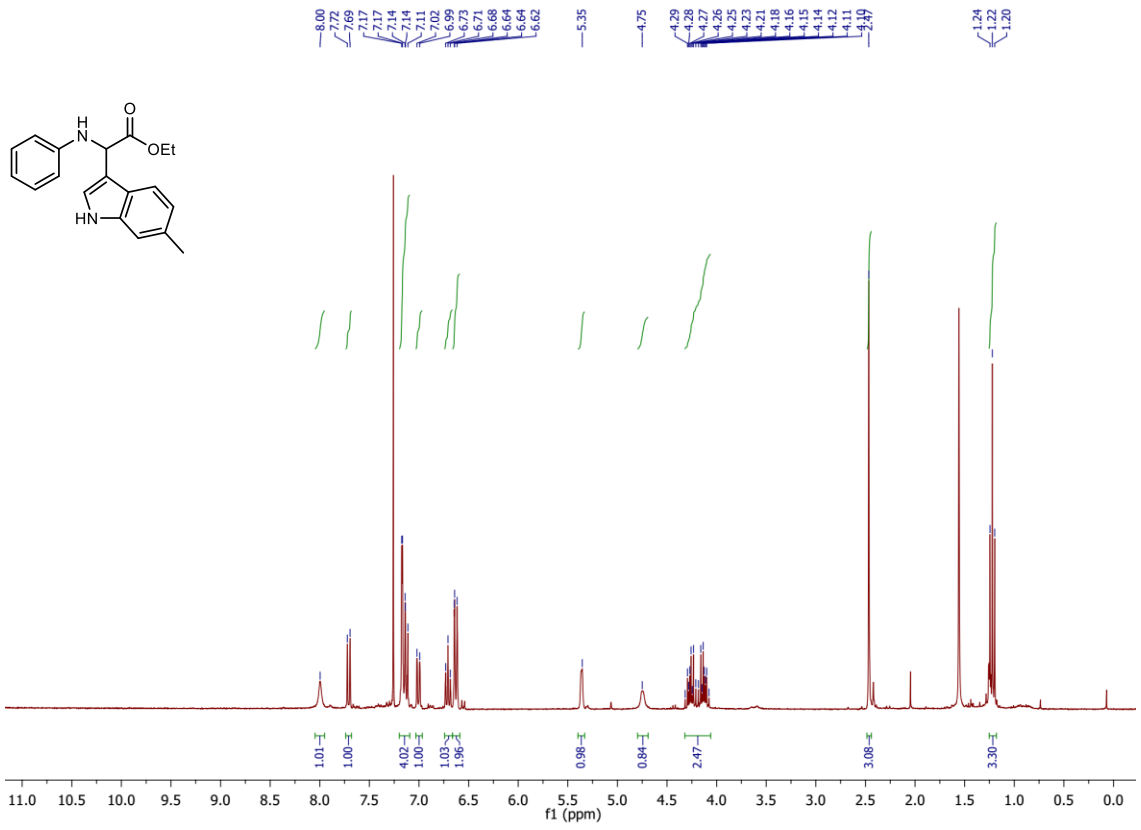

^{13}C-NMR (101 MHz, $CDCl_3$) spectrum of 6ad

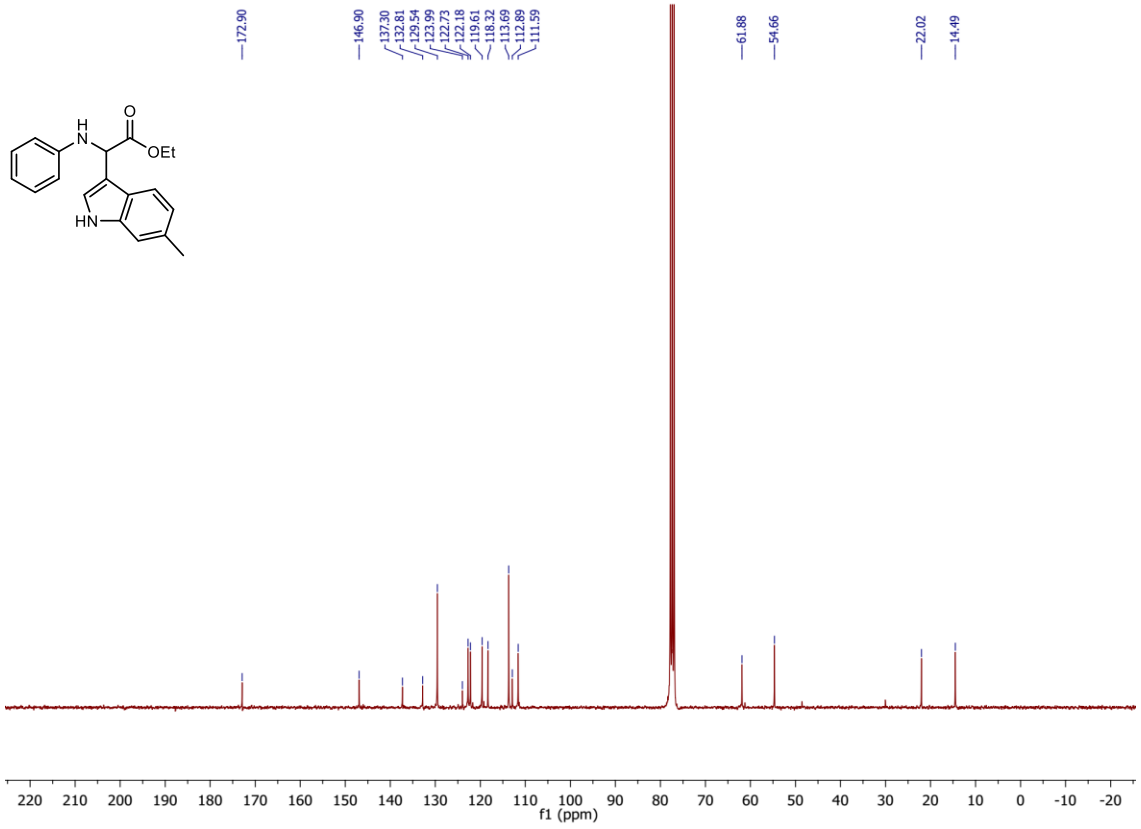

^{1}H-NMR (300 MHz, $CDCl_3$) spectrum of 6ae

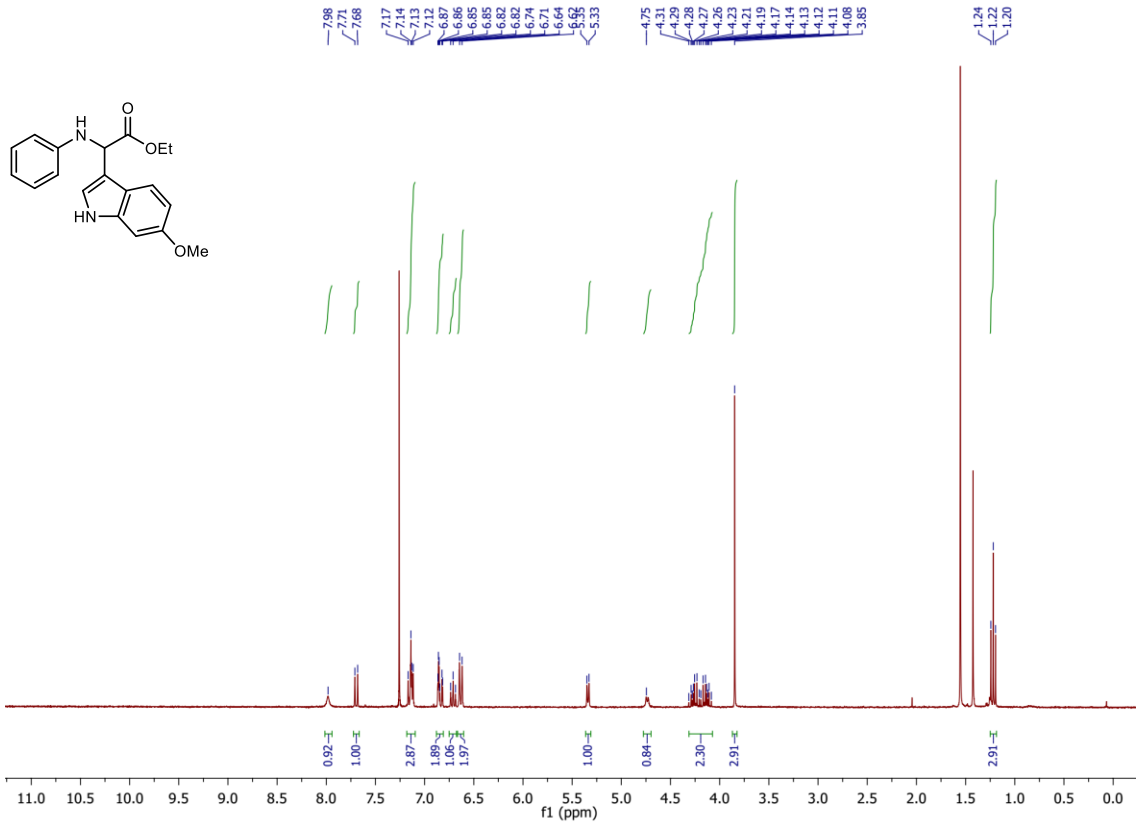

^{13}C-NMR (101 MHz, $CDCl_3$) spectrum of 6ae

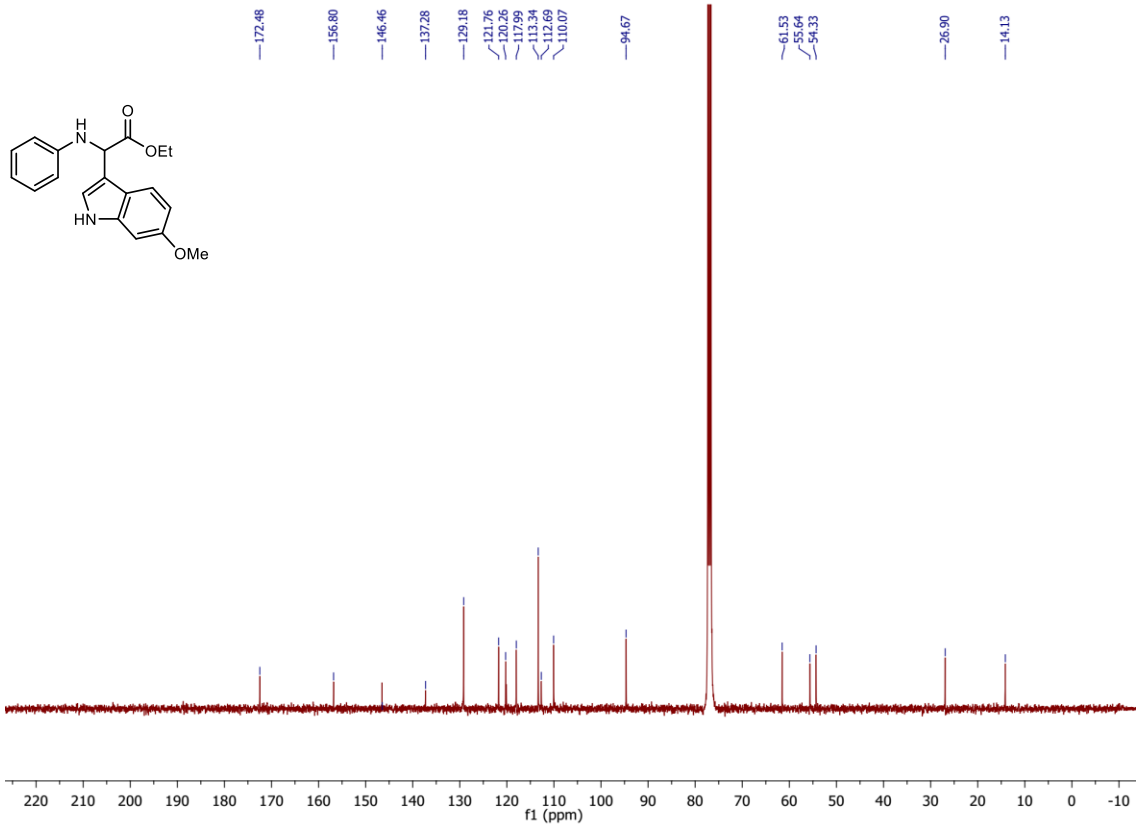

^{1}H-NMR (300 MHz, $CDCl_3$) spectrum of 6af

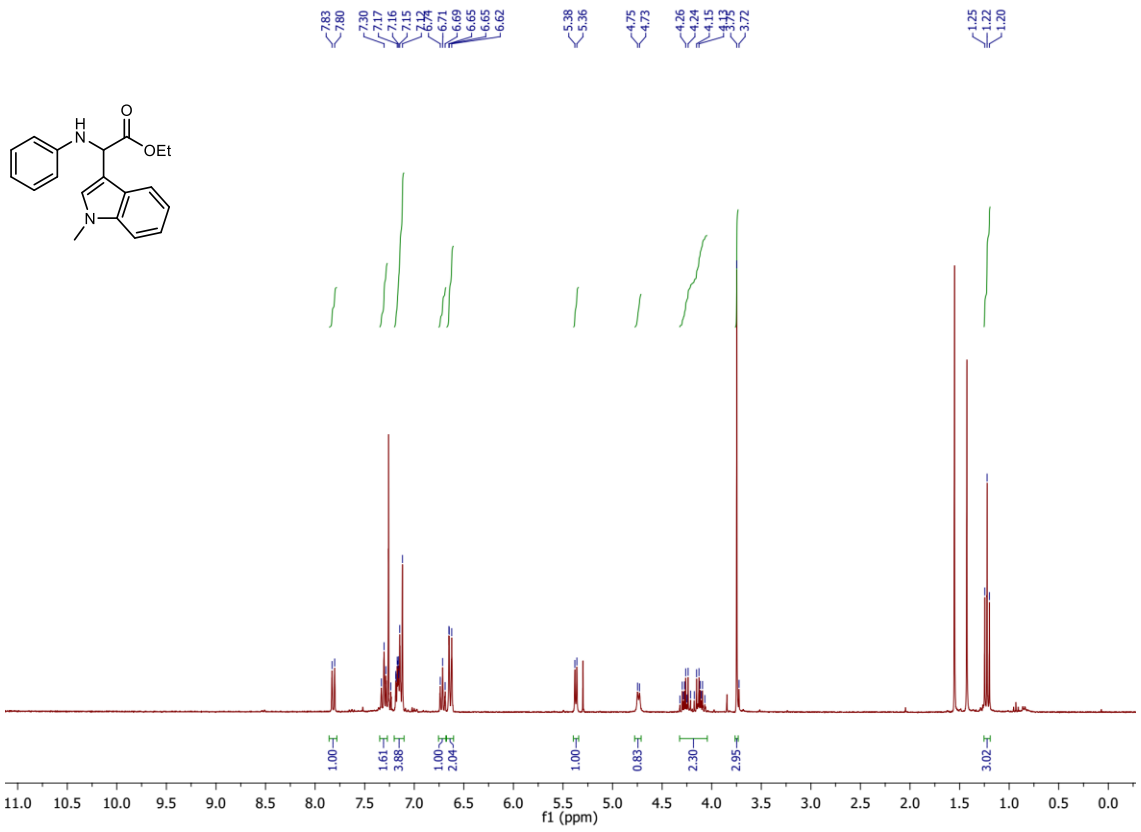

^{13}C-NMR (101 MHz, $CDCl_3$) spectrum of 6af

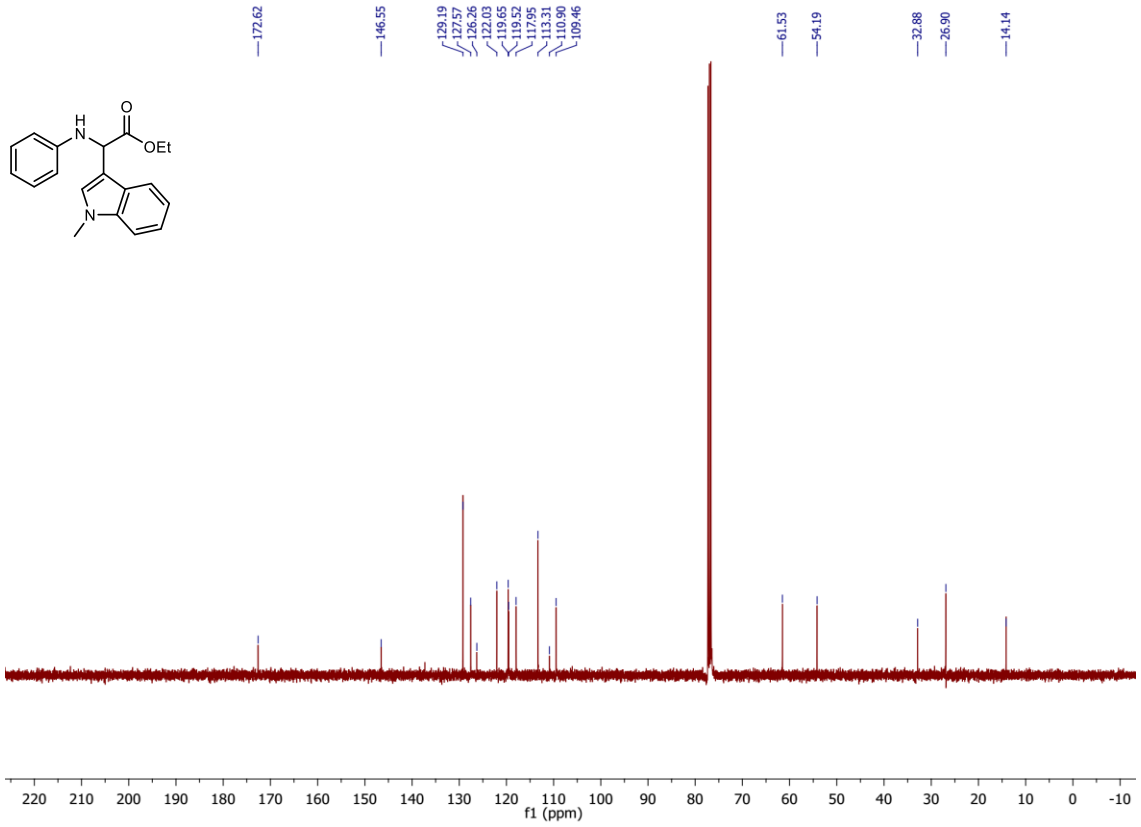

^{1}H-NMR (300 MHz, $CDCl_3$) spectrum of 6ag

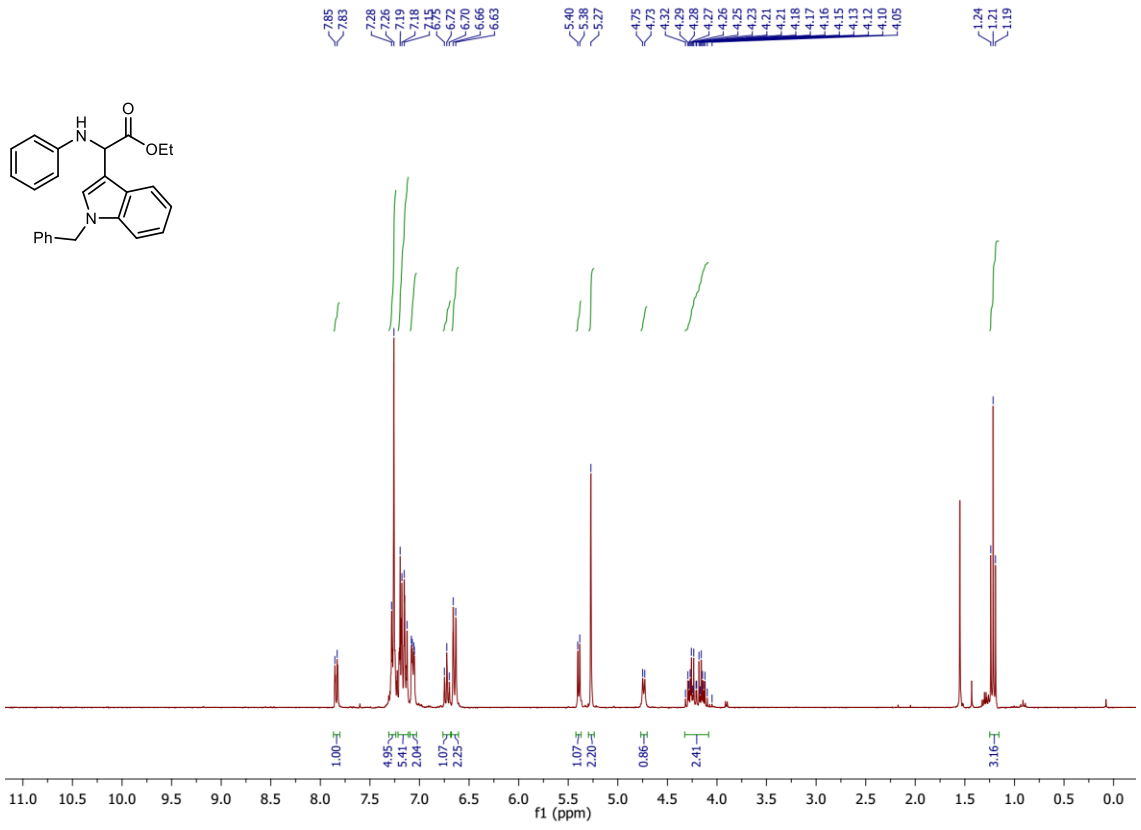

^{13}C-NMR (101 MHz, $CDCl_3$) spectrum of 6ag

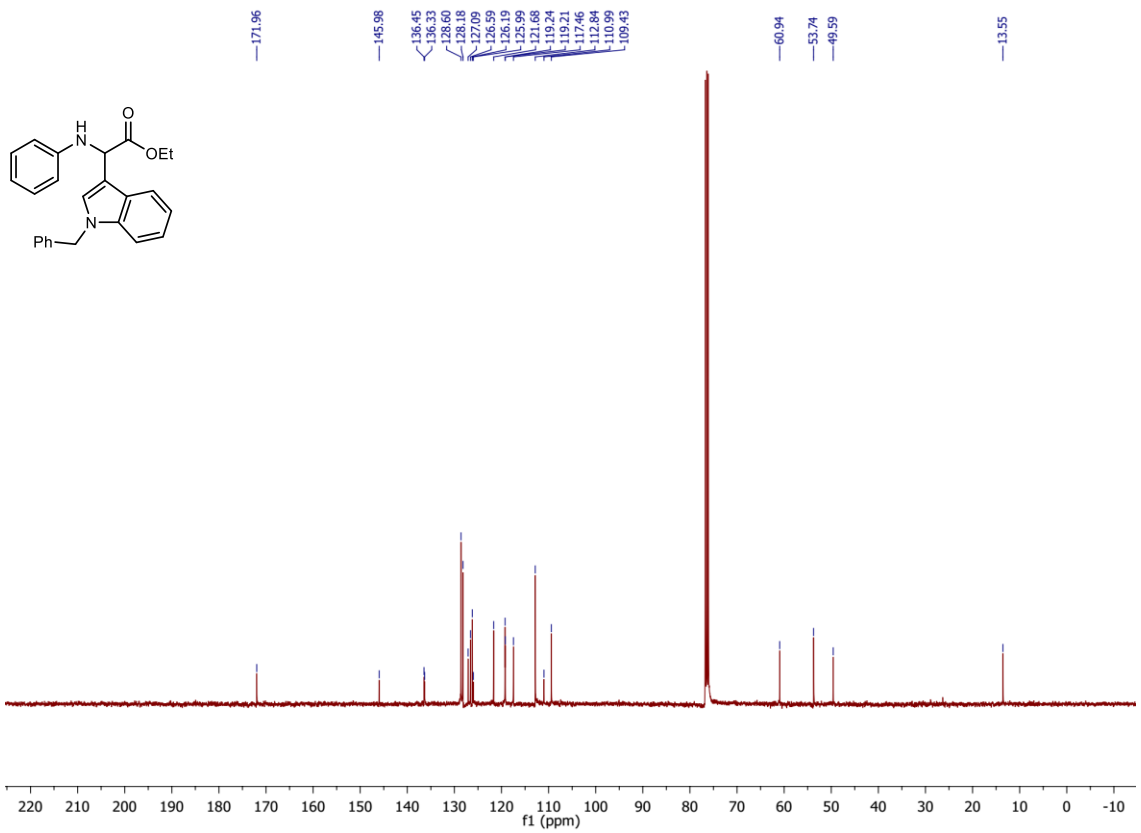

^{1}H-NMR (400 MHz, DMSO-d_6) spectrum of Ricobendazole

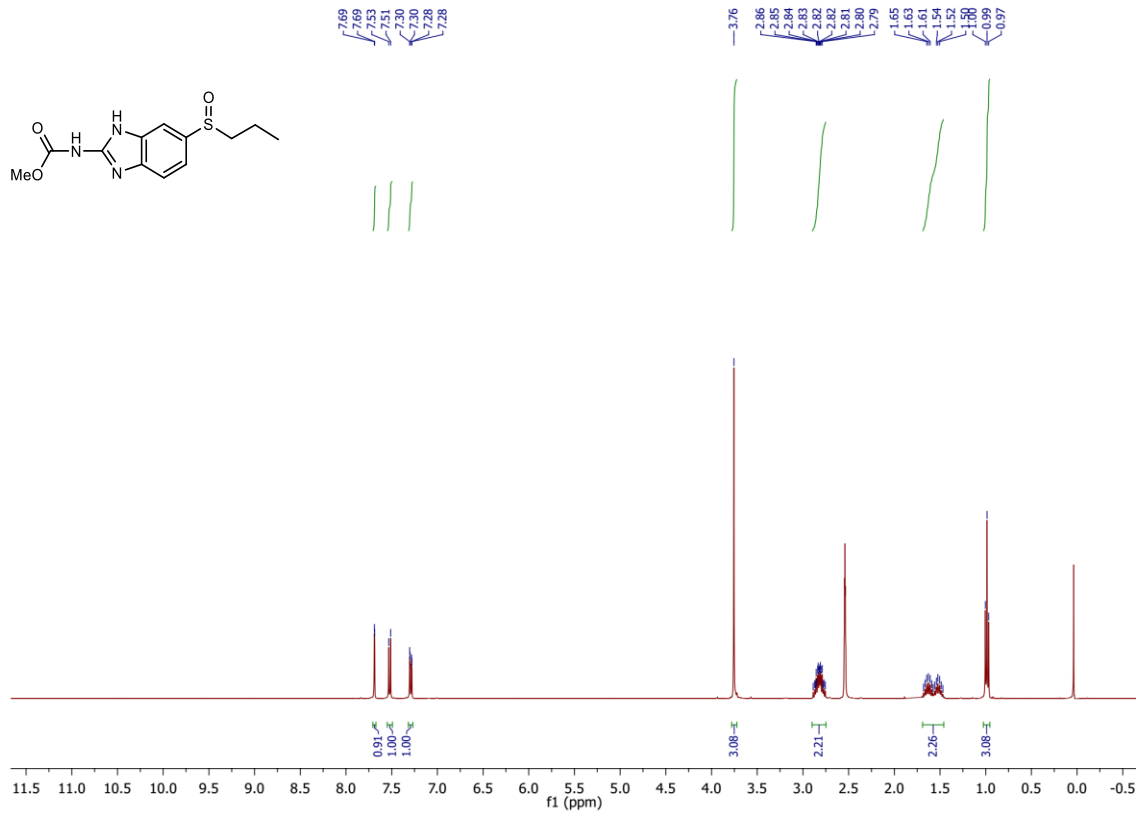

^{13}C-NMR (101 MHz, DMSO-d_6) spectrum of Ricobendazole